Systems Biology of the *Neurospora* Circadian Clock and its Response to Light and Temperature

A thesis submitted to the University of Manchester for the degree of Doctor of Philosophy in the Faculty of Life Sciences

2012

YU-YAO TSENG

Table of contents

The final word count:41553

List of Figures

List of Tables

Abstract

- The University of Manchester
- YU-YAO TSENG
- Doctor of Philosophy
- Systems Biology of the Neurospora Circadian Clock and its Response to Light and Temperature
- December 2012

Circadian clocks are internal timekeepers that aid survival by allowing organisms, from photosynthetic cyanobacteria to humans, to anticipate predictable daily changes in the environment and make appropriate adjustments to their cellular biochemistry and behaviour. Whilst many of the molecular cogs and gears of circadian clocks are known, the complex interactions of clock components in time and space that generate a reliable internal measure of external time are still under investigation. Computational modelling has aided our understanding of the molecular mechanisms of circadian clocks, nevertheless it remains a major challenge to integrate the large number of clock components and their interactions into a single, comprehensive model that is able to account for the full breadth of clock properties.

An important property of circadian clocks is their ability to maintain a constant period over a range of temperatures. Temperature compensation of circadian period is the least understood characteristic of circadian clocks. To investigate possible mechanisms underlying temperature compensation, I first constructed a comprehensive dynamic model of the *Neurospora crassa* circadian clock that incorporates its key components and their transcriptional and post-transcriptional regulation. The model is based on a compilation of published and new experimental data and incorporates facets of previously described *Neurospora* clock models. Light components were also incorporated into the model to test it and to reproduce our knowledge of light response of the clock. Also, experiments were carried out to investigate the unknown mechanisms of light response, such as the molecular mechanisms supporting the correct timing of conidiation after light to dark transfer. The model accounts for a wide range of clock characteristics including: a periodicity of 21.6 hours, persistent oscillation in constant conditions, resetting by brief light pulses, and entrainment to full photoperiods.

Next, I carried out robustness tests and response coefficient analysis to identify components that strongly influence the period and amplitude of the molecular oscillations. These data measure the influence of the parameters in the model and were beneficial for making and testing predictions in the model. Thermodynamic properties were then introduced into reactions that experimental observations suggested might be temperature sensitive. This analysis indicated that temperature compensation can be achieved if nuclear localisation of a key clock component, FRQ, decreases with increasing temperature. Experiments have been carried out to validate this hypothesis and simulations were made to explore other possible mechanisms. However, from my experimental data and modelling results, the restriction of FRQ nuclear localisation might not be the only mechanism required to achieve temperature compensation. In conclusion, temperature compensation is most likely a complex property and may involve a combination of multiple mechanisms regulating clock component activity over a range of temperatures.

Declaration

No portion of the work referred to in the thesis has been submitted in support of an application for another degree or qualification of this or any other university or other institute of learning.

Copyright statement

Acknowledgement

The grey rainy Manchester city is where I pursued my PhD. No matter how bad the weather was and how difficult the work was, I was able to go past them because of the presence of a lot of important people who accompanied and supported me.

Firstly, I would like to thank my supervisors Dr. Sue Crosthwaite and Dr. Jean-Marc Schwartz for giving me the opportunity to work in their lab, and for inspiration, careful direction and valuable assistance.

I would like to thank my advisor Dr. Simon Lovell for his valuable comments, and Dr. Christian Heintzen for his helpful advice and suggestions.

I would like to thank Dr. Delali Adiamah, Dr. Daphne Chen, Mr. Kun Tian, Ms. Caroline Paget, Dr. Suzanne Hunt, Dr. Cassie Welburn, Ms. Seona Thompson, Dr. Yamini Arthanari and all the others in the laboratories of Dr. Sue Crosthwaite, Dr. Jean-Marc Schwartz and Dr. Christian Heintzen for their various help.

I would also like to thank the Faculty of Life Sciences of the University of Manchester for providing the facilities and the environment.

I would like to thank Manchester Fo Guang Shan where I visited to calm my mind and make me focus.

I would also like to thank people whoever annoyed or hurt me. This made me stronger and better.

I would especially like to thank my girlfriend Hsin-Ying Cho for her love, company, encouragement and support.

Finally, I would like to thank my parents for their love, funding and support of living expense throughout my PhD study.

Abbreviations

Ago	Argonaute
aWCC	activated WCC
C box	Clock box
CCA1	*CIRCADIAN CLOCK ASSOCIATED1*
ccg	*clock-controlled gene*
cel	*chain elongation*
chr	*chrono*
CK-1a	casein kinase 1a
CK2	casein kinase 2
cpm	counts per minute
CT	circadian time
D-WCC	dark WCC
DC	detergent-compatible
DCL	dicer-like protein
dcl	dicer-like homologous gene
DD	constant darkness
dsRNA	double-stranded RNA
FAD	flavin mononucleotide
F_C	cytosolic FRQ
FFC	FRQ–FRH complex
FLO	FRQ-less oscillator
FMN	flavin mononucleotide
F_N	nuclear FRQ
FRH	FRQ-interacting RNA helicase
frq	*frequency*
FRQ/WCC TTFL	FRQ/WCC transcription/translation feedback loop
FRQ_c	cytosolic FRQ
FRQ_n	nuclear FRQ
FWD-1	F box/WD-40 repeat-containing protein
G1	*GIGANTEA*
hyperFRQc	cytosolic hyperphosphorylated FRQ
hyperFRQn	nuclear hyperphosphorylated FRQ
hyperWCC	hyperphosphorylated WCC
hyperWCCc	cytosolic hyperphosphorylated WCC
hyperWCCn	nuclear hyperphosphorylated WCC
hypoFRQc	cytosolic hypophosphorylated FRQ
hypoFRQn	nuclear hypophosphorylated FRQ
hypoWCC	hypophosphorylated WCC
hypoWCCc	cytosolic hypophosphorylated WCC
hypoWCCn	nuclear hypophosphorylated WCC
L-WCC	light activated WCC
laWCC	light activated WCC
LD	light to dark
lFRQ	large FRQ
LHY	*LATE ELONGATED HYPOCOTYL*

LL	constant light
LOV	light, oxygen, or voltage
miRNA	microRNA
MS	mass spectrometry
n/tFRQ	the ratio of nuclear to total FRQ
OD	optical density
ORF	open reading frame
PAS	Per: period circadian protein; Arnt: aryl hydrocarbon receptor nuclear translocator protein; Sim: single-minded
PCR	polymerase chain reaction
PKA	Protein Kinase A
PP2A	Protein Phosphatase 2A
PP4	Protein Phosphatase 4
PRC	phase response curves
prd	*period*
PYP	photoactive yellow protein
QA	quinic acid
qa-2	quinic acid-inducible promoter
qde	quelling-deficient gene
QIP	QDE-2-interacting protein
qrf	*frq* antisense RNA
RISC	RNA-induced silencing complex
RNAi	RNA interference
SCF	Skp1-Cul1-F-box-protein
SE	standard error
sFRQ	small FRQ
siRNA	short interfering RNA
Trh	Trachealess
UTR	untranslated region
vvd	*vivid*
VVDc	cytosolic VVD
VVDn	nuclear VVD
wc-1	*white collar-1*
wc-2	*white collar-2*
WC1c	cytosolic WC-1
WC2c	cytosolic WC-2
WCC	WHITE COLLAR complex
WVC	WCC-VVD complex

Chapter 1

Introduction

1. Introduction

1.1 Circadian clocks and systems biology

Circadian clocks are endogenous timekeepers that drive circadian rhythms with a period of about 24 hours. Circadian rhythms are daily periodic cycles of biochemical, physiological or behavioural process in organisms, such as conidiation in fungi (Sargent *et al*., 1966), photosynthesis (Sweeney, 1963) and leaf movement (Halaban, 1968a, 1968b) in plants, locomotor activities in fruit flies (Konopka and Benzer, 1971) and honeybees (Moore and Rankin, 1985), and hormone release and core body temperature cycle in humans (Kusanagi *et al*., 2008). Circadian rhythms are driven by circadian clocks. Circadian clocks aid survival by allowing organisms to anticipate predictable daily changes in the environment and make appropriate adjustments to their cellular biochemistry and behaviour (reviewed in Antle and Silver, 2009; Dodd *et al*., 2005). For example, DNA replication may be triggered by the circadian clock to occur at night to avoid damage of DNA by UV light (Batista et al., 2009). There are three defining characteristics of circadian clocks (reviewed in Dunlap *et al*., 2004). Firstly, the period is approximately 24 h and persists in constant conditions (Pittendrigh and Caldarola, 1973). Secondly, the rhythm can be reset by exposure to external stimuli, such as light or temperature (reviewed in Kozma-Bognar and Kaldi, 2008; Pittendrigh, 1960; reviewed in Rensing and Ruoff, 2002). Thirdly, the rhythm is temperature and nutritionally compensated (reviewed in Eckardt, 2006; Fonzo et al., 2009). Thus, the period length remains the same in a range of different conditions, when the organism is exposed to different temperatures or different carbon sources (Pittendrigh and Caldarola, 1973; Winfree, 1980).

Neurospora, a filamentous fungus, is one of the model organisms used to study circadian clocks. It is a simple eukaryote and has an easily observable circadian rhythm of asexual sporulation. Moreover, it has a well-studied circadian clock and many components of the clock are known (Dunlap and Loros, 2006).

Quantitative modelling is widely used to quantify the amounts of molecular components in biological processes, to represent interactions between components, and to make and test predictions. In addition, quantitative modelling may uncover new mechanisms and interactions. It is used to design experiments and to decide the direction of future research (reviewed in Ecker et al., 2008; Kollmann and Sourjik, 2007). Several quantitative models of the *Neurospora* circadian clock have been built (Francois, 2005; Hong *et al*., 2008a; Leloup *et al*., 1999b; Ruoff *et al*., 2005), that successfully represent known interactions of clock components. Furthermore, hypotheses have been proposed using some models for phenomena whose underlying molecular basis have not been experimentally determined. Therefore, quantitative modelling is not only helpful for precisely understanding the interactions of *Neurospora* clock components, but also useful for making and testing predictions of *Neurospora* clock mechanisms, such as mechanisms of temperature compensation.

This chapter reviews the literature related to the biology of the *Neurospora* circadian clock and the quantitative modelling of the *Neurospora* circadian clock. There are two main sections. In the first section (1.2), circadian clocks and biological rhythms will be introduced followed by detailed information on the *Neurospora* circadian clock including the key clock components and mechanisms that generate rhythmicity. Details of how the key clock components undergo posttranslational modification, translocation and function will also be described in this section. In addition, interactions between environmental factors and the *Neurospora* clock components will be described to explain how environmental changes affect the *Neurospora* circadian clock. The current understanding of temperature compensation is also discussed here. The second section (1.3) will focus on quantitative modelling. The general area of systems biology and quantitative modelling of genetic regulation will be introduced, and then it will focus on the dynamic modelling of genetic feedback loop. Next, quantitative models of the *Neurospora* circadian clock are introduced and compared. Finally, models accounting for temperature effects in this system and descriptions of how temperature compensation is modelled will be given. The aims and objectives of this project are presented at the end of this chapter (1.4).

1.2 Characteristics and molecular mechanisms of the *Neurospora* circadian clock

1.2.1 Introduction

At the molecular level, a common characteristic of circadian clocks is that there is usually an underlying transcriptional and translational feedback loop (reviewed in Dunlap, 1999). The common elements in the transcriptional-translational negative feedback loops are shown in Figure 1.1. Positive and negative elements regulate the expression of clock genes and clock-controlled genes (ccgs). For example, KaiA in *Synechococcus* (reviewed in Dong and Golden, 2008), CLK and CYC in *Drosophila* (reviewed in Zheng and Sehgal, 2008), and Clock and Bmal1 (Mop3) in mammals (reviewed in Dardente and Cermakian, 2007) are positive elements. These molecules promote the expression of the clock and clock-controlled genes. On the other hand, negative elements, such as KaiC in *Synechococcus* (reviewed in Dong and Golden, 2008), PERIOD and TIMELESS in *Drosophila* (reviewed in Zheng and Sehgal, 2008), and Cry1, Cry2, Per1 and Per2 in mammals (reviewed in Dardente and Cermakian, 2007), repress the action of positive elements. The transcriptional-translational negative feedback loops result in periodic expression of the clock genes and clock-controlled genes. Consequently, rhythmic changes in metabolism and behaviour can be observed (reviewed in Loros and Dunlap, 2001).

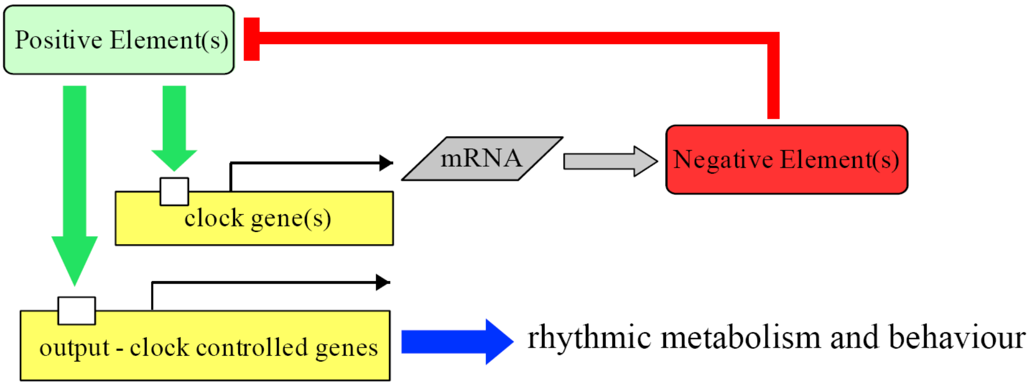

Figure 1.1 Schematic representation of common feedback loops in circadian clocks.
Positive and negative elements could be expressed from clock genes, and positively or negatively regulate the expression of clock genes. Figure redrew from (Dunlap, 1999).

The *Neurospora crassa* clock is based on molecular feedback loops that in constant conditions generate a 22 hours period (Figure 1.2). Components include the *frequency* (*frq*), *white collar-1* (*wc-1*) and *white collar-2* (*wc-2*) genes. In the positive arm, the WHITE COLLAR complex (WCC), a heterodimer of WC-1 and WC-2, activates the transcription of *frq*. The product of the *frq* gene, the FREQUENCY (FRQ) protein, transcriptionally and post-transcriptionally promotes the accumulation of WC-2 and WC-1, respectively (Cheng *et al*., 2001b; Schafmeier *et al*., 2008). In a negative feedback loop, FRQ recruits kinases, such as Casein kinase-1a (CK-1a), and facilitates WCC phosphorylation (He *et al*., 2006). The phosphorylation of WCC results in WCC inactivation and thus interferes with the binding of WCC to the *frq* promoter (Schafmeier *et al*., 2005)

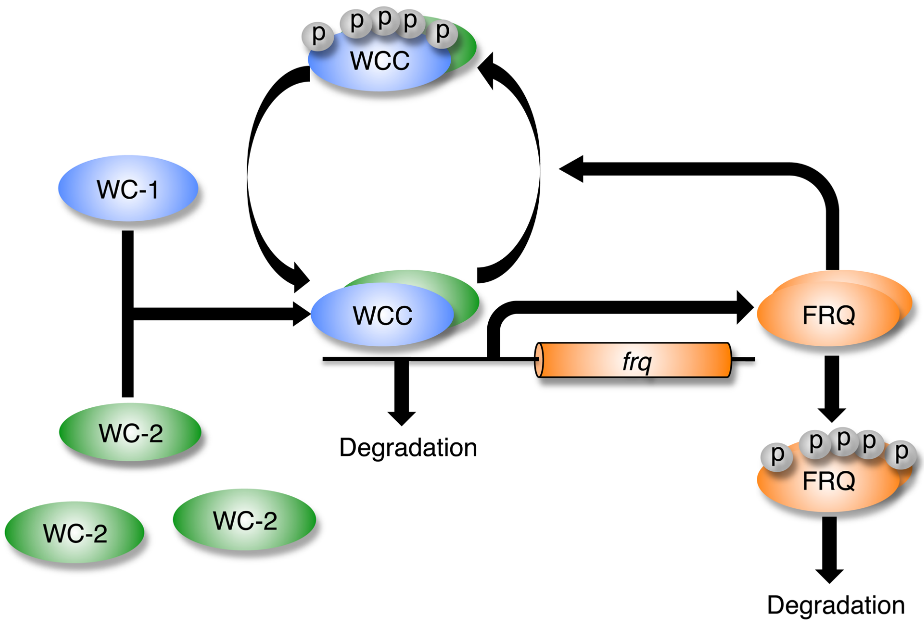

Figure 1.2 Simplified representation of the *Neurospora* circadian clock.
Transcription factors WHITE COLLAR-1 (WC-1) and WHITE COLLAR-2 (WC-2) form a heterodimeric WHITE COLLAR complex (WCC). Early in the subjective night, the hypophosphorylated form of WCC (hypoWCC) activates the transcription of the *frequency* (*frq*) gene. Once hypoWCC activates transcription, it is degraded. The FREQUENCY protein (FRQ) accumulates, peaking around midday, and is progressively phosphorylated. Hyperphosphorylated FRQ is ubiquitinated and degraded by the proteosome. FRQ promotes phosphorylation of WCC by recruiting kinases, and phosphorylated WCC (hyperWCC) is inactive thus leading to decreased transcription of *frq* and consequently negative regulation of FRQ. Phosphorylated WCC is more stable than its hypophosphorylated form, thus the increase in FRQ level leads to a rise in overall WCC level.

1.2.2 Transcription factors WHITE COLLAR-1 and WHITE COLLAR-2

WC-1 and WC-2 are both GATA-type zinc finger DNA binding proteins and are mainly localized in the nucleus (Denault *et al*., 2001; Schwerdtfeger and Linden, 2000). WC-1 and WC-2 can bind to each other to form a heterodimeric complex, the WHITE COLLAR complex (WCC). WCC binds to the Clock box (C box) in the *frequency* (*frq*) promoter and activates *frq* transcription (Crosthwaite *et al*., 1997; Froehlich *et al*., 2003; He *et al*., 2006). WHITE COLLAR-1 (WC-1) and WHITE COLLAR-2 (WC-2) proteins are PAS (Per: period circadian protein; Arnt: aryl hydrocarbon receptor nuclear translocator protein; Sim: single-minded) protein domain-containing transcription factors (Ballario *et al*., 1996; Linden and Macino, 1997). The PAS domain is a signal sensor domain, which is often involved in protein-protein interactions. It can be found in many signalling proteins, such as the F-box protein EID1 involved in light signal transduction in plants (Marrocco *et al*., 2006), the *Drosophila* transcription factor Trachealess (Trh) (Zelzer *et al*., 1997), and the bacterial photoreceptor photoactive yellow protein (PYP) (Rajagopal *et al*., 2005). WC-1 contains three PAS domains, including one light, oxygen, or voltage (LOV) domain, and WC-2 contains one PAS domain (Ballario *et al*., 1996; Linden and Macino, 1997). One of the PAS domains (PASC) in WC-1 interacts with the PAS domain of WC-2 and mediates the formation of WCC (Cheng *et al*., 2002; Cheng *et al*., 2003). On the other hand, WC-2 is critical both for WC-1 production and WCC formation (Cheng *et al*., 2002).

WC-1 not only plays an important role in activating the transcription of *frq*, but also is crucial for photo responses. The N-terminal PAS domain of WC-1 is a specialised PAS domain which is named as the LOV domain. Proteins containing a LOV domain usually function as a sensor for environmental factors (reviewed in Crosson *et al*., 2003). The LOV domain contains a flavin mononucleotide (FMN or FAD: flavin adenine dinucleotide) chromophore binding site and can trigger signal transduction to activate photoinduced reactions (Briggs and Huala, 1999). WC-1 has been identified as a blue-light photoreceptor (Froehlich *et al*., 2002; Linden *et al*., 1997). The LOV domain in WC-1 is crucial for flavin mononucleotide (FMN) involved light response (He *et al*., 2002).

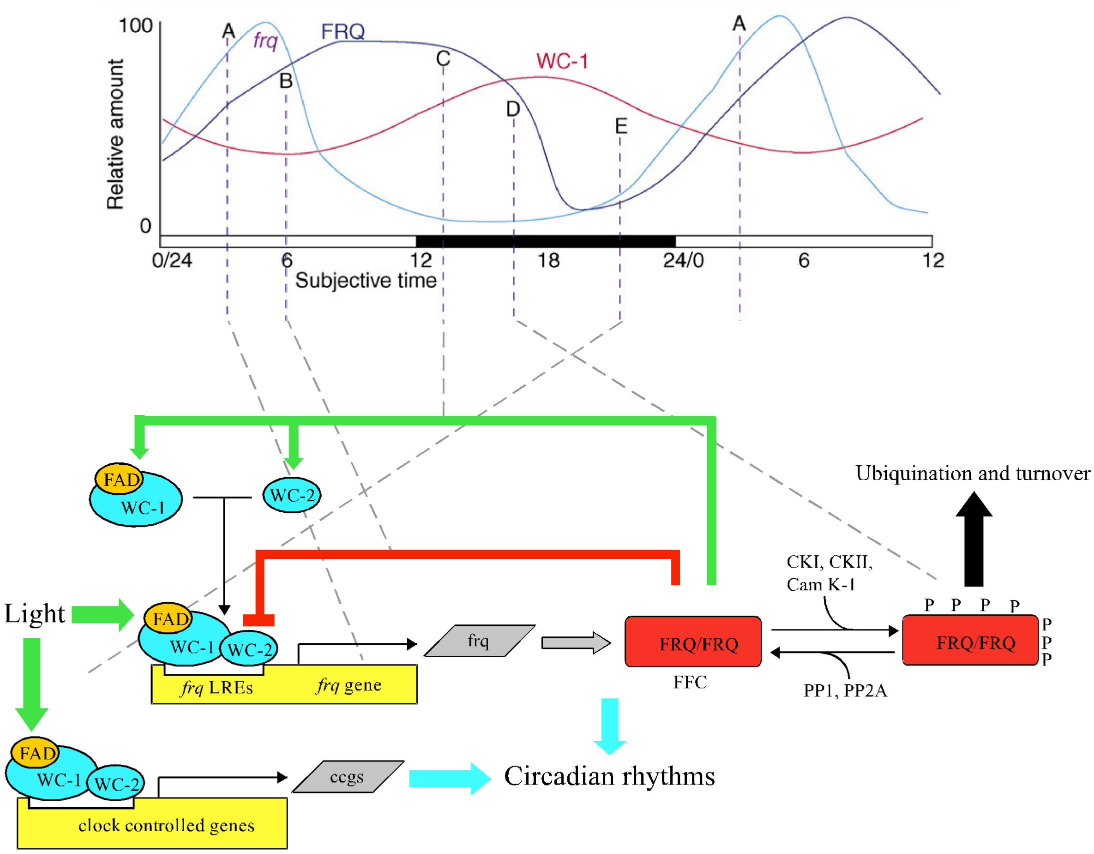

Figure 1.3 Monitoring the key components of the *Neurospora* circadian oscillator over time.
This graph is plotted from the subjective dawn, which is defined as the circadian time 0 (CT 0). Day time (white bar) is from CT 0 to CT 12, whereas night time (black bar) is from CT 12 to CT 24/0. Time A corresponds to *frq* transcription. After translation, the FFC complex is formed and translocates into the nucleus to inactivate WCC (time B). Also, FFC translationally and transcriptionally promotes the production of WC-1 and WC-2, respectively (time C). Then, FRQ is hyperphosphorylated and degraded (Time D). Next, light activates WCC and reinitiates the next cycle. Figure redrawn from (Dunlap and Loros, 2006).

1.2.3 The *frequency* gene and its products

The protein product (FRQ) of the *frequency* (*frq*) gene is a core component of the circadian oscillator in *Neurospora* (Figure 1.3). Mutation of *frq* can alter the period length of the circadian rhythm (Gardner and Feldman, 1981). In addition, the behaviour of temperature and nutritional compensation can also be lost in a *frq* mutated strain, frq^9 (Loros and Feldman, 1986). The production of FRQ is activated by its transcription factor, the WHITE COLLAR complex (WCC). After translation, FRQ becomes homodimerised and binds with the FRQ-interacting RNA helicase (FRH) to form the FRQ–FRH complex (FFC) (Cheng *et al.*, 2001a; Cheng *et al.*, 2005). The FFC complex can recruit kinases, such as casein kinase-1a (CK-1a), and facilitate WCC phosphorylation (Schafmeier *et al.*, 2005). The phosphorylation of WCC results in WCC inactivation and thus interferes with the binding of WCC to the *frq* promoter (Schafmeier *et al.*, 2005). Consequently, the levels of *frq* mRNA and FRQ decline. Degradation of FRQ depends on the level of its phosphorylation. FRQ can be phosphorylated by kinase CK-1a, CKII and CAMK-1, and dephosphorylated by phosphatase PP1 and PP2A (reviewed in Liu, 2005). Highly phosphorylated FRQ interacts with FWD-1, an F box/WD-40 repeat-containing protein and the substrate-recruiting subunit of an Skp1-Cul1-F-box-protein (SCF)-type ubiquitin ligase complex, and undergoes ubiquitination, thus phosphorylation targets FRQ protein for degradation by the proteosome (He *et al.*, 2003). When the level of FRQ is declining, WCC becomes activated and *frq* transcription as well as clock-controlled gene expression is reactivated (reviewed in Heintzen and Liu, 2007). Moreover, FRQ not only plays a critical role in negatively regulating its own expression, but also positively promotes the production of WC-1 and WC-2 (reviewed in Vitalini *et al.*, 2006). FRQ promotes the transcription of both *wc-1* and *wc-2* and posttranscriptionally promotes translation of *wc-1* mRNA (reviewed in Liu and Bell-Pedersen, 2006).

The level of WC-2 is not shown in Figure 1.3 because its level is much higher (5 to 30 times) than FRQ and WC-1 and nearly constant (Denault *et al.*, 2001). Large amounts of WC-1 accumulate in the cytosol at CT 18. This results in a gradual increase of

WCC, and thus clock genes and clock-controlled genes (ccgs) are activated. The level of *frq* mRNA peaks at CT 0-4 and FRQ is produced. Next, the concentration of *frq* mRNA declines because of the repression by its own product at CT 10. However, FRQ positively regulates the production of WC-1. Throughout the day, FRQ is phosphorylated from CT 16 to CT 20, and hyoperphosphorylated FRQ is degraded via the Ubiquitin/Proteasome pathway.

To summarise, in the positive regulation loop, FRQ facilitates the production of WC-1 and *wc-2*. Next, WCC binds to the *frq* promoter, and activates the transcription of the *frq* gene. In the negative regulation loop, FFC catalyzes WCC phosphorylation and inhibits *frq* transcription (reviewed in Heintzen and Liu, 2007).

1.2.4 FRQ phosphorylation and its function

FRQ is the essential clock component in *Neurospora*, which is not only involved in the negative limb of the *Neurospora* clock feedback loop (Aronson *et al*., 1994; Schafmeier *et al*., 2005), but also participates in the positive feedback loop (Cheng *et al*., 2001b; Lee *et al*., 2000; Schafmeier *et al*., 2006). After translation, FRQ is progressively phosphorylated over time (reviewed in Brunner and Schafmeier, 2006). In addition, high-performance tandem mass spectrometry (MS) analysis reveals phase-specific phosphorylation of FRQ (Baker *et al*., 2009). More than 75 FRQ phosphorylation sites have been identified (Baker *et al*., 2009).

Phosphorylation of FRQ strongly influences the period length of the *Neurospora* circadian clock (Liu *et al*., 2000). Early studies revealed that FRQ degradation becomes much slower and the period length is longer than 30 hours when a single serine residue (S513) is exchanged to arginine or isoleucine by the site-directed mutagenesis (Liu *et al.*, 2000). However, this residue was not found to be phosphorylated from the MS data (Baker *et al.*, 2009; Liu *et al.*, 2000). The phosphorylation of FRQ at the early stage stabilises FRQ and is able to increase period length, whereas phosphorylation at later stage leads to faster degradation of FRQ and decreases period length (Baker *et al.*, 2009). In addition, phosphorylation at residue 548 stabilises FRQ and increases period length, whereas phosphorylation at the C-terminal residue 900 increases FRQ turnover and decreases period length (Baker *et al.*, 2009). For temperature effects, Mehra *et al.* showed that casein kinase 2 (CK2) can directly phosphorylate FRQ and plays an important role in temperature compensation of the *Neurospora* clock (Mehra *et al.*, 2009). Reducing the production of CK2 subunits, β1 or α, results in a loss of temperature compensation (Mehra *et al.*, 2009). Phosphorylation may lead to conformation change of FRQ. Therefore, temperature sensitive phosphorylation possibly supports FRQ function to achieve temperature compensation.

Phosphorylation of FRQ also regulates the localisation of FRQ. Hyperphosphorylated nuclear FRQ is translocated out of the nucleus and accumulates in the cytoplasm (Diernfellner *et al.*, 2009). Hypophosphorylated nuclear FRQ shuttles into and out of the nucleus (Diernfellner *et al.*, 2009) and is progressively phosphorylated in both the cytoplasm and the nucleus (reviewed in Brunner and Schafmeier, 2006).

1.2.5 FRQ localisation

FRQ is predominantly accumulated in the cytoplasm both in constant light and in constant darkness (Cha *et al.*, 2011; Diernfellner *et al.*, 2009). In constant light the ratio of nuclear FRQ to total FRQ is about 0.2 (Cha *et al*., 2011). In constant darkness, the level of nuclear FRQ is rhythmic with the ratio of nuclear FRQ to total FRQ approximately maintained at 0.3 (Cha *et al*., 2011). From FRQ-mCh (FRQ is fused with a red fluorescent protein mCherryNC) *in vivo* experiments, a major peak of nuclear FRQ occurs at CT 4-5 whilst a minor peak occurs at CT 19 (Castro-Longoria *et al*., 2010). These results suggest that FRQ nuclear localisation is complex and time dependent.

1.2.6 WCC phosphorylation and its function

The phosphorylation of WCC is first by a priming kinase, such as Protein Kinase A (PKA), followed by FRQ-recruited kinases, such as Casein Kinase 1a (CK1a), (Huang *et al*., 2007; Schafmeier *et al*., 2005). FRQ-dependent phosphorylation of WCs is mediated by Casein Kinase 1a (CK-1a) and Casein Kinase 2 (CK2) (He *et al*., 2006). Protein Phosphatase 2A (PP2A) and Protein Phosphatase 4 (PP4) dephosphorylates both WC-1 and WC-2 (Cha *et al*., 2008; Schafmeier *et al*., 2005). Five light-independent phosphorylation sites have been identified in WC-1 (He *et al*., 2005) and up to eight residues can be phsophorylated in WC-2 (Sancar *et al*., 2009). Circadian phosphorylation of WC-1 and WC-2 determines their activities. Single (Ser-990) or double (Ser-988/Ser-990) mutation of WC-1 phosphorylation sites result in short period of conidation (He *et al*., 2005). Conidation becomes arrhythmic if three (Ser-990/Ser-992/Ser-988) or five (Ser-990/Ser-992/Ser-994/Ser-995/Ser-988) WC-1 phosphorylation sites are mutated (He *et al*., 2005). Higher level of *frq* RNA and FRQ was observed in WC-1 (Ser-990/Ser-992/Ser-994/Ser-995/Ser-988) and WC-2 (Ser-433) phosphorylation site mutation strains, suggesting that phosphorylation of the WC proteins negatively regulates WCC function (He *et al*., 2005; Sancar *et al*., 2009). The level of WCC phosphorylation depends on the presence of FRQ. WCC is hyperphosphorylated and inactive when FRQ is expressed (Schafmeier *et al*., 2005). In addition, the binding of WCC to the *frq* promoter is significantly reduced when WCC is hyperphosphorylated and inactive (He *et al*., 2006).

Phosphorylation of the WCC also regulates its cellular localisation. FRQ facilitates WCC phosphorylation and cytoplasmic accumulation (Schafmeier *et al*., 2008). Dephosphorylation of the WCC by PP4 promotes WCC nuclear localisation, whereas phosphorylation of WCC by PKA inhibits WCC nuclear localisation (Cha *et al*., 2008). Furthermore, PP2A-dependent WCC dephosphorylation activity is high in the cytoplasm and low in the nucleus (Schafmeier *et al*., 2008). Therefore, these data suggest that PP2A-dependent WCC dephosphorylation in the cytoplasm reactivates WCC and supports its nuclear re-entry.

The degradation of WCC is triggered by DNA binding (Schafmeier *et al*., 2008). As WCC phosphorylation interferes with its DNA binding (Schafmeier *et al*., 2005), FRQ positively regulates the accumulation of WCC by facilitating WCC phosphorylation since phosphorylated WCC translocates out of the nucleus and is dephosphorylated by PP2A in the cytoplasm (Schafmeier *et al*., 2008). In addition, *wc-2* transcription is promoted by FRQ and *wc-2* transcription is repressed by WCC via up-regulation of a putative repressor (Neiss *et al*., 2008).

1.2.7 VVD and its function

For the light response, VVD is the second blue light receptor in *Neurospora*. VIVID (VVD) is a small protein containing 187 amino acids. Similar to WC-1, VVD is also a PAS/LOV protein. The expression of vivid (*vvd)* is rapidly light-induced and clock-controlled, but after the first day in constant darkness its expression is much reduced (no expression can be detected by northern blot) (Heintzen *et al*., 2001). In the *vvd* mutant strain (SS692), *frq* and *vvd* RNA decrease significantly slower after light pulse comparing to wild-type (Heintzen *et al*., 2001). In addition, SS692 has a 4 hr delay of light response comparing to wild-type (Heintzen *et al*., 2001). VIVID also functions as a repressor of the light response (Chen *et al*., 2010; Heintzen *et al*., 2001; Malzahn *et al*., 2010). Furthermore, VVD influences temperature-dependent FRQ phosphorylation after light to dark transfer and supports the regulation of conidiation downstream from the clock to achieve temperature compensation (Hunt *et al*., 2007).

1.2.8 The *frq* antisense RNA, *qrf*

Interestingly, the *frq* locus encodes both sense and antisense transcripts. The expression of the *frq* antisense RNA (*qrf*) is antiphase to sense *frq* RNA in constant darkness. *frq* sense and antisense RNA are both inducible by light (Kramer *et al*., 2003). After light to dark transfer, the first band of conidiation is used to define the reference phase of the clock. Replacement of the *qrf* promoter with the *clock-controlled gene-2 (ccg-2*) promoter results in phase delay compared to wildtype (Kramer *et al*., 2003). This result suggests that *qrf* is a functional non-protein-coding transcript. Because *frq* and *qrf* are fully complementary, it is possible that they form dsRNA. This dsRNA could be cleaved by the ribonuclease protein Dicer and triggers RNAi. Therefore, *qrf* may regulate the phase after light to dark transfer by RNAi. On the other hand, experimental data suggested that DNA methylation regulates circadian phase (Belden *et al.*, 2011). DNA methylation at the *frq* promoter region was significantly reduced when the expression of *qrf* was abolished (Belden *et al.*, 2011), suggesting that *qrf* may regulate circadian phase via DNA methylation.

1.2.9 RNAi in *Neurospora*

As *qrf* RNA is expressed in *Neurospora*, *frq* might be the target of regulation by *qrf* via RNA interference (RNAi). RNAi is one of the regulation processes of gene expression. Generally, RNAi is triggered with the cleavage of double-strand RNA by the ribonuclease protein Dicer (reviewed in Chang *et al.*, 2012; reviewed in Mello and Conte, 2004). Next, short interfering RNAs (siRNAs) or microRNAs (miRNAs) produced from the cleavage are involved in the formation of the RNA-induced silencing complexes (RISCs) with the Argonaute (Ago) protein (reviewed in Carthew and Sontheimer, 2009; Hammond *et al.*, 2001). One strand of the siRNA is discarded (passenger strand) and the other one becomes the guide strand in RISC (reviewed in Carthew and Sontheimer, 2009). RISC uses this guide strand to find the complementary target of sequence and the degradation of target RNA is induced by the Ago protein (reviewed in Carthew and Sontheimer, 2009).

In *Neurospora*, there are two dicer-like homologous genes (*dcl-1* and *dcl-2*) (Catalanotto *et al.*, 2004). Dicer protein recognizes double-stranded RNA (dsRNA), binds to it and cleaves it giving rise to small-interfering RNA (siRNAs) (Figure 1.4). Three quelling-deficient genes (*qde*) have been identified in *Neurospora*, which are *qde-1*, *qde-2*, and *qde-3* (Cogoni and Macino, 1997). QDE-1 is an RNA-dependent RNA polymerase and QDE-3 is a DNA helicase. QDE-1 and QDE-3 are involved in generation of dsRNA and are not required for gene silencing. QDE-2 is an Argonaute protein and is the core of the RNA-induced silencing complex (RISC) associated with siRNA (Choudhary *et al*., 2007). In the RNAi pathway, dicer-like protein (DCL) binds to dsRNA and cleavage dsRNA to siRNA. QDE-2 is the core component of RISC. QDE-2-interacting protein (QIP) is an exonuclease that digests the passenger strand. Next, the guide strand is left in the complex and RISC is active (Maiti *et al*., 2007).

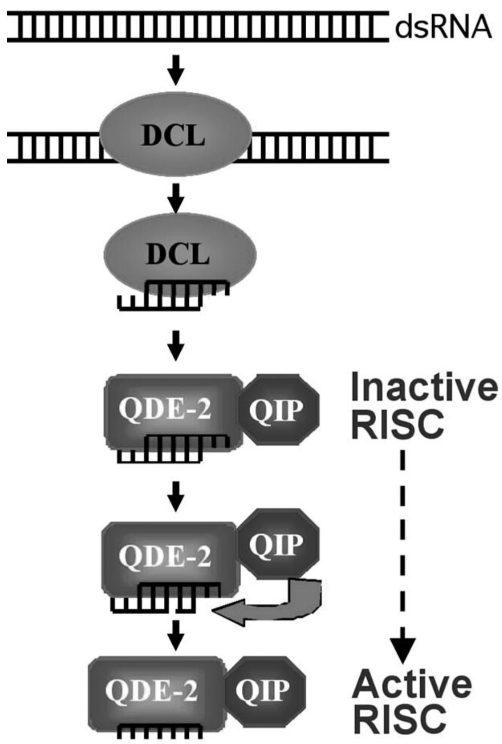

Figure 1.4 The pathway of RNAi in Neupospora.
The dicer like protein (DCL) recognise the double strain RNA (dsRNA) and digest the sequence into small-interfering RNA (siRNA). The RNA-induced silencing complex (RISC) is mainly composed of quelling-deficient protein-2 (QDE-2) and QDE-2-interacting protein (QIP). After the passenger strand is removed, the RISC complex is active. (Figure taken from (Maiti *et al*., 2007))

1.2.10 The FRQ/WCC less oscillator

In addition to the FRQ/WCC transcription/translation feedback loops (FRQ/WCC TTFL), several circadian or non-circadian molecular rhythms have been found in *Neurospora* (Christensen *et al*., 2004; Dragovic *et al*., 2002; Lakin-Thomas and Brody, 2000; Li *et al*., 2011). These rhythms are named as FRQ-less oscillators (FLOs), which may not be driven by or be part of the FRQ/WCC TTFL, suggesting that multiple feedback loops are involved in the *Neurospora* circadian clock system. Some of these rhythms are involved in metabolic rhythm and may contribute to the mechanism of nutritional compensation (Christensen *et al*., 2004). In addition, the FRQ-less oscillator (FLO) coupling with WC-1 and WC-2 is able to achieve temperature compensation (de Paula *et al*., 2006). Therefore, these data suggest that the existence of FLOs is critical for the *Neurospora* circadian clock.

1.2.11 Interactions between environmental factors and *Neurospora* oscillators

Neurospora can sense and respond to environmental stimuli to synchronise to local time (Francis and Sargent, 1979; Sargent and Briggs, 1967). The molecular mechanisms of sensing environmental change by *Neurospora* are still not totally understood. There are several mechanisms related to this behaviour. At the molecular level, the resetting of the clock by light involves photoreceptors such as WC-1 and VVD in receiving the light and results in the strong induction of *frq* expression (Crosthwaite *et al*., 1995; Froehlich *et al*., 2002; He *et al*., 2002; Schwerdtfeger and Linden, 2003). This rapid expression of *frq* changes the level of *frq* RNA and FRQ and resets the clock.

A light pulse at night (CT 12-24) can result in a phase shift of the circadian cycle. The degree of influence depends on when *Neurospora* is exposed to light. In addition, stimulus duration influences the degree of delay or advance by which the clock is reset (Figure 1.5) (Dharmananda, 1980; Huang *et al.*, 2006; Sargent and Briggs, 1967). For example, 15 seconds of light at CT 19 can result in arrhythmicity, which is known as the singularity behaviour. The singularity behaviour happens when the clock system receives a stimulus and the system is driven to its singularity point. This results in the clock being unable to measure time. In *Neurospora*, the singularity behaviour happens when the level of FRQ is varied to the intermediate level after receiving a stimulus. Whereas, 5 and 30 seconds of light only result in a phase change, but do not affect the rhythmicity.

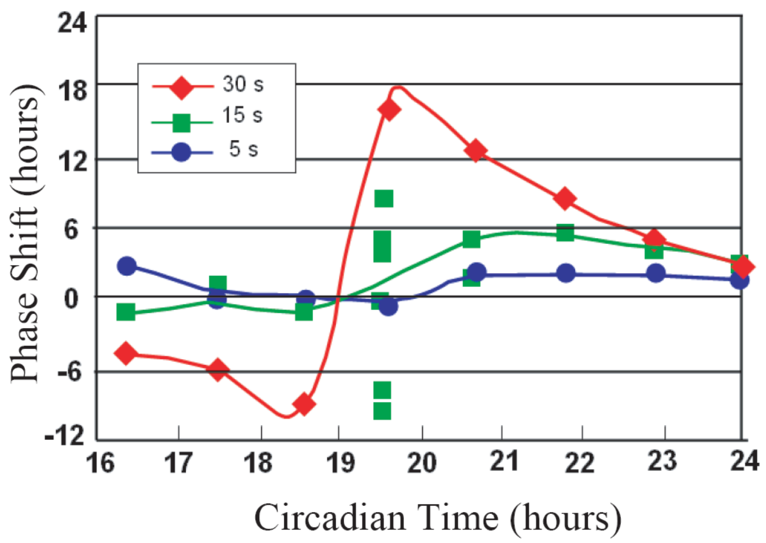

Figure 1.5 ***Neurospora*** **phase response curves (PRC) of light pulses.**
Phase shift induced by light pulses of different duration (5, 15 and 30 seconds) given at different times (CT 16-24) throughout the subjective day. The value of phase shift is calculated from the advance or delay of conidiation after stimulation. Figure redrawn from (Huang *et al.*, 2006).

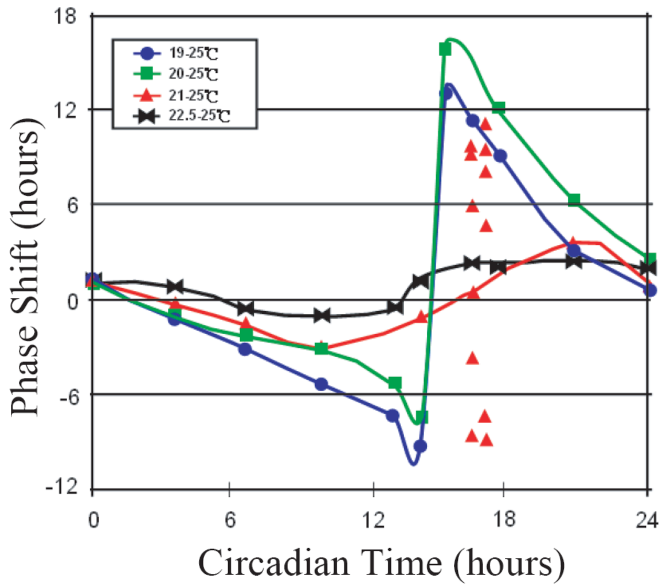

Figure 1.6 *Neurospora* phase response curves (PRC) of temperature step-ups.
A larger temperature change (19-25℃ and 20-25℃) results in a more significant phase shift. The value of the phase shift is calculated from the advance or delay of conidiation after stimulation. Figure redrawn from (Huang *et al*., 2006).

WC-1 and VIVID (VVD) proteins are known *Neurospora* blue light receptors (Froehlich *et al*., 2002; Linden and Macino, 1997; Schwerdtfeger and Linden, 2003). WC-1 is a photoreceptor and transcription factor that enhances the transcription of light-responsive genes such as *frq*, *wc-1* and *vvd* (Ballario *et al*., 1996; Correa *et al*., 2003; Froehlich *et al*., 2002; He *et al*., 2002; Smith *et al*., 2010). In addition, WCC regulates about 20 % of all genes, including the expression of 24 transcription factor genes (Smith *et al*., 2010). VIVID functions as a repressor of the light response (Chen *et al*., 2010; Heintzen *et al*., 2001; Malzahn *et al*., 2010). Both photorecpetors contain the PAS/LOV domain that binds with FAD or FMN cofactor and are able to trigger signal transduction to activate photoinduced reactions. After stimulation by light, a large photoactivated complex (L-WCC), which contains more than one WC-1 molecule, is transformed from the heterodimeric dark WCC (D-WCC), and promotes the transcription *frq*, *vvd*, and other *clock-controlled genes (ccgs)* (reviewed in Liu and Bell-Pedersen, 2006). L-WCC is a strong transcriptional activator of *frq* even in the presence of FRQ (reviewed in Heintzen and Liu, 2007). In addition, WC-2 is necessary for WC-1 in the light signalling pathway (Cheng *et al*., 2002).

In contrast VVD acts as a repressor of light-induced responses (Heintzen *et al*., 2001). The expression of VVD is dependent on L-WCC. Evidence suggests that it represses light-induced transcription by competing with L-WCC for the dimerisation with WC-1 and this results in the dissociation of L-WCC and a concomitant decrease in its ability to activate transcription (Chen *et al*., 2010; Hunt *et al*., 2010; Malzahn *et al*., 2010). Moreover, *qrf*, the antisense *frq* RNA, also contributes to the light response of the *Neurospora* circadian clock by supporting the correct timing of conidiation after light to dark transfer (Belden *et al*., 2011; Crosthwaite, 2004; Kramer *et al*., 2003).

Temperature can also synchronise the clock to local time. Temperature cycles are able to entrain the clock in *Neurospora* (Francis and Sargent, 1979). For phase resetting by temperature, Figure 1.6 shows the Phase Response curves (PRC) resulting from different magnitudes of temperature change (Huang *et al*., 2006). Larger changes in temperature result in larger phase shifts.

For the resetting of the clock by temperature, the mechanism should be more complex since temperature affects most chemical reactions. How temperature affects the clock is still unclear. Temperature regulates the splicing of mRNA in *Neurospora* (Colot *et al*., 2005; Diernfellner *et al*., 2007; Garceau *et al*., 1997). This results in different products from a single gene. Two different forms of FRQ can be produced from the *frq* mRNA. At higher temperature, the large FRQ (lFRQ: 989 amino acids) can be produced efficiently. At lower temperature, a splice form of *frq* mRNA lacking the first ATG is preferentially produced resulting in synthesis of small FRQ (sFRQ: 889 amino acids) (Diernfellner *et al*., 2005). The most significant observation of temperature effect is that the level of FRQ is tripled from 21 to 28 ºC (Liu *et al*., 1998). However, the level of *frq* RNA oscillation is unchanged (Liu *et al*., 1998). The degradation rate of FRQ is also maintained (Mehra *et al*., 2009). These results suggest that the rate of FRQ translation is dependent on temperature. The level of FRQ varies with temperature and determines phase resetting after a temperature pulse. However, the detailed mechanism of how temperature resets the clock is still unknown.

1.2.12 Temperature compensation

Living creatures usually experience a wide range of daily and seasonal temperatures. To be able to live under these conditions, temperature compensation can be observed ubiquitously at each level of biological systems. For example, the escape behaviour in the marine copepod, *Calanus finmarchius* (Lenz *et al*., 2005), and the metabolic temperature compensation in aquatic poikilotherms (Newell, 1966). The period of the circadian clocks are also temperature compensated (Pittendrigh, 1954; reviewed in Rensing and Ruoff, 2002; Tsuchiya *et al*., 2003).

For general chemical reactions, the reaction rate is usually doubled when temperature increases by 10 ºC (Harcourt, 1867; Snyder, 1908). To measure how temperature affects reaction rates, the temperature coefficient Q_{10} value is widely used to determine how the reaction rate is changed when temperature increases by 10 ºC (McLarnon *et al*., 1993; Reyes *et al*., 2008; Ruoff, 1992). The Q_{10} for most biochemical and chemical reactions is about 2-3, i.e. the rate of reaction is doubled or tripled when temperature increases by 10 ºC (Laidler *et al.*, 2003). However, the period of circadian clocks is temperature compensated, i.e. the Q_{10} for the period of the rhythm is close to 1 in a range of temperatures (reviewed in Rensing and Ruoff, 2002).

How exactly temperature affects the circadian clock is still unclear. In principle, two theories have been proposed for temperature compensation (reviewed in Ueda, 2007):

1. Temperature compensation of period may be achieved because clock component activity is unaffected by temperature (Pittendrigh, 1954).
2. Temperature affects the activity of more than one clock component such that the net effect is no change in period (Hastings and Sweeney, 1957; Ruoff, 1992; Ruoff *et al.*, 2007; Winfree, 1980).

Whilst some reaction rates are seemingly temperature-insensitive (Isojima *et al.*, 2009), temperature-dependent changes in the binding affinity, activity or conformation of the proteins involved has usually occurred (Kageyama *et al.*, 2006; Mehra *et al.*, 2009; Terauchi *et al.*, 2007). In cyanobacteria, the period of the clock is determined by the ATPase activity of KaiC (Terauchi *et al.*, 2007). ATPase activity of KaiC is independent of temperature (Murakami *et al.*, 2008). In *Drosophila*, temperature compensation may be achieved by the temperature-independent PER activity (Huang *et al.*, 1995). The competing of intermolecular (PAS-PAS) and intramolecular (PAS-C-domain) interaction of PER regulates the dimerisation of PER and results in the maintenance of dimmer PER concentration as temperature changes (Huang *et al.*, 1995). In *Arabidopsis*, the dynamic balance between *LATE ELONGATED HYPOCOTYL* (*LHY*) and *GIGANTEA* (*G1*) supports temperature compensation at high temperatures (17-27 ºC) (Gould *et al*., 2006). At low temperatures (at 12-17 ºC), *CIRCADIAN CLOCK ASSOCIATED1* (*CCA1*) replaces the dynamic balance with *LHY* (Gould *et al*., 2006). In addition, *PRR7* and *PRR9* are also involved in temperature compensation (Salome *et al*., 2010).

In *Neurospora*, there are several mutants found to be partially or totally temperature-compensation defective (Table 1). frq^{3}, frq^{7}, frq^{8} are long period *frq* mutants (Gardner and Feldman, 1981). frq^{7}, frq^{8} are temperature compensation deficient strains and frq^{3} is partially temperature compensation deficient above 25 ºC. frq^{9} and frq^{10} are null *frq* mutants. In $frq^{\triangle PEST\text{-}1}$, the PEST-1 domain is deleted in FRQ, which results in slower degradation of FRQ and a long period length. *period-6* is a short period mutant and is temperature sensitive below 21 ºC. Double mutation of *period-2* (*prd-2)* and *prd-6* lost the phenotype of temperature sensitivity in *period-6*, suggesting that temperature controls the interaction between these two genes or there is a physical interaction between their protein products (Morgan and Feldman, 1997). The *cel* mutant is a fatty acid synthesis mutant and temperature compensation is deficient in this strain. However, how are these genes are involved in temperature compensation is not known. In 2009, Mehra et al. suggested that casein kinase 2 (CK2) is the key regulator of temperature compensation of the *Neurospora* circadian clock (Mehra *et al*., 2009). Consequently, mutations of genes mentioned in this paragraph result in partial or complete deficiency of temperature compensation, suggesting that multiple genes are involved in the achievement of temperature compensation in *Neurospora*, including the central clock gene, the output genes of the clock and even genes involved in metabolism. Therefore, the mechanism of temperature compensation should be complex and it is necessary to investigate it by a more systemic approach, such as systems biology.

Table 1.1 *Neurospora* mutants with defective temperature compensation

frq gene mutants	frq^3, frq^7, frq^8, frq^9, frq^{10}, frq^{S513I}, $frq^{\triangle PEST\text{-}1}$
fatty acid synthesis mutant	*cel* (*chain elongation*)
Casein Kinase 2 (CK2) mutants	*chrono* (chr), *period-3* (*prd-3)*
Other mutants	*period-2* (*prd-2)*, *period-6* (*prd-6)*

1.3 Systems biology and quantitative modelling of oscillatory systems

1.3.1 Introduction

Conventional biological research usually focuses on understanding specific parts of biological reactions. In order to study the interactions between biological mechanisms, systems biology focuses on integrative research (Auffray *et al*., 2003; Oliver, 2006). Systems biology represents the complex interactions between biological molecules or relationships between substances and species. This may reveal a more complete view of a biological network (Bruggeman and Westerhoff, 2007; Kitano, 2002).

Quantitative modelling is one of the important strategies in systems biology. The goal of quantitative modelling is to precisely depict the concentration changes and the interactions among biological substances (Goldbeter, 1996; Goldbeter, 1997), or population relationships among species (Schuster *et al*., 1978). A comprehensive quantitative model should not only correctly depict the biological interactions, but can also be used to test assumptions/hypothesis and simulate their effect on the system in silico. This type of model can therefore be used for to make predictions and direct further research. However, the reliability of a quantitative model depends on the observed and experimental data used to create it, and on the current understanding of molecular mechanisms. Consequently, the combined use of quantitative models and experiments can result in faster and more productive research than either strategy alone.

In order to accurately demonstrate the interactions in a quantitative model, mathematical formulas are used to represent the biological mechanisms. Differential equations are widely used in research to represent chemical reactions, such as simulation of coupled chemical reactions (Gillespie, 1977). Different usages of equations or algorithms are appropriate to describe different mechanisms and relationships. For example, models for biological oscillations usually use differential formulas to describe the concentration change and interactions between molecules over time (Goodwin, 1963, 1965).

1.3.2 Modelling genetic regulation

Mathematical equations are widely used for constructing quantitative models of chemical or biological reactions. Theoretical models dealing with genetic regulation were created to easily understand the genetic regulatory interactions and the amount of change of biological molecules (Goldbeter, 1996; Winfree, 1980). The first quantitative model of genetic regulation was Goodwin's model (Goodwin, 1963). His model is based on the essential gene expression and regulatory components of a feedback loop and demonstrates these features by using differential equations. Figure 1.7 shows the scheme of this basic model. L_i is a genetic locus synthesising mRNA. X_i represents the quantity of mRNA. R stands for the cellular structure of the ribosome. Y_i is the quantity of the protein product, which is usually assumed to be an enzyme. The enzyme will translocate to a cellular locus C and undergo activation or catalyse another metabolic process. M_i is the metabolic species generated from this metabolic process. A fraction of M_i will become the repressor or co-repressor and affect the rate of mRNA synthesis.

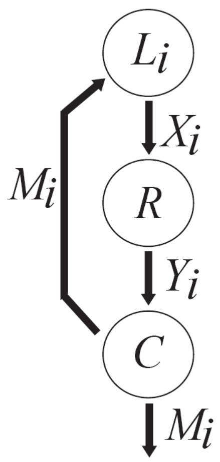

Figure 1.7 Goodwin's model of genetic regulation. Goodwin's model is a quantitative model of negative genetic feedback loop. L_i is a genetic locus synthesising mRNA X_i. R stands for the cellular structure of the ribosome. Y_i is the quantity of the protein product. Y_i will translocate to a cellular locus C. M_i is the metabolic species generated from this metabolic process. A fraction of M_i will become the repressor or co-repressor and affect the rate of mRNA synthesis. Figure taken from (Goodwin, 1963)

Two differential equations are used to examine the feedback regulation of this model. The two kinetic laws are:

$$\frac{dX_i}{dt} = \frac{a_i}{A_i + k_i Y_i} - b_i$$ (Concentration change of X_i mRNA) (1.1)

$$\frac{dY_i}{dt} = \alpha_i X_i - \beta_i$$ (Concentration change of Y_i protein) (1.2)

a_i is a constant related to mRNA synthesis. a_i/Ai is the rate of mRNA synthesis when there is no repressor. k_i is the Michaelis constant of this repression activity. The constant b_i is the rate of mRNA degradation. α_i represents the rate of protein production and the concentration of activated protein. β_i is the rate of protein degradation. After simulation, the concentration changes of the molecules over time can be plotted and the oscillations can be generated. Consequently, this makes it easier to understand the interactions between these clock components.

1.3.3 Modelling circadian clocks

Given the large number of components and processes involved in the circadian clockwork it becomes ever more difficult to interpret clock function and response to environmental factors by intuition and reasoning alone. A rigorous, quantitative model that embeds our knowledge of the circadian network should make it possible to test the consequences of experimental perturbations on the system, and reveal components and mechanisms underlying clock characteristics. Such a model would allow predictions to be made regarding the behaviour of the clockwork under a wide variety of conditions. Quantitative models of the *Neurospora* circadian clock have been built previously (Francois, 2005; Hong *et al*., 2008a; Leloup *et al*., 1999b; Ruoff *et al*., 1996; Ruoff and Rensing, 1996; Ruoff *et al*., 2005). Leloup's minimal *Neurospora* clock model concentrates on *frq* gene expression which is regulated by the concentration of FRQ protein using the Hill equation. The model was the first to successfully simulate both a period of 21.5 hours in constant darkness and entrainment of the oscillator to a 24 hour light-dark cycle. Ruoff *et al*. developed a model, based on a Goodwin-type oscillator, that introduces a switch mechanism to activate and repress *frq* transcription (Ruoff *et al*., 2005). Temperature-regulated degradation of wild type and mutant forms of FRQ was modelled by introducing the Arrhenius equation, resulting in the expected expression of *frq* mRNA and FRQ at 21°C and 28°C. This work and subsequent experiments have shown that wild type FRQ degradation is not significantly affected over this range of temperatures (Mehra *et al*., 2009). François' model considers an interaction between FRQ and *wc-1* RNA, and the inactivation of WCC through binding with FRQ homodimers (Francois, 2005). Subsequent modelling by Hong *et al*. has provided insight into the possible mechanism of FRQ action in the nucleus indicating that a one-to-one molar ratio of FRQ and WCC is not necessary for FRQ to repress WCC activity (Hong *et al*., 2008a).

As shown by the above examples, quantitative modelling has made valuable contributions to our understanding of the circadian clock mechanism in *Neurospora*. To date however, no model is able to describe the full range of observed clock phenotypes. Because the *Neurospora* circadian clockwork consists of several interlocking feedback loops, a comprehensive model is expected to shed light on circadian clock properties and mechanisms underlying its response to environmental factors, in particular temperature compensation.

1.3.4 Application of Goodwin's model into limit cycles

To focus on the characteristics of genetic feedback loops and to represent the continuous oscillatory behaviour, Goodwin modified his model to explain the repression of gene expression by the gene's protein product. Here are the equations of this model (Goodwin, 1965).

$$\frac{dX_1}{dt} = \frac{a_1}{A_1 + k_1 Z_1} - b_1 X_1 \quad \text{(Concentration change of } X_i \text{ mRNA) (1.3)}$$

$$\frac{dY_1}{dt} = \alpha_1 X_1 - \beta_1 Y_1 \quad \text{(Concentration change of } Y_i \text{ Enzyme) (1.4)}$$

$$\frac{dZ_1}{dt} = \gamma_1 Y_1 - \delta_1 Z_1 \quad \text{(Concentration change of } Z_i \text{ repressor) (1.5)}$$

This model was modified to consider the amount of degradation based on the molecules' concentration rather than constant degradation. X_1, Y_1 and Z_1 represent the concentration of mRNA, enzyme and repressor, respectively. The cooperativity (power) in Z_1 needs to be increased to 9 in order to get oscillations. It is assumed that the product of the X_1 gene is an enzyme that catalyses the formation of a repressor. The repressor negatively regulates the transcription of the X_1 gene. a_1 is a constant related to mRNA synthesis. a_1/A_1 is the rate of mRNA synthesis when there is no repressor. k_1 is the Michaelis constant (reviewed in Cornish-Bowden, 2004) of this repression process. α_1 represents the rate of protein production and the concentration of activated protein. γ_1 is the constant of repressor production. b_1, β_1 and δ_1 are the degradation constants of mRNA, enzyme and repressor, respectively.

This model reproduces three key features of the genetic feedback loop. The first feature is the diffusion delay of mRNA. This explains the time delay of the diffusion of mRNA from the nucleus to the cytoplasm. The second feature is the precursor concept of enzyme production. This concept depicts that the mechanism of protein synthesis becomes active after the translocation of mRNA to the cytosol. In addition, the precursor of the transcription factor is produced and becomes mature after a process of activation. The third feature is the metabolic sequence of gene expression regulation, which illustrates the whole regulation process of gene expression and the repression by its product.

1.3.5 Quantitative models of biological oscillations

To precisely study the molecular basis of biological time keeping, models representing biological oscillations have been created to describe the synthetic gene network of *lac* gene expression in *E. coli* (Stricker *et al*., 2008), the *Xenopus* embryonic cell cycle (Tsai *et al*., 2008), and circadian clocks in a numbers of different species (Tigges *et al*., 2009). In addition, these models are created to study the interaction between the positive and the negative arms of feedback loop, and the elements affecting the robustness and tenability of the oscillation (Gore and Oudenaarden, 2009). This report will concentrate on the modelling of the *Neurospora* circadian clock. Several models of *Neurospora* circadian clock have been published, such as Leloup *et al*. in 1999, Hong *et al*. in 2008 and François in 2005. These models will be described as follow.

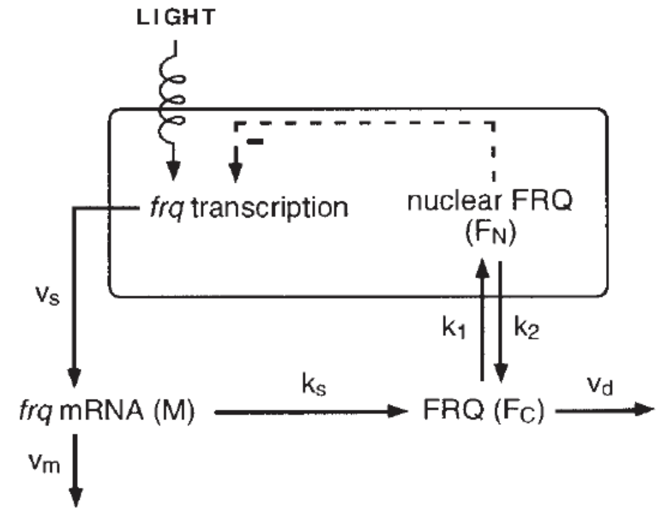

Figure 1.8 Leloup's model of *Neurospora* circadian clock.
In this model it is assumed that the transcription of frq mRNA is activated by light impulse. *frq* gene is negatively regulated by its own protein product. In this model, M, F_N and F_C represent *frq* mRNA, nuclear FRQ and cytosol FRQ, respectively. k_1, k_2, k_s, V_s, V_d and V_m are constants. Figure taken from (Leloup *et al.*, 1999b)

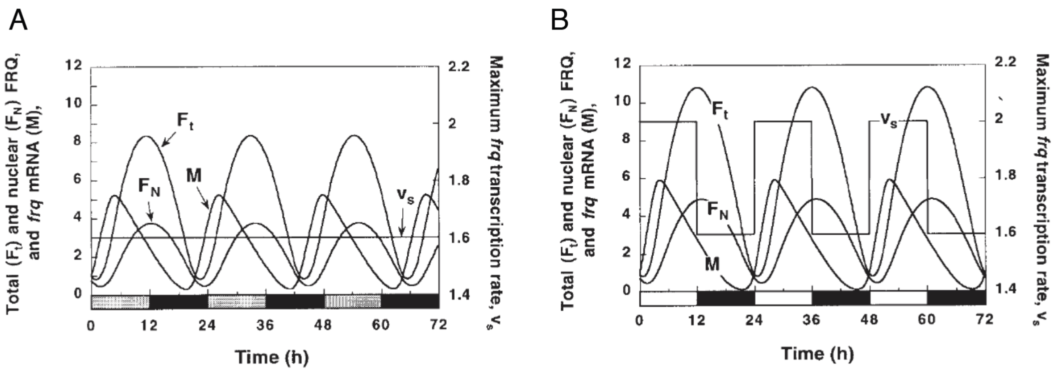

Figure 1.9 The simulated oscillations of Leloup's model.
(A) This figure shows the relative amount of *frq* mRNA, total FRQ (F_t) and nuclear FRQ (F_N) over time in continuous darkness. (B) This figure shows the relative amount of *frq* mRNA, total FRQ (F_t) and nuclear FRQ (F_N) over time entrainment by 12 h: 12 h light : dark cycle. V_S is the rate of *frq* transcription. Figure taken from (Leloup *et al.*, 1999b).

1.3.5.1 Leloup's model for the *Neurospora* circadian clock

In *Neurospora* a minimal quantitative model of the circadian clock has been reported by Leloup (Leloup *et al*., 1999a) (Figure 1.8). This model considers the translocation of FRQ protein into and out of the nucleus. When FRQ is produced, it is assumed to be shuttled into and out of the nucleus. FRQ in the nucleus will repress the transcription of its own gene. In addition, FRQ only degrades in the cytoplasm in this model. Leloup used a similar formula as in Goodwin's model to express the mechanism of repression. Leloup's model is a three-variable model containing three differential equations:

$$\frac{\mathrm{d}M}{\mathrm{d}t} = \mathrm{V_S}\frac{K_\mathrm{I}^\mathrm{n}}{K_\mathrm{I}^\mathrm{n} + F_N^n} - \mathrm{V_m}\frac{M}{K_m + M}$$

(Concentration change of *frq* mRNA) (1.6)

$$\frac{\mathrm{d}F_C}{\mathrm{d}t} = k_s M - \mathrm{V_d}\frac{F_C}{K_\mathrm{d} + F_C} - k_1 F_C + k_2 F_N$$

(Concentration change of cytoplasmic FRQ) (1.7)

$$\frac{\mathrm{d}F_N}{\mathrm{d}t} = k_1 F_C - k_2 F_N$$

(Concentration change of nuclear FRQ) (1.8)

In Leloup's work, the parameters of the model were adjusted to fit experimental observations. In these equations, M is the concentration of *frq* mRNA; F_C is the concentration of cytosolic FRQ; and F_N is the concentration of nuclear FRQ. Parameter V_S is the rate of *frq* transcription. Constant K_I is associated with the threshold of *frq* transcription repressed by F_N. n is the Hill coefficient and used for representing the degree of repression. V_m is the maximum rate of *frq* degradation and K_m is the Michaelis constant of this process. k_s is the rate constant of FRQ synthesis. V_d is the maximum rate of FRQ degradation and K_d is the Michaelis constant of this process. k_1 and k_2 are the rate constants related to the transport of FRQ into and out of the nucleus, respectively. The values of these parameters are shown in Appendix 1.

The simulated oscillation is shown in Figure 1.9. The concentration changes of the clock molecules and the period of this model successfully agree with experimental observations. However, this is a limited genetic feedback loop model of circadian clock in *Neurospora*. Therefore, models containing clock components and more parameters and equations for different processes need to be created to comprehensively explain the biological system.

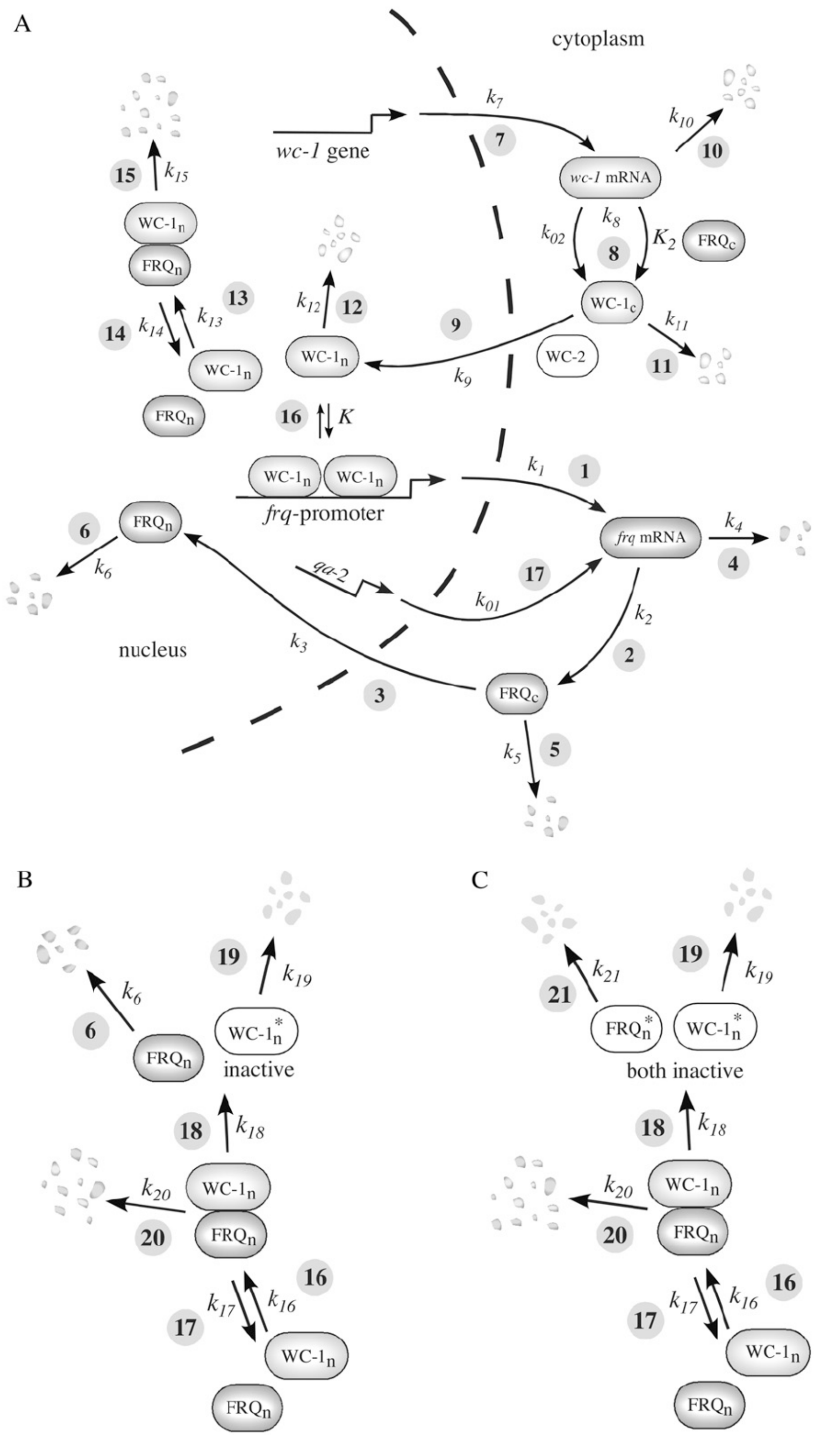

Figure 1.10 Hong's model of *Neurospora* circadian clock.
Figure (A) is the scheme of Hong's model. *frq* transcription can be negatively regulated by the binding of FRQ to WCC with a 1:1 stoichiometry (A). The other assumption of the inhibition mechanism of *frq* transcription is shown in (B), which is by a catalytic-like mechanism. Another hypothesis is shown in Figure (C). It is supposed that after the binding of FRQ_n and $WC\text{-}1_n$, both of them become inactive. Figure taken from (Hong *et al*., 2008a)

1.3.5.2 Hong's model for circadian clock in *Neurospora*

In 2008, Hong et al. developed a model to demonstrate the interaction between FREQUENCY (FRQ) protein and WHITE COLLAR-1 (WC-1) protein (Hong *et al.*, 2008b; Hong *et al.*, 2008c). This model is shown in Figure 1.10 (A).

The equations of this model are shown below. The values of the parameters are shown in Appendix 1.

$$\frac{d[\mathit{frq}\ \mathrm{mRNA}]}{dt} = k_1 \frac{[\mathrm{WC-1_n}]^2}{K+[\mathrm{WC-1_n}]^2} - k_4[\mathit{frq}\mathrm{mRNA}] + k_{01}$$

(Concentration change of *frq* mRNA) (1.9)

$$\frac{d[\mathrm{FRQ_c}]}{dt} = k_2[\mathit{frq}\ \mathrm{mRNA}] - (k_3+k_5)[\mathrm{FRQ_c}]$$

(Concentration change of cytoplasmic FRQ) (1.10)

$$\frac{d[\mathrm{FRQ_n}]}{dt} = k_3[\mathrm{FRQ_c}] + k_{14}[\mathrm{FRQ_n}:\mathrm{WC-1_n}] - [\mathrm{FRQ_n}](k_6 + k_{13}[\mathrm{WC-1_n}])$$

(Concentration change of nuclear FRQ) (1.11)

$$\frac{d[wc-1\mathrm{mRNA}]}{dt} = k_7 - k_{10}[wc-1\mathrm{mRNA}]$$

(Concentration change of *wc-1* mRNA) (1.12)

$$\frac{d[\mathrm{WC-1_c}]}{dt} = \frac{k_8[\mathrm{FRQ_c}][wc-1\mathrm{mRNA}]}{K_2+[\mathrm{FRQ_c}]} - (k_9+k_{11})[\mathrm{WC-1_c}] + k_{02}[wc-1\mathrm{mRNA}]$$

(Concentration change of cytoplasmic WC-1) (1.13)

$$\frac{d[\mathrm{WC-1_n}]}{dt} = k_9[\mathrm{WC-1_c}] - [\mathrm{WC-1_n}](k_{12}+k_{13}[\mathrm{FRQ}_n]) + k_{14}[\mathrm{FRQ}_n{:}\mathrm{WC-1_n}])$$

(Concentration change of nuclear WC-1) (1.14)

$$\frac{d[\mathrm{FRQ_n : WC-1_n}]}{dt} = k_{13}[\mathrm{FRQ_n}][\mathrm{WC-1_n}] - (k_{14} + k_{15})[\mathrm{FRQ}_n\mathrm{:WC-1_n}]$$

(Concentration change of the FRQ_n: WC-1_n complex) (1.15)

This model considers the transcription and translation of the *frequency (frq)* gene, and the translocation of FRQ into, but not out of the nucleus (steps 1~3). The degradation of *frq* mRNA, cytosolic FRQ (FRQ_c) and nuclear FRQ (FRQ_n) is also considered (steps 4~6). In addition, the expression of the *white collar-1 (wc-1)* gene and nuclear localisation of WC-1 are incorporated (steps 7~9). Degradation of *wc-1* mRNA, cytosolic WC-1 and nuclear WC-1 is also included in this model (steps 10~12). Nuclear WC-1 (WC-1_n) is used to represent the WHITE COLLAR complex (WCC) in this model. Step 16 represents the activation of *frq* transcription by the binding of WC-1_n at the promoter.

Three different hypotheses have been formulated based on this model. The first hypothesis is shown in Figure 1.10 (A) from step 13 to step 15. It is proposed that FRQ_n and WC-1_n form a complex with a 1:1 stoichiometry, and that this complex is degraded or inactivated in the nucleus. The second hypothesis is demonstrated in Figure 9 (B). It is assumed that the inactivation of WC-1_n by FRQ_n is a catalytic-like mechanism. WC-1_n is inactivated after binding to FRQ_n, but FRQ_n is still active. The third hypothesis is shown in Figure 1.10 (C). In this assumption, after the binding of FRQ_n and WC-1_n, both of them become inactive. After testing these hypotheses by computational methods, Hong et al. indicated that the process of removing the FRQ_n: WC-1_n complex is critical for generating the correct oscillations of FRQ and WC-1.

This model differs from previous models in a number of different ways. In this model, the concentration of WHITE COLLAR-2 (WC-2) is assumed as a constant. The genetic regulation of *frq* by WCC is depicted, as well as the interaction between FRQ and WCC in the nucleus. It also predicts three kinds of possibilities of how the WCC is inactivated. Furthermore, it represents that FRQ_c facilitates the accumulation of $WC\text{-}1_c$.

Figure 1.11 shows the simulated oscillation of this model. The interactions among these clock molecules are in agreement with experimental data. For example, the peak of total FRQ has a 7 hours delay after the peak of total WC-1. This represents that WC-1 positively regulates FRQ production. In addition, when the FRQ level ascends, the WC-1 level drops. This also indicates that FRQ negatively regulates the translation of WC-1.

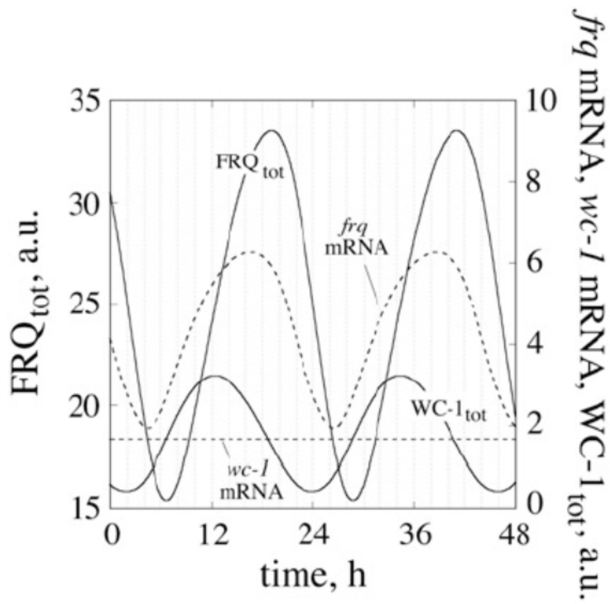

Figure 1.11 The simulated oscillations of Hong's model.
This figure shows the relative amount of *frq* and *wc-1* mRNA, total FRQ (including nuclear FRQ and cytosolic FRQ) and WC-1 over time. Figure taken from (Hong *et al.*, 2008a)

This model can also be used for modelling the period length of several *frq* mutants, such as *frq*[1], *fr*q[7] and *frq*[S513I], using different parameter values. In addition, the behaviour of quinic acid (QA) inducible system and ER24 mutant can also be modelled. (The ER24 mutant has a point mutation at the conserved position of WC-2, and therefore WC-2 has weaker binding affinity to the *frq* promoter.) In order to model the oscillation when *frq* mRNA is overexpressed by using a quinic acid inducible system, k_{01} is adjusted to test the model. It is observed that the period slightly changes when increasing the value of k_{01}. Nevertheless, if k_{01} is too large, the oscillations will stop. Furthermore, the form of equation (1.13) is changed for modelling the relationship between *frq* mRNA and WC-1 production (1.16), and the effects of *wc-1* mRNA overexpression (1.17). Furthermore, after introducing temperature compensation into the model, Hong et al. suggests that the binding of WC-1 to the *frq* promoter plays an important role in the temperature compensated *Neurospora* circadian system.

$$\frac{d[\mathrm{WC-1_c}]}{dt} = k_8[wc-1\ \mathrm{mRNA}] - (k_9 + k_{11})[\mathrm{WC-1_c}] + k_{02}[wc-1\ \mathrm{mRNA}]$$

(Concentration change of cytoplasmic WC-1) (1.16)

$$\frac{d[\mathrm{WC-1_c}]}{dt} = \frac{k_8[\mathrm{FRQ_c}]}{K_2 + [\mathrm{FRQ_c}]} \times \frac{[wc-1\ \mathrm{mRNA}]}{K_3 + [wc-1\ \mathrm{mRNA}]} - (k_9 + k_{11})[\mathrm{WC-1_c}] + k_{02}[wc-1\ \mathrm{mRNA}]$$

(Concentration change of cytoplasmic WC-1) (1.17)

1.3.5.3 François' model of circadian clock in *Neurospora*

There are two main characteristics in François' model. Firstly, this model does not consider different concentrations in the nucleus and cytoplasm. Secondly, WC-2 is assumed to quickly combine with WC-1 and become part of the WCC. There are three models presented in François' work (Francois, 2005). The one-loop model explains the basic oscillatory behaviour in *Neurospora*. The two othermodels, the first two-loop model and the second two-loop model, are extension of the one-loop model and demonstrate the enhancement of *wc-1* mRNA production by FRQ. These models are described in this section.

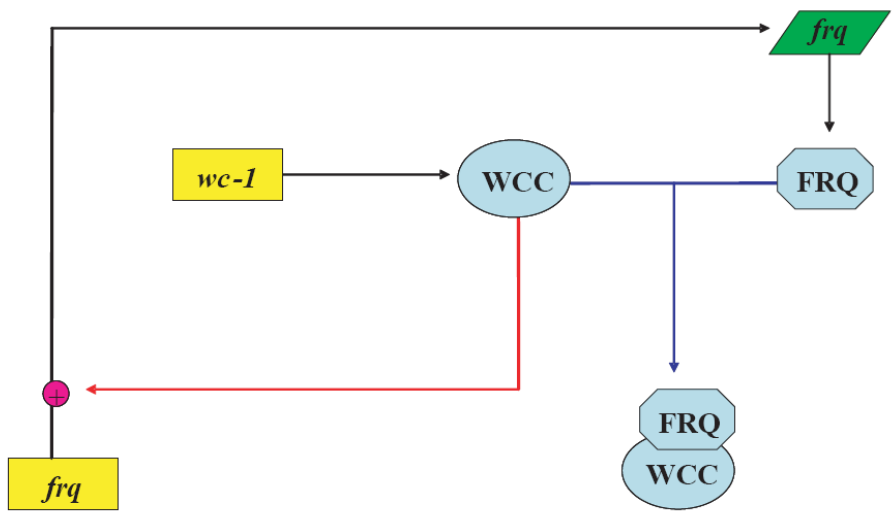

Figure 1.12 François' one loop-model of circadian clock in *Neurospora*.
François' one-loop model assumes that FRQ protein can bind to WHITE-COLLAR complex (WCC) and inhibit its own transcription.

(1) The one-loop model

The scheme of the one-loop model is shown in Figure 1.12. The concept of this model is to present the negative regulation of FRQ protein expression. FRQ protein is assumed to bind with WCC and inhibit WCC binding to the *frq* promoter.

The equations of this model are shown below. The values of the parameters are shown in Appendix 1.

$$\frac{d[frq]}{dt} = \theta[frq\text{:WCC}] - \alpha[frq][\text{WCC}]$$

(Concentration change of *frq* gene) (1.18)

$$\frac{d[\text{RNA}]}{dt} = \rho_{\text{FRQ}}[frq\text{:WCC}] - \delta_{\text{RNA}}[\text{RNA}]$$

(Concentration change of *frq* mRNA) (1.19)

$$\frac{d[\text{FRQ}]}{dt} = \beta[\text{RNA}] - \gamma[\text{FRQ}][\text{WCC}] - \delta_{\text{FRQ}}[\text{FRQ}]$$

(Concentration change of FRQ) (1.20)

$$\frac{d[\text{WCC}]}{dt} = \rho_{\text{WCC}} - \gamma[\text{FRQ}][\text{WCC}] + \theta[frq\text{:WCC}] - \alpha[frq][\text{WCC}] - \delta_{\text{WCC}}[\text{WCC}]$$

(Concentration change of WCC) (1.21)

$$\frac{d[T]}{dt} = \gamma[\text{FRQ}][\text{WCC}] - \delta_T[T]$$

(Concentration change of the multimer *T*: FRQ + WCC) (1.22)

Equation 1.18 and 1.19 model the mechanism of transcription factor binding at the promoter and the activation of transcription. [*frq*], [RNA] and [WCC] are the concentrations of *frq* gene, mRNA and WCC, respectively. [*frq*: WCC] represents the fraction of WCC binding at the *frq* promoter. θ is the releasing rate of WCC proteins from the *frq* gene. In contrast, α is the binding rate of WCC proteins to the *frq* gene. ϱ_{FRQ} and δ_{RNA} is the rate of *frq* transcription and *frq* mRNA degradation, respectively.

Equations 1.20-1.22 explain the interactions among FRQ, WCC and the *frq* promoter. WCC can either bind to FRQ or to the *frq* promoter. Only free WCC can bind to the *frq* promoter and activate transcription. [FRQ], [WCC] and [T] are the concentrations of FRQ protein, WCC complex and FRQ-WCC complex. β is the FRQ translation rate. ϱ_{WCC} is the WCC production rate. γ is the multimer T (FRQ and WCC proteins) formation rate. δ_{FRQ}, δ_{WCC} and δ_{T} are the degradation rates of FRQ, WCC and the multimer T, respectively.

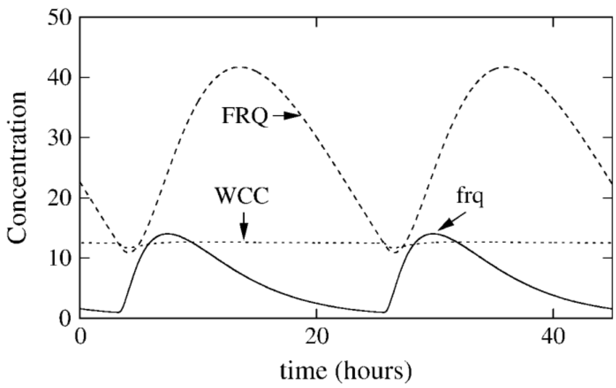

Figure 1.13 The simulated oscillations of François' one loop-model model.
The concentration of FRQ (dashed line), WCC (solid line) and *frq* mRNA (dotted line) over time is plotted in this graph. Figure taken from (Francois, 2005)

Figure 1.13 shows the simulated oscillation of this model. The results show agreement with experimental results. For example, the peak of FRQ has a delay of about 6 hours after the peak of *frq* mRNA. Also, *frq* mRNA requires 18 hours to degrade, which is in agreement with the half-life of *frq* mRNA detected from experiments.

(2) The first two-loop model

The scheme of the first two-loop model is shown in Figure 13. In this model, it is assumed that the *wc-1* transcription is enhanced by FRQ in this model. When FRQ binds to *wc-1* mRNA, the normal form of *wc-1* mRNA will becomes the enhanced form, and WC-1 will be produced with a delay τ after the interaction between WC-1 and FRQ.

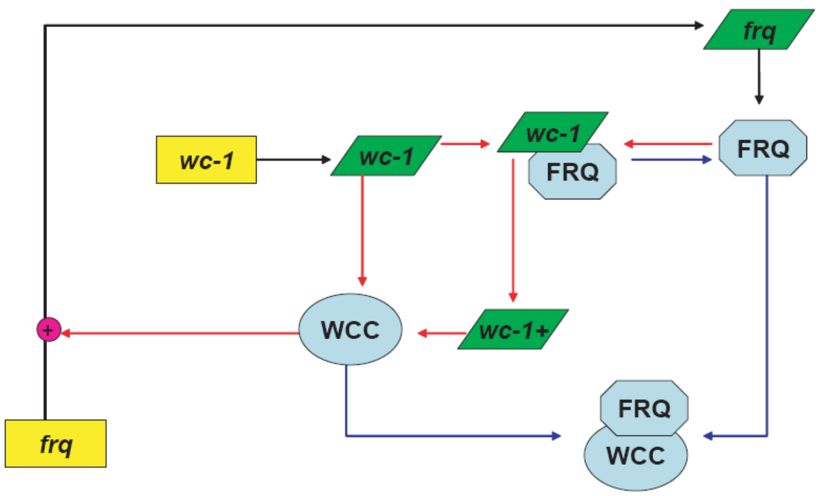

Figure 1.14 François' first two-loop model of circadian clock in *Neurospora*. François' first two-model assumes that FRQ is not only a repressor, which inhibits its own transcription, but also an activator, which enhances *wc-1* transcription. After interacting with FRQ, wc-1+ is the enhanced form of *wc-1* mRNA and is more efficient for protein synthesis. WC-1 will be produced with a delay τ after the interaction between WC-1 and FRQ. Figure redrew from (Francois, 2005).

The equations used in this model are shown below. The values of the parameters are shown in Appendix 1.

$$\frac{d[frq]}{dt} = \theta[frq\text{:WCC}] - \alpha[frq][\text{WCC}]$$

(Concentration change of *frq* gene) (1.23)

$$\frac{d[\text{RNA}]}{dt} = \rho_{\text{FRQ}}[frq\text{:WCC}] - \delta_{\text{RNA}}[\text{RNA}]$$

(Concentration change of *frq* mRNA) (1.24)

$$\frac{d[T]}{dt} = \gamma[\text{FRQ}][\text{WCC}] - \delta_T[T]$$

(Concentration change of the multimer *T*: FRQ + WCC) (1.25)

$$\frac{d[\text{RNA}_\text{W}]}{dt} = \rho_{\text{WCC}} - \delta_{\text{RNA}_\text{W}}[\text{RNA}_\text{W}] - \nu[\text{RNA}_\text{W}][\text{FRQ}] + \mu[\text{RNA}_{\text{W+}}]$$

(Concentration change of *wc-1* mRNA) (1.26)

$$\frac{d[\text{RNA}_{\text{W+}}]}{dt} = \nu[\text{RNA}_\text{W}][\text{FRQ}] - (\delta_{\text{RNA}_\text{W}} + \mu)[\text{RNA}_{\text{W+}}]$$

(Concentration change of enhanced *wc-1* mRNA) (1.27)

$$\frac{d[\text{FRQ}]}{dt} = \beta[\text{RNA}] - \gamma[\text{FRQ}][\text{WCC}] - \delta_{\text{FRQ}}[\text{FRQ}] - \nu[\text{RNA}_\text{W}][\text{FRQ}] + \mu[\text{RNA}_{\text{W+}}]$$

(Concentration change of FRQ) (1.28)

$$\frac{d[\text{WCC}]}{dt} = \beta_{\_}[\text{RNA}_\text{W}] + \beta_{+}[\text{RNA}_{\text{W+}}]_\tau - \gamma[\text{FRQ}][\text{WCC}] + \theta[frq\text{:WCC}] - \alpha[frq][\text{WCC}] - \delta_{\text{WCC}}[\text{WCC}]$$

(Concentration change of WCC) (1.29)

[*frq*], [RNA] and [WCC] are the concentrations of *frq* gene, mRNA and WCC, respectively. [*frq*: WCC] represents the fraction of WCC binding at the *frq* promoter. θ is the releasing rate of WCC proteins from the *frq* gene. In contrast, α is the binding rate of WCC proteins to the frq gene. [FRQ], [WCC] and [*T*] are the concentrations of FRQ protein, WCC complex and FRQ-WCC complex, respectively. γ is the multimer *T* (FRQ and WCC proteins) formation rate. δ_{FRQ}, δ_{RNA}, δ_{WCC} and δ_T are the degradation rates of FRQ, *frq* mRNA, WCC and the multimer *T*, respectively. In equations 1.26-1.29, [RNA_w] and [RNA_{w+}] are the concentrations of the normal form and the enhanced form of *wc-1* mRNA, respectively. δ_{RNAw} is the *wc-1* mRNA degradation rate. ϱ_{WCC} is the wc-1 transcription rate. ν is the second-order complex formation rate of normal *wc-1* mRNA and FRQ. In contrast, μ is the dissociation rate of the FRQ: *wc-1* mRNA complex. β_- and β_+ are the wc-1 translation rate of the normal form and the enhanced form of of *wc-1* mRNA. Figure 1.15 shows the simulated oscillation of this model.

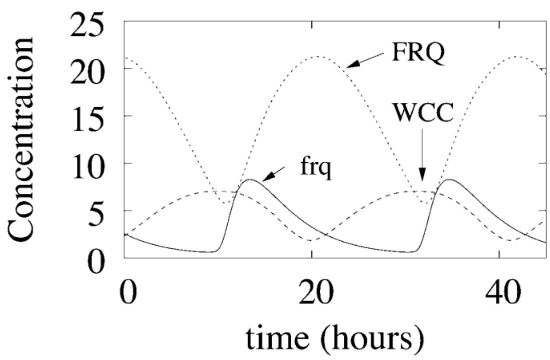

Figure 1.15 The simulated oscillations of François' first two-loop model. The concentration of WCC (dashed line), *frq* mRNA (solid line) and FRQ (dotted line) over time is plotted in this graph. Figure taken from (Francois, 2005)

(3) The second-loop model

The scheme of the second two-loop model is shown in Figure 1.16. In this model, it is supposed that the translation of *wc-1* is not delayed after the formation of the FRQ:

wc-1 mRNA complex. In addition, it is assumed that when FRQ interacts with the FRQ:*wc-1* mRNA complex and becomes a FRQ dimer, the translation of *wc-1* will be inhibited.

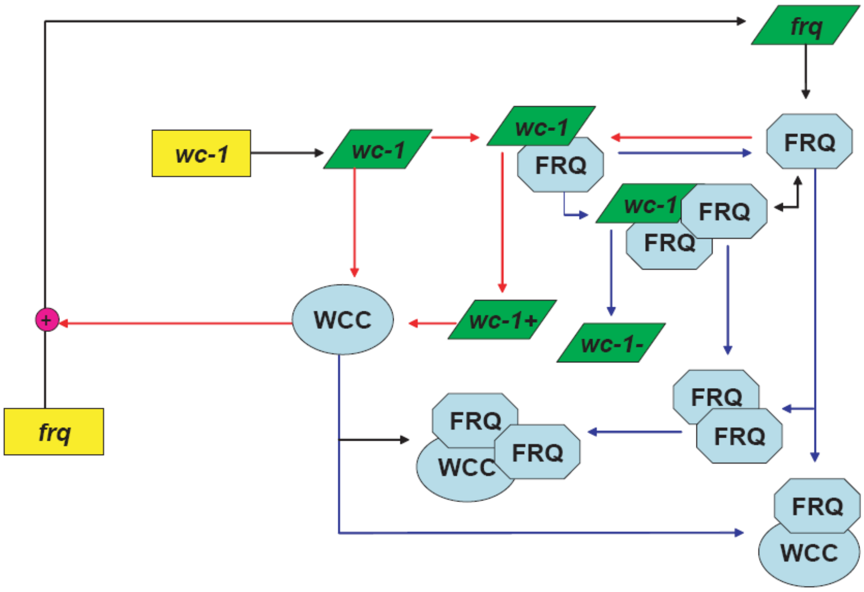

Figure 1.16 François' second two-loop model of circadian clock in *Neurospora*. François' second two-model assumes that FRQ is not only a repressor, which inhibits its own transcription, but also an activator, which enhances *wc-1* transcription. After interacting with FRQ, wc-1+ is the enhanced form of *wc-1* mRNA and is more efficient for protein synthesis. In addition, wc-1- is the negative form, which is produced when *wc-1* mRNA interact with the FRQ dimmer. The translation of *wc-1* is no delay after the formation of the FRQ: *wc-1* mRNA complex. Figure redrew from (Francois, 2005).

The equations used in this model are shown here. The values of the parameters are shown in Appendix 1.

$$\frac{d[frq]}{dt} = \theta[frq\text{:WCC}] - \alpha[frq][\text{WCC}]$$

(Concentration change of *frq* gene) (1.30)

$$\frac{d[\mathrm{RNA}]}{dt} = \rho_{\mathrm{FRQ}}[frq\mathrm{:WCC}] - \delta_{\mathrm{RNA}}[\mathrm{RNA}]$$

(Concentration change of *frq* mRNA) (1.31)

$$\frac{d[T]}{dt} = \gamma[\mathrm{FRQ}][\mathrm{WCC}] - \delta_T[T]$$

(Concentration change of the multimer *T*: FRQ + WCC) (1.32)

$$\frac{d[\mathrm{RNA_W}]}{dt} = \rho_{\mathrm{WCC}} - \delta_{\mathrm{RNA_W}}[\mathrm{RNA_W}] - \nu[\mathrm{RNA_W}][\mathrm{FRQ}] + \mu[\mathrm{RNA_{W+}}]$$

(Concentration change of *wc-1* mRNA) (1.33)

$$\frac{d[\mathrm{RNA_{W+}}]}{dt} = \nu[\mathrm{RNA_W}][\mathrm{FRQ}] - (\delta_{\mathrm{RNA_W}} + \mu)[\mathrm{RNA_{W+}}] - \eta[\mathrm{RNA_{W+}}][\mathrm{FRQ}] + \kappa[\mathrm{RNA_{W-}}]$$

(Concentration change of enhanced *wc-1* mRNA) (1.34)

$$\frac{d[\mathrm{RNA_{W-}}]}{dt} = \eta[\mathrm{RNA_{W+}}][\mathrm{FRQ}] - (\delta_{\mathrm{RNA_W}} + \kappa)[\mathrm{RNA_{W-}}]$$

(Concentration change of negative form *wc-1* mRNA) (1.35)

$$\frac{d[\mathrm{FRQ}]}{dt} = \beta[\mathrm{RNA}] - \delta_{\mathrm{FRQ}}[\mathrm{FRQ}] - \nu[\mathrm{RNA_W}][\mathrm{FRQ}] + \mu[\mathrm{RNA_{W+}}] - \eta[\mathrm{RNA_{W+}}][\mathrm{FRQ}] + \kappa[\mathrm{RNA_{W-}}] - 2\eta[\mathrm{FRQ}]^2 + 2\kappa[\mathrm{FRQ_2}]$$

(Concentration change of FRQ) (1.36)

$$\frac{d[\mathrm{FRQ_2}]}{dt} = \eta[\mathrm{FRQ}]^2 - \kappa[\mathrm{FRQ_2}] - \gamma[\mathrm{FRQ_2}][\mathrm{WCC}] - \delta_{\mathrm{FRQ}}[\mathrm{FRQ_2}]$$

(Concentration change of FRQ dimmer) (1.37)

$$\frac{d[\mathrm{WCC}]}{dt} = \beta_{-}[\mathrm{RNA_W}] + \beta_{+}[\mathrm{RNA_{W+}}] - \gamma[\mathrm{FRQ_2}][\mathrm{WCC}] + \theta[frq\mathrm{:WCC}] - \alpha[frq][\mathrm{WCC}] - \delta_{\mathrm{WCC}}[\mathrm{WCC}]$$

(Concentration change of WCC) (1.38)

$$\frac{d[\mathrm{FRQ_2:WCC}]}{dt} = \gamma[\mathrm{FRQ_2}][\mathrm{WCC}] - \delta_{\mathrm{T}}[\mathrm{FRQ_2:WCC}]$$

(Concentration change of the FRQ_2: WCC complex) (1.39)

[*frq*], [RNA] and [WCC] are the concentrations of *frq* gene, mRNA and WCC, respectively. [*frq*: WCC] represents the fraction of WCC binding at the *frq* promoter. θ is the releasing rate of WCC proteins from the *frq* gene. In contrast, α is the binding rate of WCC proteins to the *frq* gene. [FRQ], [WCC] and [T] are the concentrations of FRQ protein, WCC complex and FRQ-WCC complex, respectively. γ is the multimer T (FRQ and WCC proteins) formation rate. δ_{FRQ}, δ_{RNA}, δ_{WCC} and δ_{T} are the degradation rates of FRQ, *frq* mRNA, WCC and the multimer T, respectively. [RNA_w] and [RNA_{w+}] are the concentrations of the normal form and the enhanced form of *wc-1* mRNA, respectively.δ_{RNAw} is the *wc-1* mRNA degradation rate. ϱ_{WCC} is the wc-1 transcription rate. ν is the second-order complex formation rate of normal *wc-1* mRNA and FRQ. In contrast, μ is the dissociation rate of the FRQ: *wc-1* mRNA complex. β_- and β_+ are the wc-1 translation rate of the normal form and the enhanced form of of *wc-1* mRNA. In Equations 1.33-1.39, FRQ_2 stands for the dimerised FRQ. η is the second-order rate of FRQ homodimerisation. On the contrary, $\varkappa$ is the dissociating rate of the FRQ_2. There are three kinds of *wc-1* mRNA in this model. RNA_W is the normal form. RNA_{W+} is the enhanced form. RNA_{W-} is the negative form, which is produced when RNA_W interact with the FRQ dimmer. [RNA_{w-}] is the concentration of negative *wc-1* mRNA. Figure 1.17 shows the simulated oscillation of this model.

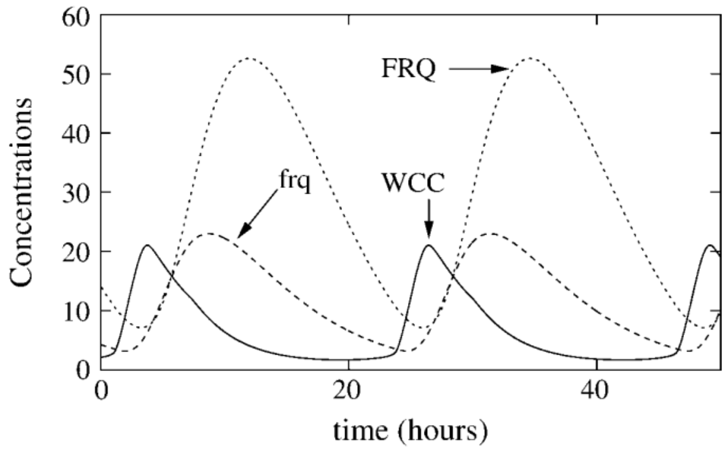

Figure 1.17 The simulated oscillations of François' first two-loop model.
The concentration of WCC (solid line), *frq* mRNA (dashed line) and FRQ (dotted line) over time is plotted in this graph. Figure taken from (Francois, 2005)

1.3.6 Temperature and biological time keeping

Temperature influences most chemical reactions. According to *Van't Hoff's rule*, the speed of a reaction increases when the temperature is increased. This law can be described as equation 1.40. Q_{10} is the ratio of reaction rate v at temperature T+10ºC to T. For general reactions, Q_{10} is usually between 2-3, suggesting that the reaction rate at least doubles when temperature is increased by 10 ºC (Laidler *et al.*, 2003). However, in organisms, the timing of biological processes is almost constant in a range of temperatures. The period of circadian clocks is a general example of a process that is temperature compensated (Pittendrigh and Caldarola, 1973). It is still unclear how organisms keep constant rhythms when exposed to temperature change. In 2007, Ruoff et al. described how temperature compensation works in a global kinetic network (Ruoff *et al.*, 2007). The idea of a global system is to consider all genetic and metabolic reactions in the system. Temperature compensation for oscillatory systems can possibly happen in a range of temperatures if equation 1.41 is satisfied (Ruoff, 1994). n is the number of positive feedback reactions and m is the number of negative feedback reactions. Temperature compensation is achieved when the reactions that increase or decrease the period are antagonistically balanced.

$$Q_{10} = \frac{v(T + 10^{\circ}\mathrm{C})}{v(T)}$$

(*Van't Hoff's rule*) (1.40)

$$\frac{\partial P}{\partial T} = \frac{1}{RT^2} \sum_{i=1}^{m+n} a_i E_i = 0$$

(Temperature compensated global kinetic network for oscillatory systems) (1.41)

$$k_i = A_i e^{-\frac{E_a^{k_i}}{RT}}$$

(The *Arrhenius* equation) (1.42)

k_i is the rate constant of reaction i. It varies depending on the absolute temperature T. The value of k_i is derived using the Arrhenius equation (equation 1.42). A_i is the collision factor or pre-exponential factor, which is a constant. R is the gas constant. T is the Kelvin temperature. Reversible reactions are separated into two reactions. N is the number of total elementary reactions. $E_a^{k_i}$ are activation enthalpies. $*C_i^{J_j}$ is the global control coefficient (Cornish-Bowden, 2004). However, because the activation energies $E_a^{k_i}$ are positive, the sum of the global control coefficients needs to be zero according to equation 1.41. Therefore, some of the global control coefficients should be negative. This suggested that negative control coefficients must be present in a temperature compensated system to oppose the positive contributions (Ruoff *et al.*, 2007). The negative control coefficients may be generated by genetic regulation, signal transduction, or the conformational change of functional proteins.

1.3.7 Modelling temperature compensation

In 1957, Hastings and Sweeney proposed that temperature compensation of the circadian clock period (temperature independence) is achieved by means of a compensation mechanism (Hastings and Sweeney, 1957). Ruoff illustrated this idea by introducing temperature compensation into the Brusselator model (Ruoff, 1992). The Brusselator model consists of four irreversible reactions.

$$\begin{aligned}&\mathrm{A}\xrightarrow{k_1}\mathrm{X}\\&\mathrm{2X+Y}\xrightarrow{k_2}\mathrm{3X}\\&\mathrm{B+X}\xrightarrow{k_3}\mathrm{Y+D}\\&\mathrm{X}\xrightarrow{k_4}\mathrm{E}\end{aligned}\qquad \text{(the Brusselator model)(1.43)}$$

X and Y are kinetic variables. The concentrations of A, B, D, E are constant in this model. These reactions can be rewritten into two differential equations.

$$\begin{aligned}&\frac{\mathrm{d[X]}}{\mathrm{dt}}=k_1[\mathrm{A}]+k_2[\mathrm{X}]^2[\mathrm{Y}]-k_3[\mathrm{B}][\mathrm{X}]-k_4[\mathrm{X}]\\&\frac{\mathrm{d[Y]}}{\mathrm{dt}}=-k_2[\mathrm{X}]^2[\mathrm{Y}]+k_3[\mathrm{B}][\mathrm{X}]\end{aligned}\qquad \text{(the Brusselator ODE model)(1.44)}$$

The relationship between period and parameters can be expressed as the following equation.

$$p=\tau_0 k_1^{a_1}k_2^{a_2}k_3^{a_3}k_4^{a_4}\qquad \text{(the relationship between period and parameters)(1.45)}$$

P is the period length of this system. τ_0 and α_i are constants. As reaction 1 and 2 are positive feedback reactions and reaction 3 and 4 are negative feedback reactions, the value of α_1 and α_2 are negative, and α_3 and α_4 are positive. To achieve temperature compensation, the following equations need to be fulfilled.

$$\frac{\partial P}{\partial T} \approx 0 \qquad \text{(period is independent of temperature change)(1.46)}$$

If we introduce the Arrhenius equation into this model, the following equation is generated.

$$\sum_i \alpha_i E_i \approx 0 \qquad \text{(temperature compensated Brusselator model)(1.47)}$$

Therefore, positive and negative feedback reactions are "opposing reactions". Different combinations of rate constant values that fulfil the above summation theorem can therefore lead to temperature compensation.

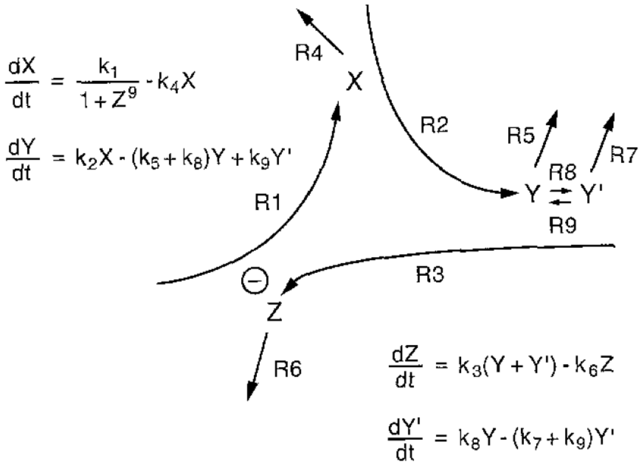

Figure 1.18 Goodwin's model for circadian clocks
X, *Y* and *Z* represent mRNA, the clock protein and the transcriptional inhibitor, respectively. Y' is a specific conformational status of the clock protein used in the *Drosophila* model. R1 is the process of transcription and repression by *Z*. R2 is the process of translation. R3 is the process of repressor activation by *Y*. R4, R5 and R6 are degradation processes of *X* mRNA, protein *Y* and repressor *Z*, respectively. Figure taken from (Ruoff *et al.*, 1996)

1.3.8 Application of Goodwin's model for temperature compensation

To model the phenomenon of temperature compensation, Ruoff considered previous models of circadian clocks (Drescher, et al., 1982; Goodwin, 1963; Goodwin, 1965; Rensing and Schill, 1985; Rensing and Schill, 1987) and modified Goodwin's model to demonstrate the possible underlying mechanism of temperature compensation (Ruoff *et al.*, 1996). The scheme of this model is shown in Figure 1.18. Temperature effects are introduced in the model by the Arrhenius equation. *Neurospora* and *Drosophila* clock properties can be reproduced in this model, including temperature compensation, phase response curves by temperature pulse and entrainment by temperature cycles (Ruoff and Rensing, 1996). In addition, period mutants such as *Neurospora frq* and *Drosophila per* mutants are accurately simulated with this model. Temperature-dependent RNA and protein degradation rates are predicted to be the main factors controlling period length of the clock and temperature compensation (Ruoff *et al*., 1996).

Ruoff further modelled the clock behaviour of the long period mutant frq^7. However, from experimental data, the peak level of frq^7 RNA is doubled compared to wild-type *frq* RNA, which could not be reproduced in the Goodwin oscillator (Ruoff *et al*., 1999). Therefore, they proposed a threshold mechanism of transcription inhibition (Ruoff *et al*., 1999). In 2005, to reproduce the rapid increase and decrease of *frq* RNA oscillation behaviour, Ruoff again proposed a threshold of *frq* transcription inhibition and a threshold for reactivating *frq* transcription (Ruoff *et al*., 2005). The scheme of this model is shown in Figure 18. His model contains three differential equations to examine feedback regulation. The three kinetic equations are:

$$\frac{\mathrm{d}X}{\mathrm{d}t} = \frac{k_1}{Z^9 + 1} - k_4 X \qquad \text{(Concentration change of } X \text{ mRNA) (1.48)}$$

$$\frac{\mathrm{d}Y}{\mathrm{d}t} = k_2 X - k_5 Y \qquad \text{(Concentration change of protein } Y\text{) (1.49)}$$

$$\frac{\mathrm{d}Z}{\mathrm{d}t} = k_3 Y - k_6 Z \qquad \text{(Concentration change of repressor } Z\text{) (1.50)}$$

X is the concentration of *X* mRNA. *Y* is the concentration of the protein which expressed by the *X* mRNA. *Z* is the concentration of the *X* mRNA repressor that inhibits the synthesis of *X* mRNA. Protein Y catalyses the formation of a repressor Z so negatively regulates the expression of its own gene. k_1-k_6 are constants. k_1 is related to the repression of mRNA transcription. k_2 is associated with the rate of Y protein synthesis. k_3 is the constant related to the formation rate of the repressor. k_4-k_6 are degradation constants.

The effect of temperature is introduced into this model by the Arrhenius equation.

$$k_i = A_i e^{-\frac{E_i}{RT}} \qquad \text{(The Arrhenius equation) (1.51)}$$

For each reaction Ri, the temperature influences the value of each constant k_i. A_i is the collision factor or pre-exponential factor, which is a constant. E_i is the activation energy. A_i and E_i are independent to temperature. R is the gas constant. T is the Kelvin temperature. Therefore, rate constants vary when the temperature changes in the model. This model successfully simulates the qualitative oscillation, and represents dynamic features of temperature-entrainment and phase resetting, which agree with experimental observations.

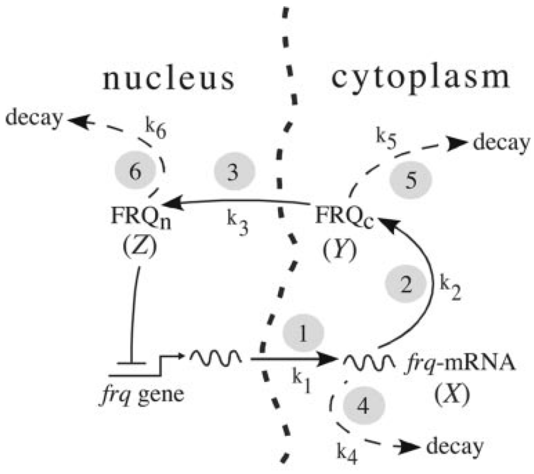

Figure 1.19 Ruoff's Temperature compensated *Neurospora* circadian clock model.
X, Y and Z stand for the *frq* mRNA, cytosolic FRQ (FRQ_c) and nuclear FRQ (FRQ_n), respectively. k_1 and k_2 are the production rate of *frq* mRNA and FRQ protein. k_3 is the rate of FRQ nuclear localisation. k_4, k_5 and k_6 are degradation constants of *frq* mRNA, FRQ_c and FRQ_n, respectively. Figure taken from (Ruoff et al., 2005).

1.3.9 Temperature compensated *Neurospora* circadian clock model

In 2005, Ruoff et al. modified the temperature compensated Goodwin's model oscillator and developed a temperature compensated model for the *Neurospora* circadian clock. The scheme of this model is shown in Figure 1.19. This model considers the concentration of FRQ protein in the nucleus and in the cytoplasm separately. Below are the equations used in this model.

$$\frac{dX}{dt} = k_1 f_{inhib} - k_4 X \quad \text{(Concentration change of } frq \text{ mRNA) (1.52)}$$

$$\frac{dY}{dt} = k_2 X - (k_3 + k_5) Y \quad \text{(Concentration change of cytosolic FRQ) (1.53)}$$

$$\frac{dZ}{dt} = k_3 Y - k_6 Z \quad \text{(Concentration change of nuclear FRQ) (1.54)}$$

X, Y and Z stand for the *frq* mRNA, cytosolic FRQ (FRQ_c) and nuclear FRQ (FRQ_n), respectively. k_1 and k_2 are the production rate of *frq* mRNA and FRQ protein. k_3 is the rate of FRQ nuclear localisation. k_4, k_5 and k_6 are degradation constants of *frq* mRNA, FRQ_c and FRQ_n, respectively.

The effect of temperature is introduced into this model using the Arrhenius equation. The activation energy of FRQ degradation is calculated by equation 1.55 and the FRQ degradation rate constant is estimated from experimental data (Ruoff et al., 2005).

$$E_a = \frac{R \times \ln\left(\frac{k_i^{25℃}}{k_i^{20℃}}\right)}{\frac{1}{293K} - \frac{1}{298K}} \qquad \text{(Activation energy of reaction Ri) (1.55)}$$

The simulated oscillation is shown in Figure 1.20. The simulated oscillations in Figure 1.20 c and d are compared to experimental observations plotted from Liu et al. (Liu *et al.*, 1998) in Figure 21 a and b. The amplitude behaviour agrees with the experimental data. This model describes the dynamic behaviour when temperature changes and explains the relationship between the stability of the FRQ protein and temperature compensation. This model could also be used to represent the positive and negative control energies in the temperature compensation system.

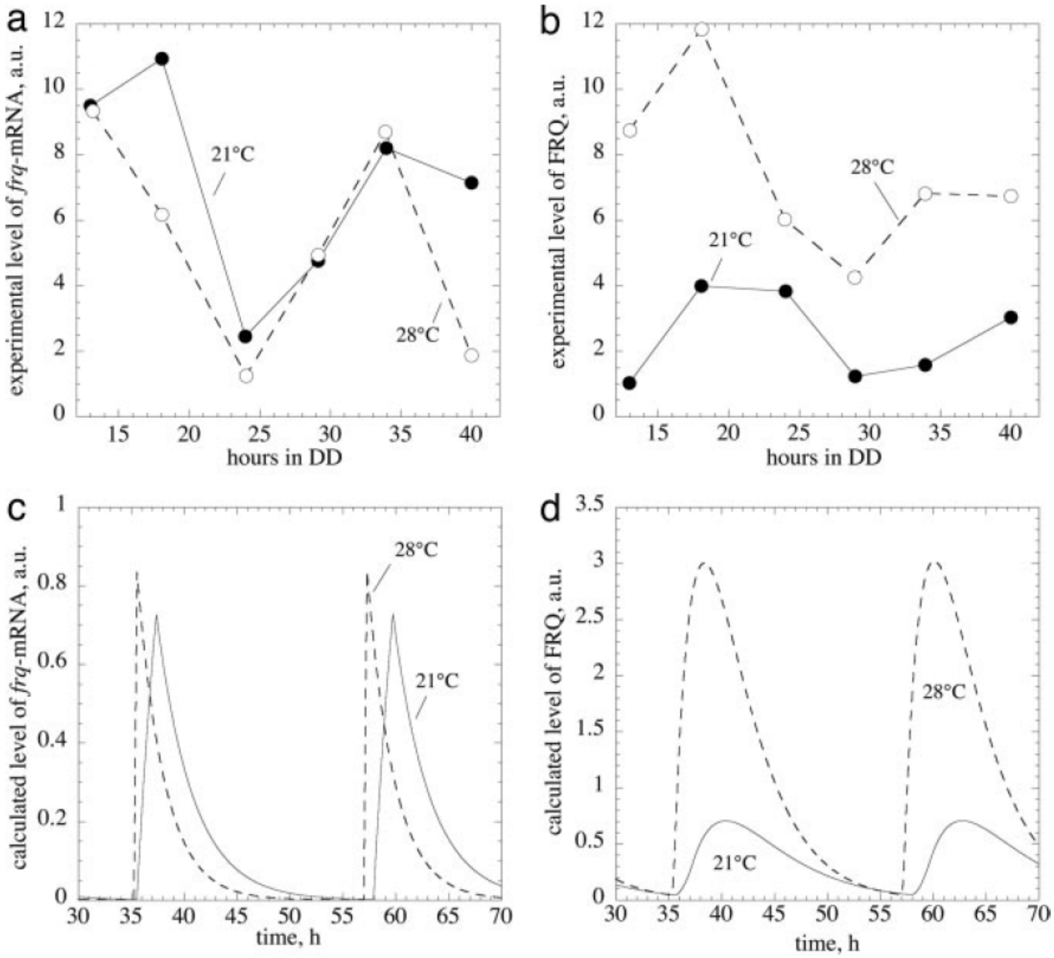

Figure 1.20 The simulated result of Ruoff's Temperature compensated *Neurospora* circadian clock model.
The simulated oscillations in Figure 21 c and c are compared to experimental observations plotted from Liu et al. (Liu et al., 1998) in figure 21 a and b. Figure taken from (Ruoff *et al*., 2005)

1.3.10 Comparisons of *Neurospora* circadian clock models

To focus on comparing the circadian clock models in *Neurospora*, there are four models considered in this section, which are Leloup 1999, Ruoff 2005, Hong 2008 and François 2005.

Leloup 1999 and Ruoff 2005 are minimal *Neurospora* circadian clock models, both of which concentrate on *frq* gene expression and regulation by its product, FRQ.

Although they both focus on the concentration changes of *frq* mRNA, cytosolic FRQ (F_C) and nuclear FRQ (F_N), there are slight differences between these two models. Firstly, Leloup's model considers the shuttle of FRQ into and out of the nucleus, whereas Ruoff's model only considers the transportation of FRQ into the nucleus. Furthermore, Ruoff et al. considered the degradation of F_N, but Leloup et al. did not. Secondly, the format of the equations is slightly different. Ruoff et al. used a constant to represent the degradation rate (k_4 for *frq* mRNA, k_5 for F_C and k_6 for F_N). In contrast, Leloup et al. introduced the idea of Michaelis constant combining with the rate constant into their model. Thirdly, temperature compensation was introduced into Ruoff's model, but not in Leloup's model.

Generally, these four models are based on *frq* gene expression feedback loop. Therefore, although they have different forms of equations to address the regulation process, they all consider the rate of *frq* transcription and translation. François' 2005 model did not consider the cell compartments, and therefore it did not discuss the nuclear localisation of FRQ, but it focuses on the physical appearance of transcription factor WCC binding and disassociation at the promoter. In addition, it also considers the dimerisation of FRQ, which is absent in other models.

Compared to the models of Leloup 1999 and Ruoff 2005, Hong 2008 and François 2005 incorporate more of the known clock molecules and reactions, and therefore are more comprehensive models. Hong 2008 and François 2005 both consider the transcription and translation of *wc-1*, and ignore *wc-2* because of the nearly constant concentration of WC-2 observed from experimental data. Furthermore, they both include the genetic regulation of *wc-1* by FRQ into their model. In Hong's 2008 model, the FRQ protein is considered as a translational or post-translational activator and can facilitate the production of WC-1. On the contrary, François' 2005 model assumes that there are different forms of *wc-1* mRNA. The enhanced form of mRNA is supposed to produce WC-1 more effectively. In addition, François' 2005 model is able to better explain the interaction between the genetic regulations of *wc-1* with other mechanisms, such as FRQ dimerisation and WCC: FRQ or WCC: FRQ_2 complex formation.

Hong 2008 and François 2005 both regard the formation of the WCC: FRQ complex. In François' work, they explain this mechanism by considering the formation and disassociation of the multimer *T* [FRQ+WCC]. In contrast, Hong suggests three different possibilities, the 1:1 binding model, the catalytic model and the inactive $WC\text{-}1_n{}^*$ and $FRQ_n{}^*$ model, and uses the models to test these possibilities.

These models always consider the degradation of the mRNAs, proteins and the complexes included in their model. However, in Leloup's 1999 model, only the degradation in the cytoplasm is considered.

1.4 Aims and objectives

The aim of this project was to discover the underlying mechanism of temperature compensation of the *Neurospora crassa* circadian clock. To be able to investigate this, the construction of a comprehensive quantitative model of the *Neurospora crassa* circadian clock model was necessary. This model needed to be accurate so that the appropriate oscillations of the known clock components based on the interactions of *wc-1, wc-2* and *frq* gene products could be simulated. In addition, circadian clock-associated genes and molecules, such as the VIVID (VVD) protein were included in the model. Light reactions were also modelled. Furthermore, the effect of temperature was also considered to investigate how the clock compensates for environmental variations in temperature to maintain a stable cycle. This model should not only describe the activity of core clock molecules, but also how the clock responds to the fluctuations in the environment. This model was then used to investigate the underlying mechanism of temperature compensation.

Molecular biology experiments were carried out to generate data to inform model building and model validation. For example, the values of missing parameters were determined, such as RNA degradation rates. Experiments for understanding light reactions of the *Neurospora* circadian clock were also carried out. In addition, to understand whether and how temperature affects the central clock, the expression of FRQ at different temperatures was also monitored. Furthermore, to examine the effect of temperature on the localisation of key clock components and to validate hypotheses derived from the model, cellular fractionation experiments were carried out to monitor the subcellular distribution of FRQ, WC-1 and WC-2 proteins.

Chapter 2

Materials and methods

2. Materials and methods

2.1 Molecular biology protocols

2.1.1 Strains

87-3 *bd* and 54-3 *bd* were used as lab wildtype. The *band (bd)* mutation strain has a T79I point mutation in *ras-1*. RAS is the small membrane-anchored G-protein and is involved in signalling cascades (Marshall, 1996). The *bd* mutation amplifies the output signal of the circadian clock and results in clear visualization of conidial banding (Belden *et al*., 2007; Sargent and Woodward, 1969). *bd, frq^{10}* (Aronson *et al*., 1994) and *bd, $wc\text{-}2^{KO}$* are *frq* and *wc-2* null mutants, respectively. Other strains used in this study are 54-6 *his-3*, *bd*, *frq^{10}* (*$his\text{-}3^{+}$*:: *qaqrf*); 54-6, *bd*, *his-3*, *frq^{10}* (*$his\text{-}3^{+}$*:: pBM120); KAJ120 (93-4 *bd*, *his-3*, (*$his\text{-}3^{+}$*:: pKAJ120), *frq^{10}* (Kramer *et al*., 2003); *his-3*, *bd*, *$dicer\text{-}1^{\Delta}$*, *$dicer\text{-}2^{RIP}$* (a kind gift from Prof Yi Liu, University of Texas Southwestern Medical School, Dallas, TX) and *his-3*, *bd*, *$dicer\text{-}1^{\Delta}$*, *$dicer\text{-}2^{RIP}$*(*$his\text{-}3^{+}$*:: *qaqrf*) (Crosthwaite laboratory strain). *his-3* gene encodes the histidine biosynthesis trifunctional protein which is involved in histidine biosynthesis (Ahmed *et al*., 1964; Legerton and Yanofsky, 1985). The usage of *his-3* mutant for transformation allowed the selection of transformants on minimal medium. Successful transformants reconstituted a wildtype version of the *his-3* gene.

2.1.2 Race tube assay

Race tube minimal medium contained 1× Vogel's salts (Vogel, 1956), 0.1% glucose, 50 ng/μL biotin, 0.17% arginine, and 1.5% agar. For race tube medium containing histidine and/or quinic acid (QA), 50 μg/mL histidine and/or 10^{-2} M QA was added to minimal medium and and the medium was adjusted to pH 6.5. The race tube is a long glass tube (about 40 cm long and 16 mm in diameter) and both ends are bent up to hold agar growth medium (about 15 ml) (Kramer, 2007). Tubes inoculated with *Neurospora* macroconidia were incubated in constant light (LL) for at least 24 hours and then transferred to constant darkness (DD) at the same temperature. The mycelial growth fronts were first marked at the light to dark (LD) transition and then every 24 h thereafter. All race tubes were analyzed using the CHRONO program (Roenneberg and Taylor, 2000). The program identified the peaks of conidial bending and the phase plots with a linear regression were made in the program. The period and phase of the rhythm can then be calculated from the linear regression in the program.

2.1.3 Isolation of microconidia

Transformants were selected on minimal plates then inoculated into slants containing 0.1 × Westergaard's salts (Westergaard and Mitchell, 1947), 0.5 % sucrose, 2 % agar, 50 ng/μL biotin, after autoclaving and cooling to 55 C, sodium idoacetate was added to a final concentration of 1 mM and 5 ml of medium was inserted into ~15 cm long and ~15 mm in diameter glass tubes. After incubation of cultures for 7 to 10 days at 25 ºC in the dark, microconidia (containing 1-2 nuclei) were mixed with 2 ml of sterile dH_2O by vortexing and filtered through a 5 μm membrane (Sartorius, minisart 17594-K) and spread on minimal sorbose media plates. The minimal sorbose media plates are prepared with 1× Vogel's salts (Davis and de Serres, 1970), 50 ng/μl biotin, 1.5 % agar and 1M sorbitol. After autoclaving, the sterile 10 X FIGS (20 % L-sorbose, 0.5 % fructose, 0.5 % glucose) was mixed with the agar medium and aliquoted into individual plates. Plates containing macroconidia were incubated at 30 ºC for 4-7 days. Individual colonies were transferred to slants containing minimal medium (1× Vogel's salts, 2 % sucrose, 1.5 % agar and 50 ng/μl biotin).

2.1.4 Genomic DNA extraction

Neurospora was grown on minimal medium slants and spores were transferred to petri dishes containing 30 ml liquid medium (1× Vogel's salts, 2 % glucose, 50 ng/μl biotin and 0.17 % arginine). After incubation of cultures for 48 hours at 30 °C DD, tissue was taken out by tweezers, press-dried between filter paper (Whatman 3030-917), and ground to a fine powder in a motor and pestle under liquid nitrogen. An equal volume of 2 × CTAB buffer (100 mM Tris-HCl, 2% (w/v) hexadecyltrimethylammonium bromide (CTAB) (Sigma, H5882), 1.4 M NaCl, 20 mM Ethylenediaminetetraacetic acid (EDTA), 1% (w/v) Sodium Bisulphite) was added to the ground tissue (ca. 1 ml) in a 15 ml tube and incubated at 60 °C for 30 minutes with occasional gentle inversion. An equal volume of 24:1 chloroform: isoamyl alcohol (ca. 1 ml) was added to the crude mixture and incubated on a rotator (Stuart) at room temperature for 15 minutes. The crude mixture was centrifuged at 2000×g for 10 minutes and the supernatant collected. An equal volume of isopropanol (ca. 0.8 ml) was added to the supernatant and mixed with gentle inversion. The mixture was then centrifuged at 18,000×g for 5 minutes. The supernatant was discarded. The pellet was washed with 400 μl 70 % ethanol and spun at 18,000×g for 5 minutes. The supernatant was discarded. The pellet was air-dried and resuspended in 100 μl dH_2O.

2.1.5 Total RNA extraction

Transcripts were extracted from vacuum-filtrated frozen tissue using the Qiagen RNeasy Mini kit according to the manufacturer's instructions for the isolation of total RNA from filamentous fungus.

2.1.6 Agarose gel electrophorsis

For DNA electrophoresis, the agarose gel was made with 1 X TAE (10 X TAE: 0.4 M Tris-base, 11.4 % glacial acetic acid, 10 mM EDTA, pH 7.6 with glacial acetic acid). Mixed solution was microwaved for 2-4 minutes to melt the agarose. After the gel solution was cooled down to 60 ºC, 0.1 μg/ml ethidium bromide was added and the gel was poured.

For total RNA electrophoresis, agarose–formaldehyde gel containing 1 X MOPs (450 mM morpholinopropanesulfonic acid, 49.8 mM NaOAc, 5 mM EDTA, pH 7) was microwaved for 2-4 minutes to melt the agarose, and 5.5 % formaldehyde and 20 ng/ml ethidium bromide was added just before the gel was poured.

2.1.7 Southern blot analysis

For DNA probes, pSA1 plasmid (Figure 2.1) DNA was digested with *Xho*I following the manufacturer's instructions and the 1.7 kb product (339-2049 bp of pSA1) was gel extracted and ~3 μg of DNA labeled with DIG using the DIG-High Prime DNA Labeling and Detection Starter Kit II (Roche) according to the manufacturer's instructions. Approximately 200 μg of genomic DNA was digested with *Pdm*I (*Xmn*I) overnight at 37 °C and electrophoresed through a 1% agarose gel made with 1 X TAE (10 X TAE: 0.4 M Tris-base, 11.4 % glacial acetic acid, 10 mM EDTA, pH 7.6 with glacial acetic acid). The size separated genomic DNA fragment was then blotted onto Hybond-N+ membrane (Amersham) according to manufacturer's instructions (https://www.gelifesciences.com/gehcls_images/GELS/Related%20Content/Files/1314774443672/litdocRPN2020BPL_Rev_E_2006_web_20110831095435.pdf), and probed with DIG-labeled probes. The signal was developed with CSPD (Roche) and exposed to Kodak BioMax MR film (Sigma-Aldrich).

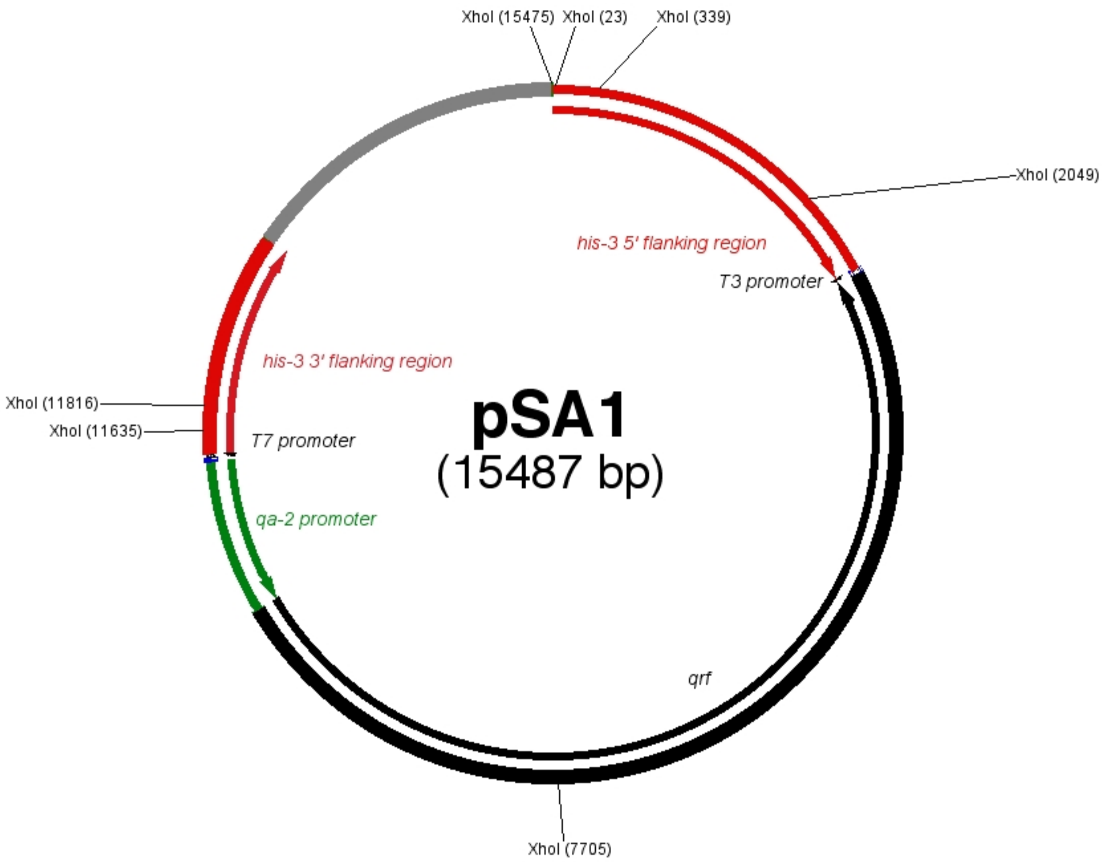

Figure 2.1 Plasmid map of the pSA1 plasmid.
his-3 5' flanking region and *his-3* 3' flanking region are shown in red. *qrf* gene (black) is promoted by the qa-2 promoter (green).

2.1.8 RNA degradation assay

mRNA degradation was assayed in the 54-3 *bd* strain of *Neurospora*. 54-3 *bd* was grown on slant minimal medium and macroconidia were transferred to petri dishes containing 30 ml liquid minimal medium. After 24 hours culture at 30 °C in DD, the mycelial mats were cut into ca. 90 mm diameter discs and each disc placed in a 100 ml. Erlenmyer flask containing 25 ml liquid medium. Discs were grown in shake culture on a rotary shaker at 125 rpm at 25 °C in constant light (LL) for at least 24 hours. After 24 hours, control samples were harvested in LL. Immediately after the light to dark (DD) transfer, thiolutin (Tocris) dissolved in dimethyl sulfoxide (DMSO) was added to a final concentration of 12 µg/ml. Samples were harvested in darkness at the times indicated.

2.1.9 Polymerase chain reaction (PCR) and gel extraction for riboprobe templates

100 ng of plasmid DNA or 1 μg of genomic DNA was used for template. Primer sequences are shown in table 2.1. Each reaction contained DNA template, 1×PCR reaction buffer, 0.2 μM forward primer, 0.2 μM reverse primer, 0.4 mM dNTP mix and 5 U Bioline Taq polymerase (Bioline). PCR products were electrophoresed through a 1% TAE agarose gel. Products were visualised under UV illumination and excised from the gel. DNA was recovered from the gel slices using the Qiaquick gel extraction kit (Qiagen) according to the manufacturer's instructions, or by phenol-chloroform extraction. For phenol-chloroform extraction, the excised gel was shredded on foil using a clean razor blade and placed in a 2 ml eppendorf tube. 0.5 ml Buffer EB (QIAGEN) was added and mixed by vortexing. An equal volume of Phenol : Chloroform : iso-Amyl alcohol (25:24:1) (VWR) was added and mixed on a rotator (Stuart) at 40 rpm for 5 minutes at room temperature. Samples were transferred to -80 ºC for 15 minutes, defrosted on a rotator (Stuart) at 40 rpm for 10 minutes at room temperature and centrifuged at full speed for 10 minutes. The

supernatant was collected and DNA was concentrated by alcohol. 2.5 volumes of -20 ºC ethanol, 0.1 volume of 3M sodium acetate and 0.01 volume of glycogen was added and briefly vortexed. The mixture was transferred to -20 ºC for at least 30 minutes and centrifuged at top speed (14,000 rpm) at 4 ºC for 30 minutes. The supernatant was discarded and the DNA pallet was briefly washed by 1 volume of -20 ºC 70 % ethanol. The mixture was centrifuged at top speed (14,000 rpm) at 4 ºC for 15 minutes. The supernatant was discarded. The DNA pallet was air dried and resuspended in 30-100 μl dH_2O.

Table 2.1 Table of primer sequences

Primer Name	Forward primer (5'-3')	Reverse primer (5'-3')
frq probe for Northern	GTAAAACGACGGCCAGT (M13/pUC sequencing primer)	CAGGAAACAGCTATGAC (M13/pUC reverse sequencing primer)
wc-1 probe for Northern	TAATCAGACTCACTATAGGGAGTG TTCCTCGTATGG	CTCGTGGAATGCCCTGATGC
wc-2 probe for Northern	CAAGCGCCGCAATTGGC	TAATAGGACTCACTATAGGGAGGCCCA ATCCGTTGT
vvd probe for Northern	GAGCCATACCGTGAACTC	TAATACGACTCACTATAGGGAGGCCCA ATCGCAGAATAAGACG

2.1.10 Northern blot analysis

Total RNA (7-10 μg) was electrophoresed through a 0.8 % agarose–formaldehyde gel in 1 X MOPs buffer. The size separated RNA was blotted onto Hybond-N+ membrane (Amersham) according to manufacturer's instructions (https://www.gelifesciences.com/gehcls_images/GELS/Related%20Content/Files/131

4774443672/litdocRPN2020BPL_Rev_E_2006_web_20110831095435.pdf), and probed using radiolabeled riboprobes complementary to the transcript of interest. Riboprobes were made using the MAXIscript T7/T3 Kit (Ambion) according to the manufacturer's instructions. Nucleotides 1630–3832 of the *frequency* open reading frame (ORF) were transcribed into an antisense riboprobe using Amersham ^{32}P-dUTP (800 Ci/mmol) to a specific activity of 10^9 counts per minute (cpm) per microgram. For *wc-1* (positions 1756-3067) and *wc-2* (positions 637-1801) gene specific riboprobes were generated by labelling PCR fragments containing T7 polymerase sites to generate antisense riboprobes. Gene-specific riboprobes of *vvd* mRNA were obtained by labeling PCR products (AF338412, positions 239–1173 for *vvd*) containing an appropriate T7 Polymerase site to generate antisense riboprobes. Membranes were pre-hybridized in 10 ml of NorthernMax Prehyb/Hyb (Ambion) at 68 ºC for at least 1 hour and then with 2×10^7 cpm/ml of *in vitro* transcribed radiolabeled probe (Ambion) at 68 ºC over night. The membrane was washed twice with 2 X SSC, 0.1 % SDS at room temperature for 20 min, and then washed twice with 0.1 X SSC, 0.1 % SDS at 68 ºC for 20 min. Membranes were exposed to Fuji screens and were scanned using a PhosphorImager (Bio-Rad). RNA data were quantified using ImageJ 1.42q (National Institutes of Health, USA) or Quantity One (Biorad).

2.1.11 Total protein extraction

Neurospora was grown on slants containing minimal medium and spores were transferred to petri dishes containing 30 ml liquid minimal medium (1× Vogel's salts, 2 % glucose, 50 ng/µl biotin and 0.17 % arginine) and incubated over night at 30 °C. 20 mm diameter discs were cut from the mycelial mats and placed into 100 ml liquid medium in 250 ml flasks. The flasks were shaken at 250 rpm on rotary shakers and incubate in constant light for at least 24 hours. Tissue was harvested onto filter paper (Whatman) by vacuum filtration at the time indicated and ground under liquid nitrogen into fine powder. An equal volume of protein extraction buffer (50 mM HEPES pH 7.4, 137 mM KCl, 10%(v/v) glycerol, 5mM EDTA, 1 μg/μl pepstatin A (Sigma, P5318), 1 μg/μl Leupeptin (Sigma, L2884), 1 mM PMSF (Sigma, P7626)) was added to the tissue powder and the samples were mixed vigorously by vortexing. EDTA and protease inhibitors were added just before use. Samples were incubated on ice for 30 minutes with occasional vortexing. The crude mixture was spun at 18,000×g for 20 min at 4 °C and the supernatant (total protein extract) was collected and stored at -80 °C.

2.1.12 Cell fractionation

The cell fractionation procedure was modified from Luo *et al*. 1998, Hong *et al*. 2008, Diernfellner *et al*. 2009, and Hunt *et al*. 2010. Tissue was cultured from conidia (1.6×10^7 conidia/l for culture at 25 °C or 8.8×10^6 conidia/l for culture at 30 °C) for at least 24 hours in constant light and then transfered to constant dark. Tissue was collected by vacuum filtration on to 2 layers of filter paper (Whatman 1001-110) and press-dried between filter paper. Tissue wrapped in aluminium foil was stored in liquid nitrogen. A small portion of each sample was used for total protein extraction (section 2.1.11). For fractionation, frozen tissue (8 g) was ground with 12 ml of buffer A (1 M sorbitol, 7% (w/v) ficoll-type 70, 20% (v/v) glycerol, 5 mM magnesium acetate, 5 mM EGTA, 3 mM $CaCl_2$, 5 mM dithiothreitol (DTT) (added just before use), 50 mM Tris-HCl, pH 7.5) and 5 ml of sterile 425-600 µm glass beads (Sigma, G9268) on ice in a chilled motor and pestle for 3 minutes. The crude mixture was filtered through a

20 μm nylon filter membrane (Millipore) into a 50 ml Corning centrifuge tube. 2 volumes of buffer B (10% (v/v) glycerol, 5 mM magnesium acetate, 5 mM EGTA, 25 mM Tris-HCl, pH 7.5) were added to the flow-through with gentle stirring on ice. To remove cell debris the homogenate was layered on 15 ml buffer C (a 1:1.7 mix of buffers A and B) and centrifuged at 3000×g in a SW28 rotor in a Ultracentrifuge (Beckman Coulter Optima L-90K) for 7 minutes at 4 °C. To pellet nuclei the supernatant (total fraction) was collected (16 ml from top) and layered on a 5 ml sucrose gradient buffer (1 M sucrose, 10% (v/v) glycerol, 5 mM magnesium acetate, 1 mM DTT (added just before use), 25 mM Tris-HCl, pH 7.5) and spun at 9000×g in a SW28 rotor for 15 minutes at 4 °C. The resulting supernatant (cytoplasmic fraction) was collected (8 ml from top) without touching the pellet and the rest was discarded. The pellet (nuclear fraction) was gently resuspended in 1 ml sucrose gradient buffer and transferred to a 1.5 ml eppendorf tube to wash the nuclei. To pallet the nuclei, this suspension of nuclei was spun at 10,000 rpm (9000×g) in a bench top centrifuge at 4 °C for 15 min. The supernatant was discarded and the nuclear pellet resuspended in 100-800 μl storage buffer (25% (v/v) glycerol, 5 mM magnesium acetate, 3 mM DTT (added just before use), 0.1 mM EDTA, 25 mM Tris-HCl, pH 7.5). 10 μg/ml leupeptin, 10 μg/ml pepstatin A and 1 mM phenylmethylsulfonyl fluoride (PMSF) were added into all buffers just before use. Samples were stored in a -80 ºC freezer.

2.1.13 FRQ antibody depletion

To decrease non-specific binding of the FRQ antibody it was incubated with total protein extracted from a frq deletion strain, *bd, frq*^{10}, *bd, frq*^{10} was grown on minimal slat at 30 ºC for 5-10 days. Spores in each minimal slant were mix with sterile dH2O and transferred to a petri dishe containing 30 ml liquid minimal medium. After 24 hours culture at 30 °C, whole mycelial mat was transferred into a 2 L flask with 1 L of liquid minimal medium. The flask was shaken at 150 rpm on a rotary mixer at 25 °C in constant light (LL) for at least 48 hours. Tissue was harvested and ground to a fine powder under liquid nitrogen. 25 ml tissue powder was aliquoted into four 50 ml Corning centrifuge tubes. Four tubes of tissue powder were used for depletion of 180 μl anti-FRQ antibody. PBS (0.01 M phosphate buffer, 0.0027 M potassium chloride and 0.137 M sodium chloride, pH 7.4) (Sigma, P4417) with 0.5 % formaldehyde was added into 12.5 ml powdered *bd,frq*^{10} tissue up to 50 ml and the crude mixture was incubate at 37 °C with occasional vortexing over 2 hours. 4 tubes of crude mixture were collected into one 500 ml centrifuge tube and spun in F10BCL 6×500y rotor at 5000×g at 4 ºC for 10 minutes. The supernatant was discarded and the pellet was washed twice in 200 ml TBS (137 mM NaCl, 2.7 mM KCl, 25 mM Tris, pH 7.4) and centrifuged at 5000×g at 4 ºC for 10 minutes after each wash. The pellet was aliquoted into 8 portions (~1 ml each) and stored at -20 °C. Anti-FRQ antibody (kindly provided by Prof. Yi Liu, University of Texas Southwestern Medical School, Dallas, TX) was diluted 1:50 in TBS (137 mM NaCl, 2.7 mM KCl, 25 mM Tris, pH 7.4) containing 1 % BSA. The first portion of tissue pellet (~1 ml) was incubated with 9 ml diluted antibody for at least 2 hours or overnight at 4 °C at 40 rpm on a rotator (Stuart). The crude mixture was spun at 5000×g for 10 minutes. The supernatant was collected and depleted another 7 times. The final supernatant was collected and used at 1:100 dilution.

2.1.14 Western blot analysis

Samples of the nuclear fraction were mixed with protein sample buffer (50 mM Tris pH6.8, 0.1 M DTT, 2 % SDS, 0.1 % bromophenol blue, 10 % glycerol) and boiled for

5 minutes in a 1.5 ml screw cap tube (Starlab E1415-2231). Samples were mixed by vortexing and centrifuged at full speed for 2 minutes. The supernatant was collected and mixed again by vortexing. For detection of FRQ, c.a. 100 μg of sample was loaded per lane onto a 7.5 % SDS-PAGE gel (Criterion Tris-HCl Gel, 345-0006) and run in SDS running buffer (192 mM glycine, 25 mM Tris, 0.1 % SDS) at 60 V for 4 hours. For detection of WC-2 and alpha-tubulin, c.a. 10 μg of sample was loaded per lane onto a 10 % SDS-PAGE gel. After electrophoresis, proteins were blotted onto Immobilon-P membrane (Millipore) by wet transfer using the Criterion blotter with plate electrodes (Bio-Rad) according to manufacturer's instructions (http://www.millipore.com/userguides.nsf/a73664f9f981af8c852569b9005b4eee/e619b2b726e40a3b85257307005ecc8d/$FILE/PR02531.pdf; http://www.bio-rad.com/webroot/web/pdf/lsr/literature/4006190b.pdf). Briefly, protein was transferred in ice cold transfer buffer (384 mM glycine, 50 mM Tris, 20 % methanol) at 70 volts for 75 minutes. Membranes were blocked in SuperBlock Blocking Buffer in TBS (Fisher Scientific, PN37535) and hybridised with either anti-FRQ (1:3000) (Prof. Yi Liu, University of Texas Southwestern Medical School, Dallas, TX), depleted anti-FRQ (1:100) (section 2.1.13), anti-alpha-tubulin antibody (1:200) (Fitzgerald, 10R-T130a), anti-WC-1 (1:3000) (kindly provided by Prof. Yi Liu, University of Texas Southwestern Medical School, Dallas, TX), anti-WC-2 (1:6000) (kindly provided by Prof. Yi Liu, University of Texas Southwestern Medical School, Dallas, TX) or anti-MYC antibody (Santa Cruz Biotechnology) in TBS (25 mM Tris, 150 mM NaCl, pH 7.2) containing 0.5 % Tween-20 as described previously (Heintzen *et al*., 2001). Immunodetection was carried out as previously described (Hunt *et al*., 2007) and the signal quantified using the ImageJ software (http://rsbweb.nih.gov/ij/).

2.1.15 Calculation of standard deviation and standard error

Standard deviation (s) was calculated using the following equation.

$$s = \sqrt{\frac{\sum_{i=1}^{i=n}(x_i - x_{av})^2}{n-1}} \qquad (2.1)$$

where n is the total number of samples. x_i is the observed value of sample i and x_{av} is the mean observation of all samples. Standard deviations can be integrated by the following equation.

$$S_{tot} = \sqrt{s_1^2 + s_2^2 + \ldots} \qquad (2.2)$$

S_{tot} is the final standard deviation. S_i are the original standard deviations.

The standard deviation can be used to calculate the standard error (SE) with the following equation.

$$SE = \frac{S_{tot}}{\sqrt{n}} \qquad (2.3)$$

where n is the number of observations.

To compare the difference of period and phase between samples, SPSS 20.0.0.1 (IBM) was used to perform the analysis. Original data such as period and phase converted to circadian time (CT) were typed into the program and One-way ANOVA and scheffe post hoc were carried out to test the significance of difference.

2.1.16 Nucleic acids concentration

To determine the concentrations of DNA and RNA the optical density (OD) at 260 mm of samples were measured in a spectrophotometer (BOECO) (1:50 dilution, 50 μl in total) or nanodrop (Thermo Scientific) (2 μl in total). The equations used for calculating DNA and RNA concentrations are as follows:

$$[\text{DNA}] = \text{OD}_{260} \times 50 \times \text{dilution factor} \qquad (2.4)$$

$$[\text{RNA}] = \text{OD}_{260} \times 40 \times \text{dilution factor} \qquad (2.5)$$

2.1.17 Protein concentration

For total protein extract, the concentration of protein was determined by Bradford Protein Assay (Bio-Rad) according to manufacturer's instructions (http://www3.bio-rad.com/LifeScience/pdf/Bulletin_9004.pdf). For nuclear fraction, the concentration of protein was determined by detergent-compatible (DC) Protein Assay (Bio-Rad) according to the manufacturer's instructions (http://www3.bio-rad.com/LifeScience/pdf/Bulletin_9005.pdf). The reaction is similar to the Lowry assay and is able to detect protein concentration with samples containing detergents such as Triton or SDS. 12.5 μl of each sample or standards were mixed with 12.5 μl of 2 X protein sample buffer by vortexing and boiled for 5 minutes prior to the assay.

2.1.18 Calculation of RNA degradation rates

The first order RNA decay is written as:

$$\frac{\mathrm{d}\left[\mathrm{RNA}\right]}{\mathrm{d}t} = -\left[\mathrm{RNA}\right] \times kd \qquad (2.6)$$

kd is the degradation constant of RNA. This equation can be solved by integrating and generates the following equation.

$$[\mathrm{RNA}]_t = [\mathrm{RNA}]_0 \times \mathrm{e}^{-kt} \qquad (2.7)$$

In this thesis $[\mathrm{RNA}]_0$ is the level of RNA at the time point of light to dark transfer. $[\mathrm{RNA}]_t$ is the level of RNA at the time t. The amount of RNA exponentially decreases as t increases. To obtain the half-life of RNA, equation (2) can be solved as:

$$\frac{[\mathrm{RNA}]_{t_{1/2}}}{[\mathrm{RNA}]_0} = \frac{1}{2} = \mathrm{e}^{-kt_{1/2}} \qquad (2.8)$$

Therefore the half-life of RNA is $t_{1/2} = \frac{\ln 2}{k}$ (2.9)

2.2 Chemical kinetics and computational modelling

2.2.1 Mass action kinetics

Chemical reactions obey the law of conservation of mass. For a generic chemical reaction (equation 2.10), the rate of the reaction (v) can be described as equation 2.11.

$$a\text{A}+b\text{B} \rightarrow c\text{C}+d\text{D}+... \quad (2.10)$$

$$v = -\frac{1}{a}\frac{d[\text{A}]}{dt} = -\frac{1}{b}\frac{d[\text{B}]}{dt} = \frac{1}{c}\frac{d[\text{C}]}{dt} = \frac{1}{d}\frac{d[\text{D}]}{dt} = ... \quad (2.11)$$

In terms of chemical kinetics, the reaction rate can be described as equation 2.12. It is affected by the concentration of reactants ([A], [B]…) and kinetic parameters (k_1, k_2).

$$v = f([\text{A}],[\text{B}]...,k) \quad (2.12)$$

The changes in reaction rates over time can be characterised by differential rate equations. Rate equations represent the relationship between the concentration of reactant(s) over time and the reaction rate. The concentration of each reactant may make different contributions to the reaction rate. For example, for a chemical reaction defined as equation 2.13, the rate equation may be described as equation 2.14.

$$\alpha\text{A}+\beta\text{B} \rightarrow \gamma\text{C} \quad (2.13)$$

$$v = \frac{d[\text{C}]}{dt} = k[\text{A}]^m[\text{B}]^n \quad (2.14)$$

α, β and γ represent the stoichiometry of this reaction. [A], [B] and [C] stand for the concentrations of component A, B and C, respectively. k is the rate constant.

Exponents *m* and *n* are partial reaction orders given by the component A and B, respectively. The sum of *m* and *n* is the order of this reaction.

2.2.2 Enzyme kinetics

In the natural world, the reaction rate of many chemical reactions is not only dependent on the concentration of reactants. Catalysts influence the rate of reactions. Positive catalysts speed up a reaction, whereas inhibitors slow down a reaction. In biology, enzymes are biological molecules that are able to change biochemical reaction rates. The Michaelis-Menten equation is the general form to describe enzyme catalysed kinetics:

$$v = \frac{k_{cat}[\mathrm{E}][\mathrm{S}]}{K_M + [\mathrm{S}]} \qquad (2.15)$$

v is the rate of reaction. k_{cat} is the rate constant. [E] is the concentration of enzyme. k_{cat}[E] can be written as V_{max}, which is the maximum rate of this reaction. $\mathrm{K_M}$ is the Michaelis constant. [S] is the concentration of substrate.

2.2.3 Order of reaction

The equations used in this study can be classified depending on the order of reaction. The classification and descriptions are shown as follows.

2.2.3.1 Zero-order reaction

In equation 2.14, if m and n are zero, the reaction rate is independent of the concentrations of the reactants. Therefore, the reaction rate is constant. For example, this kind of equation is applied to the rate of mRNA synthesis in my model.

2.2.3.2 First-order reaction

In equation 2.14, if either m or n is one and the other is zero, the reaction rate depends on either the concentration of A or B. Hence, the reaction rate is varied following the concentration of one of the reactants. This kind of equation is applied to protein synthesis, component degradation, translocation, phosphorylation, and dephosphorylation in the model.

2.2.3.3 Second-order reaction

If the reaction rate is dependent on the concentration of two reactants or the square power of one reactant, this reaction is a second-order reaction. For example, in equation 2.14, if m is two and n is zero, the reaction rate is exponentially affected by [A]. If m and n are both one, the reaction depends on both [A] and [B]. Hence, the reaction rate varies following the two reactants' concentrations. This kind of equation is applied to the rate of WCC complex formation in my model.

2.2.4 Hill equation

The Hill equation is widely used in describing the affinity of protein ligand binding (Goutelle *et al.*, 2008; Hill, 1910). The general format of the Hill equation explaining the cooperative binding of oxygen to haemoglobin can be written as follow:

$$\theta = \frac{[L]}{K_d + [L]} \tag{2.16}$$

θ is the proportion of occupied sites. $[L]$ is the concentration of the ligand. K_d is the dissociation constant. This equation can be transformed and applied to describe a nonlinear reaction rate dependent on the concentration of an enzyme:

$$v = \frac{V_{max}[E]^H}{K_d^H + [E]^H} \tag{2.17}$$

v is the reaction rate. V_{max} is the maximum reaction rate. [E] is the concentration of the enzyme. K_d is the dissociation constant, which determines the binding efficiency between the reactant and the enzyme. H is the Hill coefficient, which shows the degree of this nonlinear reaction. This type of reaction is applied to the transcription of *frq* by WCC and the phosphorylation of WCC facilitated by FRQ in my model.

On the other hand, the Hill equation can also be applied to describe the nonlinear inhibition reaction:

$$v = \frac{V_{max}K_d^H}{K_d^H + [I]^H} \tag{2.18}$$

v is the reaction rate. V_{max} is the maximum reaction rate. [I] is the concentration of the inhibitor. K_d is the dissociation constant. For simplicity, K_d can be replaced with $1/k$ and H can be defined as 1. Therefore, the equation can be rewritten as:

$$v = \frac{V_{max}}{1 + k[\mathrm{I}]} \tag{2.19}$$

This type of reaction is applied to the transcription of *wc-2* inhibited by WCC in my model.

2.2.5 The influence of temperature on rate constants

For general chemical reactions, the reaction rate is usually doubled when the temperature increases by 10 ºC (Harcourt, 1867). In 1889, Arrhenius derived an equation to describe a rate constant varying with temperature, the Arrhenius equation:

$$k = A_i e^{\frac{-Ea}{RT}} \tag{2.20}$$

A_i is the collision factor or pre-exponential factor, which is a constant; E_i is the activation energy; R is the gas constant (8.314472 J mol^{-1} K^{-1}); T is the temperature in Kelvin. A_i and E_i are independent of the temperature.

2.2.6 Model construction

In this project, we used these general kinetic laws to construct a model of the *Neurospora* circadian clock. Figure 2.2 summarises the processes of constructing this model.

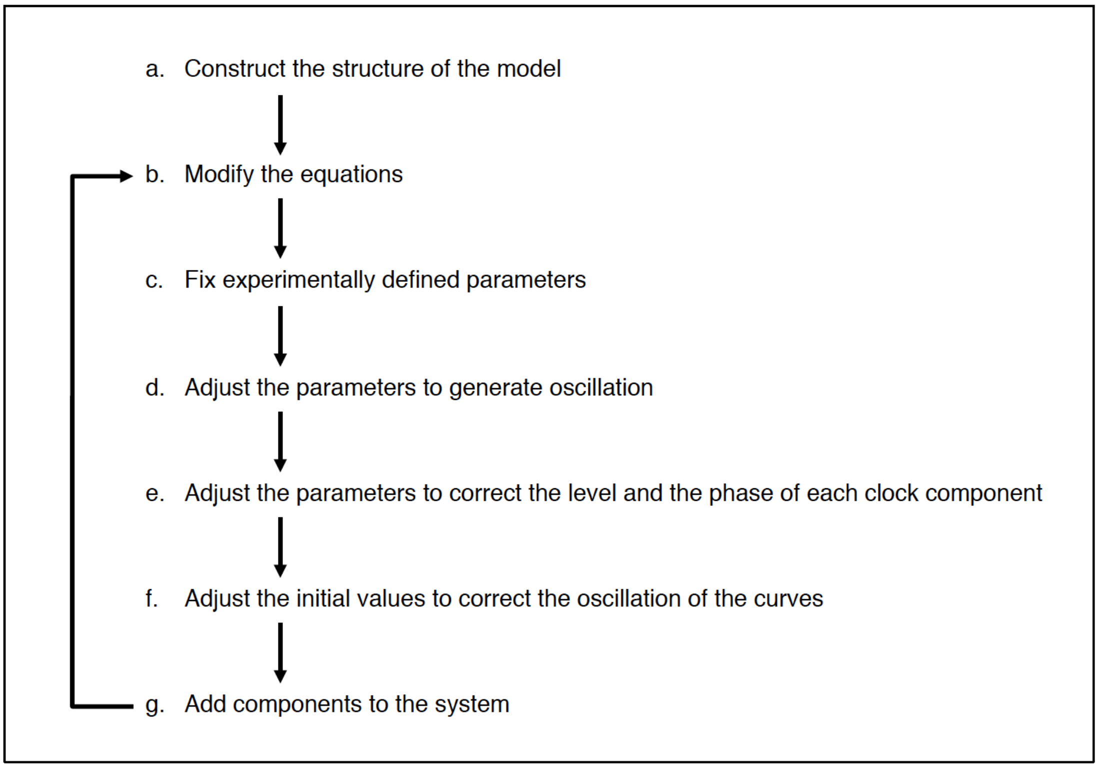

Figure 2.2 The processes of model construction.
The construction of this model started using information from previous literature (step a). Some equations were modified to better represent the molecular mechanisms of the *Neurospora* circadian clock (step b). In addition, some parameters were fixed with experimentally defined values (step c). Then, non-fixed parameters and initial values of the components were adjusted empirically to generate the correct level and phase of clock components (steps d-f). Next, new components could be added to the model (step g). Steps b-g were repeated multiple times to produce the final model. Details of the reactions included in each step are provided in Chapter 3.

2.2.7 Parameter usage

Model parameters were either derived from experimental data (*frq* ((Guo *et al.*, 2010) and our data), *wc-1* (our data), *wc-2* (our data) and *vvd* RNA degradation (our data), FRQ degradation (Ruoff *et al.*, 2005)) or estimated by comparing simulations to experimental observations.

2.2.8 Computation

The circadian clock model was manually constructed using the CellDesigner™ 4.1 or 4.2 software (Funahashi *et al.*, 2003; Funahashi *et al.*, 2008; Kitano *et al.*, 2005). The program was operated in Java Runtime Environment (JRE) Version 6 Update 16 on Windows XP or on Mac OS 10.6.8. The model is provided in SBML format Level 2 version 4 (http://www.ploscompbiol.org/article/fetchSingleRepresentation.action?uri=info:doi/10.1371/journal.pcbi.1002437.s002). Simulations were carried out in CellDesigner using SOSlib as the numerical solver.

2.2.9 Control analysis

To quantify how model components affect the period and amplitude of the oscillations, we calculated period and amplitude response coefficients. The period response coefficient R_j^T of parameter P_j was defined as the rate of change in period T divided by the rate of change of the parameter value.

$$R_j^T = \frac{\frac{\delta T}{T}}{\frac{\delta P_j}{P_j}} \qquad (2.21)$$

The amplitude response coefficient R_j^A of the parameter P_j was similarly defined as the rate of change in amplitude A divided by the rate of change of the parameter value.

$$R_j^A = \frac{\frac{\delta A}{A}}{\frac{\delta P_j}{P_j}} \tag{2.22}$$

The effect of a 3 % change in the value of each parameter was considered. 200 hours of dark simulation and 200 points per hour were calculated without changing the initial value of the components for period response coefficients. 200 hours of dark simulation and 50 points per hour are calculated without changing the initial value of the components for amplitude response coefficients. The last two peaks of *frq* mRNA level were used to calculate the period and the last peak and trough of the *frq* mRNA oscillation were used to calculate the amplitude.

2.2.10 Phase response curves

For phase response curves (PRC) simulated in the model, 0.1 or 0.01 h of duration of light was pulsed every two circadian hours. To simulate a light pulse, the light activation rate (*klact_hypoWCCn*) of WCC was changed from 0 to 5, and returned to 0 to end the pulse. The time of peak *frq* mRNA before and after the light pulse was used to calculate the advance or delay of the clock.

2.2.11 Modelling temperature compensation

To model temperature compensation the effect of temperature was introduced into temperature sensitive parameters by use of the Arrhenius equation (Ruoff and Rensing, 1996). For each reaction, the temperature influences the value of each kinetic parameter k_i according to equation 2.23 (Ruoff et al., 2005).

$$k_i = A_i e^{\frac{-E_i}{RT}} \qquad (2.23)$$

The activation energy E_a was calculated using equation 2.24 (Ruoff *et al.*, 2005).

$$E_a = \frac{R \times \ln(\frac{k_{T_2}}{k_{T_1}})}{\frac{1}{T_1} - \frac{1}{T_2}} \qquad (2.24)$$

R is the gas constant k_{T1} is the parameter value at temperature T_1 and k_{T2} is the parameter value at temperature T_2.Once the activation energy was calculated, the pre-exponential factor A was obtained by solving the Arrhenius equation.

Chapter 3

A comprehensive dynamic model of the *Neurospora* circadian clock

3. A comprehensive dynamic model of the *Neurospora* circadian clock

3.1 Introduction

As mentioned in the first chapter, *Neurospora* clock research has benefited from computational modelling (Francois, 2005; Hong *et al*., 2008a; Hong *et al*., 2008c; Leloup *et al*., 1999b; Ruoff *et al*., 1996; Ruoff *et al*., 2005). Computational modelling not only can quantify the concentration changes and represent interactions of key clock components, but also leads to the generation of testable predictions. This helps us discover new mechanisms and interactions and even helps us to design experiments and decide the direction of research. However, existing *Neurospora* models are not up-to-date with current experimental results; for example, VIVID (VVD) represses light responses by interacting with light-activated WCC (Chen *et al*., 2010; Hunt *et al*., 2010; Malzahn *et al*., 2010), and as yet no model incorporates this important interaction. In addition, WC-2 is the key component of the *Neurospora* circadian clock, but WC-2 is usually not modelled as an independent component in the published *Neurospora* models (Francois, 2005; Hong *et al*., 2008a). Therefore, developing a comprehensive model of *Neurospora* circadian clock may not only increase our understanding of entrainment, but also be enable us to accurately inspect the interactions among clock components.

The construction of my model was based on a compilation of published and new experimental data and incorporates facets of previously described *Neurospora* clock models (Hong *et al*., 2008a; Leloup *et al*., 1999b). The usage of equations and mechanisms considered in the model will be described in this chapter. In addition, in order to develop a reliable model, simulated results such as relative levels and phases of key clock components were compared with published experimental data. Furthermore, phenotypes of *Neurospora* with a mutant form of WC-2 ($wc\text{-}2^{ER24}$) or an inducible copy of the wc-1 gene (qa-WC-1) were also simulated to test the model.

Although a complex comprehensive model can be used to make and test predictions, it is still difficult and inefficient to test predictions by randomly adjusting the value of parameters. Understanding the influence of each parameter gives clues of how parameters affect the oscillatory system. Therefore, the parameter perturbation tests were performed and the results are shown in this chapter.

3.2 Results of modelling the *Neurospora* circadian clock in constant darkness

3.2.1 Model construction process and parameter determination

The development of this model began with the model from published literature (Leloup *et al.*, 1999b). Next, essential reactions, such as *wc-2* transcription and translation, FRQ and WCC phosphorylation and translocation, were added into the model. For simplicity, first order equations were first considered for newly added reactions. Furthermore, the kinetic equations used to represent the degradation of components were simplified to first order equations. For parameter values, some parameters were derived from experimental data, such as *frq* ((Guo *et al.*, 2010) and my data), *wc-1* (my data), *wc-2* (my data) and *vvd* RNA degradation (my data), and FRQ degradation (Ruoff *et al.*, 2005). The remaining parameters were adjusted to reproduce experimental observations, such as the period, relative level of molecular compounds, phase of each component, and clock behaviours. If the relative level of components or any other clock characteristic could not be reproduced by simulations, another form of equation or additional components and reactions were considered. For example, Hill equations were used for *frq* transcription and FRQ-dependent WCC phosphorylation to generate appropriate oscillations. In addition, speeding up or slowing down reactions by increasing or decreasing the values of parameters also helped to test if the model was working correctly.

3.2.2 Determination of *frq*, *qrf*, *wc-1*, *wc-2*, *vvd* RNA degradation

Parameter values obtained from experimental data would be of benefit to develop a precise model. However, the degradation rate of FRQ is currently the only accurately determined parameter value from molecular biology experiments (Mehra *et al.*, 2009;

Ruoff *et al*., 2005). The values of *frq* and *wc-1* RNA degradation rates had been optimised by monitoring from RT-PCR experimental data and from microarray data, respectively (Garceau *et al*., 1997; Ruoff *et al*., 1999; Yu *et al*., 2007), but these values might not be accurate. Therefore, experiments were carried out to obtain these parameter values. The degradation of RNA was determined by using thiolutin as a transcription inhibitor (Das *et al*., 2003; Guo *et al*., 2009). The degradation rate of RNA at light to dark transfer at 25 ºC was determined. In my model, the degradation reaction for RNA is considered as a first order reaction. Therefore, the exponent of the exponential trend line equals the degradation rate. For *frq*, *vvd* and *qrf* RNA, most of RNA was degraded within one hour after light to dark transfer (Figure 3.1 A-D). In addition, the decay of RNA is slower with thiolutin treatment compared with the control. The reason could be because thiolutin stops all transcription including genes involved in RNA degradation pathways, such as RNAse, which may result in the decrease of RNA degradation. *wc-1* and *wc-2* RNA decayed slower than *frq*, *qrf* and *vvd* RNA (Figure 3.1). *frq*, *qrf* and *vvd* RNA degradation rates were averaged with previous experiments (data not shown). RNA degradation rates are shown in table 3.1.

Table 3.1 Decay rates of RNAs

RNA	Decay rate in a.u./hour (number of experiments)
frq	2.469 (6)
qrf	1.866 (6)
wc-1	0.448 (3)
wc-2	0.585 (3)
vvd	2.099 (6)

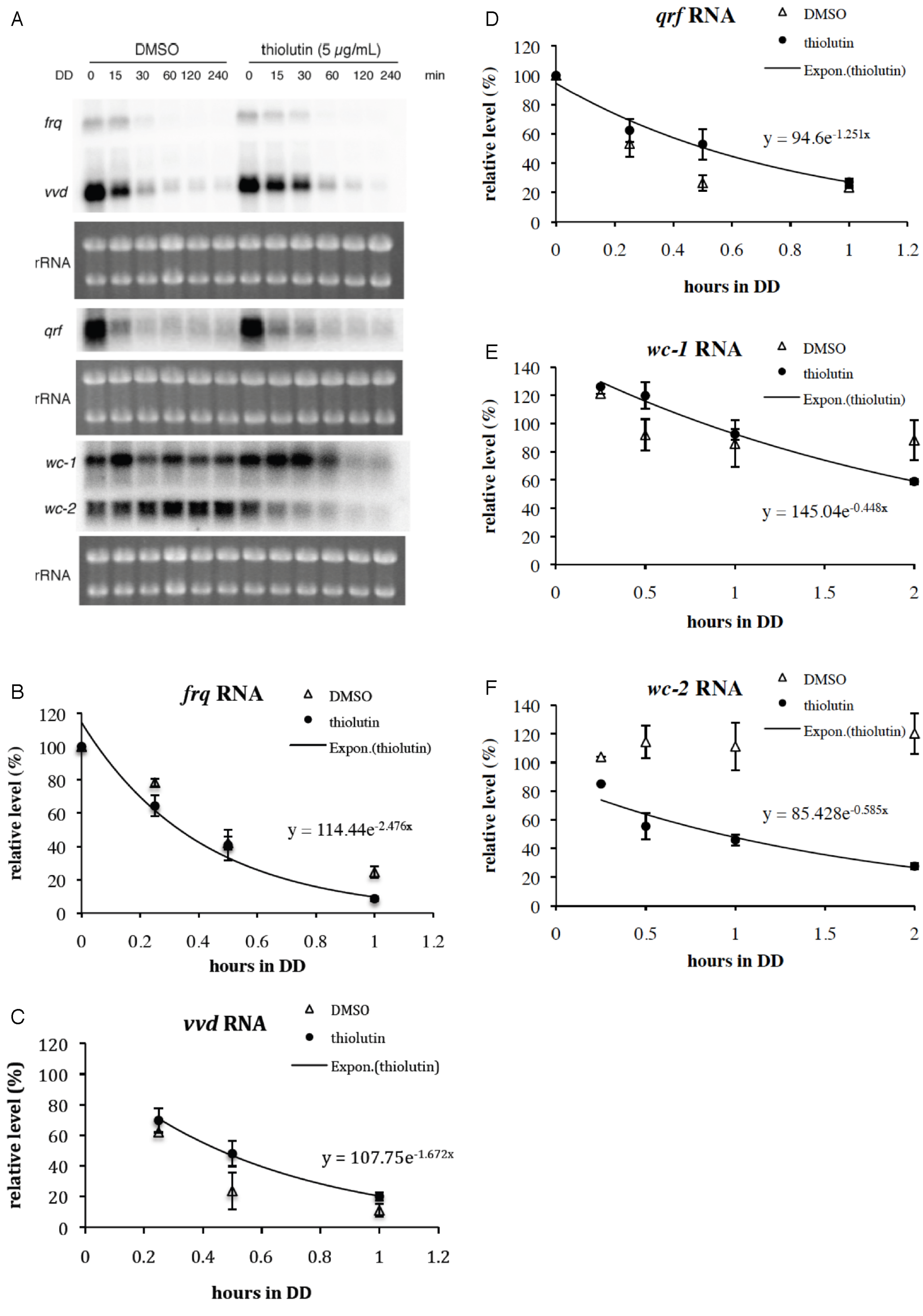

Figure 3.1 Determination of frq and vvd RNA degradation rates.
(A) Northern blot analysis shows the degradation of *frq*, *vvd*, *qrf*, *wc-1* and *wc-2* RNA after light to dark transfer. (B) The densitometric analysis of the results of *frq* RNA. (C) The densitometric analysis of the results of *vvd* RNA. (D) The densitometric analysis of the results of *qrf* RNA. (E) The densitometric analysis of the results of *wc-1* RNA. (F) The densitometric analysis of the results of *wc-2* RNA. The graphs in B - F show the results from three independent experiments. Error bars represent standard error (SE).

3.2.3 The *Neurospora crassa* circadian clock model

The *Neurospora crassa* circadian clock model was constructed through a mechanistic approach (Figure 3.2). The equations used in the model are shown in Appendix 2 and the parameters and their values used in the model are shown in Appendix 3. The model is based on a compilation of published and new experimental data and incorporates facets of previously described *Neurospora* clock models (Hong *et al*., 2008a; Leloup *et al*., 1999b). The development of this model was begun with the *frq* genetic feedback loop modelled in 1999 (Leloup *et al*., 1999b). Next, new components such as *wc-1* and *wc-2* were then added into the model and the equation formats for the degradation of components were simplified with first order equations. The equation format for the transcription regulation was applied from Hong's model (Hong *et al*., 2008a).

3.2.3.1 Modelling transcription

The model centres on the genetic interlocking positive and negative feedback loops created by the interactions of the *frq*, *wc-1* and *wc-2* genes (reviewed in Dunlap and Loros, 2006; Heintzen and Liu, 2007). The *frq*, *wc-1* and *wc-2* genes are transcribed into *frq*, *wc-1* and *wc-2* mRNA (step 1-3), respectively, and translated into hypophosphorylated cytosolic FRQ (hypoFRQc), WC-1 (WC1c) and WC-2 (WC2c) protein (step 5-7).

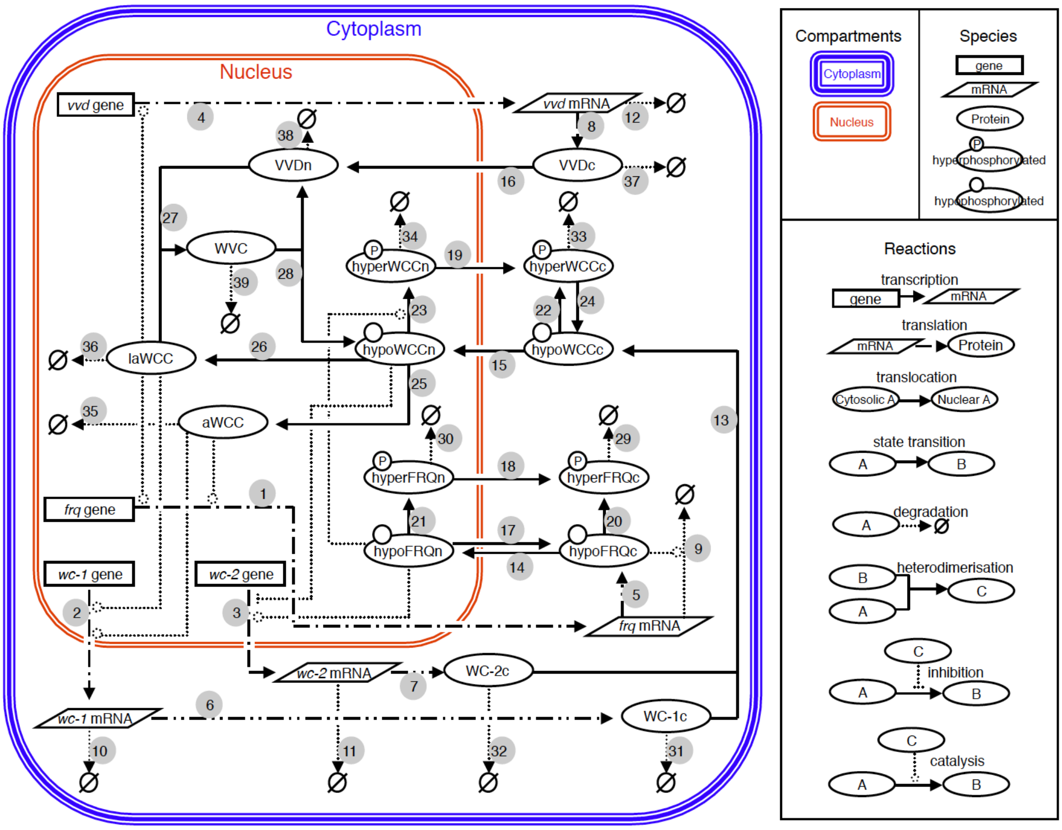

Figure 3.2 The *Neurospora* circadian clock model.
The symbol representations of compartments, species and reactions are shown in the right hand panel. Individual pathways are numbered starting with the transcription of the *frq* gene. *frq* = *frequency*, *wc-1* = *white collar-1*, *wc-2* = *white collar-2*, *vvd* = *vivid*, hypoFRQc = cytosolic hypophosphorylated FREQUENCY (FRQ) protein, hypoFRQn = nuclear hypophosphorylated FRQ, hyperFRQc = cytosolic hyperphosphorylated FRQ, hyperFRQn = nuclear hyperphosphorylated FRQ, WC-1c = cytosolic WHITE COLLAR-1 (WC-1) protein, WC-2c = cytosolic WHITE COLLAR-2 (WC-2) protein, hypoWCCc = cytosolic hypophosphorylated WHITE COLLAR COMPLEX (WCC), hypoWCCn = nuclear hypophosphorylated WCC, hyperWCCc = cytosolic hyperphosphorylated WCC, hyperWCCn = nuclear hyperphosphorylated WCC, aWCC = activated WCC, laWCC = light activated WCC, VVDc = cytosolic VIVID (VVD) protein, VVDn = nuclear VVD, WVC = WCC-VVD complex.

frq transcription is activated by the activated hypophosphorylated WCC. The Hill equation is used to represent the regulation. The kinetic equation of *frq* transcription is as follows:

$$v\_1 = k\_01 \times \frac{[\mathrm{aWCC}]^{H\_01}}{K\_01^{H\_01} + [\mathrm{aWCC}]^{H\_01}} + k\_01a \times [\mathrm{laWCC}]$$

v_1 is the rate of *frq* transcription. *k_01* is the maximum transcription rate constant of *frq*. *K_01* is the Michaelis constant and *H_01* is the Hill coefficient. [aWCC] is the concentration of the activated hypophosphorylated WCC. *k_01a* is an additional transcription rate constant when the system is exposed to light. [laWCC] is the concentration of the light activated hypophosphorylated WCC.

For *wc-1* transcription, three promoters have been identified, which are P_{dist}, P_{prox} and P_{int} (Káldi *et al*., 2006). P_{dist} and P_{prox} are located at 5'-untranslated regions (5'-UTRs). P_{dist} is dependent on WCC and P_{prox} is only dependent on WCC in light. P_{int} is located at 5' of the *wc-1* open reading frame (ORF) and promotes the transcription of a truncated WC-1 isoform. P_{int} is independent of WCC. To model *wc-1* transcription, the kinetic equation is as follows:

$$v\_2 = k\_02 + k\_02a01 \times [\mathrm{aWCC}] + k\_02a02 \times [\mathrm{laWCC}]$$

v_2 is the reaction rate of *wc-1* transcription. *k_02* is the basal transcription rate of *wc-1*, which is assumed to be promoted by P_{int}. *k_02a01* is the WCC dependent transcription rate constant, which is assumed to be promoted by P_{dist}. *k_02a02* is an additional transcription rate constant when the system is exposed to light, which is assumed to be promoted by P_{prox}..

wc-2 transcription is promoted by hypophosphorylated nuclear FRQ (hypoFRQn) (Neiss *et al*., 2008) and *wc-2* transcription is repressed by hypophosphorylated nuclear WCC (hypoWCCn) (Neiss *et al*., 2008) (step 3). To model *wc-2* transcription, the kinetic equation of *wc-2* transcription is as follows:

$$v\_3 = k\_03 \times \frac{1}{1 + [\text{hypoWCCn}] \times k\_03i} + [\text{hypoFRQn}] \times k\_03a$$

v_3 is the reaction rate of *wc-2* transcription. *k_03* is the maximum rate of *wc-2* transcription. The simplified Hill function is used to represent the repression of *wc-2* transcription by WCC. [hypoWCCn] is the concentration of the hypophosphorylated nuclear WCC. *k_03i* is the repression constant. *k_03a* is the additional transcription rate promoted by FRQ. [hypoFRQn] is the concentration of hypophosphorylated nuclear FRQ.

3.2.3.2 Modelling translation

For translation, first order reactions were considered in the model. The translation rate is dependent on the concentration of RNA. The kinetic equation for *frq*, *wc-1* and *wc-2* translation are as follows:

$$v\_5 = k\_05 \times [\textit{frq}\ \text{mRNA}]$$

$$v\_6 = k\_06 \times [wc-1\ \text{mRNA}]$$

$$v\_7 = k\_07 \times [wc\text{ - }2\ \text{mRNA}]$$

v_5-7 are the reaction rates of *frq*, *wc-1*, *wc-2* and *vvd* translation, respectively. *k_05-07* are translation rate constants of *frq*, *wc-1*, *wc-2* and *vvd* translation, respectively. [*frq* mRNA], [*wc-1* mRNA] and [*wc-2* mRNA] are concentrations of *frq*, *wc-1* and *wc-2* RNAs, respectively.

3.2.3.3 Modelling RNA degradation

Step 9 is the degradation of *frq* mRNA. *frq* mRNA degradation is facilitated by the FRQ-FRH complex and the degradation rate is dependent on FRQ concentration (Guo *et al*., 2009; Guo *et al*., 2010). The kinetic equation is as follows:

$$v\_9 = [\textit{frq}\ \text{mRNA}] \times (k\_09 + [\text{hypoFRQc}] \times k\_09a)$$

v_9 is the reaction rate of *frq* RNA degradation. *k_09* is the basal degradation rate constant of *frq* RNA. *k_09a* is the additional degradation rate constant of *frq* RNA facilitated by FRQ. [hypoFRQc] is the concentration of hypophosphorylated cytosolic FRQ.

Steps 10 and 11 are degradation reactions *wc-1* and *wc-2* mRNA. Degradation reactions of *wc-1* mRNA and *wc-2* mRNA were considered as first order reactions in the model. The degradation rate is dependent on the concentration of RNA. The kinetic equations for *wc-1* and *wc-2* RNA degradation are as follows:

$$v\_10 = k\_10 \times [wc\text{-}1 \text{ mRNA}]$$

$$v\_11 = k\_11 \times [wc\text{-}2 \text{ mRNA}]$$

$$v\_12 = k\_12 \times [vvd \text{ mRNA}]$$

v_10-12 are the reactions of *wc-1*, *wc-2* and *vvd* RNA degradation, respectively. *k_10-12* are degradation rates of *wc-1*, *wc-2* and *vvd* RNA, respectively.

3.2.3.4 Modelling WCC

Once translated, cytoplasmic WC-1 (WC1c) and WC-2 (WC2c) bind to each other to form the hypophosphorylated cytosolic WHITE-COLLAR complex (hypoWCCc) (step 13). The formation rate of WCC is dependent on the concentration of WC-1 and WC-2 in the model. The kinetic equation is as follows:

$$v\_13 = k\_13 \times [\text{WC1c}] \times [\text{WC2c}]$$

v_13 is the reaction rate of WCC formation. *k_13* is the WCC formation rate constant. [WC-1c] and [WC-2c] are concentrations of cytoplasmic WC-1 and WC-2, respectively.

After WCC is produced, WCC translocates into the nucleus (step 15). The kinetic equation of hypophosphorylated WCC nuclear localisation is as follows:

$$v\_15 = k\_15 \times [\mathrm{hypoWCCc}]$$

The reaction rate of hypophosphorylated WCC (hypoWCCc) nuclear localisation is dependent on the concentration of hypoWCCc. *v_15* is the reaction rate of hypoWCCc nuclear localisation. [hypoWCCc] is the concentration of hypoWCCc.

In the model, only a small fraction of WCC is activated (activated WCC) from nuclear hypophosphorylated WCC (hypoWCCn) (step 25) (Schafmeier *et al*., 2008). The kinetic equation is as follows:

$$v\_25 = k\_25 \times [\mathrm{hypoWCCn}]$$

The activation rate of WCC is dependent on the concentration of hypoWCCn. *v_25* is the reaction rate of WCC activation and *k_25* is the WCC activation rate constant. Activated WCC promotes the transcription of *frq* and *wc-1* genes (steps 1 and 2) (Froehlich *et al*., 2003; Káldi *et al*., 2006) and as a consequence is degraded (Schafmeier *et al*., 2008) (step 35).

Hypophosphorylated cytosolic WCC (hypoWCCc) and nuclear WCC (hypoWCCn) can be phosphorylated in the cytoplasm and in the nucleus (step 22 and 23). The kinetic equations are as follows:

$v\_22 = k\_22 \times [\text{hypoWCCc}]$

$$v\_23 = k\_23 \times [\text{hypoWCCn}] \times \frac{[\text{hypoFRQn}]^{H\_23}}{K\_02^{H\_23} + [\text{hypoFRQn}]^{H\_23}}$$

v_22-23 are the reaction rates of cytoplasmic and nuclear WCC phosphorylation, respectively. In the cytoplasm, the phosphorylation of WCC is dependent on its own concentration. *k_22* is the rate constant of cytoplasmic WCC phosphorylation. [hypoWCCc] is the concentration of hypoWCCc. In the nucleus, this reaction is promoted by hypoFRQn. *k_23* is the maximum phosphorylation rate constant of nuclear WCC phosphorylation. [hypoWCCn] is the concentration of hypophosphorylated nuclear WCC. The Hill function is also used here to represent the facilitating of WCC phosphorylation by FRQ. *K_02* is the Michaelis constant and *H_23* is the Hill coefficient. [hypoFRQn] is the concentration of hypophosphorylated nuclear FRQ. Hypophosphorylated nuclear FRQ (hypoFRQn) facilitates the phosphorylation of hypoWCCn (Schafmeier *et al*., 2005) (step 23) and clearance of WCC from the nucleus (Schafmeier *et al*., 2008). Thus, FRQ negatively regulates its own expression and positively regulates the accumulation of WCC.

Hyperphosphorylated nuclear WCC (hyperWCCn) is translocated out of the nucleus (step 19) to the cytoplasm where it can be dephosphorylated (step 24) (Schafmeier *et al*., 2008). The kinetic equations are as follows:

$v\_19 = k\_19 \times [\text{hyperWCCn}]$

$v\_24 = k\_24 \times [\text{hyperWCCc}]$

v_19 and v_24 are the reaction rates of hyperWCCn translocation out of the nucleus and cytosolic WCC dephosphorylation. k_19 and k_24 are hyperWCCn translocation rate out of the nucleus and cytosolic WCC dephosphorylation rate, respectively. [hyperWCCn] and [hyperWCCc] are the concentration of hyperphosphorylated cytosolic WCCn and hyperphosphorylated cytosolic WCC, respectively.

3.2.3.5 Modelling FRQ

Once translated, FRQ forms a homodimer that interacts with the FRQ-interacting helicase FRH (Cheng *et al*., 2005); in the model this complex is represented by FRQ. Hypophosphorylated FRQ (hypoFRQ) shuttles into (step 14) and out of (step 17) the nucleus (Diernfellner *et al*., 2009) and is progressively phosphorylated in both the cytoplasm (step 20) and the nucleus (step 21) (reviewed in Brunner and Schafmeier, 2006). For hypoFRQ translocation, the kinetic equations are as follows:

$v\_14 = k\_14 \times [\text{hypoFRQc}]$

$v\_17 = k\_17 \times [\text{hypoFRQn}]$

v_14 and v_17 are the reaction rates of hypoFRQ shuttling into and out of the nucleus, respectively. k_14 and k_17 are rate constants. [hypoFRQc] and [hypoFRQn] are concentrations of cytoplasmic and nuclear hypophosphorylated FRQ, respectively.

For FRQ phosphorylation, the kinetic equations are shown as follow:

$v\_20 = k\_20 \times [\text{hypoFRQc}]$

$v\_21 = k\_21 \times [\text{hypoFRQn}]$

v_20-21 are the reaction rates of cytosolic and nuclear FRQ, respectively. *k_20-21* are phosphorylation rates of cytosolic and nuclear, respectively.

Hyperphosphorylated nuclear FRQ (hyperFRQn) is translocated out of the nucleus (step 18) and accumulates in the cytoplasm (Diernfellner *et al*., 2009). This is represented by:

$v\_18 = k\_18 \times [\text{hyperFRQn}]$

v_17-19 are the reactions of hypophosphorylated FRQ, hyperphosphorylated FRQ and hyperphosphorylated WCC translocation out of the nucleus, respectively. *k_17-19* are their translocation rates out of the nucleus, respectively. [hypoFRQn], [hyperFRQn] and [hypoWCCn] are concentrations of hypophosphorylated nuclear FRQ, hyperphosphorylated nuclear FRQ, hypophosphorylated nuclear, respectively.

$v\_14 = k\_14 \times [\text{hypoFRQc}]$

$v\_15 = k\_15 \times [\text{hypoWCCc}]$

v_14-15 are the reactions of FRQ and WCC nuclear localisation, respectively. *k_14-15* are nuclear localisation rates of FRQ and WCC, respectively. [hypoFRQc] and [hypoWCCc] are concentrations of hypophosphorylated cytosolic FRQ and hypophosphorylated cytosolic WCC, respectively.

3.2.3.6 Modelling protein degradation

Steps 29-36 are degradation reactions of protein components in the model. FRQ can be degraded in the cytoplasm (step 29) and nucleus (step 30). Step 31 and 32 are degradation of cytoplasmic WC-1 and WC-2, respectively. WCC can be degraded in the cytoplasm (step 33) and nucleus (step 34). hyperWCCn and activated WCC, respectively. Step 31 and 32 are degradation of activated WCC and light activated WCC. The kinetic equations are as follows:

$v\_29 = k\_29 \times$[hyperFRQc]

$v\_30 = k\_30 \times$[hyperFRQn]

$v\_31 = k\_31 \times$[WC1c]

$v\_32 = k\_32 \times$[WC2c]

$v\_33 = k\_33 \times$[hyperWCCc]

$v\_34 = k\_34 \times$[hyperWCCn]

$v\_35 = k\_35 \times$[aWCC]

$v\_36 = k\_36 \times$[laWCC]

The degradation rate is dependent on the protein component's own concentration. *v_29-36* are degradation rates of the protein components in the model and *k_29-36* are degradation rate constants of each reaction.

3.2.4 Clock simulation in constant darkness

From experimental data, *frq* mRNA and protein is rhythmically expressed in continuous darkness (DD). *frq* mRNA is peaking at CT 0-4 with a period of 21.6 h and FRQ protein peaking 3-7 hours later (Figure 3.3A) (Garceau *et al.*, 1997). A plot of the simulated oscillations of *frq* mRNA and FRQ protein (Figure 3.3B) shows that the period (21.6 h) and amplitude of *frq* mRNA and FRQ are similar to experimental results. The delay between peak levels of *frq* and FRQ is 4.3 hours, which lies inside the range of experimental results. The simulated behaviours of these core clock components are in agreement with the experimental data from Garceau *et al*. (1997).

For *wc-1* expression, the *wc-1* transcript is constantly produced and the level is not rhythmic. However, the WC-1 protein oscillates with peak levels around 18-20 hours after the light to dark transition, 8 hours after the peak levels of FRQ (Figure 3.4A) (Lee *et al*., 2000). These properties are correctly reproduced by the model (Figure 3.4B).

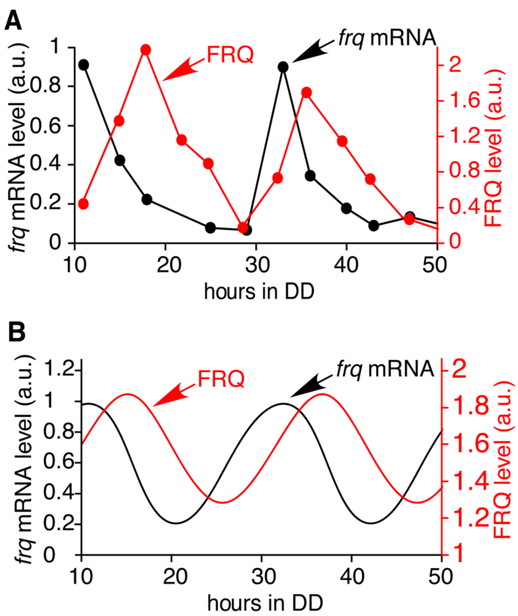

Figure 3.3 Continuous dark simulations of *frq* mRNA and FRQ oscillation.
(A) Experimental data showing the oscillation of *frq* mRNA and FRQ protein levels (Garceau *et al*., 1997). The period length is approximately 22 hours, and FRQ (red line) peaks 3-7 hours after *frq* mRNA (black line). (B) Simulated results showing the oscillation of *frq* mRNA and FRQ protein levels has a period of 21.6 hours, and FRQ peaks 4.4 hours after *frq* mRNA. Simulation begins 10 hours after a light to dark transfer, 10 data points per hour.

wc-2 transcription is also not rhythmic and the level of *wc-2* RNA is similar to *wc-1* RNA level (data not shown). From experimental data, the level of WC-2 protein is 5-30 times higher than the average level of FRQ and WC-1 protein (Figure 3.7A) (Denault *et al*., 2001). However, after 18 hours in constant darkness, the level of WC-2 is about 5 times higher than the level of FRQ and WC-1 oscillation. The relative levels of FRQ, WC-1 and WC-2 are successfully reproduced by the model. Figure 3.5A and 3.5B show that there is a good match between experimentally determined (Denault *et al*., 2001) and simulated levels of clock proteins.

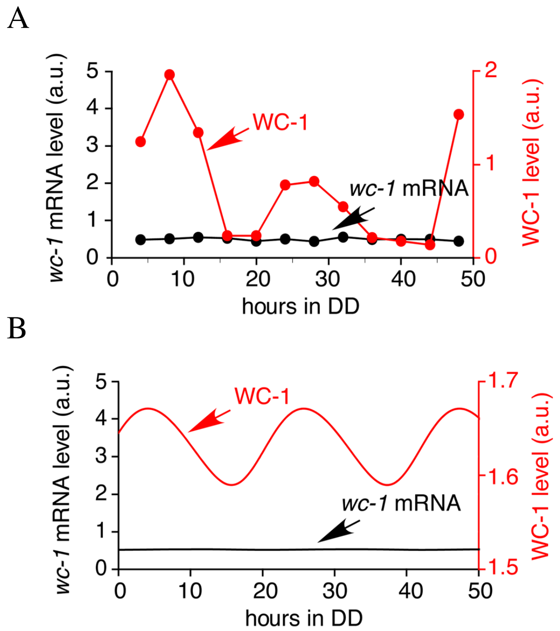

Figure 3.4 Continuous dark simulations of *wc-1* mRNA and WC-1 expression. (A) Experimental data showing *wc-1* mRNA and WC-1 protein levels (Lee *et al*., 2000). The level of *wc-1* mRNA is nearly constant. WC-1 protein expression oscillates. (B) Simulated results. *wc-1* mRNA (black line) level is constant and WC-1 oscillates. Simulation begins at the light to dark transfer, 10 data points per hour.

A

B

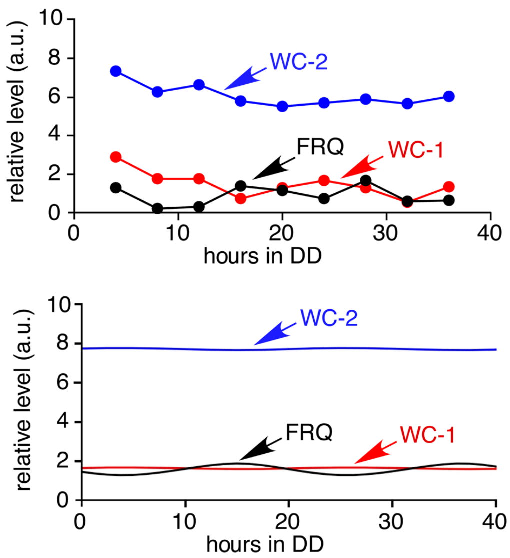

Figure 3.5 Continuous dark simulations of FRQ, WC-1 and WC-2.
(A) The level of WC-2 protein is 5-30 times higher than the average level of FRQ and WC-1 protein (Denault *et al*., 2001). (B) In the model WC-2 protein is 10 times higher than the average level of FRQ and WC-1 proteins. Simulation begins at the light to dark transfer, 10 data points per hour are plotted.

3.2.5 Model robustness to parameter perturbation

Robustness of the model was determined by testing a range of parameter values to discover the limits within which the period and amplitude of *frq* RNA was maintained within experimentally defined values. To evaluate the robustness of the model, I determined the range of each parameter value in which rhythmicity was maintained, and in which the period and amplitude of the rhythm remained within experimentally defined limits. The oscillation of *frq* RNA was used as the reference for these tests. To determine how much each parameter value can change while still generating oscillations, each parameter was increased and decreased until *frq* RNA oscillation was lost (Table 3.2). The results show that 8 parameters are restricted to a fairly small range of values, 12 parameters can be decreased to zero, 8 parameters can be increased to infinity and 4 parameters can take any value without losing oscillations.

Table 3.2 Parameter sensitivity test for oscillations

For each parameter, the table gives the lower and upper value that conserves *frq* RNA oscillations, as well as the percentage change with respect to its reference value.

ID	Parameter name	Reference value	Lowest value generating oscillations	Highest value generating oscillations	Percentage change for lowest value	Percentage change for highest value
k_10	*kd_wc1*	2.4	1.206	2.471	-49.75	2.96
k_35	*kd_aWCC*	1.29	0.633	1.3266	-50.93	2.84
k_06	*k_WC1*	0.226	0.218	0.455	-3.54	101.33
k_02	*k_wc1*	1.19	1.148	2.47	-3.53	107.56
k_25	*kact_hypoWCCn*	0.15	0.0545	0.301	-63.67	100.67
k_02a01	*ka_wc1*	1.2	0.68	18.1	-43.33	1408.33
k_01	*k_frq*	7.3	6.5	125	-10.96	1612.33
k_05	*k_FRQ*	0.19	0.168	3.3	-11.58	1636.84
k_09	*kd_frq*	2	0	2.202	-100.00	10.10
k_21	*kp_hypoFRQn*	0.1	0	0.1146	-100.00	14.60
k_20	*kp_hypoFRQc*	0.1	0	0.1163	-100.00	16.30
k_33	*kd_hyperWCCc*	0.05	0	0.0601	-100.00	20.20
k_22	*kp_hypoWCCc*	0.3	0	0.3615	-100.00	20.50
k_17	*kout_hypoFRQn*	0.1	0	0.1216	-100.00	21.60
k_11	*kd_wc2*	2.5	0	3.71	-100.00	48.40
k_09a	*kd_frq_FRQ*	0.356	0	0.564	-100.00	58.43
k_32	*kd_WC2*	0.085	0	0.1405	-100.00	65.29
k_31	*kd_WC1*	0.135	0	0.224	-100.00	65.93
k_34	*kd_hyperWCCn*	0.05	0	0.123	-100.00	146.00
k_03i	*ki_wc2*	0.03	0	0.86	-100.00	2766.67
k_14	*kin_hypoFRQc*	0.1	0.09	∞	-10.00	∞
k_15	*kin_hypoWCCc*	0.3	0.245	∞	-18.33	∞
k_24	*kdp_hyperWCCc*	0.3	0.243	∞	-19.00	∞
k_07	*k_WC2*	1	0.674	∞	-32.60	∞
k_03	*k_wc2*	1.6	1.075	∞	-32.81	∞
k_13	*k_WCC*	0.472	0.285	∞	-39.62	∞
k_23	*kp_hypoWCCn*	0.6	0.346	∞	-42.33	∞
k_19	*kout_hyperWCCn*	0.29	0.062	∞	-78.62	∞
k_03a	*ka_wc2*	0.03	0	∞	-100.00	∞
k_18	*kout_hyperFRQn*	0.3	0	∞	-100.00	∞
k_29	*kd_hyperFRQc*	0.27	0	∞	-100.00	∞
k_30	*kd_hyperFRQn*	0.27	0	∞	-100.00	∞

Parameters are sorted into four categories: (1) parameters constrained to a fairly small range of values, (2) parameters that can decrease to zero, (3) parameters that can increase to infinity, and (4) parameters that can take any value without losing oscillations. The average absolute percentage difference is used to rank the parameters according to their sensitivity.

To understand how parameters affect the period and how it is comparable to experimental data, I first determined how much each parameter value can change while the period of *frq* RNA remains compatible with the experimental wild-type *Neurospora* clock period, taking a reference value of 21.6 hours and an experimental standard error of 0.6 hours (estimated from race tube experiments). Each parameter was increased and decreased until the period was increased or decreased outside the range of 21.6 ± 0.6 hours (Table 3.3). Some parameters are highly sensitive since the oscillation is lost before the target increase or decrease of period can be reached, such as *kd_aWCC, kin_hypoFRQc, kd_frq,* and *kd_wc2*. Other parameters can be modified in a certain range of values while remaining compatible with the experimental range of observed periodicity, such as *k_wc1, k_WC1, kd_wc1* and *k_FRQ*.

Table 3.3 Parameter sensitivity test for period

For each parameter, the table gives the lower and upper value for which a period of 21.6 ± 0.6 hours is obtained for *frq* RNA oscillations, as well as the percentage change with respect to its reference value.

ID	Parameter name	Reference value	Value for 21 h period	Value for 22.2 h period	Percentage change for 21 h period	Percentage change for 22.2 h period
k_35	*kd_aWCC*	1.29	1.232	arrhythmic	-4.50	arrhythmic
k_14	*kin_hypoFRQc*	0.1	0.112	arrhythmic	12.00	arrhythmic
k_09	*kd_frq*	2	1.595	arrhythmic	-20.25	arrhythmic
k_11	*kd_wc2*	2.5	0.5	arrhythmic	-80.00	arrhythmic
k_17	*kout_hypoFRQn*	0.1	arrhythmic	0.006	arrhythmic	-94.00
k_02a01	*ka_wc1*	1.2	2.34	arrhythmic	95.00	arrhythmic
k_31	*kd_WC1*	0.135	0	arrhythmic	-100.00	arrhythmic
k_32	*kd_WC2*	0.085	0	arrhythmic	-100.00	arrhythmic
k_23	*kp_hypoWCCn*	0.6	1.648	arrhythmic	174.67	arrhythmic
k_07	*k_WC2*	1	6.2	arrhythmic	520.00	arrhythmic
k_13	*k_WCC*	0.472	3.35	arrhythmic	609.75	arrhythmic
k_03	*k_wc2*	1.6	28	arrhythmic	1650.00	arrhythmic
k_03i	*ki_wc2*	0.03	n/a	arrhythmic	n/a	arrhythmic
k_09a	*kd_frq_FRQ*	0.356	n/a	arrhythmic	n/a	arrhythmic
k_20	*kp_hypoFRQc*	0.1	n/a	arrhythmic	n/a	arrhythmic
k_21	*kp_hypoFRQn*	0.1	n/a	arrhythmic	n/a	arrhythmic
k_02	*k_wc1*	1.19	1.24	1.152	4.20	-3.19
k_06	*k_WC1*	0.226	0.2352	0.2184	4.07	-3.36
k_10	*kd_wc1*	2.4	2.29	2.47	-4.58	2.92
k_05	*k_FRQ*	0.19	0.21	0.17	10.53	-10.53
k_01	*k_frq*	7.3	8.3	6.63	13.70	-9.18
k_25	*kact_hypoWCCn*	0.15	0.17	0.135	13.33	-10.00
k_15	*kin_hypoWCCc*	0.3	0.36	0.256	20.00	-14.67
k_24	*kdp_hyperWCCc*	0.3	0.36	0.255	20.00	-15.00
k_33	*kd_hyperWCCc*	0.05	0.04	0.06	-20.00	20.00
k_22	*kp_hypoWCCc*	0.3	0.24	0.36	-20.00	20.00
k_19	*kout_hyperWCCn*	0.29	0.45	0.21	55.17	-27.59
k_34	*kd_hyperWCCn*	0.05	0.015	0.11	-70.00	120.00
k_03a	*ka_wc2*	0.03	20	n/a	66566.67	n/a
k_18	*kout_hyperFRQn*	0.3	n/a	n/a	n/a	n/a
k_29	*kd_hyperFRQc*	0.27	n/a	n/a	n/a	n/a
k_30	*kd_hyperFRQn*	0.27	n/a	n/a	n/a	n/a

Parameters are sorted into different categories: (1) the clock becomes arrhythmic before the target value of the period can be reached, (2) the target period values are reached for a fixed change in the parameter value, (3) the oscillations are maintained but no parameter value is able to achieve the desired period length (n/a).

A similar approach was taken to determine how much each parameter value can change while remaining compatible with the experimental amplitude of *frq* RNA oscillations, taking an uncertainty of ± 5 %. Each parameter was increased and decreased until the *frq* RNA oscillation amplitude was increased or decreased by 5 % of its original value (Table 3.4). Most parameters are highly constrained by the amplitude; 25 parameters cannot be changed by more than 10 % without changing the amplitude by more than 5 %. The remaining 7 parameters can take a large range of values without affecting the amplitude strongly.

Taken together, these tests show that with the exception of *ka_wc2* (FRQ-induced transcription of *wc-2*), *kout_hyperFRQn* (translocation of phosphorylated FRQ out of the nucleus), *kd_hyperFRQc* and *kd_hyperFRQn* (degradation of phosphorylated FRQ in the cytoplasm and nucleus, respectively), most parameters are highly constrained. The low sensitivity of FRQ-induced transcription of *wc-2* (*ka_wc2*) is expected because the basal transcription level of *wc-2* is high in comparison to *ka_wc2*. The low sensitivity of hyperphosphorylated FRQ related parameters is due to the fact that hyperphosphorylated FRQ has no function in creating oscillations in the model. The high sensitivity of other parameters suggests that if the clock properties are to be maintained over a wide range of environmental conditions, complex adjustments of multiple parameters are necessary.

Table 3.4 Parameter sensitivity test for amplitude

For each parameter, the table gives the lower and upper value for which the amplitude of *frq* RNA of oscillations is changed by ± 5 %, as well as the percentage change with respect to its reference value.

ID	Parameter name	Reference value	Value for 5 % decrease of amplitude (0.741)	Value for 5 % increase of amplitude (0.819)	Percentage change for 5 % decrease of amplitude (0.741)	Percentage change for 5 % increase of amplitude (0.819)
k_35	*kd_aWCC*	1.29	1.294	1.2856	0.31	-0.34
k_10	*kd_wc1*	2.4	2.4076	2.3916	0.32	-0.35
k_06	*k_WC1*	0.226	0.22529	0.2268	-0.31	0.35
k_02	*k_wc1*	1.19	1.186	1.1945	-0.34	0.38
k_01	*k_frq*	7.3	7.235	7.372	-0.89	0.99
k_09	*kd_frq*	2	2.02	1.978	1.00	-1.10
k_05	*k_FRQ*	0.19	0.18795	0.19242	-1.08	1.27
k_14	*kin_hypoFRQc*	0.1	0.0987	0.1015	-1.30	1.50
k_21	*kp_hypoFRQn*	0.1	0.10173	0.0978	1.73	-2.20
k_33	*kd_hyperWCCc*	0.05	0.05095	0.04898	1.90	-2.04
k_20	*kp_hypoFRQc*	0.1	0.10196	0.0977	1.96	-2.30
k_22	*kp_hypoWCCc*	0.3	0.3063	0.2932	2.10	-2.27
k_24	*kdp_hyperWCCc*	0.3	0.293432	0.3074	-2.19	2.47
k_15	*kin_hypoWCCc*	0.3	0.293043	0.3081	-2.32	2.70
k_17	*kout_hypoFRQn*	0.1	0.1025	0.09724	2.50	-2.76
k_02a01	*ka_wc1*	1.2	1.141	1.265	-4.92	5.42
k_09a	*kd_frq_FRQ*	0.356	0.376	0.3344	5.62	-6.07
k_11	*kd_wc2*	2.5	2.64	2.34	5.60	-6.40
k_07	*k_WC2*	1	0.946	1.068	-5.40	6.80
k_23	*kp_hypoWCCn*	0.6	0.566	0.64	-5.67	6.67
k_03	*k_wc2*	1.6	1.512	1.712	-5.50	7.00
k_32	*kd_WC2*	0.085	0.0908	0.0784	6.82	-7.76
k_31	*kd_WC1*	0.135	0.1445	0.1245	7.04	-7.78
k_13	*k_WCC*	0.472	0.4408	0.512	-6.61	8.47
k_34	*kd_hyperWCCn*	0.05	0.0547	0.0453	9.40	-9.40
k_25	*kact_hypoWCCn*	0.15	0.1212	n/a	-19.20	n/a
k_19	*kout_hyperWCCn*	0.29	0.21725	n/a	-25.09	n/a
k_03i	*ki_wc2*	0.03	0.13	n/a	333.33	n/a
k_03a	*ka_wc2*	0.03	n/a	0.326	n/a	986.67
k_18	*kout_hyperFRQn*	0.3	n/a	n/a	n/a	n/a
k_29	*kd_hyperFRQc*	0.27	n/a	n/a	n/a	n/a
k_30	*kd_hyperFRQn*	0.27	n/a	n/a	n/a	n/a

Parameters are sorted into two categories: (1) the target amplitude values are reached for a fixed change in the parameter value, (2) no parameter value is able to achieve the desired amplitude (n/a).

3.3 Summary

This chapter presents a comprehensive model of the *Neurospora* circadian clock. This model successfully reproduces a variety of clock characteristics in constant darkness, including a period of 21.6 hours, correct levels and phases of key clock components, and the phenotypes of *Neurospora* with a mutant form WC-2 ($wc\text{-}2^{ER24}$) or an inducible copy of *wc-1* (qa-WC-1). In addition, while developing the model, some reactions were found to be important for generating oscillations and to have the correct phase of clock components. For example, the Hill coefficient of *frq* transcription needed to be larger than 4 to generate oscillations. The basal level of *wc-1* transcription is important for reproducing the antiphasic behaviour between FRQ and WCC. In addition, the effects of parameters on the period and amplitude of the central oscillator *frq* RNA were quantified. Consequently, this model is a powerful tool to analyse circadian rhythms in *Neurospora* and can be used to make and test predictions of light and temperature effects on the clock.

Chapter 4

Light resetting of the clock and modeling of light reactions

4. Light resetting of the clock and modeling of light reactions

4.1 Introduction

One of the major properties of circadian clocks is that the clock can be reset and entrained by environmental factors. Light is an important environmental time cue that circadian clocks interact with. In the previous chapter I showed that the *Neurospora* circadian clock model is working properly in constant darkness. To further test if the model is able to reproduce interactions of the clock with the environment, the effect of light needed to be introduced into the model.

In *Neurospora*, WC-1 and VVD are blue light receptors for the clock. Therefore, to model the clock's interaction with light, *vvd* components and mechanisms of light activation and photoadaptation were introduced into the model. Simulated results showed that the *Neurospora* circadian clock model is working properly with light and successfully reproducing several characteristics of the light response, including resetting the clock by light pulses, light-dark cycles, photoadaptation and phase response curves. However, the simulated results showed that the phase of *frq* mRNA was delayed by approximately two hours compared to the experimentally determined phase. Experiments were carried out to discover the possible mechanism of supporting the phase resetting after light to dark transfer and the results suggested that *qrf* may regulate *frq* expression by affecting the stability of *frq* mRNA.

4.2 Modelling light response

Light is one of the main environmental time cues for the circadian clock of *Neurospora*. Stimulation of light resets the phase of the clock and 12 h: 12 h light: dark cycles entrain the period of the clock to 24 h (Dharmananda, 1980). At the molecular level, WC-1 and VVD are blue light receptors (Froehlich *et al.*, 2002; Linden *et al.*, 1997; Schwerdtfeger and Linden, 2003). The activation of WC-1 by light results in homo-dimerisation of WCC and rapid expression of light controlled genes, including *frq*, *wc-1* and *vvd* (Chen *et al.*, 2010; Heintzen *et al.*, 2001; Malzahn *et al.*, 2010). VVD is the repressor of light response. VVD interacts with the light activated WCC (L-WCC) and competes with the dimerisation of L-WCC. This results in the formation of the WCC VVD complex (WVC) and inactivates L-WCC (Chen *et al.*, 2010; Heintzen *et al.*, 2001; Malzahn *et al.*, 2010).

4.2.1 Incorporating light components into the model

To simulate the response of the *Neurospora* clock to light, the reaction of WCC light activation and an additional component, light-activated WCC (L-WCC), were incorporated into the model (step 26 in Figure 3.4); L-WCC was activated from nuclear hypophosphorylated WCC. The kinetic equation of WCC light activation is as follows:

$$v\_26 = k\_26 \times [\text{hypoWCCn}]$$

v_26 is the reaction rate of WCC light activation. *k_26* is the WCC light activation rate constant. The value of *k_26* was set to 0 in dark and 5 in light, which assumes that 5 is the maximum value of the WCC light activation rate constant in full light.

These parameter values were determined by the results of simulations in light so as to reproduce the phenotypes of light response, such as the relative level of clock components in light and the phase of *frq* RNA after light to dark transfer. [hypoWCCn] is the concentration of nuclear hypophosphorylated WCC. Furthermore, step 36 is the degradation of L-WCC. The kinetic equation is as follow:

$v\_36 = k\_36 \times$ [laWCC]

v_36 is the degradation rate of L-WCC. *k_36* is the degradation rate constant of L-WCC.

To model the mechanism of light reactions and photoadaptation, the *vvd* gene, *vvd* RNA and its protein product VVD were also introduced into the model. The expression of *vvd* is clock-controlled, but after the first day in constant darkness its expression is much reduced (no expression can be detected by northern blot). L-WCC was found to bind to the light response element (LRE) of the *vvd* promoter (He and Liu, 2005). Therefore, *vvd* transcription is assumed to be activated only by L-WCC in the model. Step 4, 8 and 16 in Figure 3.4 are reactions of *vvd* transcription, translation, and nuclear localisation of VVD. The kinetic equations are as follow:

$v\_4 = k\_04 \times$ [laWCC]

$v\_8 = k\_08 \times$ [*vvd* mRNA]

$v\_16 = k\_16 \times$ [VVDc]

v_4, 8 and *16* are the reaction rates of *vvd* transcription, translation, and nuclear localisation of VVD, respectively. *k_04, 08* and *16* are the rate constants of *vvd* transcription, translation, and nuclear localisation of VVD, respectively. [laWCC], [*vvd* mRNA] and [VVDc] are the concentrations of light-activated WCC (L-WCC), vvd mRNA and cytosolic VVD, respectively. The transcription of *vvd* is only activated in light. The degradation of *vvd* component was also considered (step 12, 37 and 38). The kinetic equations are as follow:

$$v\_12 = k\_12 \times [vvd \text{ mRNA}]$$

$$v\_37 = k\_37 \times [\text{VVDc}]$$

$$v\_38 = k\_38 \times [\text{VVDn}]$$

v_12, 37 and *38* are the degradation rates of *vvd* mRNA, cytoplasmic VVD (VVDc), and nuclear VVD (VVDn), respectively. *k_12, 37* and *38* are the degradation rate constants of *vvd* mRNA, VVDc, and VVDn, respectively. [*vvd* mRNA], [VVDc] and [VVDn] are the concentrations of of *vvd* mRNA, VVDc, and VVDn, respectively.

L-WCC also strongly activates transcription of *frq* and *wc-1* (step 1 and 2). As described in chapter 3, the additional transcription step activated by L-WCC is included in step 1 and 2:

$$v\_1 = k\_01 \times \frac{[\text{aWCC}]^{H\_01}}{K\_01^{H\_01} + [\text{aWCC}]^{H\_01}} + k\_01a \times [\text{laWCC}]$$

$$v\_2 = k\_02 + k\_02a01 \times [\text{aWCC}] + k\_02a02 \times [\text{laWCC}]$$

In the last part of both of the equations, *k_01a* and *02a02* are the rate constants of light-activated *frq* and *wc-1* transcription, respectively. The additional transcription is dependent on the concentration of L-WCC ([laWCC]).

Photoadaptation occurs as L-WCC function is quickly diminished by the formation of the L-WCC VVD complex (WVC) (step 27). The kinetic equation is as follow:

$v\_27 = k\_27 \times [\text{laWCC}] \times [\text{VVDn}]$

v_27 is the rate of WVC formation. *k_27* is the rate constant of WVC formation. The formation of WVC is dependent on the concentration of L-WCC ([laWCC]) and VVDn ([VVDn]). After interacting with VVD, the L-WCC dissociates and returns to its dark state (step 28) (Malzahn *et al*., 2010). The kinetic equation is as follow:

$v\_28 = k\_28 \times [\text{WVC}]$

v_28 is the rate of WVC disassociation. *k_28* is the rate constant of WVC dissociation. The dissociation of WVC is dependent on the concentration of WVC ([WVC]). The degradation of WVC is also modelled. The kinetic equation is as follow:

$v\_39 = k\_39 \times [\text{WVC}]$

v_39 is the rate of WVC degradation. *k_39* is the rate constant of WVC degradation. The degradation of WVC is dependent on the concentration of WVC ([WVC]).

4.2.2 Simulation of light resetting

Light results in a rapid but transient increase of *frq* mRNA and FRQ protein (Crosthwaite *et al*., 1995; Merrow *et al*., 2001), after which levels of *frq* RNA and FRQ quickly drop to a level close to their peak levels in darkness (Figure 4.1). When light turns off, levels of *frq* RNA and FRQ decreased to the trough in darkness and then the cycle of *frq* RNA and FRQ expression starts. The model successfully simulates the phenotypes of the clock in constant light and in constant darkness. Although the phase of the clock is delayed by approximately two hours in simulations compared to the experimentally determined phase, the magnitude of the delay can be increased or decreased by changing the kinetics of FRQ-dependent *frq* RNA degradation (Guo *et al*., 2009) and of VVD's interaction with light-activated WCC.

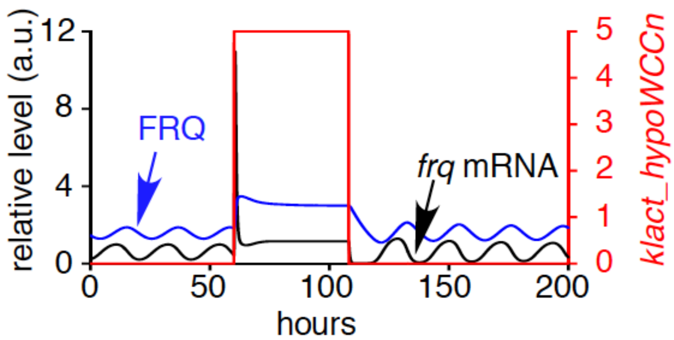

Figure 4.1 Simulated results of light resetting.
The simulation consists of 60 h dark, 48 h constant light, 92 h constant dark. 10 data points per hour are plotted. The red line indicates light intensity. After the dark to light transfer, *frq* mRNA and FRQ protein levels increase and the oscillation is lost. Rhythmic expression begins without delay on return to darkness.

4.2.3 Simulation of light/dark cycles

To synchronize the clock with local time, circadian clocks are entrained by environmental cycles, such as light. Figure 4.2 shows a simulation of several light/dark cycles. The period of cycling *frq* RNA and protein is entrained to 24 hours in the light dark cycles (12 h light: 12h dark), and on return to continuous dark the clock exhibits its free running periodicity of 21.6 h.

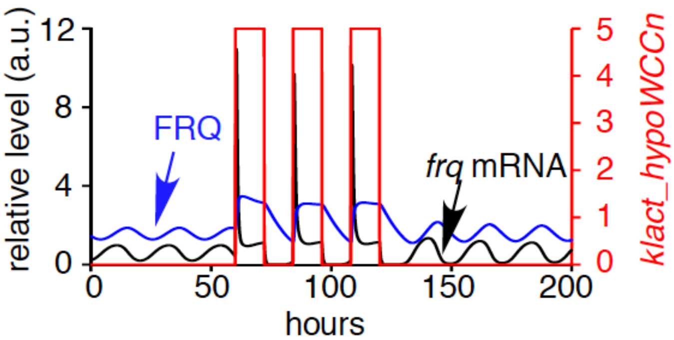

Figure 4.2 Simulated entrainment by light / dark (LD) cycles.
The simulation began with continuous dark for 60 hours, followed by three cycles of 12 h light: 12h dark, before transfer to constant dark. The simulated clock can be entrained to 24 h with 12 h: 12 h light : dark cycle.

4.2.4 Photoadaptation

Photoadaptation occurs when *Neurospora* is transferred from constant dark to constant light. Light-activated genes are rapidly induced at the beginning of constant light conditions, then repressed to their steady state level. In agreement with experimental data (Malzahn *et al*., 2010) (Figure 4.3A), the simulation results shows that on exposure to light of increasing intensity, after a transient increase of *frq* RNA and protein, photo-adaptation occurs and the photo-adapted steady state of gene expression depends on light intensity (Figure 4.3B). These data are consistent with results that show that VVD plays a role in setting the phase of the clock at the light dark transition (Elvin *et al*., 2005; Heintzen *et al*., 2001; Hunt *et al*., 2007).

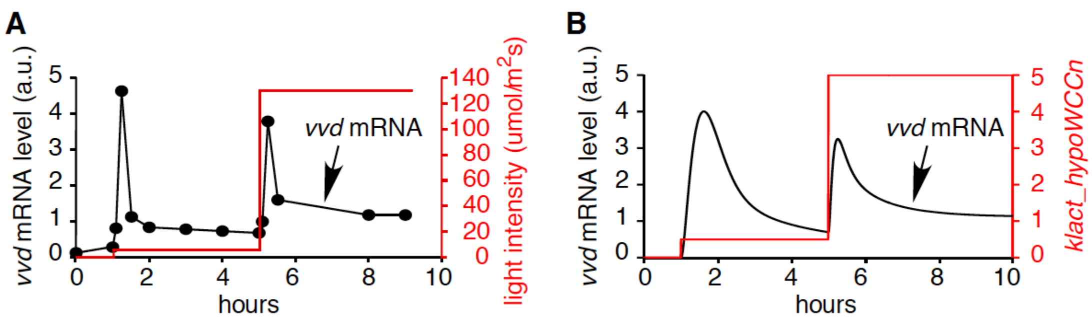

Figure 4.3 Simulated photoadaptation
(A) Experimental data shows the molecular behaviour of photoadaptation (Malzahn *et al*., 2010). Light intensity (red line) of 5 mol/m^2s for 4 hours and 130 mol/m^2s for 5 h. *vvd* mRNA level (black line) is rapidly and transiently induced to high levels immediately after exposure to light. (B) The behaviour of *vvd* mRNA photoadaptation is reproduced in the model. A second increase in light intensity results in a rapid increase of *vvd* RNA. The levels soon fall but remain at a higher level compared to levels at the lower light intensity. 100 data points per hour were plotted.

4.2.5 Simulated phase response curves by light stimulation

A universal characteristic of circadian clocks is their phase response to light. Light exposure during the late subjective night advances their phase of oscillation. In contrast, light exposure late in the subjective day results in phase delays and light exposure during the day results in little or no change in clock time (Figure 4.4A) (Johnson, 1999; Sargent and Briggs, 1967). To examine the effect of light pulses on my model clock, the system was pulsed with light (duration 0.1 or 0.01 h) at 2 hour intervals covering one circadian day. In the model, large phase shifts are induced during the (late) subjective day and early morning (Figure 4.4B), which is in agreement with the published literature (Crosthwaite *et al*., 1995) (Figure 4.4A). Moreover, simulating the phase shift behaviour with different amounts of light reproduces the experimentally observed dependency of phase shift magnitude on the amount of light (Dharmananda, 1980) (Figure 4.4B, dotted line).

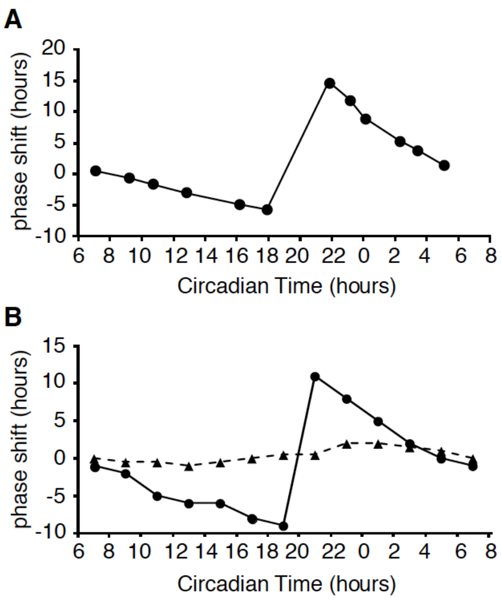

Figure 4.4 Simulated phase response curves by light stimulation.
(A) Plot of experimental data showing light-induced phase shifts (Crosthwaite *et al*., 1995). Light pulses given during the late subjective night and early morning result in large phase shifts. (B) Light-induced phase shifts are reproduced in the model. 0.1 h light pulses (solid line) cause larger phase shifts than 0.01 h light pulses (dashed line). Large phase shifts occurred during the late subjective night and early morning. 20 and 200 data points/h were plotted for simulated 0.1 and 0.01 h light pulse respectively.

4.3 How is the phase of conidiation is regulated after light to dark transfer in *Neurospora*?

As presented in the previous sections, this model successfully reproduces a variety of light response phenotypes from the clock, including resetting by light pulses, entrainment with light-dark cycles and photoadaptation. However, several phenotypes were still not accurately reproduced in the model. For example, the level of *frq* mRNA and FRQ determines the delay of the first *frq* mRNA peak after light to dark transfer. The mechanisms of FRQ-dependent *frq* RNA degradation and VVD's interaction with L-WCC are not sufficient to generate the correct phase of *frq* mRNA peaking after light to dark transfer. This suggests that other critical light response mechanisms still need to be considered. One possibility is that the non-coding *frq* antisense transcript *qrf* influences *frq* stability or regulates the production of *frq* RNA or FRQ and results in setting the correct phase of conidiation after light to dark transfer.

4.3.1 *qrf* constructs and their response to light

Further understanding of processes occurring during light to dark transfer is necessary. Some evidence shows that *qrf* regulates the phase of conidiation: The *frq* antisense RNA *qrf* was observed to be involved in generating the correct phase of conidiation after light to dark transfer (Belden *et al*., 2011; Kramer, 2007). *qrf* is an antisense frq transcript and is expressed at 180˚ phase to the frq RNA (Kramer *et al*. 2003). Replacement of the *qrf* promoter with 3' untranslated region (UTR) of the clock-controlled gene *ccg-2* results in a small phase delay after light to dark transfer (Kramer et al., 2003). Therefore, when *qrf* expression is reduced, *frq* RNA is more stable. As the RNA sequence of *frq* and *qrf* RNA are complementary to each other, *frq*: *qrf* double strain RNA (dsRNA) may be present in *Neurospora* and becomes the material of RNA interference (RNAi). This suggests that RNAi could be the potential mechanism regulating the phase of conidiation after light to dark transfer.

Several constructs have been created to explore the role of *qrf* in the light response. In *frq*^{10}*KAJ120* (54-6 *his-3, bd, frq*^{10} (*his-3*$^{+}$:: *pKAJ120*)), the endogenous *frq* locus is replaced with *hph* but a WT copy of *frq* has been inserted at the *histidine-3* (*his-3*) locus, and this rescues rhythmicity. In *frq*^{10}*frqccg-2* (54-6 *his-3, bd, frq*^{10} (*his-3*$^{+}$:: *frqccg-2*)), the 3' end of the *frq* locus was replaced with the 3' untranslated region (UTR) of a transcriptionally controlled *Neurospora* gene, *eas* (*ccg-2*) (Kramer *et al*., 2003) (Figure 4.5) and inserted at *his-3*. Anson (2009) constructed a *frq*^{10}*qa-2qrf* strain (54-6 *his-3, bd, frq*^{10} (*his-3*$^{+}$:: *qa-2qrf*)) in which the expression of *qrf* is driven by the *quinic acid-2 promoter* (*qa-2*) (Figure 4.5). Without QA, this strain displays delayed conidiation following a light to dark transfer. In the presence of increasing amounts of QA, the phase of conidiation is rescued. In addition, *frq*^{10}*PBM120* (54-6 *his-3, bd, frq*^{10} (*his-3*$^{+}$:: *pBM120*)) is a similar construct to *frq*^{10}*KAJ120* (Figure 4.5). The period and phase of conidiation of *frq*^{10}*PBM120* and *frq*^{10}*qa-2qrf* were analysed in race tubes and compared with the wildtype (*87-3 bd*) phenotype (Figure 4.6). In the absence of QA, the period of conidiation among these strains is not significantly different. With the induction of QA, the period of conidiation in *frq*^{10}*qa-2qrf* is significantly shorter than in *frq*^{10}*PBM120* (Figure 4.6). Furthermore, in *frq*^{10}*qa-2qrf*, the phase of conidiation is rescued with the induction of QA, which confirms the results from Anson (2009). These results suggest that *qrf* regulates the phase of conidiation after light to dark transfer. However, how *qrf* regulates the phase of conidiation is still unknown.

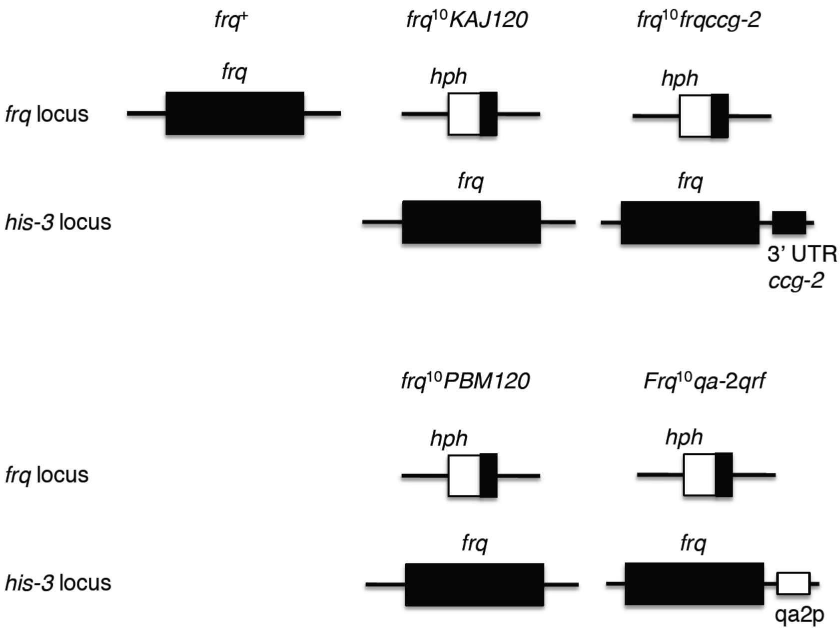

Figure 4.5 The insertion of *frq* construct into *frq*^{10}*KAJ120*, *frq*^{10}*frqccg-2*, *frq*^{10}*PBM120* and *frq*^{10}*qaqrf his-3* locus.

In *frq*^{10}, *frq* is deleted and replaced with the sequence of *hygromycin phosphotransferase* (*hph*). *KAJ120* or *frqccg-2* inserted into the *his-3* locus of *frq*^{10}. Thick filled boxes show FRQ ORF. Open boxes are the sequence of *hph*. Thin filled box indicates the 3' UTR sequences of *ccg-2*.

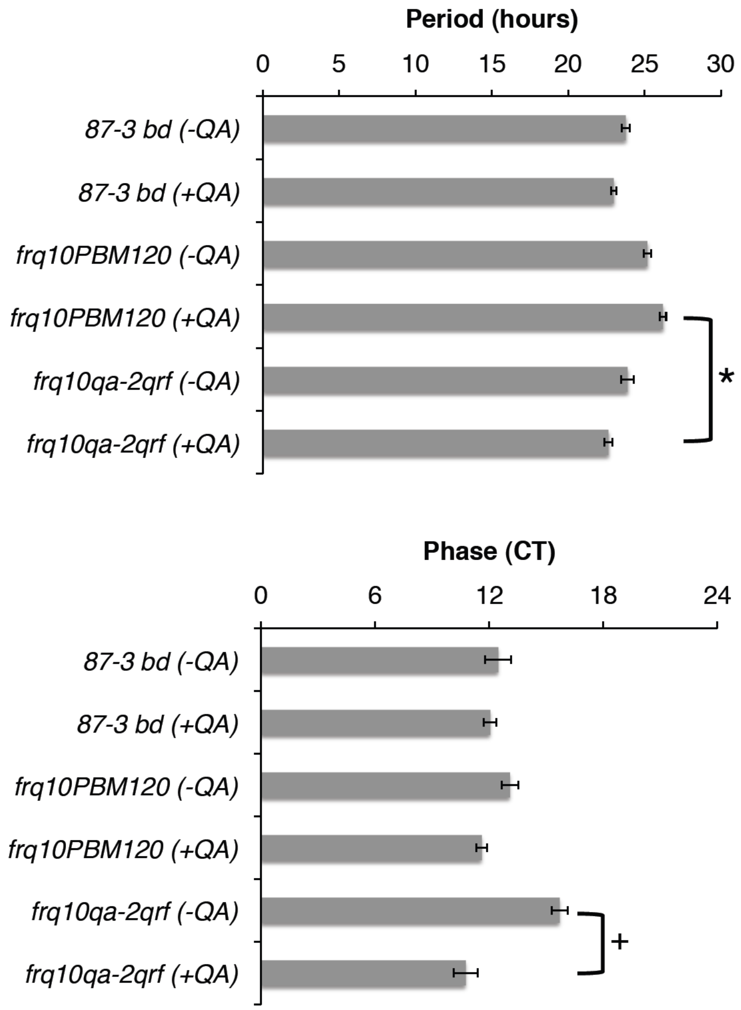

Figure 4.6 Period and phase of conidiation in wildtype, ddicer, qaqrf, PBM120 strains.

Neurospora strains were grown in constant light (LL) for at least 24 hours and then transferred to DD at 25 ºC. Medium contains histidine. Growth fronts were first marked at the LD transition and then every 24 h thereafter. All race tubes were analyzed using the CHRONO program. n = 12 in 87-3 bd (-QA), 12 in 87-3 bd (+QA), 18 in frq^{10}*PBM120* (-QA), 18 in frq^{10}*PBM120* (+QA), 18 in frq^{10}*qa-2qrf* (-QA) and 16 in frq^{10}*qa-2qrf* (-QA). Data from two independent experiments are combined together in frq^{10}*PBM120* and frq^{10}*qa-2qrf*. Error bars indicate ±1 standard error. One-way ANOVA and scheffe post hoc were carried out to test the significance of difference. * : p = 0.000. + : p = 0.000.

4.3.2 Is RNAi involved in phase resetting after a light to dark transfer?

In the RNA interference (RNAi) pathway, QDE-2 is an Argonaute protein and is the core of the RNA-induced silencing complex (RISC) complex associated with siRNA (Choudhary *et al*., 2007). QDE-2-interacting protein (QIP) is an exonuclease that digests the passenger strand, which results in the activation of RISC (Maiti *et al*., 2007). To understand if QDE-2 dependent RNAi is involved in phase setting after light to dark transfer, the period and phase of conidiation of *bd, qde-2*$^{\Delta}$ were analysed in race tubes and compared with the wildtype phenotype. The results show that the period of conidiation among these strains is not significantly different (Figures 4.7). The phase of *bd, qde-2*$^{\Delta}$ advances compared to a *bd* strain isolated from the same cross as the *bd, qde-2*$^{\Delta}$ strain but is similar to other *bd* strains i.e. 54-3*bd* and 87-3*bd*. However, these data are combined from two independent experiments and only one experiment shows the phase of *bd, qde-2*$^{\Delta}$ is significantly different with the *bd* strain isolated from the same cross as the *bd, qde-2*$^{\Delta}$ strain, suggesting that deletion of *qde-2* does not affect the phase of conidiation after light to dark transfer.

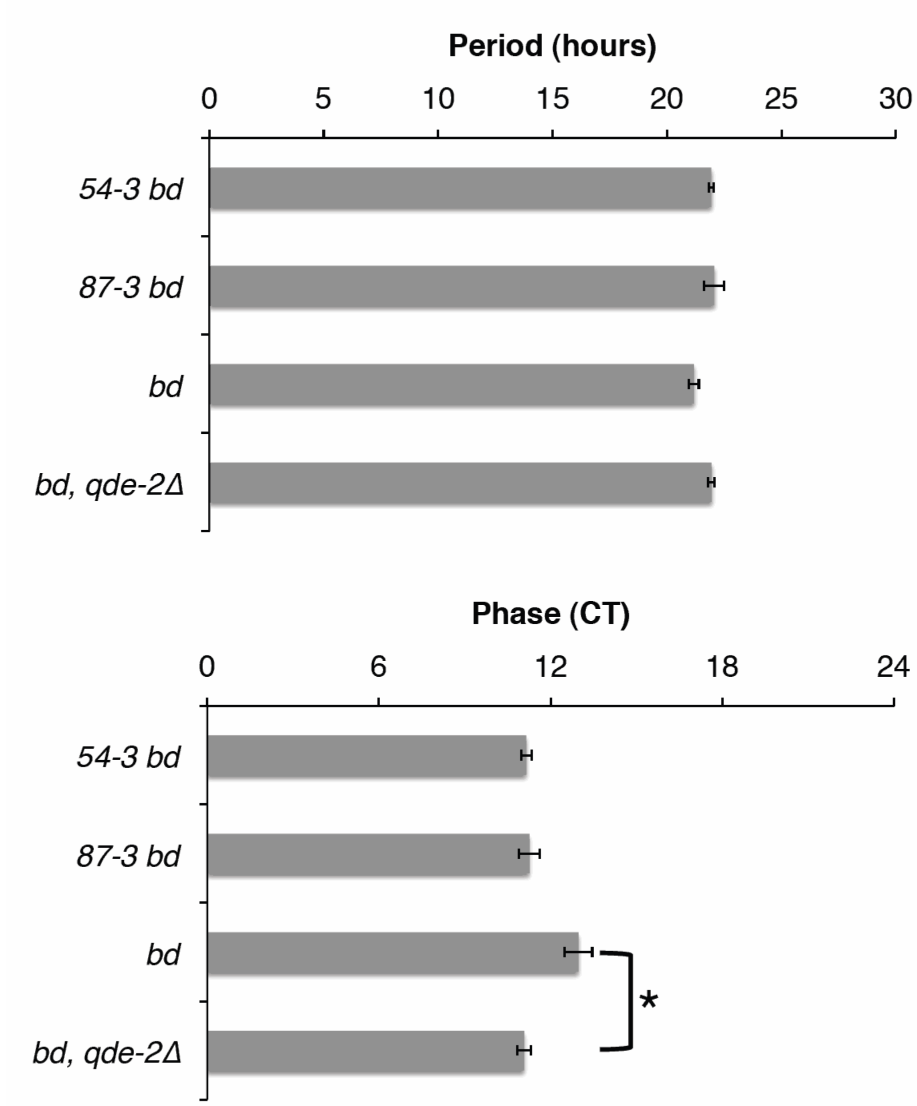

Figure 4.7 Period and phase of conidiation in wildtypes and the *bd, qde-2*$^{\Delta}$ strain. *Neurospora* strains were grown in constant light (LL) for at least 24 hours and then transferred to DD at 25 ºC. Growth fronts were first marked at the LD transition and then every 24 h thereafter. All race tubes were analyzed using the CHRONO program. n = 24 in 54-3 bd, 23 in 87-3 bd, 24 in bd and 23 in *bd, qde-2*$^{\Delta}$. Data from two independent experiments are combined together. Error bars indicate ±1 standard error. One-way ANOVA and scheffe post hoc were carried out to test the significance of difference. * : p = 0.002.

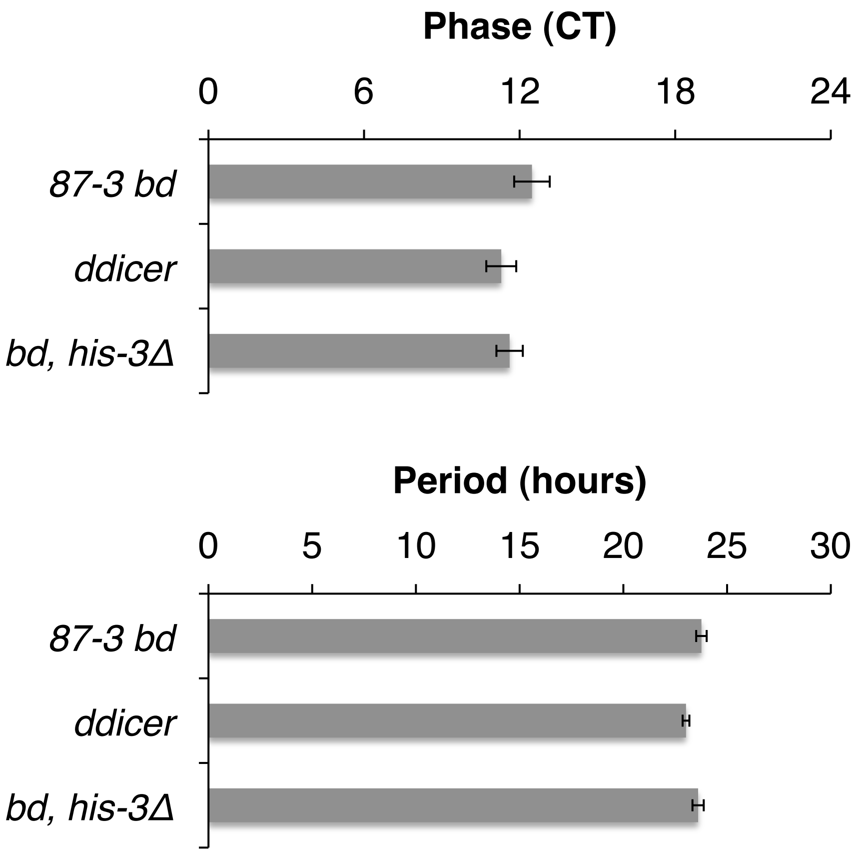

Figure 4.8 Period and phase of conidiation in wildtype (87-3 bd), *ddicer* and *his-3*$^{\Delta}$ strains.

Neurospora strains were grown in constant light (LL) for at least 24 hours and then transferred to DD at 25 ºC. Medium contains histidine. Growth fronts were first marked at the LD transition and then every 24 h thereafter. All race tubes were analyzed using the CHRONO program. n = 12 in *87-3 bd*, 17 in *ddicer* and 16 in *bd, his-3*$^{\Delta}$. Data from two independent experiments are combined together in *ddicer* and *bd, his-3*$^{\Delta}$. Error bars indicate ±1 standard error. One-way ANOVA and scheffe post hoc were carried out to test the significance of difference.

4.3.3 Is DICER involved in *qrf* RNA-regulated phase resetting by light?

The DICER protein is involved in RNAi by recognising double-strand RNA (dsRNA), binds to it and cleaves it giving rise to small-interfering RNA (siRNAs) (reviewed in Chang *et al*., 2012). *qrf* may down regulate *frq* RNA expression by RNAi and the DICER protein may be involved in this mechanism (Catalanotto *et al*., 2004). A race tube assay was also carried out to analyse the phase setting in the *ddicer* strain (*his-3, bd, dicer-1^{RIP}, dicer^{KO}*) compared to the wild-type (*87-3 bd*) and the *bd, his-3$^{\Delta}$* strain. The results are shown in Figure 4.8. The period and phase of conidiation among these strains are not significantly different, suggesting that the phase setting after light to dark transfer may not require DICER.

To further test that whether DICER is involved in phase resetting by light with *qrf* RNA, a the two *dicer* genes were mutated was transformed with *qa-qrf* to give (*his-3, bd, dicer-1^{RIP}, dicer^{KO}* (*his-3^{+}::qa-2qrf*)) and used to test this hypothesis. The double *dicer* deletion strain was transformed with *qaqrf his-3* targeting plasmid (pSA1). Transformants were selected on minimal plates then microconidia containing 1-2 nuclei were generated and the genotypes of single colonies were further confirmed by Southern blotting.

Genomic DNA was digested with *Xmn*1. The *his-3* target length will be 5.9 kb in the parental strain and 8.3 kb with the *qa-2qrf* insertion. pSA1 was digested with *Xho*1 to obtain a 1.7 kb sequence of *his-3* fragment for the probe. The *qa-2 qrf* cassette was successfully inserted into the *his-3* locus in transformant 3-4 and 3-5 (Figure 4.9).

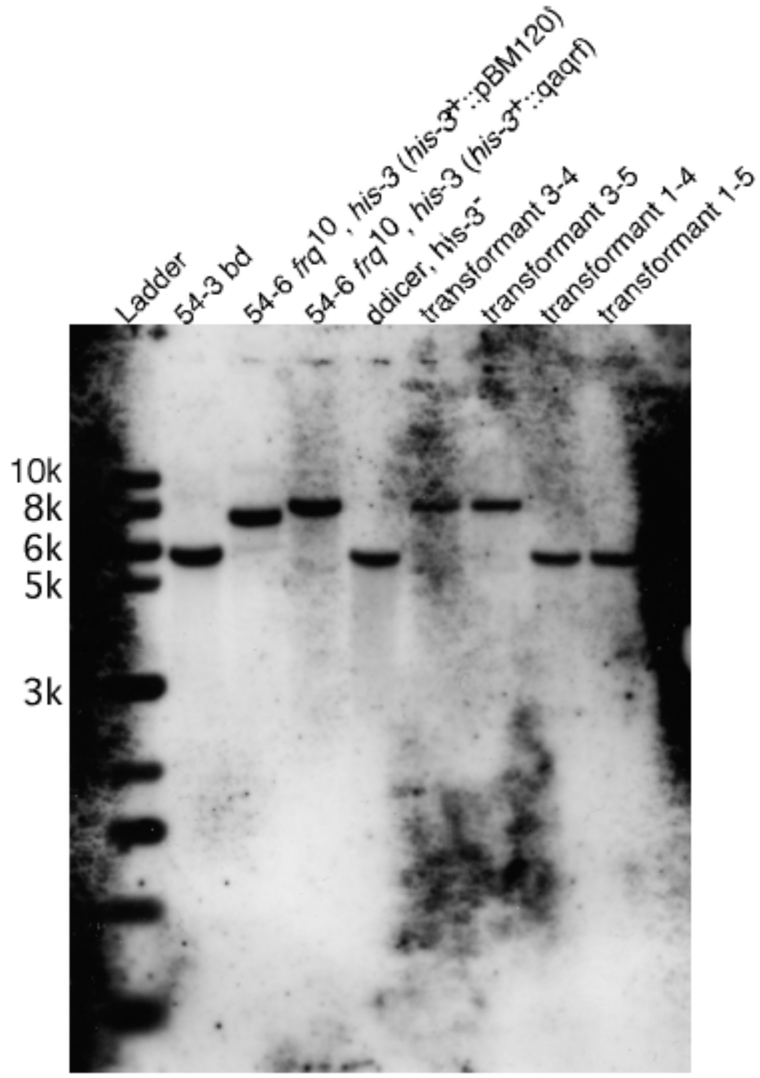

Figure 4.9 Southern blot analysis of *ddicer*, *qa-2qrf* transformants.
Genomic DNA was extracted from 54-3 bd, PBM120, *qaqrf*, *ddicer* strains and transformants. Genomic DNA was digested with *Xmn*1 and probed with a DIG-labeled *his-3* specific probe.

A race tube assay was also carried out to analyse the phase setting in transformants compared with *frq[10]PBM120* and *frq[10]qa-2qrf* and the phase when *qrf* is induced by QA. The results are shown in Figure 4.10 and Figure 4.11. Induction of *qrf* expression by QA can advance the conidiation (comparing with + or – QA in *frq[10]qa-2qrf*), but no effect was observed on ddicer strains (comparing with ddicer microconidia 3-4 and 1-4). However, no significant difference was found in this experiment, suggesting that *qrf*-dependent phase setting does not require DICER.

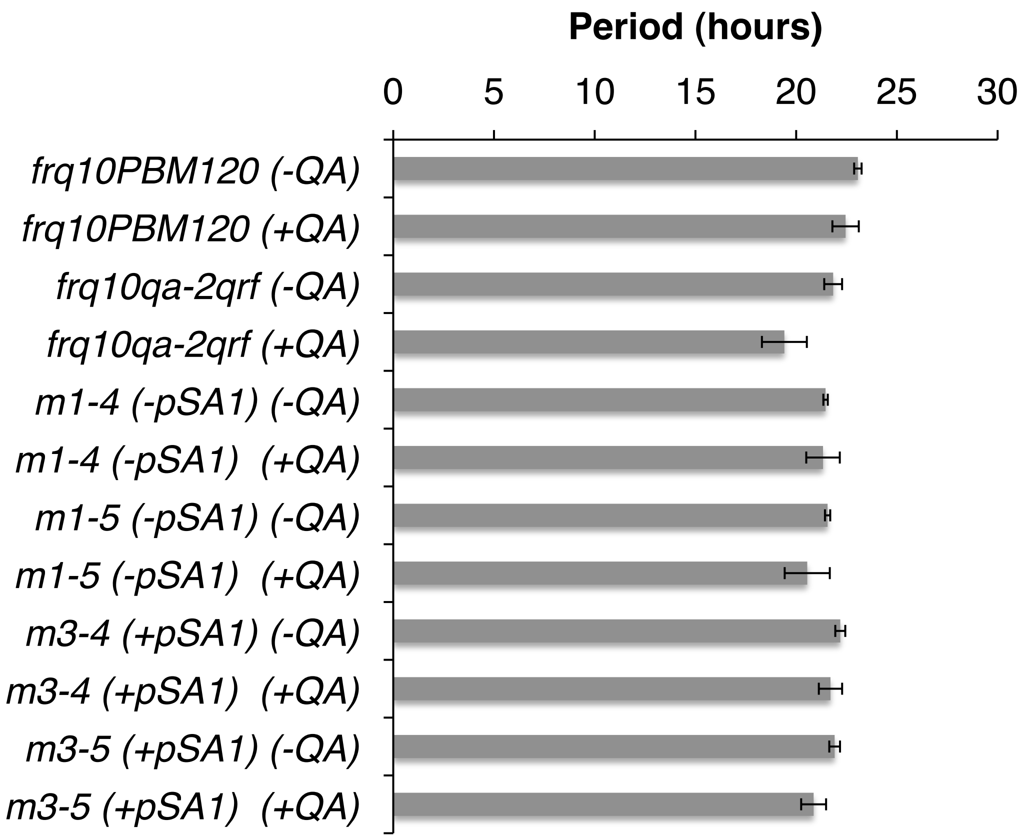

Figure 4.10 Period of conidiation in *frq[10]PBM120*, *frq[10]qa-2qrf* and ddicer strains. *Neurospora* strains were grown in constant light (LL) for at least 24 hours and then transferred to DD at 25 ºC. Medium does not contain histidine. Growth fronts were first marked at the LD transition and then every 24 h thereafter. Transformant m1-4 and m1-5: *ddicer, his-3*$^-$. Transformant m3-4 and m3-5: *bd, his-3, ddicer* (*his-3*$^+$:: *qaqrf*). All race tubes were analyzed using the CHRONO program. n = 3 in *frq[10]PBM120* (-QA), 3 in *frq[10]PBM120* (+QA), 3 in *frq[10]qa-2qrf* (-QA), 2 in *frq[10]qa-2qrf* (+QA), 3 in m1-4 (-QA), 3 in m1-4 (+QA), 3 in m1-5 (-QA), 2 in m1-5 (+QA), 3 in m3-4 (-QA), 3 in m3-4 (+QA), 3 in m3-5 (-QA) and 3 in m3-5 (+QA). Error bars indicate ±1 standard error. One-way ANOVA and scheffe post hoc were carried out to test the significance of difference.

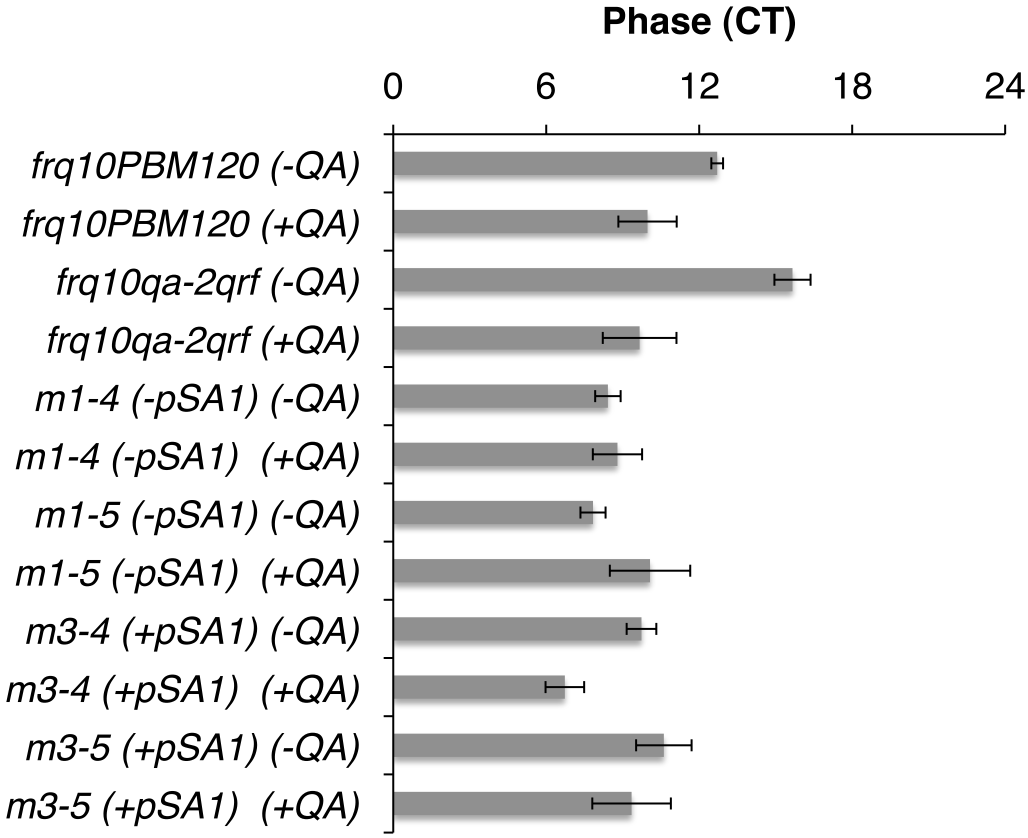

Figure 4.11 Phase of conidiation in frq10PBM120, frq10qa-2qrf and ddicer strains.

Neurospora strains were grown in constant light (LL) for at least 24 hours and then transferred to DD at 25 ºC. Medium does not contain histidine. Growth fronts were first marked at the LD transition and then every 24 h thereafter. Transformant 1-4 and 1-5: *ddicer, his-3*$^{-}$. Transformant 3-4 and 3-5: *bd, his-3, ddicer* (*his-3*$^{+}$:: *qaqrf*). All race tubes were analyzed using the CHRONO program. n = 3 in *frq*^{10}*PBM120* (-QA), 3 in *frq*^{10}*PBM120* (+QA), 3 in *frq*^{10}*qa-2qrf* (-QA), 2 in *frq*^{10}*qa-2qrf* (+QA), 3 in m1-4 (-QA), 3 in m1-4 (+QA), 3 in m1-5 (-QA), 2 in m1-5 (+QA), 3 in m3-4 (-QA), 3 in m3-4 (+QA), 3 in m3-5 (-QA) and 3 in m3-5 (+QA). Error bars indicate ±1 standard error. One-way ANOVA and scheffe post hoc were carried out to test the significance of difference.

4.3.4 *frq* expression profiles after light to dark transfer in wild type, *frq*^{10}*frqccg-2*, *frq*^{10}qa-2qrf, and *ddicer* strains.

To understand if *qrf* regulates the expression of *frq* RNA and FRQ, the level of *frq* RNA in *frq*^{10}KAJ120 and *frq*^{10}*frqccg-2* was monitored by Northern blot analysis. Tissues were harvested in LL and 1, 3, 5 h in DD. The results are shown in Figure 4.12. In LL, *frq* mRNA level is similar in *frq*^{10}KAJ120 and *frq*^{10}*frqccg-2* (Figure 4.12A). No *qrf* is detected in *frq*^{10}*frqccg-2* (Figure 4.12B). However, in DD *frq* mRNA level in *frq*^{10}KAJ120 is lower than in *frq*^{10}*frqccg-2*, suggesting that *qrf* down regulating *frq* RNA in DD. The FRQ level in *frq*^{10}*KAJ120* (control), *frq*^{10}*frqccg-2*, *frq*^{10}*qa-2qrf,* and *frq*^{10}*PMB120* (control) was also monitored by Western blot analysis (Figure 4.12C and Figure 4.13). The level of FRQ in *frq*^{10}KAJ120 is significantly lower than in *frq*^{10}*frqccg-2*. However, when *qrf* is overexpressed by QA induction, FRQ level is still high (Figure 4.13). The level of FRQ is similar in *frq*^{10}*qa-2qrf* with and without the induction of QA, suggesting that the presence of *qrf* does not affect FRQ expression.

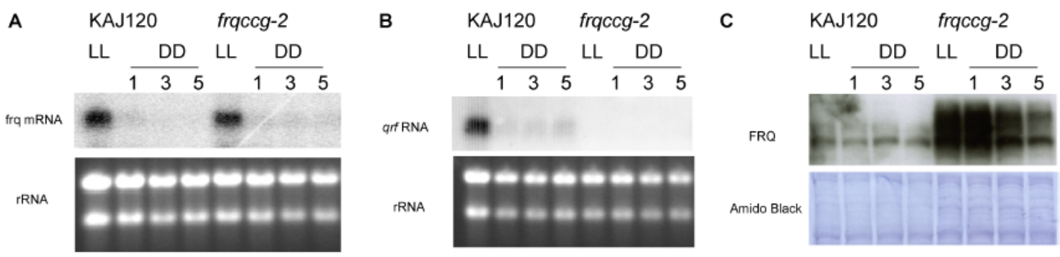

Figure 4.12 *frq* mRNA, *qrf* RNA and FRQ level in KAJ120 and *frqccg-2* strains. (A) Northern blot analysis of *frq* mRNA shows the level of *frq* mRNA in LL, at DD 1, DD 3 and DD 5. (B) Northern blot analysis of *qrf* RNA shows the level of *qrf* RNA in LL, at DD 1, DD 3 and DD 5. rRNA level was used as a concentration control in (A) and (B). (C) Western blot analysis of FRQ shows the level of FRQ in LL, at DD 1, DD 3 and DD 5. Amido black stained membrane shows each sample was evenly load.

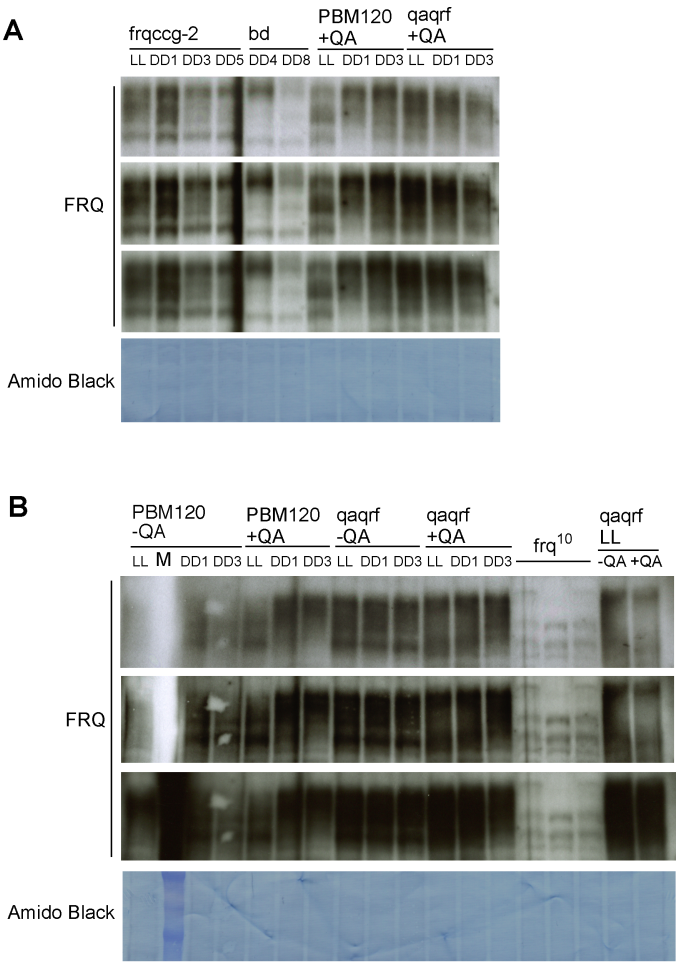

Figure 4.13 FRQ level in KAJ120, frqccg-2, PBM120 and *qaqrf* strains.
(A) Western blot analysis of FRQ shows the level of FRQ in KAJ120, *frqccg-2*, PBM120 and *qaqrf*. (B) Western blot analysis of FRQ shows the level of FRQ with or without QA in PBM120 and *qaqrf*. Three different durations of exposure are shown to compare the level of FRQ in (A) and (B). M is the ladder and Amido black stained membrane shows each sample was evenly load.

4.3.5 Comparison of *frq* mRNA degradation rates in KAJ120 and *frqccg-2*

To understand whether *qrf* RNA is able to regulate *frq* expression by facilitating its RNA degradation, the half-life of *frq* RNA in *frq^{10}*KAJ120 and *frq^{10}frqccg-2* was determined. The degradation rate was tested at light to dark transfer at 25 ºC. The results are shown in Figure 4.14. The degradation rate of *frq* mRNA in *frq^{10}*KAJ120 is faster than in *frq^{10}frqccg-2*, suggesting that the degradation rate of *frq* mRNA is regulated by *qrf* or by the *frq* 3'UTR.

A

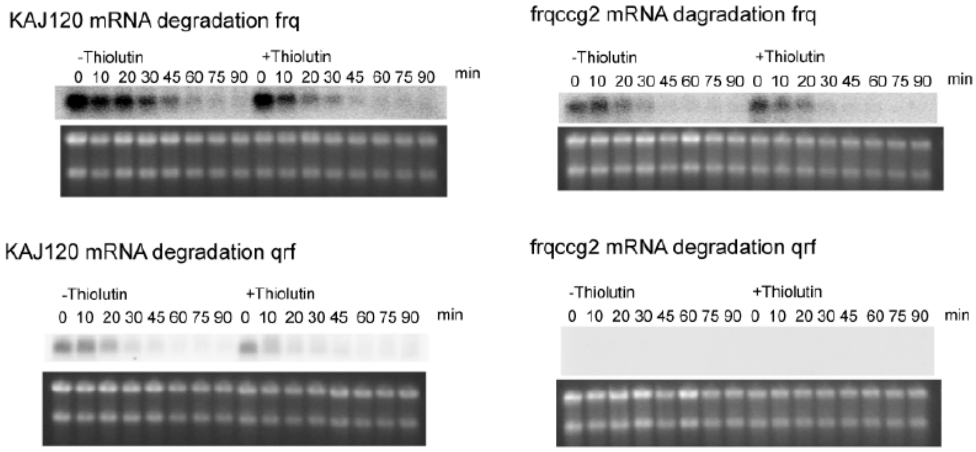

B

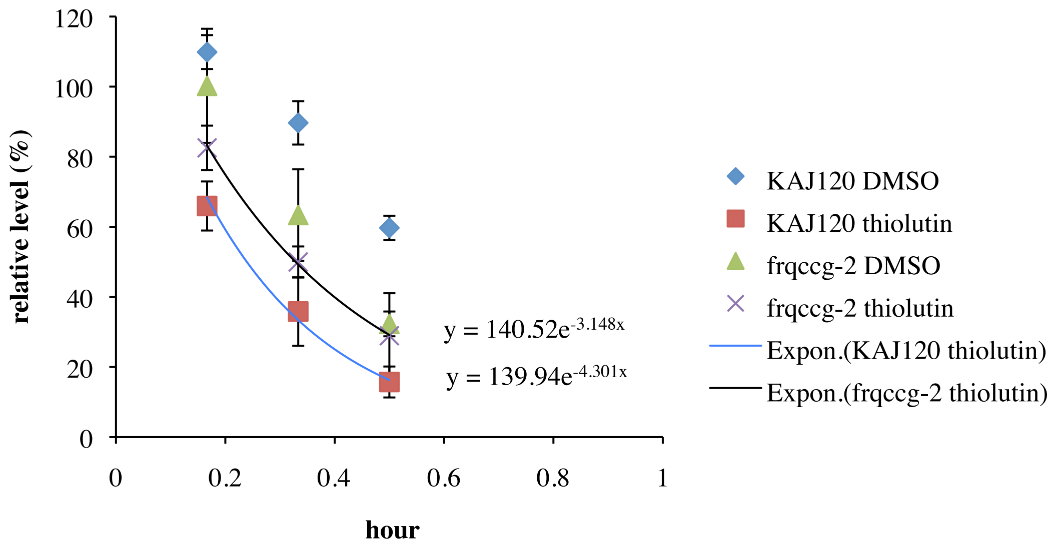

Figure 4.14 Determination of *frq* RNA degradation rates in KAJ120 and *frqccg-2*. (A) Northern blot analysis shows the degradation of *frq* RNA after light to dark transfer at 25 °C. The densitometric analysis of the results of *frq* RNA. The graph shows the results from three independent experiments. Error bars represent standard error (SE).

qrf dependent RNAi was proposed to be a potential mechanism regulating the phase after light to dark transfer. However, experimental data show that the deletion of *qde-2* or the deletion of *qde-2* or double deletion of two dicer genes (*dicer-1 and dicer-2*) does not affect the phase after light to dark transfer. Overexpressing *qrf* RNA in the *ddicer* strain does not advance the phase after light to dark transfer. Moreover, overexpressing *qrf* RNA did not decrease the FRQ level. These data suggest that *qrf* RNA is not involved in the regulation of *frq* expression and phase setting of conidiation after light to dark transfer by RNAi. Nevertheless, the degradation rate of *frq* RNA in KAJ120 is faster than in frqccg-2, suggesting that *qrf* controls the degradation of *frq* RNA. These data suggest that *qrf* RNA is involved in the regulation of *frq* expression possibly by RNAi or by the *frq* 3'UTR. Overall, how *qrf* regulates the phase setting of conidiation after light to dark transfer is still not clear. The regulation of *frq* RNA stability by *qrf* RNA is able to test in the model. If this mechanism is still not sufficient to reproduce the correct phase of *frq* RNA after light to dark transfer, other mechanisms such as FRQ phosphorylation or FRQ nuclear localisation could be considered and tested in the model.

4.4 Conclusion

This model successfully reproduces a variety of light response phenotypes of the *Neurospora* circadian clock, including resetting the clock by light, entrainment of the clock by light and dark cycles, photoadaptation and phase response curves. Although additional experimental data are required to accurately understand the mechanisms of phase resetting after light to dark transfer, this model is suitable to test and make predictions to advance our understanding of the circadian clock's response to light. For example, *qrf* component and its possible function such as the formation of *frq*: *qrf* dsRNA and the regulation of *frq* RNA or FRQ expression can be added and tested in the model. Next, other important environmental factors such as temperature need to be incorporated into the model.

Chapter 5

Modelling temperature compensation.

5. Modelling temperature compensation.

5.1 Introduction

The change of temperature affects the majority of chemical reactions. However, temperature compensation keeps the pace of circadian clocks so that the period of the clock is maintained constant in a range of temperatures. Temperature compensation is one of the most important characteristics of circadian clocks. This results in correct timing of phenotype appearance of circadian rhythms, such as conidiation in fungi, leaf movement in plants and feeding in animals. The balance model and the robust model are the two theoretical mechanisms to achieve temperature compensation (reviewed in Hogenesch and Ueda, 2011). However, what is the underlying mechanism to achieve temperature compensation is the least understood question in clock biology.

Previous chapters showed that the *Neurospora* circadian clock model provides a correct depiction of many clock phenotypes and can be used for hypothesising possible mechanisms underlying temperature compensation. However, before making and testing predictions, several experiments had to be carried out to understand what is happening in the *Neurospora* circadian clock when the temperature changes, including observing the period and phase of conidiation in wild type *Neurospora* and monitoring FRQ expression profile at different temperatures. In addition, response coefficient analyses were carried out to quantify the effects of parameters on the period and the amplitude of the oscillation, which depicts the characteristics of each parameter in the system, and the results will be shown in this chapter.

With the help of the period response coefficient test, I hypothesise that temperature compensation can be achieved by the simultaneously change of two reaction rates with increasing temperature: 1. The translation of FRQ protein increases. 2. FRQ nuclear import decreases. This hypothesis is further tested with the fractionation experiment and the results will be shown in this chapter.

5.2 The period and phase of conidiation is temperature compensated from 21 ºC to 28 ºC

To obtain data over a the range of temperatures where the period is compensated, race tube assays were carried out to observe the period and phase of conidiation in constant darkness (DD) at 15, 18, 21, 25, 28, 31 and 34 ºC. The results show that the period of conidiation is temperature compensated from 18 to 31 ºC with a slight decrease below 18 ºC and above 31 ºC (Figure 5.1), which is in agreement with published literature (Gardner and Feldman, 1981). The phase of conidiation is also temperature compensated from 18 to 31 ºC with a slight delay below 18 ºC and above 31 ºC.

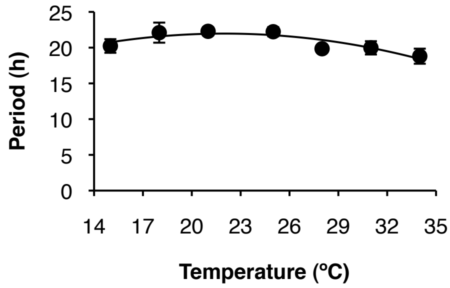

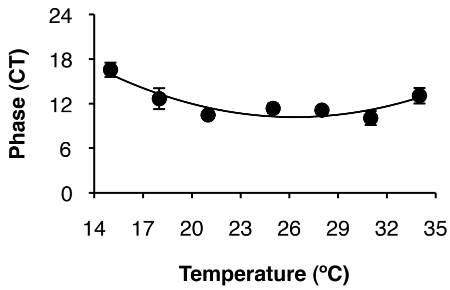

Figure 5.1 Period and phase of conidiation in constant darkness at 15, 18, 21, 25, 28, 31 and 34 ºC.
Wild type *Neurospora* (*bd*) was grown in constant light (LL) for at least 24 hours at 15, 18, 21, 25, 31 and 34 ºC and then transferred to DD at the same temperature. Growth fronts were first marked at the LD transition and then every 24 h thereafter. All race tubes were analyzed using the CHRONO program. (n= 10 for 15 ºC, 12 for 18 ºC, 11 for 21 ºC, 11 for 25 ºC, 12 for 28 ºC and 11 for 34 ºC)

5.3 FRQ oscillation level is at least doubled from 21 ºC to 28 ºC

To understand how *frq* is expressed at different temperatures, western blot analysis was carried out to monitor FRQ oscillation levels at 21 ºC and 28 ºC. Tissue was grown at either 21 ºC or 28 ºC for at least 24 hours in constant light (LL), transferred to constant darkness (DD) at the same temperature and harvested from DD 6 to DD 24 with 2 hours interval. The result shows that the peak (around at DD 20-22) and trough (around at DD10-12) of FRQ oscillation were similar at 21 ºC and 28 ºC (Figure 5.2). However, overall the level of FRQ oscillation was higher at 28 ºC than at 21 ºC. The peak of FRQ oscillation is at least doubled from 21 ºC to 28 ºC. These results are similar to those from literature (Liu *et al*., 1998).

A

B

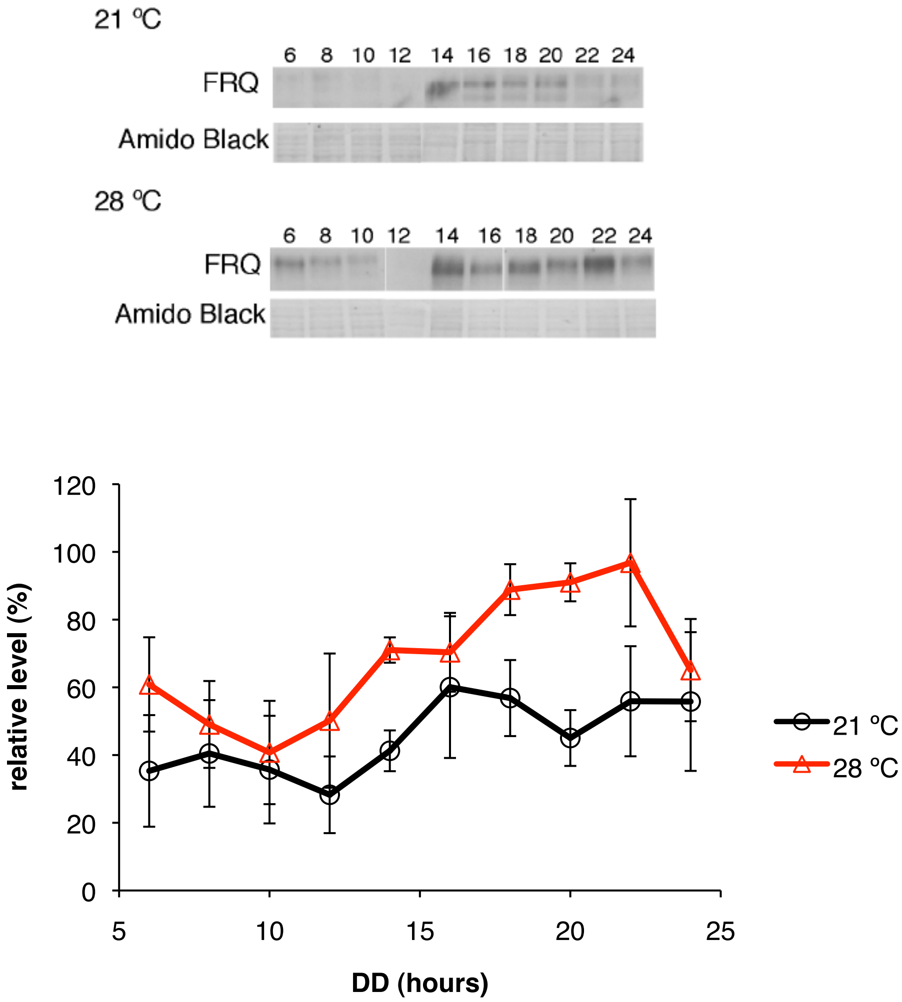

Figure 5.2 FRQ level time course at 21 °C and 28 °C.
(A) Western blot analysis of FRQ shows the level of FRQ from DD 6 to DD 24 with 2 h resolution. (B) The densitometric analysis of the results of FRQ from three independent experiments. Amido black stained membrane shows each sample was evenly load. Error bars represent standard error (SE).

5.4 The troughs of FRQ oscillation are both at DD 11.5-12 at 21 °C and 28 °C

Experimental data from Liu *et al*. suggested that the peak level of FRQ oscillation is tripled from 21 °C to 28 °C and the average level of FRQ oscillation is higher at 28°C than at 21°C (Liu *et al*., 1998). In addition, the phase of FRQ oscillation is similar at 21 °C and 28 °C. However, the resolution of Liu's data is 5 hours. To further monitor

FRQ oscillation at 21 ºC and 28 ºC with higher resolution, samples from a DD9.5-15 time course with 0.5 h resolution were recognised with the depleted FRQ antibody. Although the antibody is depleted, it is still not sensitive enough to look at the trough of FRQ oscillation. Longer exposure times result in high background signal. The assumed position of FRQ is indicated in the Figure 5.3. The result shows that troughs levels of FRQ at both 21 ºC and 28 ºC are located around DD 11.5-12 (Figure 5.3). Generally, FRQ level is higher at 28 ºC than at 21 ºC.

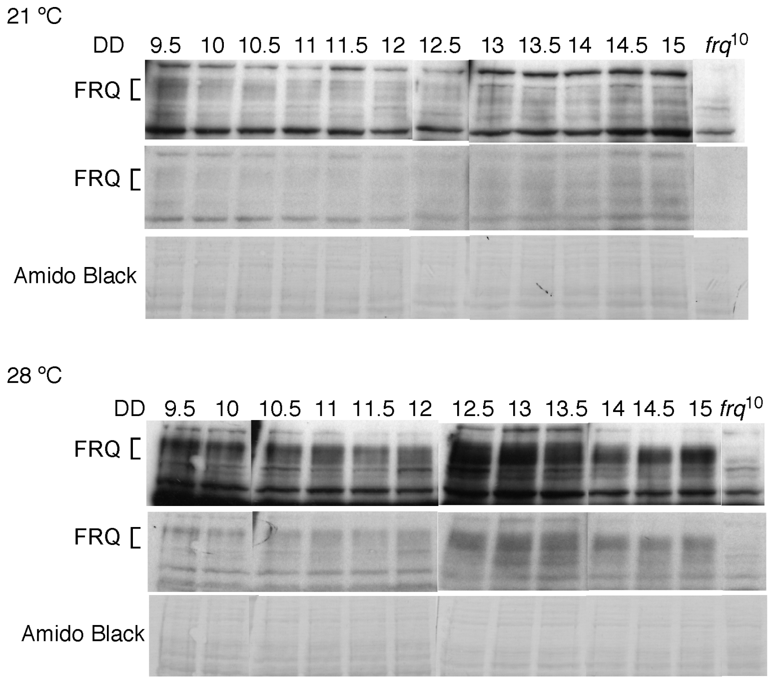

Figure 5.3 FRQ oscillation time course at 21 ºC and 28 ºC with higher resolution. Western blot analysis of FRQ shows the level of FRQ from DD 9.5 to DD15 with 2 h resolution at 21 and 28 ºC. Amido black stained membrane shows sample loading.

5.5 Response coefficient test quantifies the effects of parameters on the period of the clock

Before making and testing predictions of the model, we should understand the influence of each parameter. As we were interested in temperature compensation, the response coefficient analysis was carried out to quantify the effects of parameters on the period. Each of the parameters was increased or decreased by 3 % and the variation of period was estimated. The period response coefficient is the ratio of the relative change of period to the relative change of parameter. The averaged period response coefficient for each parameter is shown in Figure 5.4. In addition, the amplitude (of *frq* mRNA) response coefficient was also calculated and the results are shown in Figure 5.5. The results indicate that the period of the oscillator and the amplitude of *frq* mRNA are most sensitive to the Michaelis constant of *frq* transcription, the rate of basal transcription of *wc-1*, *wc-1* translation, degradation of *wc-1* mRNA, and degradation of activated WCC (Figures 5.4 and 5.5). A 10 % decrease of *wc-1* basal transcription or translation rate, or a 10 % increase of the Michaelis constant of *frq* transcription, degradation of activated WCC or *wc-1* mRNA, all result in a substantially dampened oscillator (Figure 5.6) with a longer period (e.g. decreasing the basal *wc-1* transcription rate by 10 % results in a period of 25.8 hours). A negative correlation is observed between period and amplitude response coefficients of most clock components, showing that an increase in the amplitude of oscillations would result in faster regulation through feedback loops, if not compensated (Figure 5.6).

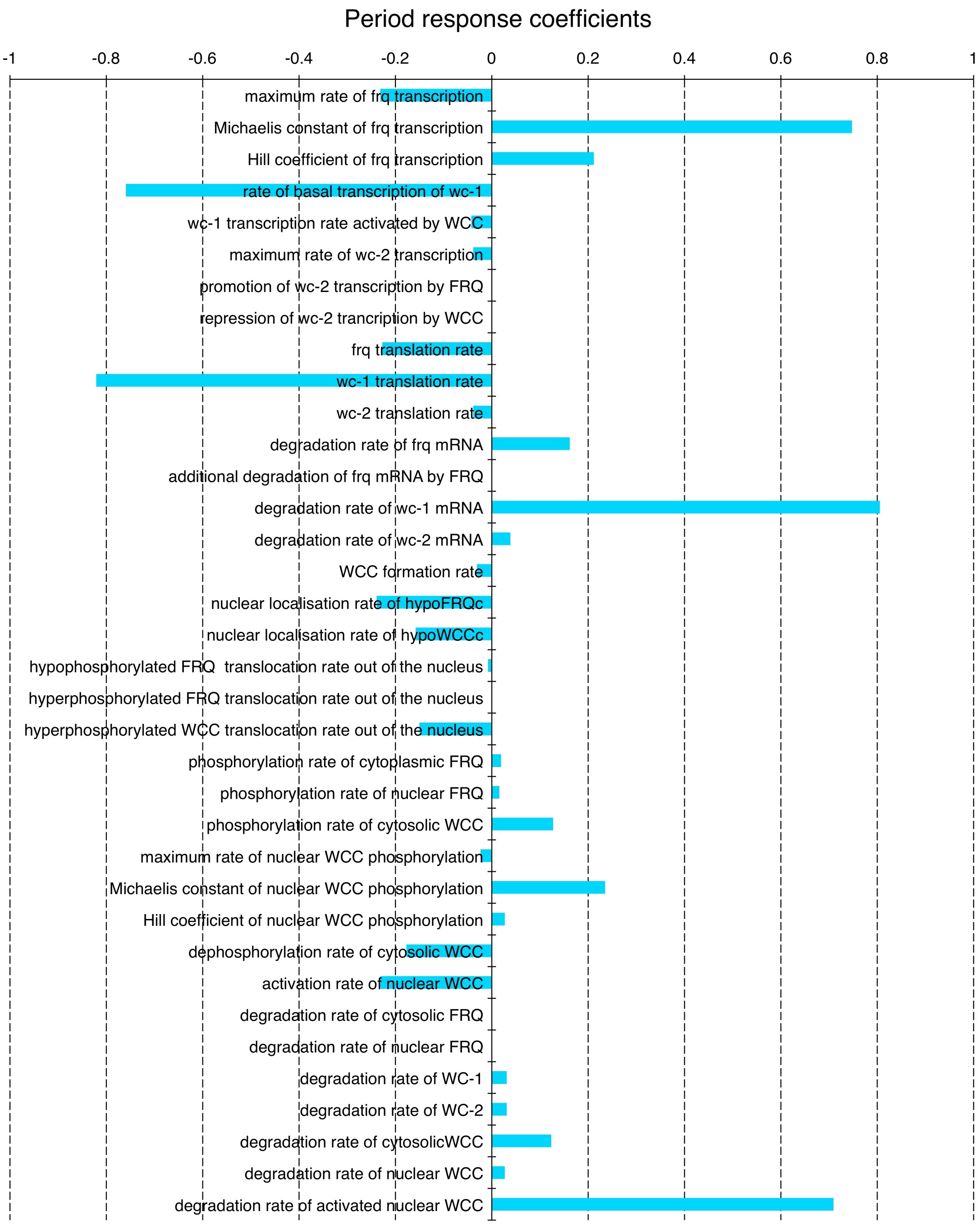

Figure 5.4 Period response coefficients.
Values of averaged period response coefficients for ± 3 % variation in each parameter value. 200 points per hour and 200 hours in total were simulated. The last two peaks of *frq* mRNA were used to determine the period.

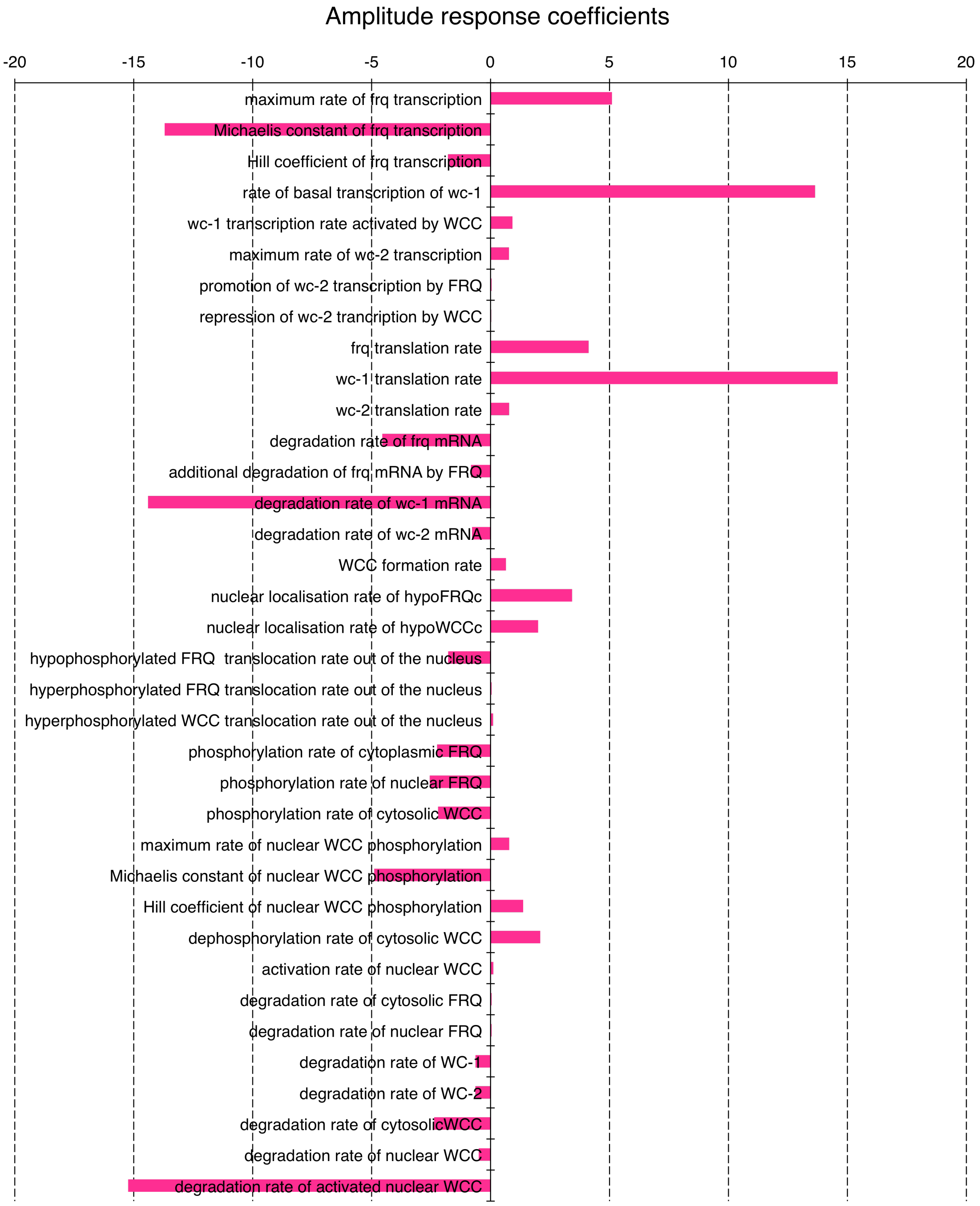

Figure 5.5 Amplitude response coefficients.

Values of averaged amplitude response coefficients for ± 3 % variation in each parameter value. 50 points per hour and 200 hours in total were simulated. The last peak and trough of *frq* mRNA were used to determine the amplitude.

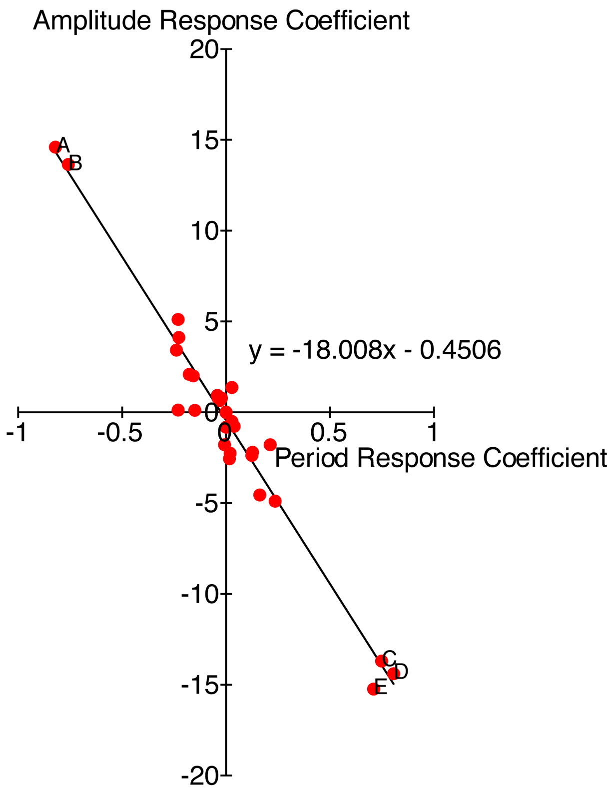

Figure 5.6 Distribution of parameters based on the value of their period and amplitude response coefficients.
The trend line indicates that period and amplitude response coefficients are negatively correlated. A= *wc-1* translation, B= constant minimum *wc-1* transcription, C=dissociation constant of WCC binding to the *frq* promoter, D=degradation of *wc-1* mRNA, E=degradation of activated WCC.

5.6 Phenotypes of *Neurospora* with a mutant form WC-2 or an inducible copy of *wc-1*

From the response coefficient analysis, I found that changes in the basal transcription rate of *wc-1* and the dissociation constant of WCC binding to the *frq* promoter (*K_frq*) have a large effect on the period and amplitude of the oscillator (Figure 5.7). Phenotypes resulting from altered transcription of *wc-1* and binding of the WCC are seen in mutant and engineered strains of *Neurospora*. For example *wc-2*^{ER24} is a *Neurospora* mutant that displays reduced WCC binding at the *frq* promoter due to a mutation at a conserved position in its Zn finger DNA-binding domain (Collett *et al.*, 2001). *wc-2^ER24^* has a long period (~29.7 hours) and becomes arrhythmic after 3-4 circadian days at 25°C (Collett *et al*., 2001). In *wc-2^ER24^*, *frq* mRNA levels are lower and peak levels of *frq* are delayed compared to wild-type. In addition, the oscillation of FRQ protein dampens with time (Collett *et al*., 2001). Figure 5.7 shows the simulation of light to dark transfer of wild-type *Neurospora*. When the dissociation constant of WCC binding to the *frq* promoter *K_frq* is increased by 10%, the model successfully reproduces the characteristics of the *wc-2^ER24^* mutant (Figure 5.7).

Experimentally, the basal rate of *wc-1* transcription has been altered by introducing an inducible copy of the *wc-1* gene (qa-WC-1). In the qa-WC-1 strain the WC-1 ORF is fused to the quinic acid-inducible promoter (*qa-2*) (Cheng *et al*., 2001b) and transcription of *wc-1* is controlled by the concentration of quinic acid (QA) in the medium. Conidiation in a qa-WC-1 expressing strain is arrhythmic when the concentration of QA is low (1×10^{-7} M), but shows sustained rhythmicity at 1×10^{-4} M QA. At 1×10^{-5} M QA, conidial rhythms rapidly dampen after 3-4 cycles. In the model, *k_wc1* is the rate of basal transcription of *wc-1*. Similar to *K_frq*, *k_wc1* is also sensitive to the period and the amplitude of oscillation. Decreasing *k_wc1* by 10 % results in a substantially dampened oscillation, successfully reproducing the behaviour of qa-WC-1 banding at 1×10^{-5} M QA (Figure 5.7).

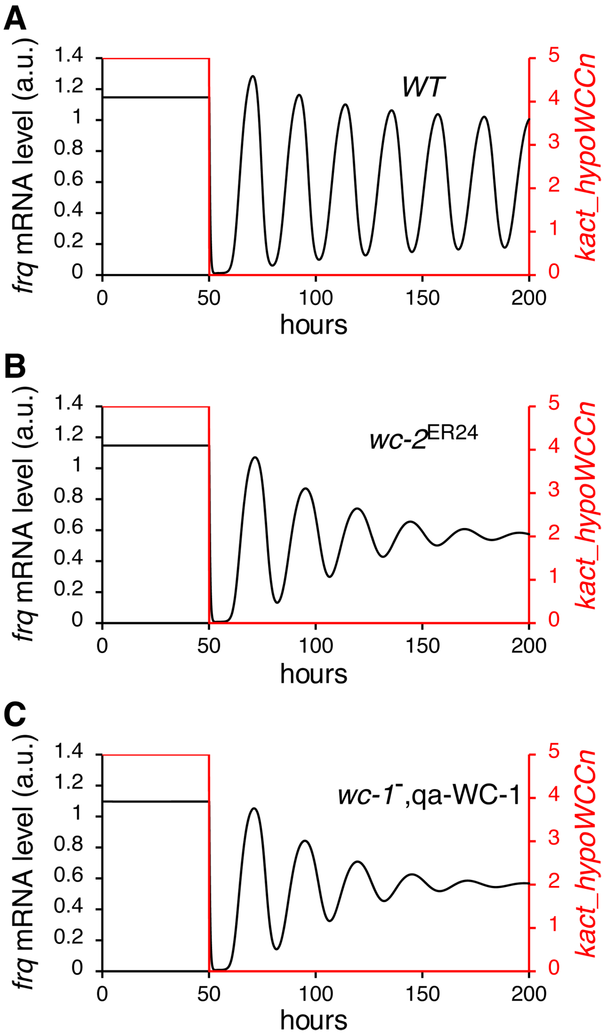

Figure 5.7 Reproduction of *wc-2*$^{\text{ER24}}$ mutant and *wc-1*$^{-}$, qa-WC-1 behaviour.
(A) Simulated results showing levels of *frq* RNA and light-activated WCC$_{\text{n}}$ before and after a light to dark transfer. 10 data points/h are plotted. When the light (red line) is turned off after 50 h, *frq* mRNA levels oscillate. (B) Simulated *frq* mRNA behaviour of the *wc-2*$^{\text{ER24}}$ mutant and (C) the *wc-1*$^{-}$, qa-WC-1 strain. In (B) and (C) *frq* mRNA oscillates in the dark but the oscillation dampens with time.

5.7 Modelling temperature compensation

As confirmed from previous experimental data and from published results (Liu *et al*., 1998; Tseng *et al*., 2012), the level of *frq* mRNA remains the same at different temperatures, but the peak level of FRQ is tripled from 21ºC to 28ºC. However, the FRQ degradation rate remains the same over this range of temperature (Mehra *et al*., 2009). This finding indicates that the translation rate of *frq*, *k_FRQ*, is increased as temperature increases. The reference value (at 25 ºC) of *frq* translation rate constant is 0.19. If the value of *frq* translation rate constant is defined as 0.165 at 21 ºC, the activation energy of *frq* translation can be calculated from equation (2.24) in chapter 2. Figure 5.8A shows the results of a simulation where the rate of *frq* translation is temperature-dependent and the activation energy is 25692 J/mol. Since *k_FRQ* is a negative response coefficient parameter, the increase of *frq* translation results in a shorter period (Figure 5.8A).

To counterbalance this effect, another reaction should be able to increase the period, maintain the same level of *frq* mRNA at different temperatures and also accumulate FRQ at higher temperatures. After testing each of the parameters with the help of the results from the period response coefficient test, I found that only two possible reactions can fulfil these conditions: 1. As the temperature increases, the transport rate of FRQ into the nucleus, *kin_hypoFRQc*, decreases. 2. As the temperature increases, the dissociation constant of FRQ and WCC, *Kp_hypoWCCn*, increases. However, the first hypothesis is better able to maintain the period at higher temperatures (data not shown).

The period response coefficient table shows that the transport rate of FRQ into the nucleus, *kin_hypoFRQc*, is a negative response coefficient parameter, as is *k_FRQ*. Thus, decreasing *kin_hypoFRQc* increases the period of the clock, which counterbalances the effect on the period of increasing *k_FRQ*. Therefore, I hypothesise that with increasing temperature the translation of FRQ protein increases and the first order reaction rate constant of FRQ nuclear import decreases. Simulation results show that temperature compensation can be achieved with this hypothesis

(Figure 5.8B). The reference value of *frq* translation rate constant (*k_FRQ*) and the nuclear localisation rate constant of hypophosphorylated FRQ (*kin_hypoFRQc*) is 0.19 and 0.1, respectively. If the value of *k_FRQ* and *kin_hypoFRQc* are defined respectively as 0.227 and 0.085 at 28 ºC, both of the activation energies can be calculated from equation (2.24) in chapter 2. In this simulation, the activation energies of *frq* translation and FRQ nuclear localisation are 44232 J/mol and -40401 J/mol, respectively. The level of *frq* mRNA remains almost constant between 20-30ºC and FRQ level increases as the temperature increases. However, the FRQ level is not tripled from 21-28ºC, but from experimental data the fold increase in FRQ level is greater between 25-28ºC than between 21-25ºC (Tseng *et al*., 2012), indicating that the dependence of *frq* translation on temperature is not linear. This observation led us to introduce different activation energies below and above 25ºC for *frq* translation. If *k_FRQ* is defined as 0.118 at 21 ºC and 0.65 at 28 ºC, the activation energies of *k_FRQ* below and above 25ºC are 86747 J/mol and 305762 J/mol, respectively. If *kin_hypoFRQc* is defined at 0.18 at 21 ºC the activation energy is -107043 J/mol. As a result, the FRQ level is now tripled from 21-28ºC and doubled from 25-28ºC (Figure 5.8C). Temperature compensation of the period is achieved and the level of *frq* mRNA remains nearly constant within 20-30ºC, which is in agreement with experimental observations (Tseng *et al*., 2012).

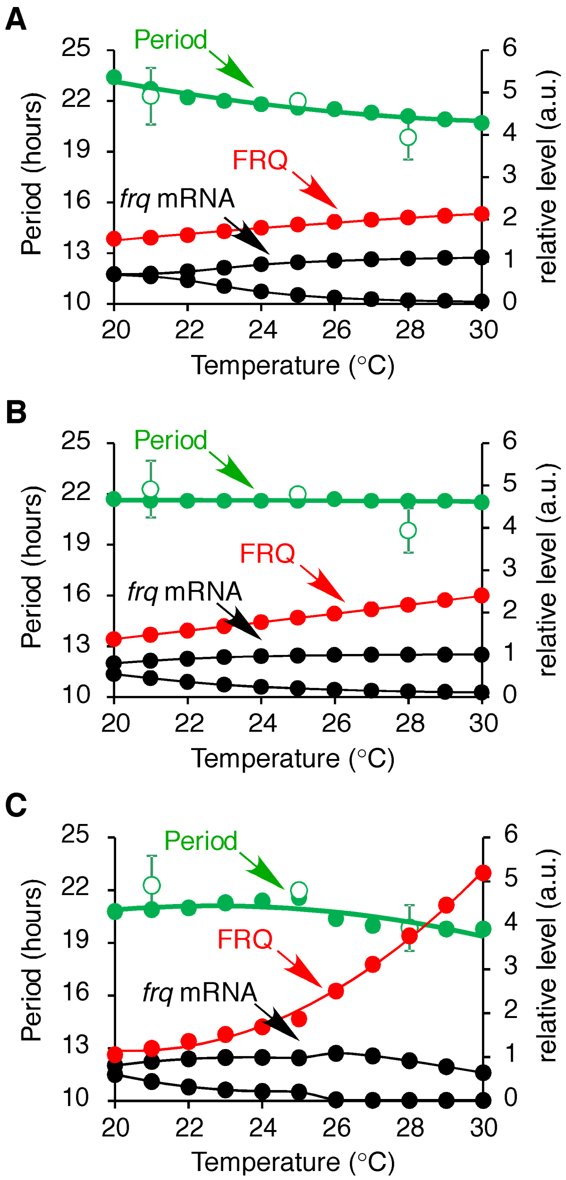

Figure 5.8 Simulated results showing the clock period and *frq* RNA and FRQ protein levels between 20 and 30 °C.

In (A) Only frq translation rate changes with temperature. In (B) translation of frq and the translocation of FRQ into the nucleus are temperature-dependent. (C) The translation of frq and the translocation of FRQ into the nucleus are temperature-dependent and frq translation has different activation energies above and below 25 °C. Simulated period = closed green circles, experimentally derived period = open green circles. Peak levels of FRQ (closed red circles) and peak and trough levels of frq mRNA (closed black circles).

5.8 The level of nuclear FRQ is higher at 30 ºC than at 25 ºC, but the ratio of nuclear FRQ to total FRQ is smaller at 30 ºC than at 25 ºC

To validate the temperature compensation hypothesis, a fractionation experiment was carried out. Tissue was grown at either 25 ºC or 30 ºC for at least 24 hours in constant light (LL) and transferred to constant darkness (DD) at the same temperature. The results show that although the level of nuclear FRQ is higher at higher temperature (Figure 5.9A and B), the ratio of nuclear FRQ to total FRQ is smaller at higher temperature (Figure 5.9C), suggesting that nuclear localisation of FRQ is slightly restricted with temperature. Two independent experiments were carried out and gave similar results. In addition, the level of WC-1 and WC-2 are slightly higher at 30 ºC than at 25 ºC. WC-1 moves slower in the nuclear fraction than the total extract, suggesting that the conformation and phosphorylation status of WC-1 is different depending on its localisation. Although the level of alpha-tubulin was significantly lower in the nuclear fraction than in the total extract, detectable alpha-tubulin in the nuclear fraction indicates that the nuclear fraction was slightly contaminated with cytoplasmic fraction. Therefore, the level of FRQ from the nuclear fraction might be lower if the purity of nuclear fraction is perfect, suggesting that more FRQ might be restricted to or translocated into the nucleus as expected from these data. Nevertheless, because FRQ nuclear localisation is not significantly restricted, this mechanism might not be sufficient to achieve temperature compensation. In this case, there should be other mechanisms that support temperature compensation.

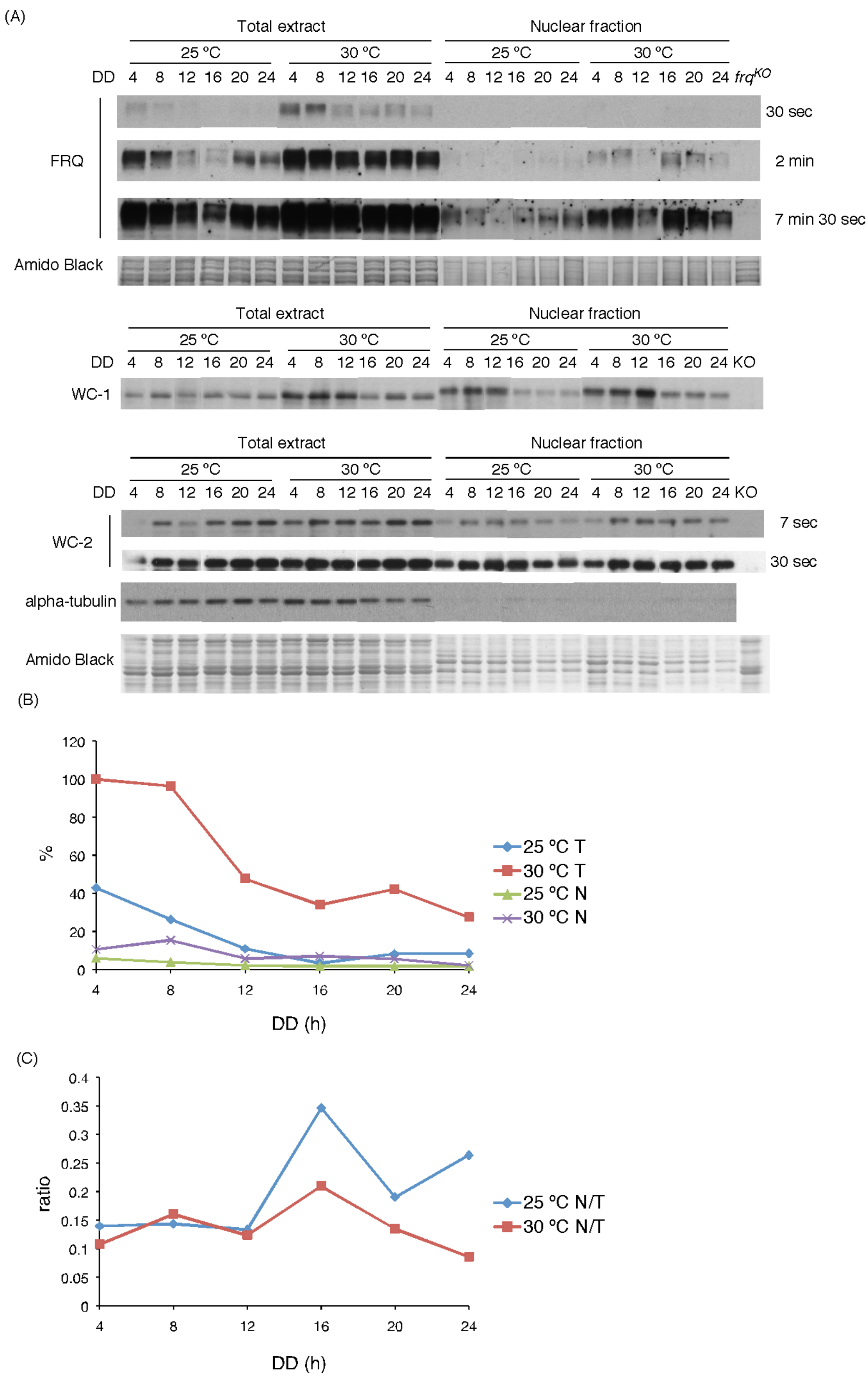

Figure 5.9 Subcellular distribution of FRQ at 25 and 30 ºC.
(A) Western blot analysis shows the level of FRQ, WC-1, WC-2 and alpha-tubulin from DD 4 to DD 24 with 4 hours interval. (B) The densitometric analysis of the results of FRQ. (C) The ratio of nuclear (N) to total (T) FRQ at 25 ºC and 30 ºC. Amido black stained membrane shows each sample was evenly load. Another two experiments were carried out and had similar results.

5.9 Summary

The period and the phase of *Neurospora* conidiation is temperature compensated from 18 ºC to 31 ºC. Our results from experimental data and response coefficient test, as well as results from literature, led us to hypothesise a possible mechanism to achieve temperature compensation: As the temperature increases, *frq* translation increases and FRQ nuclear localisation decreases. The results show that although the level of nuclear FRQ is higher at 30 ºC than at 25 ºC, FRQ nuclear localisation is slightly restricted at higher temperature, confirming the mechanism predicted by our model . However, the reduction of FRQ nuclear localisation alone is unlikely to account in full for temperature compensation. Other mechanisms supporting temperature compensation are probably present.

Chapter 6

Discussion, summary and future work

6. Discussion, summary and future work

6.1 Introduction

Biological systems are usually complex and it is thus difficult to fully understand the interactions between multiple components in systems, such as circadian clocks. To study a dynamic circadian system, a quantitative model is necessary. This quantitative model not only can be used to prove our understanding of the system, but also gives a platform to discuss the effects of interactions between components, test new hypotheses and discover novel properties.

In my work, a comprehensive *Neurospora* circadian clock model was constructed, which represents the current understanding of the *Neurospora* circadian clock. This model incorporated key clock components of the *Neurospora* circadian clock and reproduced a variety of clock characteristics, including the correct period, phase and relative level of *frq* expression and other key clock components, and light responses. In addition, this model led me to propose an underlying mechanism of temperature compensation: *frq* translation increases and FRQ nuclear import decreases simultaneously at higher temperatures. Furthermore, this model gives a unique opportunity of testing the coupling between light and temperature effects at the same time.

In this chapter, issues including the antiphasic behaviour of FRQ and WCC, the phase of the clock after light to dark transfer, temperature compensation in biology and in modelling, FRQ subcellular distribution and its contribution on temperature compensation and parameters chosen for temperature compensation will be discussed. Summary and future work will be presented at the end of this chapter.

6.1 The antiphasic behaviour of FRQ and WCC is reproduced in the model

In constant darkness, transcriptional regulation of *frq* by the WCC is a key step in *Neurospora*'s circadian oscillator and periodic transcription by WCC is dependent on its phosphorylation state (Schafmeier *et al*., 2005). Whereas hypophosphorylated WCC is degraded after activating *frq* transcription, phosphorylated WCC is more stable and can be shuttled out of the nucleus into the cytoplasm where dephosphorylation may occur (Schafmeier *et al*., 2008). The latter pathway results in the reappearance of hypophosphorylated WCC in the nucleus, which ensures the availability of WCC for the next cycle of transcription activation. My model recapitulates these experimental observations: degradation of WCC as a consequence of its role as a transcriptional activator of *frq* results in the reduction of WCC during the increasing phase of *frq* transcription. Furthermore, when FRQ levels peak, phosphorylation of the WCC, promoted by rising levels of FRQ, allows the complex to escape degradation and enter the cycle of nuclear cytoplasmic translocation. As levels of WCC reach their zenith, FRQ gradually decreases because of the decreased activation of *frq* transcription by WCC. Thus, WCC promotes *frq* transcription when the level of FRQ is low. Another possible pathway leading to the degradation of WCC centres on WCC phosphorylation state. This hypothesis was tested by modelling WCC degradation via phosphorylation. In this case my model predicts that when FRQ decreases, a delay occurs before the synthesis of new WCC and no antiphasic behaviour between WCC and FRQ is seen. Consequently, my model supports the hypothesis that degradation of WCC via transcription activation is a key factor for antiphasic FRQ and WCC expression. A putative WCC binding site exists in the *wc-1* promoter (Káldi *et al*., 2006) but a mutation of WC-2 Zn finger DNA-binding domain does not affect the expression of WC-1 (Schafmeier *et al*., 2008) indicating that a transcription factor other than the WCC regulates expression of *wc-1*. The model shows that the inferred transcription factor is necessary for antiphasic expression of WC-1 and FRQ.

6.2 The phase of the clock after light to dark transfer is delayed in the model

An important aspect of circadian clocks is their ability to integrate signals from their environment, such as light. When exposed to light, *frq* mRNA level is elevated and variable (Crosthwaite *et al*., 1995), FRQ is maintained at approximately twice the level seen in the dark (Elvin *et al*., 2005) and the *Neurospora* oscillator dampens (Elvin *et al*., 2005). On transfer from light to dark, *frq* RNA and protein are degraded and rhythmic expression of *frq* resumes (Garceau *et al*., 1997; Guo *et al*., 2009). My model incorporates a mechanism by which VVD-mediated inactivation of WCC reduces *frq* mRNA transcription at the light to dark boundary as well as the role of the FRQ-FRH complex in facilitating *frq* mRNA degradation in a FRQ concentration dependent manner (Chen *et al*., 2010; Guo *et al*., 2009; Guo *et al*., 2010; Hunt *et al*., 2010; Malzahn *et al*., 2010). However, the peak phase of *frq* mRNA after light to dark transfer is usually at DD 12-16 from experimental data (Kramer *et al*., 2003). In the model, the phase is delayed by 6 hours. Adjusting the values of the VVD interaction parameters and the FRQ-FRH-dependent *frq* mRNA degradation constant does not solve this problem, suggesting that other mechanism(s) need to be included in the model. In the model, after light to dark transfer, *frq* mRNA and FRQ are quickly degraded and maintained at a low level for a few hours. Therefore, the high level of *frq* mRNA and FRQ in light is efficiently cleared after light to dark transfer. Nevertheless, it seems that the repression of FRQ is so strong that the *frq* expression in dark is difficult to start. From experimental data, the ratio of nuclear to total FRQ (n/tFRQ) is about 0.3 in constant darkness and about 0.2 in constant light at 25 ºC (Cha *et al*., 2011). In my model, the n/tFRQ ratio is 0.276 in constant darkness and 0.286 in constant light, suggesting that FRQ phosphorylation status as well as the subcellular distribution of FRQ might be changed from light to dark. In the model, only hypo- and hyper- phosphorylated FRQ forms are considered whereas more than 70 phosphorylation sites have been identified in FRQ (Baker *et al*., 2009). From experimental data, the phosphorylation status of FRQ determines its localisation (Diernfellner *et al*., 2009). Hypophosphorylated FRQ is able to shuttle into and out of the nucleus, whereas as FRQ is further phosphorylated, the nuclear localisation of FRQ is restricted (Diernfellner *et al*., 2009). In addition, FRQ is highly phosphorylated in constant light (Collett *et al*., 2002). Therefore, adding new components of FRQ representing different status of phosphorylation and increasing the rate of FRQ phosphoryaltion in light may improve the phase delay of *frq* mRNA and correct the n/tFRQ ratio after light to dark transfer.

6.3 Temperature compensation of circadian clocks

The least understood characteristic of circadian clocks, namely temperature compensation of circadian rhythmicity, has been an important focus of this study. Temperature compensation may be achieved in a number of different ways, involving either true or apparent constancy of reaction rates. For example, a seemingly temperature insensitive reaction rate has been reported for the phosphorylation of the mammalian clock protein PER2 by CK1ε and CK1δ (Isojima *et al*., 2009) and this is thought to be important for temperature compensation. On the other hand, ATPase activity of KaiC is independent of temperature (Murakami *et al.*, 2008). In *Drosophila*, temperature compensation may be achieved by the temperature-independent PER activity (Huang *et al.*, 1995). More complex regulations in clock protein activities have been proposed in *Arabidopsis*, where not just one but many different clock components apparently participate to various degrees in the oscillation at different temperatures (Gould *et al.*, 2009; Salome *et al.*, 2010). The dynamic balance between *LATE ELONGATED HYPOCOTYL* (*LHY*) and *GIGANTEA* (*GI*) supports temperature compensation at high temperatures (17-27 ºC) (Gould *et al.*, 2006). At low temperatures (at 12-17 ºC), *CIRCADIAN CLOCK ASSOCIATED1* (*CCA1*) replaces the dynamic balance with *LHY* (Gould *et al.*, 2006). In addition, *PRR7* and *PRR9* are also involved in temperature compensation (Salome *et al.*, 2010).

6.4 Modelling temperature compensation

Modelling of circadian clocks is an effective approach to investigate the network properties of the underlying oscillators and to understand how they interact with the environment. For example, In *Arabidopsis*, modelling provides quantitative understanding and helps to suggest further experiments (Gould *et al.*, 2006; Locke *et al.*, 2005a; Locke *et al.*, 2005b). A recent model of the *Arabidopsis* circadian clock depicts the complexity of the clock and predicted a critical role for PRR5 (Pseudo response regulator 5) in the clock-control of morning gene expression (Pokhilko *et al.*, 2010). In addition, modelling the phosphorylation of different sites of the mammalian clock protein PER showed that PER phosphorylation by casein kinase CKI can explain the period decrease and phase advance associated with some mood disorders (Leloup and Goldbeter, 2011). In cyanobacteria, whose circadian clock can be reconstituted *in vitro*, modelling of the oscillations of two populations of Kai proteins, including the phosphorylation/dephosphorylation of KaiC and monomer reshuffling between KaiC hexamers, has provided insight into the mechanism by which clock time is maintained when new hypophosphorylated Kai proteins are synthesized (Nagai *et al*., 2010). More recent cyanobacterial circadian clock model suggested that temperature compensation can be achieved when the total amount of KaiA is maintained and the phosphorylation rate of KaiC is dependent on the concentration of free KaiA (not binding with KaiC) (Hatakeyama and Kaneko, 2012). They also proposed a simplified model, which can be used explain how temperature compensation is achieved by autonomous regulation of catalyst concentration for other (bio)chemical oscillators (Hatakeyama and Kaneko, 2012).

In this work, a comprehensive *Neurospora* circadian clock model was constructed and successfully simulated clock component oscillations with accurate relative levels and phases of clock components. Light responses such as phase resetting by light, entrainment to a light dark cycle and photoadaptation are also successfully predicted by the model. This model allows us to postulate that temperature compensation is achieved by a concomitant increase in *frq* translation and inhibition of FRQ nuclear localisation.

6.5 FRQ subcellular distribution and its contribution on temperature compensation

How might subcellular localisation of FRQ be regulated? Nuclear translocation may be regulated by FRQ phosphorylation, although more recent evidence suggests that this is not the case and that at least at 25 °C, FRQ's interaction with FRH and overall conformation plays a greater role (Cha *et al*., 2011). The results from FRQ-mCh (FRQ is fused with a red fluorescent protein mCherryNC) *in vivo* experiments suggest that FRQ nuclear localisation should be complex and time dependent (Castro-Longoria *et al*., 2010). This being true one would predict that some other posttranslational modification and/or change in conformation of FRQ regulates nuclear localisation with temperature. If my prediction is correct, nuclear localisation of FRQ should be restricted at high temperature. If the ratio of cytoplasmic FRQ to nuclear FRQ is similar at low and high temperature, this would suggest that although FRQ level is essentially increased, the activity of FRQ may be diminished at higher temperature, ensuring that levels of WCC phosphorylation are maintained.

Our data imply that temperature-dependent changes in the localisation of FRQ are an important aspect of temperature compensation. My experimental data shows that although the level of nuclear FRQ increases at higher temperatures, the ratio of nuclear to total FRQ (n/tFRQ) decreases. In my hypothesis derived from the model, the peak level of nuclear FRQ is increased as temperature increases. However, the n/tFRQ ratio at 21 ºC, 25 ºC and 28 ºC is 0.402, 0.276 and 0.189, respectively, which is similar to the behaviour seen in experimental results. These results suggest that FRQ nuclear localisation is not greatly restricted at high temperatures, but the rate constant of nuclear import is decreased, supporting temperature compensation of the period.

6.6 Parameter chosen for temperature compensation hypothesis

Highly period-sensitive parameters (Figure 5.4) might not significantly contribute to temperature compensation whereas low period-sensitive parameters might be important for temperature compensation. The parameters chosen for making the temperature compensation hypothesis should be able to reproduce temperature sensitive phenotypes. To be valid, the proposed mechanism of temperature compensation has to be in agreement with a certain number of experimental observations. Between 21 ºC and 28 ºC: (1) *frq* RNA levels are unchanged, (2) FRQ protein levels increase by 3-4 fold, (3) the degradation rate of FRQ is unchanged. Thus, the increase in FRQ levels must be due to an increase in *frq* translation. However, if the *frq* translation rate is increased significantly, the model predicts that the *frq* RNA level would decrease and the period shorten. Hence, the increase in *frq* translation has to be compensated by other reactions that: (1) increase the period, (2) increase the *frq* RNA level, and (3) triple the FRQ level. Firstly, an individual reaction parameter was tested to see whether these conditions could be fulfilled over a range of temperatures. When a fixed activation energy for *frq* translation was considered, no parameter variations could fulfil all three conditions and the oscillation was lost at lower temperatures. Secondly, different activation energies below and above 25 ºC for *frq* translation were considered. The reason why *frq* translation may have different activation energies may lie in the complexity of the mechanisms of translation where multiple enzymes are involved. In addition, the structure of mRNA and the conformation of FRQ may be changed at different temperatures. Supporting the use of different acticvation energies, translation in rabbit reticulocytes and mouse L-cells was found to have two different activation energies below and above 24 ºC for protein synthesis and below and above 25 ºC for protein elongation and release (Craig, 1975). Similarly, Hong *et al.* (Hong *et al.*, 2008a) employed a curved Arrhenius plot for WCC binding to the *frq* promoter and the degradation of FRQ, and used different activation energies depending on the range of temperature (20-25 °C or

25-30 °C) to explain temperature compensation. Using different activation energies for frq translation, I observed that when: (1) the Michaelis constant of nuclear WCC phosphorylation is increased with increasing temperature, or (2) the nuclear localisation of FRQ is decreased with increasing temperature, the three conditions are fulfilled. The second modification leads to simulations that are in better agreement with experimental data. The period of the clock decreased more at higher temperatures when the first hypothesis was modelled than when the second hypothesis was modelled (less temperature compensated).

How is the restriction of FRQ nuclear localisation at high temperatures possible? For general chemical reactions, the activation energy must be positive, which means that the reaction rate always increases with increasing temperature. However, some biochemical reactions do have negative activation energy, such as the GTPase activity in human guanylate binding protein-1 (hGBP1) (Rani *et al*., 2012). The reason of having a negative activation energy is because these biochemical reactions usually contain more than one elementary step of reaction and multiple components are involved in that reaction. If the increase of one or multiple elementary steps of reaction significantly decreases the overall reaction rate at higher temperature, the activation energy will possibly be negative. Temperature regulates a variety of biochemical reactions such as temperature-dependent alternative splicing (Akman *et al*., 2008; Diernfellner *et al*., 2007; James *et al*., 2012; Majercak *et al*., 1999), which may result in negative activation energy for a certain group of reaction. In addition, temperature dependent translocation of proteins has been reported in other organisms, for example in rat fibroblasts the temperature-sensitive mutant of p53 ($p53^{val-5}$) is predominantly in the cytoplasm at 37.5 °C but moves to the nucleus at 32.5 °C

(Ginsberg *et al.*, 1991). Another example of a protein whose localisation is temperature-dependent is the *Antirrhinum* Tam3 transposase, which is restricted to the cytoplasm at 25 °C, but translocates into the nucleus at 15 °C (Fujino *et al.*, 2011). Interestingly, translocation between cytoplasm and nucleus of the *Drosophila* clock protein PER is restricted in the *ritsu* mutant at higher temperatures, resulting in lengthening the period of the clock (Matsumoto *et al.*, 1999).

In addition, the hypothesis proposed in this thesis only considered the criteria of *frq* components and may not be sufficient to achieve temperature compensation. Other conditions such as the level of WC-1, WC-2 and VVD and their nuclear to cytoplasmic protein ratio should also be considered if they are temperature sensitive. New components such as *qrf* RNA and partially phosphorylated FRQ may need to be included into the model to reproduce temperature compensation characteristics and the level and phase of temperature sensitive clock components. Consequently, multiple mechanisms would be considered and simulated at the same time to achieve comprehensive temperature compensation.

6.7 Summary and future work

In summary, I have built a comprehensive model of the *Neurospora* circadian clock and its responses to acute and chronic changes in light and temperature. The model predicts a role for FRQ nuclear localisation in temperature compensation and makes predictions that can be experimentally tested in the future to further refine our understanding of circadian oscillators. Both light and temperature can entrain and reset the clock (Dharmananda, 1980; Gooch *et al.*, 1994; Johnson, 1999; Liu *et al.*, 1998), and in reality organisms are exposed to these conditions simultaneously. An advantage of having a model that incorporates both light response and temperature dependency is that the coupling between both types of environmental signals can be studied to provide a comprehensive understanding of the detailed molecular interactions of the clock.

Although my model successfully reproduces a variety of clock characteristics, such as the correct period of the clock, the correct phase of key clock components, the entrainment to 24 hours period by 12 h: 12 h light/dark cycles, the light phase response curve and photoadaptation, there are several aspects of the model that could be updated, corrected and refined:

1. To update the degradation rates of RNAs determined from experiments.
2. To add components of FRQ representing different status of phosphorylation and localisation of cell compartments.
3. To add the *qrf* RNA into the model and consider its regulation function *frq* mRNA degradation.
4. After light to dark transfer, the expression of *vvd* RNA on the first day is observed from experiments. This should be incorporated into the model since VVD is important for generating the correct phase of conidiation (Heintzen *et al*., 2001; Hunt *et al*., 2007) after light to dark transfer and is involved in temperature compensation of phase (Hunt *et al*., 2007).
5. To correct the phase of *frq* RNA after light to dark transfer.
6. To correct and refine the ratio of hypophosphorylated FRQ to hyperphosphorylated FRQ.
7. To correct and refine the ratio of nuclear FRQ to cytoplasmic FRQ.

8. The level of WC-1 and WC-2 are dominantly in the nucleus.
9. The ratio of nuclear WC-1 to cytoplasmic WC-1 is needed to be refined, as well as WC-2.

As well as up-dating the model, tests to understand the characteristics of the parameters in the model and to validate the model should be carried out:

1. How much is the period of the clock affected by each of the parameters before the oscillation of the clock is lost? How are the period and phase affected when certain gene is over expressed? These results can be compared with experimental data, such as qa-FRQ, qa-WC-1 and qa-WC-2 constructs.
2. How are the phase response curves by temperature pulse if we consider the hypothesis: *frq* translation increases and FRQ nuclear import decreases simultaneously at higher temperatures. In addition, if we consider more mechanisms, such as the phosphorylation rate of WCC facilitated by FRQ, how are the level and phase of key clock components in these conditions?

Several experiments can also be carried out to measure parameters for the model and validate the model:

1. Although the level of *frq* RNA oscillation is similar at 21 and 28 ºC (Liu *et al*., 1998; Tseng *et al*., 2012), it is still uncertain whether the transcription and the degradation of *frq* RNA is the same at 21 and 28ºC. In addition, from the response coefficient analysis, the reaction rates of transcription and degradation of RNAs are usually sensitive to the period of the clock,

especially for *frq* and *wc-1*. Therefore, experiments to determine the degradation rates of RNAs at different temperatures should be carried out.

2. From published literature (Ruoff *et al*., 1996) and the response coefficient analysis, the stability of the clock components sensitively affects period. Although the degradation of FRQ is temperature compensated (Mehra *et al*., 2009), is the effect of temperature on the degradation rate of other clock proteins such as WC-1, WC-2 and VVD is still unknown. Therefore, testing the degradation rates of clock proteins at different temperatures would not only be helpful to determine the parameter value in the model, but also help to discover the mechanisms of temperature compensation.

3. Localisation of clock proteins determines the interaction between clock components, such as phosphorylation, complex formation and function. In addition to subcellular fractionation, *in vivo* subcellular monitoring of FRQ, WC-1, WC-2, VVD at different temperatures would be helpful to validate the hypothesis of temperature compensation.

The regulation of the output of the circadian clock also determines the timing of clock-regulated processes. The conidiation of *Neurospora* is controlled by the clock. Experimental data suggested that VVD is involved in temperature compensation and influences the time of conidiation downstream from the clock (Hunt *et al*., 2007). However, what are the downstream underlying mechanisms triggering conidiation? Is temperature compensation of conidiation achieved because the phases of clock components are temperature compensated or because the downstream mechanisms are temperature compensated? These hypotheses can be tested by further incorporating the output pathways into the model. The model can be converted into a more generalised model to study how circadian clocks mediate between biochemical and behavioural processes. It would then be possible to not only focus on what is happening within the central molecular clock, but also to investigate how the clock and other biological systems interact with each other. For example how circadian clocks interact with the cell cycle (Hunt and Sassone-Corsi, 2007), stress (Sanchez *et al.*, 2011) and metabolism (Sancar *et al.*, 2012; Zhang and Kay, 2010).

References

Ahmed A, Case ME, Giles NH (1964) The Nature of Complementation among Mutants in the Histidine-3 Region of Neurospora Crassa. Brookhaven Symp Biol 17: 53-65.

Akman OE, Locke JC, Tang S, Carre I, Millar AJ, et al. (2008) Isoform switching facilitates period control in the *Neurospora crassa* circadian clock. Mol Syst Biol 4: 164.

Antle MC, Silver R (2009) Neural basis of timing and anticipatory behaviors. Eur J Neurosci 30: 1643-1649.

Aronson BD, Johnson KA, Loros JJ, Dunlap JC (1994) Negative feedback defining a circadian clock: autoregulation of the clock gene frequency. Science 263: 1578-1584.

Auffray C, Imbeaud S, Roux-Rouquié M, Hood L (2003) From functional genomics to systems biology: concepts and practices. C R Biol 326: 879-892.

Baker CL, Kettenbach AN, Loros JJ, Gerber SA, Dunlap JC (2009) Quantitative proteomics reveals a dynamic interactome and phase-specific phosphorylation in the *Neurospora* circadian clock. Mol Cell 34: 354-363.

Ballario P, Vittorioso P, Magrelli A, Talora C, Cabibbo A, et al. (1996) White collar-1, a central regulator of blue light responses in *Neurospora*, is a zinc finger protein. EMBO J 15: 1650-1657.

Batista LFZ, Kaina B, Meneghini R, Menck CFM (2009) How DNA lesions are turned into powerful killing structures: Insights from UV-induced apoptosis. Mutat Res 681: 197-208.

Belden WJ, Larrondo LF, Froehlich AC, Shi M, Chen CH, et al. (2007) The band mutation in *Neurospora crassa* is a dominant allele of ras-1 implicating RAS signaling in circadian output. Genes Dev 21: 1494-1505.

Belden WJ, Lewis ZA, Selker EU, Loros JJ, Dunlap JC (2011) CHD1 remodels chromatin and influences transient DNA methylation at the clock gene *frequency*. PLoS Genet 7: e1002166.

Briggs WR, Huala E (1999) Blue-light photoreceptors in higher plants. Annu Rev Cell Dev Biol 15: 33-62.

Bruggeman FJ, Westerhoff HV (2007) The nature of systems biology. Trends Microbiol 15: 45-50.

Brunner M, Schafmeier T (2006) Transcriptional and post-transcriptional regulation of the circadian clock of cyanobacteria and *Neurospora*. Genes Dev 20: 1061-1074.

Carthew RW, Sontheimer EJ (2009) Origins and mechanisms of miRNAs and siRNAs. Cell 136: 642-655.

Castro-Longoria E, Ferry M, Bartnicki-Garcia S, Hasty J, Brody S (2010) Circadian rhythms in *Neurospora crassa*: dynamics of the clock component frequency visualized using a fluorescent reporter. Fungal Genet Biol 47: 332-341.

Catalanotto C, Pallotta M, ReFalo P, Sachs MS, Vayssie L, et al. (2004) Redundancy of the two dicer genes in transgene-induced posttranscriptional gene silencing in *Neurospora crassa*. Mol Cell Biol 24: 2536-2545.

Cha J, Chang SS, Huang G, Cheng P, Liu Y (2008) Control of WHITE COLLAR localization by phosphorylation is a critical step in the circadian negative feedback process. EMBO J 27: 3246-3255.

Cha J, Yuan H, Liu Y (2011) Regulation of the activity and cellular localization of the circadian clock protein FRQ. J Biol Chem 286: 11469-11478.

Chang SS, Zhang Z, Liu Y (2012) RNA interference pathways in fungi: mechanisms and functions. Annu Rev Microbiol 66: 305-323.

Chen CH, DeMay BS, Gladfelter AS, Dunlap JC, Loros JJ (2010) Physical interaction between VIVID and white collar complex regulates photoadaptation in *Neurospora*. Proc Natl Acad Sci U S A 107: 16715-16720.

Cheng P, Yang Y, Heintzen C, Liu Y (2001a) Coiled-coil domain mediated FRQ-FRQ interaction is essential for its circadian clock function in *Neurospora*. EMBO J 20: 101-108.

Cheng P, Yang Y, Liu Y (2001b) Interlocked feedback loops contribute to the robustness of the *Neurospora* circadian clock. Proc Natl Acad Sci U S A 98: 7408-7413.

Cheng P, Yang Y, Gardner KH, Liu1 Y (2002) PAS domain-mediated WC-1/WC-2 interaction is essential for maintaining the steady-state level of WC-1 and the function of both proteins in circadian clock and light responses of Neurospora. Mol Cell Biol 22: 517-524.

Cheng P, Yang Y, Wang L, He Q, Liu Y (2003) WHITE COLLAR-1, a multifunctional neurospora protein involved in the circadian feedback loops, light sensing, and transcription repression of *wc-2*. J Biol Chem 278: 3801-3808.

Cheng P, He Q, He Q, Wang L, Liu1 Y (2005) Regulation of the *Neurospora* circadian clock by an RNA helicase. Genes Dev 19: 234-241.

Choudhary S, Lee HC, Maiti M, He Q, Cheng P, et al. (2007) A double-stranded-RNA response program important for RNA interference efficiency. Mol Cell Biol 27: 3995-4005.

Christensen MK, Falkeid G, Loros JJ, Dunlap JC, Lillo C, et al. (2004) A nitrate-induced frq-less oscillator in *Neurospora crassa*. J Biol Rhythms 19: 280-286.

Cogoni C, Macino G (1997) Isolation of quelling-defective (qde) mutants impaired in posttranscriptional transgene-induced gene silencing in *Neurospora crassa*. Proc Natl Acad Sci U S A 94: 10233-10238.

Collett MA, Dunlap JC, Loros JJ (2001) Circadian clock-specific roles for the light response protein WHITE COLLAR-2. Mol Cell Biol 21: 2619-2628.

Collett MA, Garceau N, Dunlap JC, Loros JJ (2002) Light and clock expression of the *Neurospora* clock gene *frequency* is differentially driven by but dependent on WHITE COLLAR-2. Genetics 160: 149-158.

Colot HV, Loros JJ, Dunlap JC (2005) Temperature-modulated alternative splicing and promoter use in the Circadian clock gene *frequency*. Mol Biol Cell 16: 5563-5571.

Cornish-Bowden A (2004) Introduction to enzyme kinetics. Fundamentals of Enzyme Kinetics. 3rd ed. ed. London: Portland Press. pp. 23-70.

Correa A, Lewis ZA, Greene AV, March IJ, Gomer RH, et al. (2003) Multiple oscillators regulate circadian gene expression in *Neurospora*. Proc Natl Acad Sci U S A 100: 13597-13602.

Craig N (1975) Regulation of translation in rabbit reticulocytes and mouse L-cells; comparison of the effects of temperature. J Cell Physiol 87: 157-166.

Crosson S, Rajagopal S, Moffat K (2003) The LOV domain family: photoresponsive signaling modules coupled to diverse output domains. Biochemistry (Mosc) 42: 2-10.

Crosthwaite SK, Loros JJ, Dunlap JC (1995) Light-induced resetting of a circadian clock is mediated by a rapid increase in *frequency* transcript. Cell 81: 1003-1012.

Crosthwaite SK, Dunlap JC, Loros JJ (1997) *Neurospora wc-1* and *wc-2*: transcription, photoresponses, and the origins of circadian rhythmicity. Science 276: 763-769.

Crosthwaite SK (2004) Circadian clocks and natural antisense RNA. FEBS Lett 567: 49-54.

Dardente H, Cermakian N (2007) Molecular circadian rhythms in central and peripheral clocks in mammals. Chronobiol Int 24: 195 - 213.

Das B, Butler JS, Sherman F (2003) Degradation of normal mRNA in the nucleus of *Saccharomyces cerevisiae*. Mol Cell Biol 23: 5502-5515.

Davis RH, de Serres FJ (1970) Genetic and microbial research techniques for *Neurospora crassa*. Methods Enzymol 17: 79-143.

de Paula RM, Lewis ZA, Greene AV, Seo KS, Morgan LW, et al. (2006) Two circadian timing circuits in *Neurospora crassa* cells share components and regulate distinct rhythmic processes. J Biol Rhythms 21: 159-168.

Denault DL, Loros JJ, Dunlap JC (2001) WC-2 mediates WC-1-FRQ interaction within the PAS protein-linked circadian feedback loop of *Neurospora*. EMBO J 20: 109-117.

Dharmananda S (1980) Studies of the circadian clock of *Neurospora crassa*: light-induced phase shifting [PhD Thesis]. Santa Cruz, California: University of California, Santa Cruz.

Diernfellner A, Colot HV, Dintsis O, Loros JJ, Dunlap JC, et al. (2007) Long and short isoforms of *Neurospora* clock protein FRQ support temperature-compensated circadian rhythms. FEBS Lett 581: 5759-5764.

Diernfellner ACR, Schafmeier T, Merrow MW, Brunner M (2005) Molecular mechanism of temperature sensing by the circadian clock of *Neurospora crassa*. Genes Dev 19: 1968-1973.

Diernfellner ACR, Querfurth C, Salazar C, Höfer T, Brunner M (2009) Phosphorylation modulates rapid nucleocytoplasmic shuttling and cytoplasmic accumulation of *Neurospora* clock protein FRQ on a circadian time scale. Genes Dev 23: 2192-2200.

Dodd AN, Salathia N, Hall A, Kevei E, Toth R, et al. (2005) Plant circadian clocks increase photosynthesis, growth, survival, and competitive advantage. Science 309: 630-633.

Dong G, Golden SS (2008) How a cyanobacterium tells time. Curr Opin Microbiol 11: 541-546.

Dragovic Z, Tan Y, Gorl M, Roenneberg T, Merrow M (2002) Light reception and circadian behavior in 'blind' and 'clock-less' mutants of *Neurospora crassa*. EMBO J 21: 3643-3651.

Dunlap JC (1999) Molecular bases for circadian clocks. Cell 96: 271-290.

Dunlap JC, Loros JJ, DeCoursey PJ (2004) Chronobiology: Biological Timekeeping. Sunderland, Mass.: Sinauer Associates.

Dunlap JC, Loros JJ (2006) How fungi keep time: circadian system in *Neurospora* and other fungi. Curr Opin Microbiol 9: 579-587.
Eckardt NA (2006) A wheel within a wheel: temperature compensation of the circadian clock. Plant Cell 18: 1105-1108.
Ecker GF, Stockner T, Chiba P (2008) Computational models for prediction of interactions with ABC-transporters. Drug Discov Today 13: 311-317.
Elvin M, Loros JJ, Dunlap JC, Heintzen C (2005) The PAS/LOV protein VIVID supports a rapidly dampened daytime oscillator that facilitates entrainment of the *Neurospora* circadian clock. Genes Dev 19: 2593-2605.
Fonzo LSN, Golini RS, Delgado SM, Ponce IT, Bonomi MR, et al. (2009) Temporal patterns of lipoperoxidation and antioxidant enzymes are modified in the hippocampus of vitamin A-deficient rats. Hippocampus 19: 869-880.
Francis CD, Sargent ML (1979) Effects of temperature perturbations on circadian conidiation in *Neurospora*. Plant Physiol 64: 1000-1004.
Francois P (2005) A model for the *Neurospora* circadian clock. Biophys J 88: 2369-2383.
Froehlich AC, Liu Y, Loros JJ, Dunlap JC (2002) White Collar-1, a circadian blue light photoreceptor, binding to the *frequency* promoter. Science 297: 815-819.
Froehlich AC, Loros JJ, Dunlap JC (2003) Rhythmic binding of a WHITE COLLAR-containing complex to the *frequency* promoter is inhibited by FREQUENCY. Proc Natl Acad Sci U S A 100: 5914-5919.
Fujino K, Hashida S-n, Ogawa T, Natsume T, Uchiyama T, et al. (2011) Temperature controls nuclear import of Tam3 transposase in *Antirrhinum*. Plant J 65: 146-155.
Funahashi A, Morohashi M, Kitano H, Tanimura N (2003) CellDesigner: a process diagram editor for gene-regulatory and biochemical networks. Drug Discov Today Biosilico 1: 159-162.
Funahashi A, Matsuoka Y, Jouraku A, Morohashi M, Kikuchi N, et al. (2008) CellDesigner 3.5: A versatile modeling tool for biochemical networks. Proc IEEE Inst Electr Electron Eng 96: 1254-1265.
Garceau NY, Liu Y, Loros JJ, Dunlap JC (1997) Alternative initiation of translation and time-specific phosphorylation yield multiple forms of the essential clock protein FREQUENCY. Cell 89: 469-476.
Gardner GF, Feldman JF (1981) Temperature compensation of circadian period length in clock mutants of *Neurospora crassa*. Plant Physiol 68: 1244-1248.
Gillespie DT (1977) Exact stochastic simulation of coupled chemical ceactions. J Phys Chem 81: 2340-2361.
Ginsberg D, Michael-Michalovitz D, Ginsberg D, Oren M (1991) Induction of growth arrest by a temperature-sensitive p53 mutant is correlated with increased nuclear localization and decreased stability of the protein. Mol Cell Biol 11: 582-585.
Goldbeter A (1996) Biochemical oscillations and cellular rhythms: The molecular bases of periodic and chaotic behaviour. Cambridge: Cambridge University Press.
Goldbeter A (1997) Modelling biochemical oscillations and cellular rhythms. Curr Sci 73: 933-939.

Gooch VD, Wehseler RA, Gross CG (1994) Temperature effects on the resetting of the phase of the *Neurospora* circadian rhythm. J Biol Rhythms 9: 83-94.
Goodwin BC (1963) Temporal organization in cells; a dynamic theory of cellular control processes. New York: Academic Press.
Goodwin BC (1965) Oscillatory behavior in enzymatic control processes. Adv Enzyme Regul 3: 425-438.
Gore J, Oudenaarden Av (2009) The yin and yang of nature. Nature 457: 271-272.
Gould PD, Locke JC, Larue C, Southern MM, Davis SJ, et al. (2006) The molecular basis of temperature compensation in the *Arabidopsis* circadian clock. Plant Cell 18: 1177-1187.
Gould PD, Diaz P, Hogben C, Kusakina J, Salem R, et al. (2009) Delayed fluorescence as a universal tool for the measurement of circadian rhythms in higher plants. Plant J 58: 893-901.
Goutelle S, Maurin M, Rougier F, Barbaut X, Bourguignona L, et al. (2008) The Hill equation: a review of its capabilities in pharmacological modelling. Fundam Clin Pharmacol 22: 633-648.
Guo J, Cheng P, Yuan H, Liu Y (2009) The exosome regulates circadian gene expression in a posttranscriptional negative feedback loop. Cell 138: 1236-1246.
Guo J, Cheng P, Liu Y (2010) Functional significance of FRH in regulating the phosphorylation and stability of *Neurospora* circadian clock protein FRQ. J Biol Chem 285: 11508–11515.
Halaban R (1968a) The Circadian Rhythm of Leaf Movement of Coleus blumei x C. frederici, a Short Day Plant. 2. The Effects of Light and Temperature Signals. Plant Physiol 43: 1887-1893.
Halaban R (1968b) The Circadian Rhythm of Leaf Movement of Coleus blumei x C. frederici, a Short Day Plant. 1. Under Constant Light Conditions. Plant Physiol 43: 1883-1886.
Hammond SM, Boettcher S, Caudy AA, Kobayashi R, Hannon GJ (2001) Argonaute2, a link between genetic and biochemical analyses of RNAi. Science 293: 1146-1150.
Harcourt AGV (1867) On the observation of the course of chemical change. Journal of the Chemical Society 20: 460-492.
Hastings JW, Sweeney BM (1957) On the mechanism of temperature independence in a biological clock. Proc Natl Acad Sci U S A 43: 804-811.
Hatakeyama TS, Kaneko K (2012) Generic temperature compensation of biological clocks by autonomous regulation of catalyst concentration. Proc Natl Acad Sci U S A 109: 8109-8114.
He Q, Cheng P, Yang Y, Wang L, Gardner KH, et al. (2002) White collar-1, a DNA binding transcription factor and a light sensor. Science 297: 840-843.
He Q, Cheng P, Yang Y, He Q, Yu H, et al. (2003) FWD1-mediated degradation of FREQUENCY in *Neurospora* establishes a conserved mechanism for circadian clock regulation. EMBO J 22: 4421-4430.
He Q, Liu Y (2005) Molecular mechanism of light responses in *Neurospora*: from light-induced transcription to photoadaptation. Genes Dev 19: 2888-2899.
He Q, Shu H, Cheng P, Chen S, Wang L, et al. (2005) Light-independent phosphorylation of WHITE COLLAR-1 regulates its function in the

Neurospora circadian negative feedback loop. J Biol Chem 280: 17526-17532.
He Q, Cha J, Lee HC, Yang Y, Liu Y (2006) CKI and CKII mediate the FREQUENCY-dependent phosphorylation of the WHITE COLLAR complex to close the *Neurospora* circadian negative feedback loop. Genes Dev 20: 2552-2565.
Heintzen C, Loros JJ, Dunlap JC (2001) The PAS protein VIVID defines a clock-associated feedback loop that represses light input, modulates gating, and regulates clock resetting. Cell 104: 453-464.
Heintzen C, Liu Y (2007) The *Neurospora crassa* circadian clock. Adv Genet 58: 25-66.
Hill AV (1910) The possible effects of the aggregation of the molecules of haemoglobin on its dissociation curves. J Physiol 40: iv–vii.
Hogenesch JB, Ueda HR (2011) Understanding systems-level properties: timely stories from the study of clocks. Nat Rev Genet 12: 407-416.
Hong CI, Jolma IW, Loros JJ, Dunlap JC, Ruoff P (2008a) Simulating dark expressions and interactions of *frq* and *wc-1* in the *Neurospora* circadian clock. Biophys J 94: 1221-1232.
Hong CI, Jolma IW, Loros JJ, Dunlap JC, Ruoff P (2008b) Simulating Dark Expressions and Interactions of frq and wc-1 in the *Neurospora* Circadian Clock. Biophys J 94: 1221-1232.
Hong CI, Ruoff P, Loros JJ, Dunlap JC (2008c) Closing the circadian negative feedback loop: FRQ-dependent clearance of WC-1 from the nucleus. Genes Dev 22: 3196-3204.
Huang G, Wang L, Liu Y (2006) Molecular mechanism of suppression of circadian rhythms by a critical stimulus. EMBO J 25: 5349-5357.
Huang G, Chen S, Li S, Cha J, Long C, et al. (2007) Protein kinase A and casein kinases mediate sequential phosphorylation events in the circadian negative feedback loop. Genes Dev 21: 3283-3295.
Huang ZJ, Curtin KD, Rosbash M (1995) PER protein interactions and temperature compensation of a circadian clock in *Drosophila*. Science 267: 1169-1172.
Hunt SM, Elvin M, Crosthwaite SK, Heintzen C (2007) The PAS/LOV protein VIVID controls temperature compensation of circadian clock phase and development in *Neurospora crassa*. Genes Dev 21: 1964-1974.
Hunt SM, Thompson S, Elvin M, Heintzen C (2010) VIVID interacts with the WHITE COLLAR complex and FREQUENCY-interacting RNA helicase to alter light and clock responses in *Neurospora*. Proc Natl Acad Sci U S A 107: 16709-16714.
Hunt T, Sassone-Corsi P (2007) Riding tandem: circadian clocks and the cell cycle. Cell 129: 461-464.
Isojima Y, Nakajima M, Ukai H, Fujishima H, Yamada RG, et al. (2009) CKIepsilon/delta-dependent phosphorylation is a temperature-insensitive, period-determining process in the mammalian circadian clock. Proc Natl Acad Sci U S A 106: 15744-15749.
James AB, Syed NH, Bordage S, Marshall J, Nimmo GA, et al. (2012) Alternative splicing mediates responses of the *Arabidopsis* circadian clock to temperature changes. Plant Cell 24: 961-981.
Johnson CH (1999) Forty years of PRCs--what have we learned? Chronobiol Int 16: 711-743.

Kageyama H, Nishiwaki T, Nakajima M, Iwasaki H, Oyama T, et al. (2006) Cyanobacterial circadian pacemaker: Kai protein complex dynamics in the KaiC phosphorylation cycle in vitro. Mol Cell 23: 161-171.

Káldi K, González BH, Brunner M (2006) Transcriptional regulation of the *Neurospora* circadian clock gene *wc-1* affects the phase of circadian output. EMBO Rep 7: 199-204.

Kitano H (2002) Computational systems biology. Nature 420: 206-210.

Kitano H, Funahashi A, Matsuoka Y, Oda K (2005) Using process diagrams for the graphical representation of biological networks. Nat Biotechnol 12: 961-966.

Kollmann M, Sourjik V (2007) In silico biology: from simulation to understanding. Curr Biol 17: R132-R134.

Konopka RJ, Benzer S (1971) Clock mutants of *Drosophila melanogaster*. Proc Natl Acad Sci U S A 68: 2112-2116.

Kozma-Bognar L, Kaldi K (2008) Synchronization of the fungal and the plant circadian clock by light. Chembiochem 9: 2565-2573.

Kramer C, Loros JJ, Dunlap JC, Crosthwaite SK (2003) Role for antisense RNA in regulating circadian clock function in *Neurospora crassa*. Nature 42: 948-952.

Kramer C (2007) Rhythmic conidiation in *Neurospora crassa*. Methods Mol Biol 362: 49-65.

Kusanagi H, Hida A, Satoh K, Echizenya M, Shimizu T, et al. (2008) Expression profiles of 10 circadian clock genes in human peripheral blood mononuclear cells. Neurosci Res 61: 136-142.

Laidler KJ, Meiser JH, Sanctuary BC (2003) Physical chemistry. Boston, Mass.: Houghton Mifflin.

Lakin-Thomas PL, Brody S (2000) Circadian rhythms in *Neurospora crassa*: lipid deficiencies restore robust rhythmicity to null frequency and white-collar mutants. Proc Natl Acad Sci U S A 97: 256-261.

Lee K, Loros JJ, Dunlap JC (2000) Interconnected feedback loops in the *Neurospora* circadian system. Science 289: 107-110.

Legerton TL, Yanofsky C (1985) Cloning and characterization of the multifunctional his-3 gene of Neurospora crassa. Gene 39: 129-140.

Leloup J-C, Gonze D, Goldbeter1 A (1999a) Limit Cycle Models for Circadian Rhythms Based on Transcriptional Regulation in *Drosophila* and *Neurospora*. J Biol Rhythms 14: 433-448.

Leloup J-C, Gonze D, Goldbeter1 A (1999b) Limit cycle models for circadian rhythms based on transcriptional regulation in *Drosophila* and *Neurospora*. J Biol Rhythms 14: 433-448.

Leloup J-C, Goldbeter A (2011) Modelling the dual role of Per phosphorylation and its effect on the period and phase of the mammalian circadian clock. IET Syst Biol 5: 44-49.

Lenz PH, Hower AE, Hartline DK (2005) Temperature compensation in the escape response of a marine copepod, *Calanus finmarchicus* (Crustacea). Biol Bull 209: 75-85.

Li S, Motavaze K, Kafes E, Suntharalingam S, Lakin-Thomas P (2011) A new mutation affecting FRQ-less rhythms in the circadian system of *Neurospora crassa*. PLoS Genet 7: e1002151.

Linden H, Macino G (1997) White collar 2, a partner in blue-light signal transduction, controlling expression of light-regulated genes in *Neurospora crassa*. EMBO J 16: 98-109.
Linden H, Rodriguez-Franco M, Macino G (1997) Mutants of *Neurospora crassa* defective in regulation of blue light perception. Mol Gen Genet 254: 111-118.
Liu Y, Merrow M, Loros JJ, Dunlap JC (1998) How temperature changes reset a circadian oscillator. Science 281: 825.
Liu Y, Loros J, Dunlap JC (2000) Phosphorylation of the *Neurospora* clock protein FREQUENCY determines its degradation rate and strongly influences the period length of the circadian clock. Proc Natl Acad Sci U S A 97: 234-239.
Liu Y (2005) Analysis of posttranslational regulations in the *Neurospora* circadian clock. Methods Enzymol 393: 379-393.
Liu Y, Bell-Pedersen D (2006) Circadian rhythms in *Neurospora* crassa and other filamentous fungi. Eukaryot Cell 5: 1184-1193.
Locke JC, Millar AJ, Turner MS (2005a) Modelling genetic networks with noisy and varied experimental data: the circadian clock in *Arabidopsis thaliana*. J Theor Biol 234: 383-393.
Locke JC, Southern MM, Kozma-Bognar L, Hibberd V, Brown PE, et al. (2005b) Extension of a genetic network model by iterative experimentation and mathematical analysis. Mol Syst Biol 1: 2005 0013.
Loros JJ, Feldman JF (1986) Loss of temperature compensation of circadian period length in the *frq-9* mutant of *Neurospora crassa*. J Biol Rhythms 1: 187-198.
Loros JJ, Dunlap JC (2001) Genetic and molecular analysis of circadian rhythms in *Neurospora*. Annu Rev Physiol 63: 757-794.
Maiti M, Lee HC, Liu Y (2007) QIP, a putative exonuclease, interacts with the *Neurospora* Argonaute protein and facilitates conversion of duplex siRNA into single strands. Genes Dev 21: 590-600.
Majercak J, Sidote D, Hardin PE, Edery I (1999) How a circadian clock adapts to seasonal decreases in temperature and day length. Neuron 24: 219-230.
Malzahn E, Ciprianidis S, ldi KK, Schafmeier T, Brunner M (2010) Photoadaptation in *Neurospora* by competitive interaction of activating and inhibitory LOV domains. Cell 142: 762-772.
Marrocco K, Zhou Y, Bury E, Dieterle M, Funk M, et al. (2006) Functional analysis of EID1, an F-box protein involved in phytochrome A-dependent light signal transduction. Plant J 45: 423438.
Marshall CJ (1996) Ras effectors. Curr Opin Cell Biol 8: 197-204.
Matsumoto A, Tomioka K, Chiba Y, Tanimura T (1999) timrit lengthens circadian period in a temperature-dependent manner through suppression of PERIOD protein cycling and nuclear localization. Mol Cell Biol 19: 4343-4354.
McLarnon JG, Hamman BN, Tibbits GF (1993) Temperature dependence of unitary properties of an ATP-dependent potassium channel in cardiac myocytes. Biophys J 65: 2013-2020.
Mehra A, Shi M, Baker CL, Colot HV, Loros JJ, et al. (2009) A role for Casein Kinase 2 in the mechanism underlying circadian temperature compensation. Cell 137: 749-760.

Mello CC, Conte D, Jr. (2004) Revealing the world of RNA interference. Nature 431: 338-342.
Merrow M, Franchi L, Dragovic Z, Gorl M, Johnson J, et al. (2001) Circadian regulation of the light input pathway in *Neurospora crassa*. EMBO J 20: 307-315.
Moore D, Rankin MA (1985) Circadian locomotor rhythms in individual honeybees. Physiological Entomology 10: 191-197.
Morgan LW, Feldman JF (1997) Isolation and characterization of a temperature-sensitive circadian clock mutant of *Neurospora crassa*. Genetics 146: 525-530.
Murakami R, Miyake A, Iwase R, Hayashi F, Uzumaki T, et al. (2008) ATPase activity and its temperature compensation of the cyanobacterial clock protein KaiC. Genes Cells 13: 387-395.
Nagai T, Terada TP, Sasai M (2010) Synchronization of circadian oscillation of phosphorylation level of KaiC in vitro. Biophys J 98: 2469-2477.
Neiss A, Schafmeier T, Brunner M (2008) Transcriptional regulation and function of the *Neurospora* clock gene *white collar 2* and its isoforms. EMBO Rep 9: 788–794.
Newell RC (1966) Effect of temperature on the metabolism of poikilotherms. Nature 212: 426-428.
Oliver SG (2006) From genomes to systems: the path with yeast. Philos Trans R Soc Lond B Biol Sci 361: 477-482.
Pittendrigh CS (1954) On temperature independence in the clock system controlling emergence time in *Drosophila*. Proc Natl Acad Sci U S A 40: 1018-1029.
Pittendrigh CS (1960) Circadian rhythms and the circadian organization of living systems. Cold Spring Harb Symp Quant Biol 25: 159-184.
Pittendrigh CS, Caldarola PC (1973) General homeostasis of the frequency of circadian oscillations. Proc Natl Acad Sci U S A 70: 2697-2701.
Pokhilko A, Hodge SK, Stratford K, Knox K, Edwards KD, et al. (2010) Data assimilation constrains new connections and components in a complex, eukaryotic circadian clock model. Mol Syst Biol 6.
Rajagopal S, Anderson S, Srajer V, Schmidt M, Pahl R, et al. (2005) A structural pathway for signaling in the E46Q mutant of photoactive yellow protein. Structure 13: 55-63.
Rani A, Pandita E, Rahman S, Deep S, Sau AK (2012) Insight into temperature dependence of GTPase activity in human guanylate binding protein-1. PLoS ONE 7: e40487.
Rensing L, Ruoff P (2002) Temperature effect on entrainment, phase shifting, and amplitude of circadian clocks and its molecular bases. Chronobiol Int 19: 807-864.
Reyes BA, Pendergast JS, Yamazaki S (2008) Mammalian peripheral circadian oscillators are temperature compensated. J Biol Rhythms 23: 95-98.
Roenneberg T, Taylor W (2000) Automated recordings of bioluminescence with special reference to the analysis of circadian rhythms. Methods Enzymol 305: 104-119.
Ruoff P (1992) Introducing temperature-compensation in any reaction kinetic oscillator model. J Interdiscipl Cycle Res 23: 92-99.

Ruoff P (1994) General homeostasis in period- and temperature-compensated chemical clock mutants formed by random selection conditions. Naturwissenschaften 81: 456-459.

Ruoff P, Mohsenzadeh S, Rensing L (1996) Circadian rhythms and protein turnover: the effect of temperature on the period lengths of clock mutants simulated by the Goodwin oscillator. Naturwissenschaften 83: 514-517.

Ruoff P, Rensing L (1996) The temperature compensated Goodwin model simulates many circadian clock properties. J Theor Biol 179: 275-285.

Ruoff P, Vinsjevik M, Monnerjahn C, Rensing L (1999) The Goodwin oscillator: on the importance of degradation reactions in the circadian clock. J Biol Rhythms 14: 469-479.

Ruoff P, Loros JJ, Dunlap JC (2005) The relationship between FRQ-protein stability and temperature compensation in the *Neurospora* circadian clock. Proc Natl Acad Sci U S A 102: 17681-17686.

Ruoff P, Zakhartsev M, Westerhoff HV (2007) Temperature compensation through systems biology. FEBS J 274: 940-950.

Salome PA, Weigel D, McClung CR (2010) The role of the Arabidopsis morning loop components CCA1, LHY, PRR7, and PRR9 in temperature compensation. Plant Cell 22: 3650-3661.

Sancar G, Sancar C, Brunner M, Schafmeier T (2009) Activity of the circadian transcription factor White Collar Complex is modulated by phosphorylation of SP-motifs. FEBS Lett 583: 1833-1840.

Sancar G, Sancar C, Brunner M (2012) Metabolic compensation of the *Neurospora* clock by a glucose-dependent feedback of the circadian repressor CSP1 on the core oscillator. Genes Dev 26: 2435-2442.

Sanchez A, Shin J, Davis SJ (2011) Abiotic stress and the plant circadian clock. Plant Signal Behav 6: 223-231.

Sargent ML, Briggs WR, Woodward DO (1966) Circadian nature of a rhythm expressed by an invertaseless strain of *Neurospora crassa*. Plant Physiol 41: 1343-1349.

Sargent ML, Briggs WR (1967) The effects of light on a circadian rhythm of conidiation in *Neurospora*. Plant Physiol 42: 1504-1510.

Sargent ML, Woodward DO (1969) Genetic determinants of circadian rhythmicity in Neurospora. J Bacteriol 97: 861-866.

Schafmeier T, Haase A, Káldi K, Scholz J, Fuchs M, et al. (2005) Transcriptional feedback of *Neurospora* circadian clock gene by phosphorylation-dependent inactivation of its transcription factor. Cell 122: 235-246.

Schafmeier T, Káldi K, Diernfellner A, Mohr C, Brunner M (2006) Phosphorylation-dependent maturation of *Neurospora* circadian clock protein from a nuclear repressor toward a cytoplasmic activator. Genes Dev 20: 297-306.

Schafmeier T, Diernfellner A, Schafer A, Dintsis O, Neiss A, et al. (2008) Circadian activity and abundance rhythms of the *Neurospora* clock transcription factor WCC associated with rapid nucleo-cytoplasmic shuttling. Genes Dev 22: 3397–3402.

Schuster P, Sigmund K, Wolff R (1978) Dynamical systems under constant organization I. Topological analysis of a family of non-linear differential equations—A model for catalytic hypercycles. Bull Math Biol 40: 743-769.

Schwerdtfeger C, Linden H (2000) Localization and light-dependent phosphorylation of White collar-1 and 2, the two central components of blue light signaling in *Neurospora crassa*. Eur J Biochem 267: 414-421.
Schwerdtfeger C, Linden H (2003) VIVID is a flavoprotein and serves as a fungal blue light photoreceptor for photoadaptation. EMBO J 22: 4846-4855.
Smith KM, Sancar G, Dekhang R, Sullivan CM, Li S, et al. (2010) Transcription factors in light and circadian clock signaling networks revealed by genomewide mapping of direct targets for neurospora white collar complex. Eukaryot Cell 9: 1549-1556.
Snyder CD (1908) Comparative study of the temperature coefficients of the velocities of various physiological actions. Am J Physiol 22: 309-334.
Stricker J, Cookson S, Bennett MR, Mather WH, Tsimring LS, et al. (2008) A fast, robust and tunable synthetic gene oscillator. Nature 456: 516-519.
Sweeney BM (1963) Resetting the Biological Clock in *Gonyaulax* with Ultraviolet Light. Plant Physiol 38: 704-708.
Terauchi K, Kitayama Y, Nishiwaki T, Miwa K, Murayama Y, et al. (2007) ATPase activity of KaiC determines the basic timing for circadian clock of cyanobacteria. Proc Natl Acad Sci U S A 104: 16377-16381.
Tigges M, Marquez-Lago TT, Stelling J, Fussenegger M (2009) A tunable synthetic mammalian oscillator. Nature 457: 309-312.
Tsai TY-C, Choi YS, Ma W, Pomerening JR, Tang C, et al. (2008) Robust, tunable biological oscillations from interlinked positive and negative feedback loops. Science 321: 126-129.
Tseng YY, Hunt SM, Heintzen C, Crosthwaite SK, Schwartz JM (2012) Comprehensive modelling of the *Neurospora* circadian clock and its temperature compensation. PLoS Comput Biol 8: e1002437.
Tsuchiya Y, Akashi M, Nishida E (2003) Temperature compensation and temperature resetting of circadian rhythms in mammalian cultured fibroblasts. Genes Cells 8: 713-720.
Ueda HR (2007) Systems biology of mammalian circadian clocks. Cold Spring Harb Symp Quant Biol 72: 365-380.
Vitalini MW, Paula RMd, Park WD, Bell-Pedersen D (2006) The rhythms of life: circadian output pathways in *Neurospora*. J Biol Rhythms 21: 432-444.
Vogel HJ (1956) A convenient growth medium for *Neurospora*. Microbial Genetics Bulletin 13: 42-43.
Westergaard M, Mitchell HK (1947) A synthetic medium favoring sexual reproduction. Am J Bot 34: 573-577.
Winfree AT (1980) The geometry of biological time. New York: Springer.
Yu Y, Dong W, Altimus C, Tang X, Griffith J, et al. (2007) A genetic network for the clock of *Neurospora crassa*. Proc Natl Acad Sci U S A 104: 2809-2814.
Zelzer E, Wappner P, Shilo B-Z (1997) The PAS domain confers target gene specificity of Drosophila bHLH/PAS proteins. Genes Dev 11: 2079-2089.
Zhang EE, Kay SA (2010) Clocks not winding down: unravelling circadian networks. Nat Rev Mol Cell Biol 11: 764-776.
Zheng X, Sehgal A (2008) Probing the relative importance of molecular oscillations in the circadian clock. Genetics 178: 1147-1155.

Appendix

Appendix 1. The parameters and their values used in the Models.

	Leloup 1999	Ruoff 2005	Hong 2008 (a,b)	François 2005
frq Transcription	v_s = 1.6 (dark)nMh^{-1} = 2 (light)nMh^{-1} K_I(nFRQ,repression) = 1 nM n (Hill coefficient)= 4	k_1 = 0.3 h^{-1}	k_1 = 1.8 a.u. h^{-1} K(WC-1_n:DNA,dissociation) = 1 .25 a.u. (*frq*$^+$) = 8.5 a.u. (ER24) k_{01} (by QA) = 0.002 a.u. h^{-1}	ϱ_{FRQ} = 7.5 mol h^{-1} (one-loop model) = 10 mol h^{-1} (first two-loop model) = 75 mol h^{-1} (second two-loop model) θ(WCC:DNA, releasing) =0.35 h^{-1}(one-loop model) = 0.6 h^{-1} (first two-loop model) = 0.25 h^{-1} (second two-loop model) α (WCC:DNA, binding) = 10 mol^{-1} h^{-1} (one-loop model) = 1 mol^{-1} h^{-1} (first two-loop model) = 0.003 mol^{-1} h^{-1} (second two-loop model)
FRQ Translation	k_s = 0.5 h^{-1}	k_2 = 0.3 h^{-1}	k_2 = 1.8 a.u. h^{-1}	β = 0.7 h^{-1} (one-loop model) = 0.6 h^{-1} (first two-loop model) = 1 h^{-1} (second two-loop model)
FRQ Translocation	k_1(into n)=0.5 h^{-1} k_2(out of n)=0.6 h^{-1}	k_3 (into n) = 0.3 h^{-1}	k_3 (into n) = 0.05 h^{-1}	
FRQ dimerisaion				η = 3000 mol h^{-1} (dimerise) ϰ = 10 h^{-1} (dissociate)

Appendix 1. (Continued) The parameters and their values used in the Models.

	Leloup 1999	Ruoff 2005	Hong 2008 (a,b)	François 2005
wc-1 Transcription			$k_7 = 0.16$ a.u. h^{-1}	ϱ_{WCC} (wc-1 transcription in two-loop model) $= 3.75$ mol h^{-1} (WCC production rate, 1-loop model) $= 0.3$ mol h^{-1} (first two-loop model) $= 2.5$ mol h^{-1} (second two-loop model)
wc-1 Translation			k_8 (FRQ promoted WC-1c accumulation) $= 0.8$ a.u. h^{-1} K_2 (FRQ_c: mRNA, dissociation) $= 1.0$ a.u. k_{02} (WC-1c synthesis without FRQ) $= 0.001$ a.u. h^{-1}	ν(FRQ: mRNA, formation) $= 0.2$ $mol^{-1}h^{-1}$(first two-loop model) $= 8000$ mol^{-1} h^{-1} (second two-loop model) μ(FRQ: mRNA, dissociation) $= 0.01$ h^{-1} (first two-loop model) $= 0.1$ h^{-1} (second two-loop model) β^- (normal form) $= 1h^{-1}$(first two-loop model) $= 0.001$ h^{-1}(second two-loop model) β^+ (complexed form) $= 40$ h^{-1}(first two-loop model) $= 10$ h^{-1}(second two-loop model) τ(the translation delay of the second type of RNA) $= 7$ h
WC-1c Translocation			k_9 (into n) $= 40.0$ a.u. h^{-1}	

Appendix 1. (Continued) The parameters and their values used in the Models. (Continued)

	Leloup 1999	Ruoff 2005	Hong 2008 (a,b)	François 2005
WC-1_n:FRQ_n complex			k_{13}(binding) = 50.0 a.u. h^{-1}(a) = 0 (a:catalytic-like model = 50 ~ 50000 a.u. h^{-1}(b) k_{16} (binding) = 50.0 a.u. h^{-1}(a) = 0 or 100 a.u. h^{-1} (b) k_{14}(dissociation) = 0.0 h^{-1} (a:catalytic-like model) = 1.0 h^{-1} (a,b) k_{17} =0 (a), 100 (b) a.u. h^{-1} k_{18} (dissociation, WC-1_n* formation w/wo FRQ_n*) = 1.0 (a), 5 (b) a.u. h^{-1}	γ(multimer T [FRQ + WCC] formation) = 2000 mol^{-1} h^{-1} (one-loop model) = 100 $mol^{-1}h^{-1}$(first two-loop model) = 1600 mol^{-1} h^{-1}(second two-loop model)

Appendix 1. (Continued) The parameters and their values used in the Models. (Continued)

Degradation				
	Leloup 1999	**Ruoff 2005**	**Hong 2008**	**François 2005**
frq mRNA	v_m = 0.505 nMh^{-1} K_m(Michaelis constant)=0.5nM	k_4= 0.27 h^{-1}	k_4= 0.23 h^{-1}	δ_{RNA} = 0.2 h^{-1}
FRQ	v_d = 1.4 nMh^{-1} K_d (Michaelis constant)= 0.13nM	k_5 (cFRQ) = 0.2 h^{-1} k_6 (nFRQ) = 0.2 h^{-1}	k_5 (cFRQ) = 0.27 h^{-1} k_6 (nFRQ) = 0.07 h^{-1} (a,b) = 1.2 h^{-1} (a:catalytic-like model) k_{21} (FRQ_n*) = ??	δ_{FRQ} = 0.05 h^{-1} (one-loop model and first two-loop model) = 0.3 h^{-1} (second two-loop model)
wc-1 mRNA			k_{10}= 0.1 h^{-1}	δ_{RNAW} (normal form) = 3 h^{-1}(first two-loop model) = 1 h^{-1} (second two-loop model)
WC			k_{11} (WC-1_c) = 0.05 h^{-1} k_{12} (WC-1_n) = 0.02 h^{-1} k_{19} (WC-1_n*)= 1.0 a.u. h^{-1}	δ_{WCC} (WCC) = 0.3 h^{-1}
FRQ_n:WC-1_n complex			k_{15} (in model A) = 0 h^{-1} (a:catalytic-like model, b) = 5.0 h^{-1} (a) k_{20} (in model B and C) = 3.0 × 10^{-2} a.u. h^{-1}	δ_T (multimer T [FRQ + WCC]) = 0.3 h^{-1}

Appendix 2 Kinetic equations used in the model

The rate of reaction *i* is noted *v_i*.

$$v\_1 = k\_01 \times \frac{[\text{aWCC}]^{H\_01}}{K\_01^{H\_01} + [\text{aWCC}]^{H\_01}} + k\_01a \times [\text{laWCC}]$$

$$v\_2 = k\_02 + k\_02a01 \times [\text{aWCC}] + k\_02a02 \times [\text{laWCC}]$$

$$v\_3 = k\_03 \times \frac{1}{1 + [\text{hypoWCCn}] \times k\_03i} + [\text{hypoFRQn}] \times k\_03a$$

$$v\_4 = k\_04 \times [\text{laWCC}]$$

$$v\_5 = k\_05 \times [\textit{frq}\ \text{mRNA}]$$

$$v\_6 = k\_06 \times [\textit{wc} - \textit{1}\ \text{mRNA}]$$

$$v\_7 = k\_07 \times [\textit{wc} - \textit{2}\ \text{mRNA}]$$

$$v\_8 = k\_08 \times [\textit{vvd}\ \text{mRNA}]$$

$$v\_9 = [\textit{frq}\ \text{mRNA}] \times (k\_09 + [\text{hypoFRQc}] \times k\_09a)$$

$$v\_10 = k\_10 \times [\textit{wc} - \textit{1}\ \text{mRNA}]$$

$$v\_11 = k\_11 \times [\textit{wc} - \textit{2}\ \text{mRNA}]$$

$$v\_12 = k\_12 \times [\textit{vvd}\ \text{mRNA}]$$

$$v\_13 = k\_13 \times [\text{WC1c}] \times [\text{WC2c}]$$

$$v\_14 = k\_14 \times [\text{hypoFRQc}]$$

$$v\_15 = k\_15 \times [\text{hypoWCCc}]$$

$$v\_16 = k\_16 \times [\text{VVDc}]$$

$$v\_17 = k\_17 \times [\text{hypoFRQn}]$$

$$v\_18 = k\_18 \times [\text{hyperFRQn}]$$

$$v\_19 = k\_19 \times [\text{hyperWCCn}]$$

$$v\_20 = k\_20 \times [\text{hypoFRQc}]$$

$v\_21 = k\_21 \times [\text{hypoFRQn}]$

$v\_22 = k\_22 \times [\text{hypoWCCc}]$

$$v\_23 = k\_23 \times [\text{hypoWCCn}] \times \frac{[\text{hypoFRQn}]^{H\_23}}{K\_02^{H\_23} + [\text{hypoFRQn}]^{H\_23}}$$

$v\_24 = k\_24 \times [\text{hyperWCCc}]$

$v\_25 = k\_25 \times [\text{hypoWCCn}]$

$v\_26 = k\_26 \times [\text{hypoWCCn}]$

$v\_27 = k\_27 \times [\text{laWCC}] \times [\text{VVDn}]$

$v\_28 = k\_28 \times [\text{WVC}]$

$v\_29 = k\_29 \times [\text{hyperFRQc}]$

$v\_30 = k\_30 \times [\text{hyperFRQn}]$

$v\_31 = k\_31 \times [\text{WC1c}]$

$v\_32 = k\_32 \times [\text{WC2c}]$

$v\_33 = k\_33 \times [\text{hyperWCCc}]$

$v\_34 = k\_34 \times [\text{hyperWCCn}]$

$v\_35 = k\_35 \times [\text{aWCC}]$

$v\_36 = k\_36 \times [\text{laWCC}]$

$v\_37 = k\_37 \times [\text{VVDc}]$

$v\_38 = k\_38 \times [\text{VVDn}]$

$v\_39 = k\_39 \times [\text{WVC}]$

Appendix 3 List and values of model parameters

ID	Name	Description	Value
k_01	*k_frq*	maximum rate of *frq* transcription	7.3
K_01	*K_frq*	Michaelis constant of *frq* transcription	0.1
H_01	*H_frq*	Hill coefficient of *frq* transcription	4
k_01a	*kl_frq*	light induced *frq* transcription	320
k_02	*k_wc1*	rate of basal transcription of *wc-1*	1.19
k_02a01	*ka_wc1*	*wc-1* transcription rate activated by WCC	1.2
k_02a02	*kl_wc1*	light induced *wc-1* transcription	90
k_03	*k_wc2*	maximum rate of *wc-2* transcription	1.6
k_03a	*ka_wc2*	promotion of *wc-2* transcription by FRQ	0.03
k_03i	*ki_wc2*	repression of *wc-2* transcription by WCC	0.03
k_04	*kl_vvd*	light induced *vvd* transcription	800
k_05	*k_FRQ*	*frq* translation rate	0.19
k_06	*k_WC1*	*wc-1* translation rate	0.226
k_07	*k_WC2*	*wc-2* translation rate	1
k_08	*k_VVD*	*vvd* translation rate triggered by light activated WCC	0.68
k_09	*kd_frq*	degradation rate of *frq* mRNA	2
k_09a	*kd_frq_FRQ*	additional degradation of *frq* mRNA by FRQ	0.356
k_10	*kd_wc1*	degradation rate of *wc-1* mRNA	2.4
k_11	*kd_wc2*	degradation rate of *wc-2* mRNA	2.5
k_12	*kd_vvd*	degradation rate of *vvd* mRNA	6.2
k_13	*k_WCC*	WCC formation rate	0.472
k_14	*kin_hypoFRQc*	nuclear localisation rate of hypoFRQc	0.1
k_15	*kin_hypoWCCc*	nuclear localisation rate of hypoWCCc	0.3
k_16	*kin_VVDc*	nuclear localisation rate of VVD	0.3
k_17	*kout_hypoFRQn*	hypophosphorylated FRQ translocation rate out of the nucleus	0.1
k_18	*kout_hyperFRQn*	hyperphosphorylated FRQ translocation rate out of the nucleus	0.3
k_19	*kout_hyperWCCn*	hyperphosphorylated WCC translocation rate out of the nucleus	0.29
k_20	*kp_hypoFRQc*	phosphorylation rate of cytoplasmic FRQ	0.1
k_21	*kp_hypoFRQn*	phosphorylation rate of nuclear FRQ	0.1
k_22	*kp_hypoWCCc*	phosphorylation rate of cytosolic WCC	0.3
k_23	*kp_hypoWCCn*	maximum rate of nuclear WCC phosphorylation	0.6
K_23	*Kp_hypoWCCn*	Michaelis constant of nuclear WCC phosphorylation	0.475
H_23	*Hp_hypoWCCn*	Hill coefficient of nuclear WCC phosphorylation	12
k_24	*kdp_hyperWCCc*	dephosphorylation rate of cytosolic WCC	0.3
k_25	*kact_hypoWCCn*	activation rate of nuclear WCC	0.15
k_26	*klact_hypoWCCn*	activation rate of light activated WCC	0
k_27	*k_WVC*	formation rate of WVC	20
k_28	*kdis_WVC*	disassociation rate of WVC	1.8
k_29	*kd_hyperFRQc*	degradation rate of cytosolic FRQ	0.27
k_30	*kd_hyperFRQn*	degradation rate of nuclear FRQ	0.27
k_31	*kd_WC1*	degradation rate of WC-1	0.135
k_32	*kd_WC2*	degradation rate of WC-2	0.085
k_33	*kd_hyperWCCc*	degradation rate of cytosolic WCC	0.05
k_34	*kd_hyperWCCn*	degradation rate of nuclear WCC	0.05
k_35	*kd_aWCC*	degradation rate of activated nuclear WCC	1.29
k_36	*kd_laWCC*	degradation rate of light activated WCC	6
k_37	*kd_VVDc*	degradation rate of cytosolic VVD	0.24
k_38	*kd_VVDn*	degradation rate of nuclear VVD	0.24
k_39	*kd_WVC*	degradation rate of WVC	0.75

Comprehensive Modelling of the *Neurospora* Circadian Clock and Its Temperature Compensation

Yu-Yao Tseng[1,2], Suzanne M. Hunt[1], Christian Heintzen[1], Susan K. Crosthwaite[1]*, Jean-Marc Schwartz[2]*

1 Faculty of Life Sciences, University of Manchester, Manchester, United Kingdom, **2** Manchester Interdisciplinary Biocentre, Faculty of Life Sciences, University of Manchester, Manchester, United Kingdom

Abstract

Circadian clocks provide an internal measure of external time allowing organisms to anticipate and exploit predictable daily changes in the environment. Rhythms driven by circadian clocks have a temperature compensated periodicity of approximately 24 hours that persists in constant conditions and can be reset by environmental time cues. Computational modelling has aided our understanding of the molecular mechanisms of circadian clocks, nevertheless it remains a major challenge to integrate the large number of clock components and their interactions into a single, comprehensive model that is able to account for the full breadth of clock phenotypes. Here we present a comprehensive dynamic model of the *Neurospora crassa* circadian clock that incorporates its key components and their transcriptional and post-transcriptional regulation. The model accounts for a wide range of clock characteristics including: a periodicity of 21.6 hours, persistent oscillation in constant conditions, arrhythmicity in constant light, resetting by brief light pulses, and entrainment to full photoperiods. Crucial components influencing the period and amplitude of oscillations were identified by control analysis. Furthermore, simulations enabled us to propose a mechanism for temperature compensation, which is achieved by simultaneously increasing the translation of *frq* RNA and decreasing the nuclear import of FRQ protein.

Citation: Tseng Y-Y, Hunt SM, Heintzen C, Crosthwaite SK, Schwartz J-M (2012) Comprehensive Modelling of the *Neurospora* Circadian Clock and Its Temperature Compensation. PLoS Comput Biol 8(3): e1002437. doi:10.1371/journal.pcbi.1002437

Editor: Jason A. Papin, University of Virginia, United States of America

Received September 29, 2011; **Accepted** February 6, 2012; **Published** March 29, 2012

Funding: This work was supported by a Biotechnology and Biological Sciences Research Council (UK) studentship to SH. The funders had no role in study design, data collection and analysis, decision to publish, or preparation of the manuscript.

Competing Interests: The authors have declared that no competing interests exist.

* E-mail: susan.crosthwaite@manchester.ac.uk (SKC); jean-marc.schwartz@manchester.ac.uk (JMS)

These authors contributed equally to this work.

Introduction

Circadian clocks are essential endogenous timekeepers that are present in most organisms. They impose temporal order on inter- and intracellular events [1], regulating the cell cycle [2], cell physiology [3] and behaviour [4]. Circadian rhythmicity emerges from a network of positive and negative feedback regulation acting on clock genes and clock proteins [5,6]. Ubiquitous characteristics of circadian clocks include: a periodicity of approximately 24 h, the ability to be entrained to the external rhythmic environment, and temperature compensation of period [7]. Synchronisation of circadian clocks to local time allows organisms to anticipate and prepare for cyclical changes in their environment. Of the defining clock characteristics, temperature compensation is the least understood.

At the molecular level, a common characteristic of circadian clocks is that there is usually an underlying transcriptional and translational feedback loop [reviewed in 8]. Positive and negative elements regulate the expression of clock genes and clock-controlled genes. For example, KaiA in *Synechococcus* [reviewed in 9], CLK and CYC in *Drosophila* [reviewed in 10], and Clock and Bmal1 (Mop3) in mammals [reviewed in 11] are positive elements. These molecules promote the expression of the clock and clock-controlled genes. On the other hand, negative elements, such as KaiC in *Synechococcus* [reviewed in 9], PERIOD and TIMELESS in *Drosophila* [reviewed in 10], and Cry1, Cry2, Per1 and Per2 in mammals [reviewed in 11], repress the action of positive elements. The rhythmic regulation results in periodic expression of the clock genes and clock-controlled genes. Consequently, rhythmic changes in metabolism and behaviour can be observed [reviewed in 12].

The *Neurospora crassa* clock is based on molecular feedback loops that in constant conditions generate a 22 hour period (Figure 1). Components include the *frequency* (*frq*), *white collar-1* (*wc-1*) and *white collar-2* (*wc-2*) genes. In the positive loop, the White Collar Complex (WCC), a heterodimer of WC-1 and WC-2, activates the transcription of *frq*. The product of the *frq* gene, the FREQUENCY (FRQ) protein, transcriptionally and post-transcriptionally promotes the accumulation of WC-2 and WC-1, respectively [13,14]. In a negative feedback loop, FRQ recruits kinases, such as casein kinase-1a (CK-1a), and facilitates WCC phosphorylation [15]. The phosphorylation of WCC results in WCC inactivation and thus interferes with the binding of WCC to the *frq* promoter [16]. Moreover, the WCC represses *wc-2* transcription via up-regulation of a putative repressor [17].

Interaction between environmental factors, such as light, and the *Neurospora* clock components is well-studied [18]. WC-1 and VIVID (VVD) proteins are known blue light receptors [19,20,21]. Light stimulates the formation of a large photoactivated WCC (laWCC), containing more than one WC-1 molecule. laWCC is transformed from the heterodimeric dark WCC, and even in the

Author Summary

Circadian clocks are internal timekeepers that integrate signals from the environment and orchestrate cellular events to occur at the most favourable time of day. Circadian clocks in animals, plants, fungi and bacteria have similar characteristic properties and molecular architecture. They have a periodicity of approximately 24 hours, persist in constant conditions and can be reset by environmental time cues such as light and temperature. Another essential property, whose molecular basis is poorly understood, is that the period is temperature compensated i.e. it remains the same over a range of temperatures. Computational modelling has become a valuable tool to predict and understand the underlying mechanisms of such complex molecular systems, but existing clock models are often restricted in the scope of molecular reactions they cover and in the breadth of conditions they are able to reproduce. We therefore built a comprehensive model of the circadian clock of the fungus *Neurospora crassa*, which encompasses existing knowledge of the biochemistry of the *Neurospora* clock. We validated this model against a wide range of experimental phenotypes and then used the model to investigate possible molecular explanations of temperature compensation. Our simulations suggest that temperature compensation of period is achieved by changing the abundance and cellular localisation of a key clock protein.

presence of FRQ is a strong transcriptional activator of *frq*, as well as *vvd* and a number of clock-controlled genes [reviewed in 5]. The blue light receptor VVD acts as a repressor of light-induced responses [22]. Evidence suggests that VVD competes with laWCC for the homodimerisation of laWCC and this results in the dissociation of laWCC and a concomitant decrease in its ability to activate transcription [23,24,25].

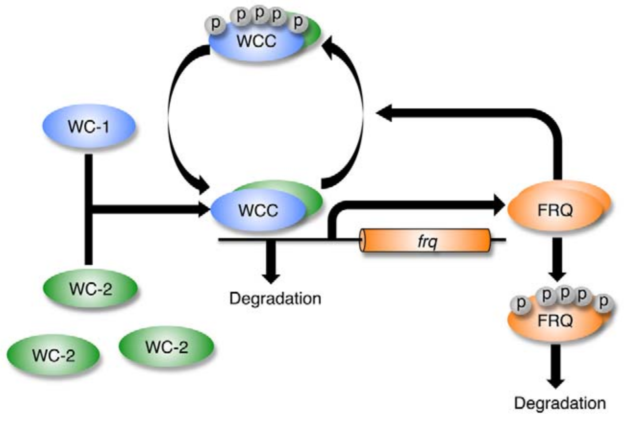

Figure 1. Simplified representation of the *Neurospora* circadian clock. Transcription factors WHITE COLLAR-1 (WC-1) and WHITE COLLAR-2 (WC-2) form a heterodimeric WHITE COLLAR COMPLEX (WCC). Early in the subjective night, the hypophosphorylated form of WCC (hypoWCC) activates the transcription of the *frequency* (*frq*) gene. Once hypoWCC activates transcription, it is degraded. The FREQUENCY protein (FRQ) accumulates, peaking around midday, and is progressively phosphorylated. Hyperphosphorylated FRQ is ubiquitinated and degraded by the proteosome. FRQ promotes phosphorylation of WCC by recruiting kinases, and phosphorylated WCC (hyperWCC) is inactive thus leading to decreased transcription of *frq* and consequently negative regulation of FRQ. Phosphorylated WCC is more stable than its hypophosphorylated form, thus the increase in FRQ level leads to a rise in overall WCC level.
doi:10.1371/journal.pcbi.1002437.g001

Given the large number of components and processes involved in the circadian clockwork it becomes ever more difficult to interpret its functioning and response to environmental factors by intuition and reasoning alone. A rigorous, quantitative model that embeds our knowledge of the circadian network should make it possible to test the consequences of experimental perturbations on the system, and reveal components and mechanisms underlying clock characteristics. Such a model would allow predictions to be made regarding the behaviour of the clockwork under a wide variety of conditions. Quantitative models of the *Neurospora* circadian clock have been built previously [26,27,28,29,30,31]. Leloup's minimal *Neurospora* clock model concentrates on *frq* gene expression which is regulated by the concentration of FRQ protein using the Hill equation. The model was the first to successfully simulate both a period of 21.5 hours in constant darkness and entrainment of the oscillator to a 24 hour light-dark cycle. Ruoff *et al.* developed a model, based on a Goodwin-type oscillator, that introduces a switch mechanism to activate and repress *frq* transcription [30]. Temperature-regulated degradation of wild type and mutant forms of FRQ was modelled by introducing the Arrhenius equation, resulting in the expected expression of *frq* mRNA and FRQ at 21°C and 28°C. This work and subsequent experiments have shown that wild type FRQ degradation is not significantly affected over this range of temperatures [32]. François' model considers an interaction between FRQ and *wc-1* RNA, and the inactivation of WCC through binding with FRQ homodimers [29]. Subsequent modelling by Hong *et al.* has provided insight into the possible mechanism of FRQ action in the nucleus indicating that a one-to-one molar ratio of FRQ and WCC is not necessary for FRQ to repress WCC activity [31].

As shown by the above examples, quantitative modelling has made valuable contributions to our understanding of circadian clock mechanism in *Neurospora*. To date however, no model is able to describe the full range of observed clock phenotypes. Because the *Neurospora* circadian clockwork consists of several interlocking feedback loops, a comprehensive model is expected to shed light on circadian clock properties and mechanisms underlying its response to environmental factors, in particular temperature compensation. Our model incorporates the majority of the known clock components and the mechanisms through which they interact, and successfully accounts for a wide range of clock characteristics including: a periodicity of approximately 24 hours, persistent oscillation in conditions of constant darkness and temperature, arrhythmicity in constant light, resetting of the clock by brief pulses of light, photoadaptation, and entrainment to full photoperiods. Relative levels of clock gene transcripts and clock proteins mimic the experimentally derived values in constant darkness, after light pulses and in light/dark conditions. Control analysis carried out on the model and comparisons between model simulations and experimental data allow us to propose a mechanism underlying temperature compensation.

Results

The *Neurospora crassa* circadian clock model

Our circadian clock model was constructed through a mechanistic approach (Figure 2). The model is based on a compilation of published and new (this paper) experimental data and incorporates facets of previously described *Neurospora* clock models [28,29,31]. The model centres on the genetic interlocking positive and negative feedback loops created by the interactions of the *frq*, *wc-1* and *wc-2* genes [reviewed in 5,33]. The *frq*, *wc-1* and

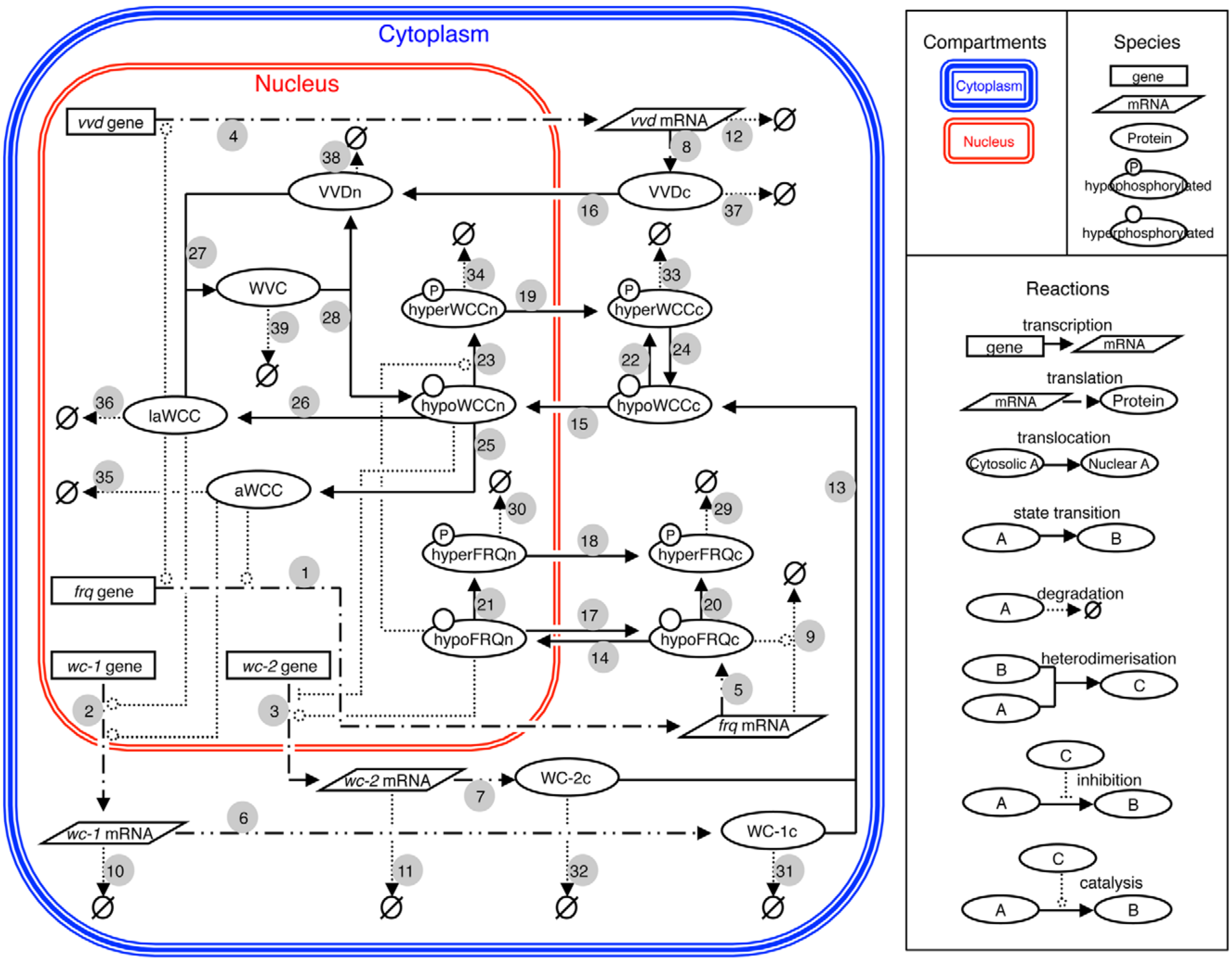

Figure 2. The *Neurospora* circadian clock model. The symbol representations of compartments, species and reactions are shown in the right hand panel. Individual pathways are numbered starting with the transcription of the *frq* gene. *frq* = *frequency*, *wc-1* = *white collar-1*, *wc-2* = *white collar-2*, *vvd* = *vivid*, hypoFRQc = cytosolic hypophosphorylated FREQUENCY (FRQ) protein, hypoFRQn = nuclear hypophosphorylated FRQ, hyperFRQc = cytosolic hyperphosphorylated FRQ, hyperFRQn = nuclear hyperphosphorylated FRQ, WC-1c = cytosolic WHITE COLLAR-1 (WC-1) protein, WC-2c = cytosolic WHITE COLLAR-2 (WC-2) protein, hypoWCCc = cytosolic hypophosphorylated WHITE COLLAR COMPLEX (WCC), hypoWCCn = nuclear hypophosphorylated WCC, hyperWCCc = cytosolic hyperphosphorylated WCC, hyperWCCn = nuclear hyperphosphorylated WCC, aWCC = activated WCC, laWCC = light activated WCC, VVDc = cytosolic VIVID (VVD) protein, VVDn = nuclear VVD, WVC = WCC-VVD complex.
doi:10.1371/journal.pcbi.1002437.g002

wc-2 genes are transcribed into *frq*, *wc-1* and *wc-2* mRNA (step 1–3), respectively, and translated into hypophosphorylated cytosolic FRQ (hypoFRQc), WC-1 (WC1c) and WC-2 (WC2c) protein (step 5–7). Steps 9–11 are degradation reactions of *frq* mRNA, *wc-1* mRNA, and *wc-2* mRNA.

Once translated, cytoplasmic WC-1 (WC1c) and WC-2 (WC2c) bind to each other to form the hypophosphorylated cytosolic WHITE-COLLAR complex (hypoWCCc) (step 13) which translocates into the nucleus (step 15) where a small fraction of hypoWCCn is activated (activated WCC) (step 25) [14]. Activated WCC promotes the transcription of *frq* and *wc-1* genes (steps 1 and 2) [34,35] and as a consequence is degraded [14] (step 35). Hypophosphorylated cytosolic WCC (hypoWCCc) and nuclear WCC (hypoWCCn) can be phosphorylated in the cytoplasm and in the nucleus (step 22 and 23). Hyperphosphorylated nuclear WCC (hyperWCCn) is translocated out of the nucleus (step 19) to the cytoplasm where it can be dephosphorylated (step 24) [14]. Once translated, FRQ forms a homodimer that interacts with the FRQ-interacting helicase FRH [36]; in our model this complex is represented by FRQ. Hypophosphorylated nuclear FRQ (hypoFRQn) facilitates the phosphorylation of hypoWCCn [16] (step 23) and clearance of WCC from the nucleus [14]. Thus, FRQ negatively regulates its own expression and positively regulates the accumulation of WCC.

Steps 31–35 are degradation reactions of WC-1c, WC-2c, hyperWCCc, hyperWCCn and activated WCC, respectively. hypoFRQ shuttles into (step 14) and out of (step 17) the nucleus [37] and is progressively phosphorylated in both the cytoplasm (step 20) and the nucleus (step 21) [reviewed in 38]. Hyperphosphorylated nuclear FRQ (hyperFRQn) is translocated out of the nucleus (step 18) and accumulates in the cytoplasm [37]. Hyperphosphorylated FRQ can be degraded in the cytoplasm (step 29) and nucleus (step 30). In addition, *wc-2* transcription is promoted by hypophosphorylated nuclear FRQ (hypoFRQn) [17] and *wc-2* transcription is repressed by hypophosphorylated nuclear WCC (hypoWCCn) [17] (step 3).

The main blue-light response components, i.e. WCC and VVD are incorporated in the model. WC-1 is a photoreceptor and transcription factor which enhances the transcription of light responsive genes [20,39,40]. VIVID functions as a repressor of the light response [22,23,24,25]. WCC can be activated by light (step 26) and promotes transcription of *frq* (step 1), *wc-1* (step 2) and *vvd* (step 4). The expression of *vvd* is clock-controlled, but after the first day in constant darkness its expression is much reduced (no expression can be detected by northern blot). Activated WCC induces *vvd* in the light (step 4) [22]. Once translated (step 8) VIVID (VVD) is transported into the nucleus (step 16), where it interferes with the function of light activated WCC (laWCC) by competing with laWCC subunits and preventing their homodimerisation [23,25]. Steps 27 and 28 describe the formation and the disassociation of the WCC-VVD complex (WVC). Steps 12, 36–39 are degradation reactions of light activated WCC (laWCC), *vvd* mRNA, cytosolic VVD (VVDc), nuclear VVD (VVDn) and the WCC-VVD complex (WVC). The full set of kinetic equations and parameter values used in the model are presented in Tables S1 and S2.

Clock simulation in constant darkness

A comparison of model simulations and experimental data from the literature is shown in Figure 3. Rhythmic expression of *frq* mRNA and protein is seen in continuous darkness (DD) with *frq* mRNA peaking at CT 0–4 with a period of 21.6 h and FRQ protein peaking 3–7 hours later (Figure 3A) [41]. A plot of the simulated oscillations of *frq* mRNA and FRQ protein (Figure 3B) shows that the period (21.6 h) and amplitude of *frq* mRNA and FRQ are similar to experimental results. The delay between peak levels of *frq* and FRQ is 4.3 hours, which lies inside the range of experimental results. The simulated behaviours of these core clock components are in agreement with the experimental data from Garceau *et al.* (1997). While *wc-1* transcription is not rhythmic, WC-1 oscillates with peak levels around 18–20 hours after the light to dark transition, 8 hours after peak levels of FRQ (Figure 3C [42] and 3D (simulated results)). Figure 3E and 3F show that there is a good match between experimentally determined [43] and simulated levels of clock proteins.

Model robustness to parameter perturbation

To evaluate the robustness of the model we determined the range of each parameter value within which rhythmicity was maintained, and in which the period and amplitude of the rhythm remained within experimentally defined limits. The oscillation of *frq* RNA was used as the reference for these tests. To determine how much each parameter value can change while still generating oscillations, each parameter was increased and decreased until *frq* RNA oscillation was lost (Table S3). Our results show that 8 parameters are restricted to a fairly small range of values, 12 parameters can be decreased to zero, 8 parameters can be increased to infinity and 4 parameters can take any value without losing oscillations.

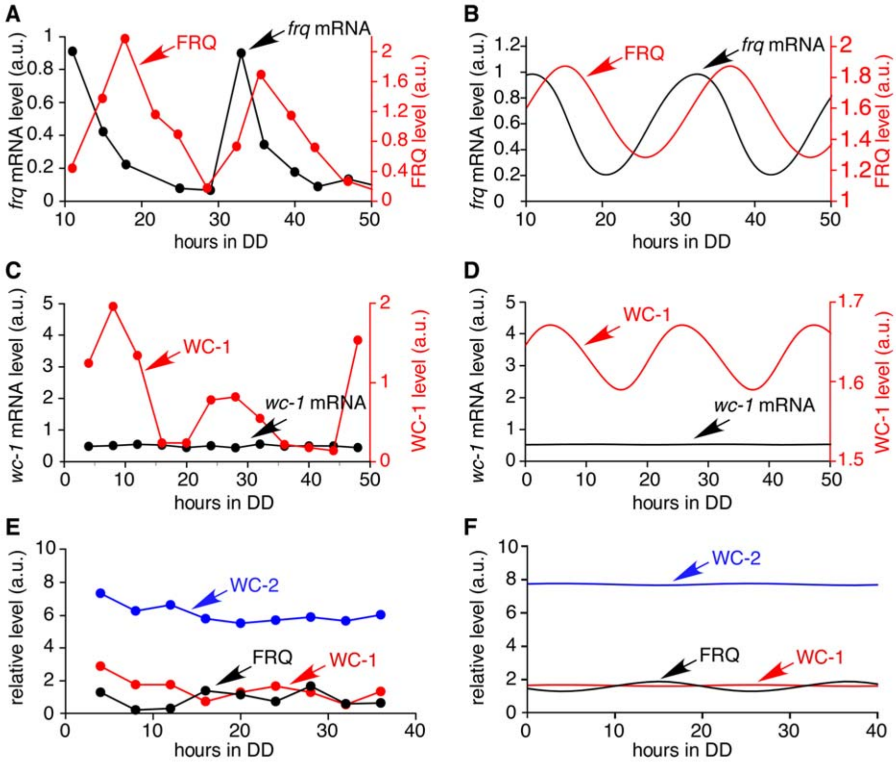

Figure 3. Continuous dark simulations. (A) Experimental data showing the oscillation of *frq* mRNA and FRQ protein levels [41]. The period length is approximately 22 hours, and FRQ (red line) peaks 3–7 hours after *frq* mRNA (black line). (B) Simulated results showing the oscillation of *frq* mRNA and FRQ protein levels has a period of 21.6 hours, and FRQ peaks 4.4 hours after *frq* mRNA. Simulation begins 10 hours after a light to dark transfer, 10 data points per hour. (C) Experimental data showing *wc-1* mRNA and WC-1 protein levels [42]. The level of *wc-1* mRNA is nearly constant. WC-1 protein expression oscillates. (D) Simulated results. *wc-1* mRNA (black line) level is constant and WC-1 oscillates. Simulation begins at the light to dark transfer, 10 data points per hour. (E) The level of WC-2 protein is 5–30 times higher than the average level of FRQ and WC-1 protein [43]. (F) In the model WC-2 protein is 10 times higher than the average level of FRQ and WC-1 proteins. Simulation begins at the light to dark transfer, 10 data points per hour are plotted.
doi:10.1371/journal.pcbi.1002437.g003

We determined how much each parameter value can change while remaining compatible with the experimental wild-type *Neurospora* clock period, taking a reference value of 21.6 hours and an experimental standard error of 0.6 hours (estimated from race tube experiments). Each parameter was increased and decreased until the period was increased or decreased outside the range of 21.6±0.6 hours (Table S4). Some parameters are highly sensitive since the oscillation is lost before the target increase or decrease of period can be reached. Other parameters can be modified in a certain range of values while remaining compatible with the experimental range of observed periodicity.

A similar approach was taken to determine how much each parameter value can change while remaining compatible with the experimental amplitude of *frq* RNA oscillations, taking an uncertainty of ±5%. Each parameter was increased and decreased until the amplitude of *frq* RNA was increased or decreased by 5% of its original value (Table S5). Most parameters are highly constrained by the amplitude; 25 parameters cannot be changed by more than 10% without changing the amplitude by more than 5%. The remaining 7 parameters can take a large range of values without affecting the amplitude strongly.

Taken together, these tests show that with the exception of *ka_wc2* (FRQ-induced transcription of *wc-2*), *kout_hyperFRQn* (translocation of phosphorylated FRQ out of the nucleus), *kd_hyperFRQc* and *kd_hyperFRQn* (degradation of phosphorylated FRQ in the cytoplasm and nucleus, respectively), most parameters are highly constrained. The low sensitivity of FRQ-induced transcription of *wc-2* is expected because the basal transcription level of *wc-2* is high in comparison. The low sensitivity of hyperphosphorylated FRQ related parameters is due to the fact that hyperphosphorylated FRQ has no function in the model. The high sensitivity of other parameters suggests that if the clock properties are to be maintained over a wide range of environmental conditions, complex adjustments of multiple parameters are necessary.

Response coefficient analysis indicates that the period of the oscillator and the amplitude of *frq* mRNA is most sensitive to the Michaelis constant of *frq* transcription, the rate of basal transcription of *wc-1*, *wc-1* translation, degradation of *wc-1* mRNA, and degradation of activated WCC (Figures S1 and S2). A 10% decrease of *wc-1* basal transcription or translation rate, or a 10% increase of the Michaelis constant of *frq* transcription, degradation of activated WCC or *wc-1* mRNA, all result in a substantially dampened oscillator (Figure 4) with a longer period (e.g. decreasing basal *wc-1* transcription rate by 10% results in a period of 25.8 hours). A negative correlation is observed between period and amplitude response coefficients of most clock components, showing that an increase in the amplitude of oscillations would result in faster regulation through feedback loops, if not compensated (Figure 4).

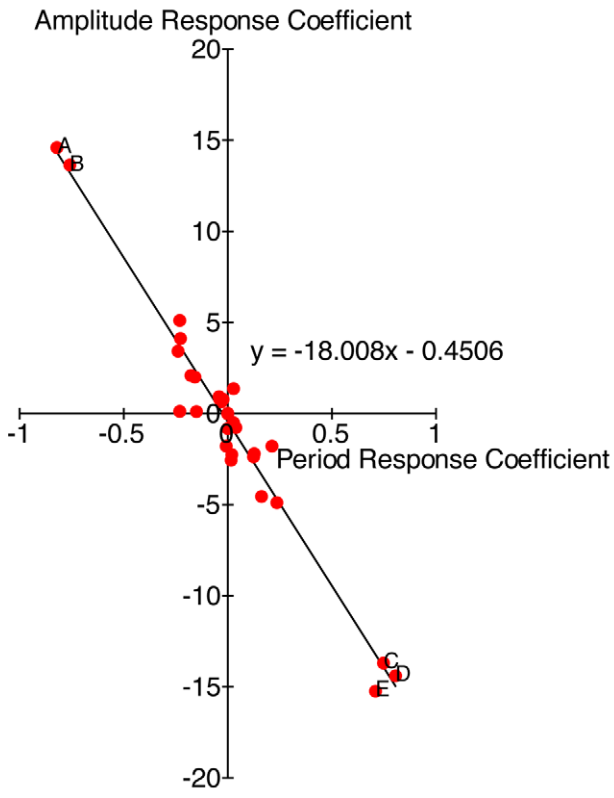

Figure 4. Distribution of parameters based on the value of their period and amplitude response coefficients. The trend line indicates that period and amplitude response coefficients are negatively correlated. A = *wc-1* translation, B = rate of basal transcription of *wc-1*, C = Michaelis constant of *frq* transcription, D = degradation of *wc-1* mRNA, E = degradation of activated WCC.
doi:10.1371/journal.pcbi.1002437.g004

Phenotypes of *Neurospora* with a mutant form WC-2 or an inducible copy of *wc-1*

From the response coefficient analysis we found that changes in the basal transcription rate of *wc-1* and the dissociation constant of WCC binding to the *frq* promoter (*K_frq*) have a large effect on the period and amplitude of the oscillator (Figure 5). Phenotypes resulting from altered transcription of *wc-1* and binding of the WCC are seen in mutant and engineered strains of *Neurospora*. For example *wc-2*^{ER24} is a *Neurospora* mutant that displays reduced WCC binding at the *frq* promoter due to a mutation at a conserved position in its Zn finger DNA-binding domain [44]. *wc-2*^{ER24} has a long period (~29.7 hours) and becomes arrhythmic after 3–4 circadian days at 25°C [44]. In *wc-2*^{ER24}, *frq* mRNA levels are lower and peak levels of *frq* are delayed compared to wild-type. In addition, the oscillation of FRQ protein dampens with time [44]. Figure 5A shows the simulation of light to dark transfer of wild-type *Neurospora*. When we increase the dissociation constant of WCC binding to the *frq* promoter *K_frq* by 10% our model successfully reproduces the characteristics of the *wc-2*^{ER24} mutant (Figure 5B).

Experimentally, the basal rate of *wc-1* transcription has been altered by introducing an inducible copy of the *wc-1* gene (qa-WC-1). In the qa-WC-1 strain the WC-1 ORF is fused to the quinic acid-inducible promoter (*qa-2*) [13] and transcription of *wc-1* is controlled by the concentration of quinic acid (QA) in the medium. Conidiation in a qa-WC-1 expressing strain is arrhythmic when the concentration of QA is low (1×10^{-7} M), but shows sustained rhythmicity at 1×10^{-4} M QA. At 1×10^{-5} M QA, conidial rhythms rapidly dampen after 3–4 cycles. In the model, *k_wc1* is the rate of basal transcription of *wc-1*. Similar to *K_frq*, *k_wc1* is also sensitive to the period and the amplitude of oscillation. Decreasing *k_wc1* by 10% results in a substantially dampened oscillation, successfully reproducing the behaviour of qa-WC-1 banding at 1×10^{-5} M QA (Figure 5C).

Simulation of light response phenotypes

To simulate the response of the *Neurospora* clock to light we incorporated light-activated WCC (laWCC) into the model (step 26 in Figure 2). laWCC strongly activates transcription of *frq*, *wc-1* and *vvd* (step 1, 2 and 4). Photoadaptation occurs as laWCC

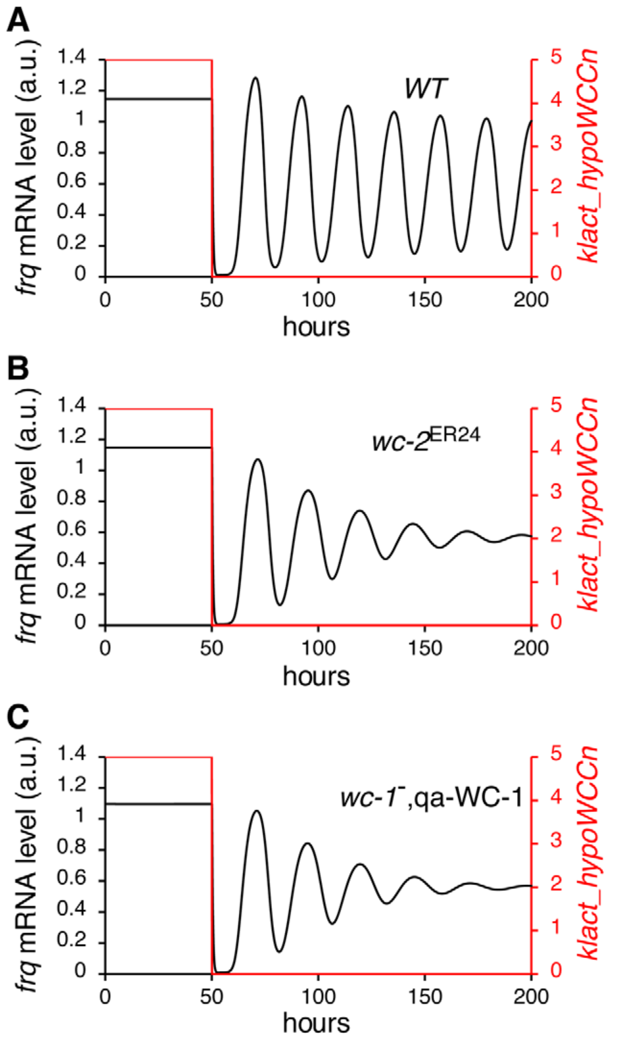

Figure 5. Reproduction of *wc-2*^{ER24} mutant and *wc-1*$^{-}$, qa-WC-1 behaviour. (A) Simulated results showing levels of *frq* RNA and light-activated WCC_n before and after a light to dark transfer. 10 data points/h are plotted. When the light (red line) is turned off after 50 h, *frq* mRNA levels oscillate. (B) Simulated *frq* mRNA behaviour of the *wc-2*^{ER24} mutant and (C) the *wc-1*$^{-}$, qa-WC-1 strain. In (B) and (C) *frq* mRNA oscillates in the dark but the oscillation dampens with time.
doi:10.1371/journal.pcbi.1002437.g005

function is quickly diminished by the formation of the laWCC VVD complex (WVC) (step 27). After interacting with VVD, the laWCC dissociates and returns to its dark state (hypoWCCn) (step 28) [25]. Light results in a rapid but transient increase of *frq* mRNA and FRQ protein [45,46], after which levels of *frq* and FRQ quickly drop to a level close to their peak levels in darkness (Figure 6A). Figure 6B shows a simulation of light/dark cycles. The period of cycling *frq* RNA and protein is entrained to 24 hours in the light dark cycles, and on return to continuous dark the clock exhibits its free running periodicity of 21.6 h. Although the phase of the clock is delayed by approximately two hours compared to the experimentally determined phase, the magnitude of the delay can be increased or decreased by changing the kinetics of FRQ-dependent *frq* RNA degradation [47] and of VVD's interaction with light-activated WCC. These data are consistent with results that show that VVD plays a role in setting the phase of the clock at the light dark transition [22,48,49]. In agreement with experimental data [25] (Figure 6C), on exposure to light of increasing intensity, after a transient increase of *frq* RNA and protein, photo-adaptation occurs and the photo-adapted steady state of gene expression depends on light intensity (Figure 6D).

A universal characteristic of circadian clocks is their phase response to light. Light exposure during the late subjective night advances their phase of oscillation. In contrast, light exposure late in the subjective day results in phase delays and light exposure during the day results in little or no change in clock time (Figure 7A) [50,51]. To examine the effect of light pulses on our model clock, the system was pulsed with light (duration 0.1 or 0.01 h) at 2 hour intervals covering one circadian day. In the model, large phase shifts are induced during the (late) subjective day and early morning (Figure 7B), which is in agreement with the published literature [45] (Figure 7A). Moreover, simulating the phase shift behaviour with different amounts of light reproduces the dependency of phase shift magnitude on the amount of light [52] (Figure 7B, dotted line).

Temperature compensation

In principle temperature compensation of period may be achieved because clock component activity is unaffected by temperature, or because temperature affects the activity of more than one clock component such that the net effect is no change in period [53,54,55,56]. Whilst some reaction rates are seemingly temperature-insensitive, temperature-dependent changes in the binding affinity, activity or conformation of the proteins involved has usually occurred [32,57,58]. For example, though the degradation rate of FRQ is temperature compensated, as the temperature rises different sites on the protein are phosphorylated by CK2. It is likely that these sites become available for phosphorylation due to a temperature-induced change in FRQ conformation or/and temperature-induced changes in the binding activity of CK2. As a result of this phosphorylation the degradation rate of FRQ is temperature compensated between 22–30 °C [32]. In other cases it is apparent from the change in relative levels of clock components that reaction rates are temperature-dependent. We know that as the temperature is raised FRQ levels oscillate around a higher mean level with no change in periodicity [59]. Since levels of *frq* RNA do not change [59] this increase in FRQ protein must be due to either increased translation or increased half-life. Since FRQ positively regulates levels of WC-1, with increasing temperature one would also expect increased levels of WC-1. With more WC-1 complexing with WC-2 (which is present in excess), more FRQ might be required to repress WCC binding to the FRQ promoter. That is, because of the positive and negative actions of FRQ, increased FRQ levels might not necessarily lead to decreased period but, depending on FRQ's activity at the new temperature, the clock is self-regulatory.

To date the effects of temperature on the *Neurospora* circadian clock have centred on the regulation of FRQ [59] and more recently on VVD [49] but there is no dataset that includes the effect of temperature on the products of the blue-light photoreceptor WC-1 and its interaction partner WC-2. To reveal the extent to which these clock components are affected by temperature, we assayed their levels over 24 hours at different temperatures. We first assayed *frq*, *wc-1* and *wc-2* transcript levels at 21 and 28°C at 4 hour intervals (Figure 8). As previously reported [59] *frq* RNA levels were not significantly different at different temperatures and peaked at DD12 (CT 5). Levels of *wc-1* RNA are lower in the first half of the day at 21°C compared to 28°C, with significant differences observed between temperatures at DD4 and DD16. *wc-2* RNA levels were comparable at most time points between 21 and 28°C. Confirming published work [41,59] we found that peak FRQ levels were significantly higher at

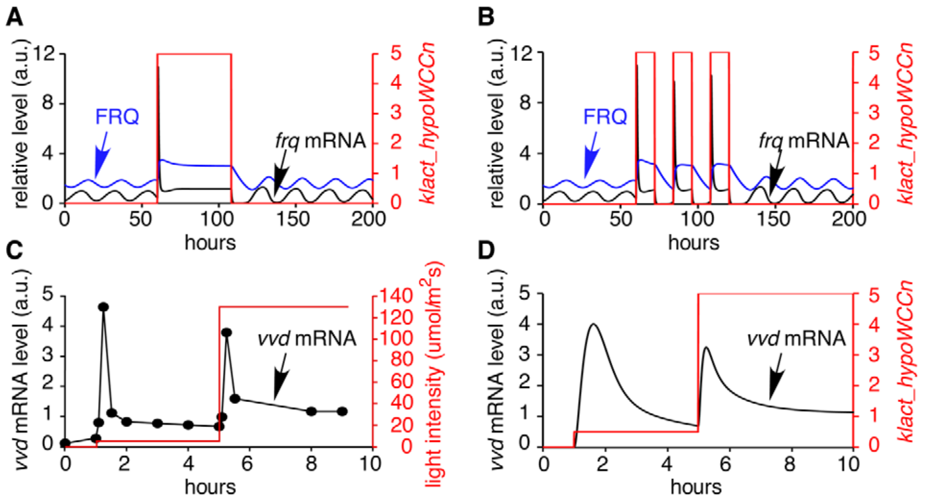

Figure 6. Simulated results of light resetting, entrainment by light/dark (LD) cycles, and photoadaptation. (A) The simulation consists of 60 h dark, 48 h constant light, 92 h constant dark. 10 data points per hour are plotted. The red line indicates light intensity. After the dark to light transfer, *frq* mRNA and FRQ protein increase and the oscillation is lost. Rhythmic expression begins without delay on return to darkness. (B) The simulation began with continuous dark for 60 hours, followed by three cycles of 12 h light: 12 h dark, before transfer to constant dark. The simulated clock can be entrained to 24 h with 12 h: 12 h light: dark cycles. (C) Experimental data shows the molecular behaviour of photoadaptation [25]. Light intensity (red line) of 5 mol·m^{-2}·s^{-1} for 4 hours and 130 mol·m^{-2}·s^{-1} for 5 h. *vvd* mRNA level (black line) is rapidly and transiently induced to high levels immediately after exposure to light. (D) The behaviour of *vvd* mRNA photoadaptation is reproduced in the model. A second increase in light intensity results in a rapid increase of *vvd* RNA. The levels soon fall but remain at a higher level compared to levels at the lower light intensity. 100 data points per hour were plotted.
doi:10.1371/journal.pcbi.1002437.g006

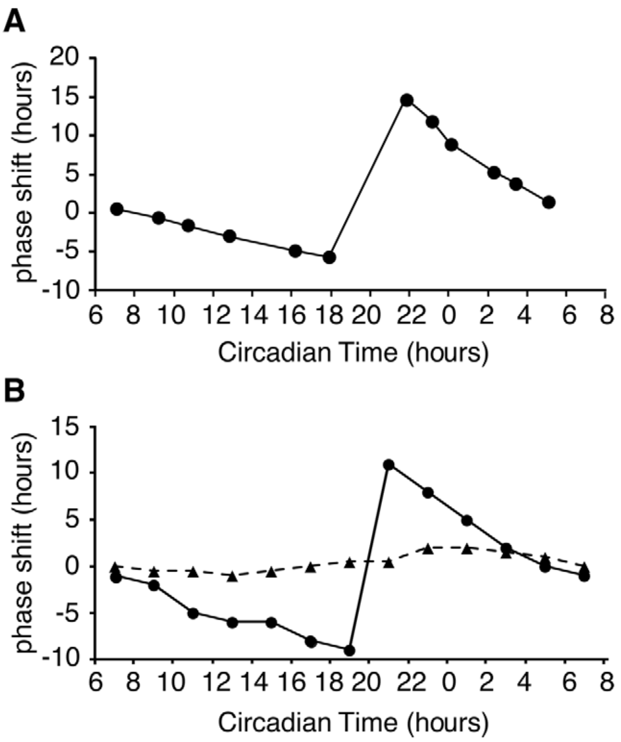

Figure 7. Phase response curves. (A) Plot of experimental data showing light-induced phase shifts [45]. Light pulses given during the late subjective night and early morning result in large phase shifts. (B) Light-induced phase shifts are reproduced in the model. 0.1 h light pulses (solid line) cause larger phase shifts than 0.01 h light pulses (dashed line). Large phase shifts occurred during the late subjective night and early morning. 20 and 200 data points/h were plotted for simulated 0.1 and 0.01 h light pulse respectively.
doi:10.1371/journal.pcbi.1002437.g007

higher temperatures and the phosphorylation pattern of FRQ, represented by the distance the bands travel on the gel, changed throughout the day (Figure 8). At DD4, FRQ levels at all temperatures were high and the majority of FRQ is highly phosphorylated. At DD8 and DD12 FRQ levels trough at all temperatures investigated and begin to rise again at DD16. At this time hypophosphorylated forms of FRQ are detected. WC-1 levels were not found to be consistently rhythmic over time at any of the temperatures investigated. A trend towards WC-1 levels being higher at higher temperatures was observed but these differences were not significant (Figure 8D). Large and small isoforms of WC-2 [17] are detected by western blot. WC-2 levels are lower at 21°C compared to 25 and 28°C. This change in WC-2 can be incorporated into our model without affecting clock properties (data not shown).

From experimental data, the level of *frq* mRNA remains the same at different temperatures, but the peak level of FRQ is tripled from 21 to 28°C [59] (Figure 8). However, the FRQ degradation rate remains the same over this range of temperature [32]. This finding indicates that the translation rate of *frq*, *k_FRQ*, is increased at high temperature. Figure 9A shows the results of a simulation where the rate of *frq* translation is temperature-dependent and the activation energy is 25.7 kJ/mol. Since *k_FRQ* is a negative response coefficient parameter, the increase of *frq* translation results in a shorter period (Figure 9A). FRQ can have both positive and negative regulatory effects in the model. A slight increase in *frq* translation elevates the level of *frq* mRNA and FRQ protein because FRQ positively regulates *wc-2* transcription and increases the accumulation of WCC in the nucleus. Nevertheless, a further increase of *frq* translation results in a reduction of *frq* mRNA and FRQ levels because FRQ facilitates the inactivation of WCC (data not shown). To maintain the same level of *frq* mRNA at different temperatures and accumulate FRQ at higher temperatures we investigated the effect of regulating FRQ nuclear localisation. The period response coefficient table shows that the transport rate of

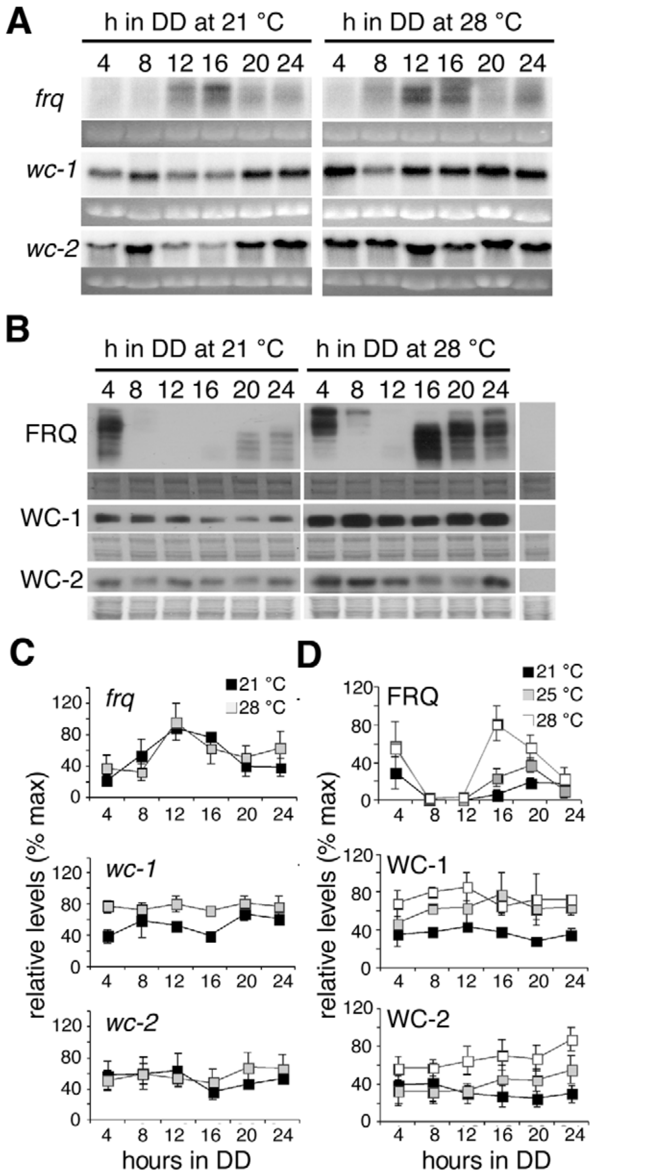

Figure 8. Clock components levels at 21 and 28°C. (A) Northern blot analysis of clock-specific transcript levels in strains grown in DD at either 21°C (left panel) or 28°C (right panel). Mycelial discs from wild-type or *wc1-myc* were grown in liquid culture at 21 or 28°C and tissue harvested at four-hour intervals in the first day of DD. Ethidium bromide stained gels were used to correct for loading. (B) The effects of temperature on clock-specific protein levels. Western blot analysis of clock-specific protein levels in strains grown in DD at either 21°C (left panel), 25°C (representative blot not shown) or 28°C (right panel). Amido black stained membranes were used to correct for loading. (C) Quantitative analysis of Northern blot data shown in A. Maximum transcript levels were set to 100%. (D) Quantitative analysis of western blot data shown in B. Maximum protein levels were set to 100%. The graphs in (C) and (D) represent three independent experiments. Error bars indicate ±1 standard error.
doi:10.1371/journal.pcbi.1002437.g008

FRQ into the nucleus, *kin_hypoFRQc*, is a negative response coefficient parameter as is *k_FRQ*. Thus, decreasing *kin_hypoFRQc* increases the period of the clock which counterbalances the effect on period of increasing *k_FRQ*. This is consistent with the concept that temperature compensation can be achieved with balancing positive and negative contributions [54,56]. Therefore, we hypothesise that with increasing temperature the translation of FRQ protein increases and the first order reaction rate of FRQ nuclear import decreases. Simulation results show that temperature compensation can be achieved with this hypothesis (Figure 9B). In this simulation, the activation energies of *frq* translation and FRQ nuclear localisation are 44.2 kJ/mol and −40.4 kJ/mol, respectively. The level of *frq* mRNA remains almost constant between 20–30°C and FRQ level increases as temperature increases. However, FRQ level is not tripled from 21–28°C, but as shown in Figure 8 the fold increased in FRQ level is greater between 25–28°C than between 21–25°C, indicating that the dependence of *frq* translation on temperature is not linear (Figure 8D). This observation led us to introduce different activation energies below and above 25°C for *frq* translation. A similar observation was made by Hong *et al.* [31] who noted that curved Arrhenius plots are needed in order to describe the temperature dependency of some kinetic parameters. As a result, the FRQ level is now tripled from 21–28°C and doubled from 25–28°C (Figure 9C). In this simulation, the activation energy of FRQ nuclear localisation (*kin_hypoFRQc*) is −107 kJ/mol, and the activation energies of *frq* translation (*k_FRQ*) below and above 25°C are 86.7 kJ/mol and 305.7 kJ/mol, respectively. Temperature compensation of period is achieved and the level of *frq* mRNA remains nearly constant within 20–30°C, in agreement with experimental observations.

Discussion

Modelling of circadian clocks is an effective approach to investigate the network properties of the underlying oscillators and to understand how they interact with the environment. For example, modelling the phosphorylation of different sites of the mammalian clock protein PER showed that PER phosphorylation by casein kinase CKI can explain the period decrease and phase advance associated with some mood disorders [60]. A recent model of the *Arabidopsis* circadian clock depicts the complexity of the clock and predicted a critical role for PRR5 (Pseudo response regulator 5) in the clock-control of morning gene expression [61]. In cyanobacteria, whose circadian clock can be reconstituted *in vitro*, modelling of the oscillations of two populations of Kai proteins, including the phosphorylation/dephosphorylation of KaiC and monomer reshuffling between KaiC hexamers, has provided insight into the mechanism by which clock time is maintained when new hypophosphorylated Kai proteins are synthesized [62]. In this work, we constructed a comprehensive *Neurospora* circadian clock model and successfully simulated clock component oscillations with accurate relative levels and phases of clock components. Light responses such as phase resetting by light, entrainment to a light dark cycle and photoadaptation are also successfully predicted by the model. This model allows us to postulate that temperature compensation is achieved by a concomitant increase in *frq* translation and inhibition of FRQ nuclear localisation.

In constant darkness, transcriptional regulation of *frq* by the WCC is a key step in *Neurospora*'s circadian oscillator and periodic transcription by WCC is dependent on its phosphorylation state [16]. Whereas hypophosphorylated WCC is degraded after activating *frq* transcription, phosphorylated WCC is more stable and can be shuttled out of the nucleus into the cytoplasm where dephosphorylation may occur [14]. The latter pathway results in the reappearance of hypophosphorylated WCC in the nucleus, which ensures the availability of WCC for the next cycle of transcription activation. Our model recapitulates these experimental observations: degradation of WCC as a consequence of its

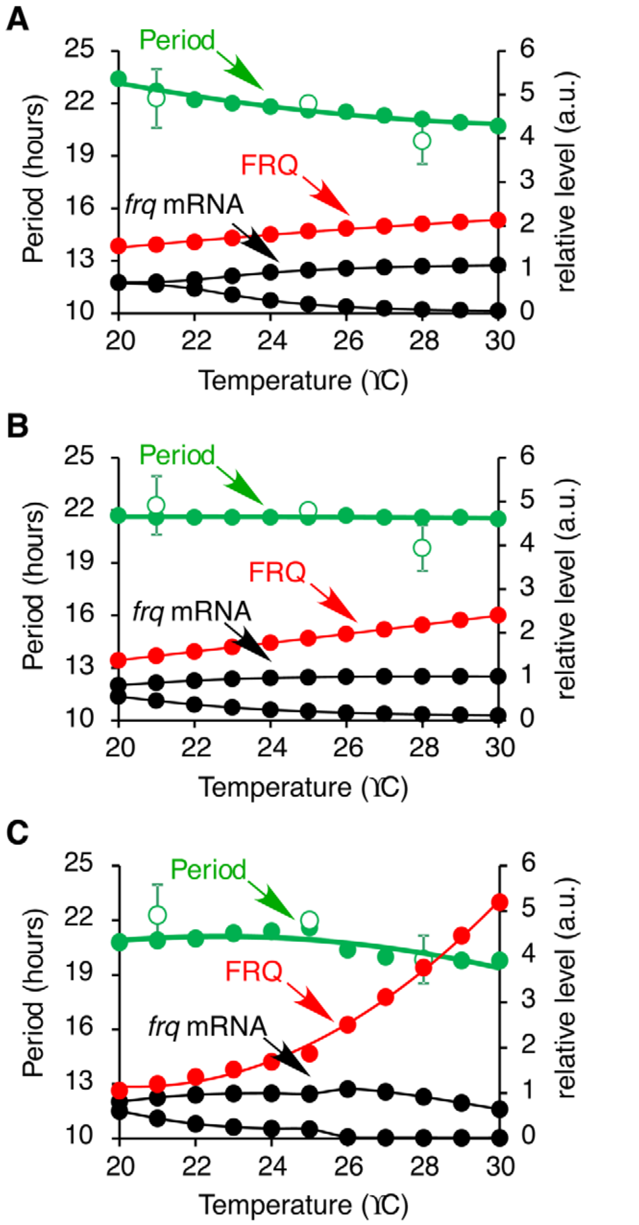

Figure 9. Simulated results showing the clock period and *frq* RNA and FRQ protein levels between 20 and 30°C. In (A) Only *frq* translation rate changes with temperature. In (B) translation of *frq* and the translocation of FRQ into the nucleus are temperature-dependent. (C) The translation of *frq* and the translocation of FRQ into the nucleus are temperature-dependent and *frq* translation has different activation energies above and below 25°C. Simulated period = closed green circles, experimentally derived period = open green circles. Peak levels of FRQ (closed red circles) and peak and trough levels of *frq* mRNA (closed black circles).
doi:10.1371/journal.pcbi.1002437.g009

role as a transcriptional activator of *frq* results in the reduction of WCC during the increasing phase of *frq* transcription. Furthermore, when FRQ levels peak, phosphorylation of the WCC, promoted by rising levels of FRQ, allows the complex to escape degradation and enter the cycle of nuclear cytoplasmic translocation. As levels of WCC reach their zenith, FRQ gradually decreases because of the decreased activation of *frq* transcription by WCC. Thus, WCC promotes *frq* transcription when the level of FRQ is low. Another possible pathway leading to the degradation of WCC centres on WCC phosphorylation state. We tested this hypothesis by modelling WCC degradation via phosphorylation. In this case our model predicts that when FRQ decreases, a delay occurs before the synthesis of new WCC and no antiphasic behaviour between WCC and FRQ is seen. Consequently, our model supports the hypothesis that degradation of WCC via transcription activation is a key factor for antiphasic FRQ and WCC expression. A putative WCC binding site exists in the *wc-1* promoter [35] but a mutation of WC-2 Zn finger DNA-binding domain does not affect the expression of WC-1 [14] indicating that a transcription factor other than the WCC regulates expression of *wc-1*. The model shows that the inferred transcription factor is necessary for antiphasic expression of WC-1 and FRQ.

An important aspect of circadian clocks is their ability to integrate signals from their environment. When exposed to light *frq* mRNA level is elevated and variable [45], FRQ is maintained at approximately twice the level seen in the dark [48] and the *Neurospora* oscillator dampens [48]. On transfer from light to dark, *frq* RNA and protein are degraded and rhythmic expression of *frq* resumes [41,47]. Our model incorporates a mechanism by which VVD-mediated inactivation of WCC reduces *frq* mRNA transcription at the light to dark boundary as well as the role of the FRQ-FRH complex in facilitating *frq* mRNA degradation in a FRQ concentration dependent manner [23,24,25,47,63]. In our model both mechanisms are essential and sufficient for initiating the oscillation after the light to dark transfer.

The least understood characteristic of circadian clocks, namely temperature compensation of circadian rhythmicity, has been a focus of this study. Temperature compensation may be achieved in a number of different ways, involving either true or apparent constancy of reaction rates. For example, a seemingly temperature insensitive reaction rate has been reported for the phosphorylation of the mammalian clock protein PER2 by CK1ε and CK1δ [64] and this is thought to be important for temperature compensation. On the other hand, in *Synechococcus* the phosphorylation cycle of KaiC depends on, but also influences, the protein's ATPase activity. Whilst the ATPase activity of KaiC is apparently temperature compensated, this is not an inherent property of the ATPase but is thought to be due to an inbuilt feedback inhibition in KaiC that downregulates its ATPase activity with increasing temperature due to a conformational change in the KaiC hexamer itself. It is speculated that the energy produced from the hydrolysis of ATP is held by KaiC resulting in an altered conformation of the protein that counterbalances changes in its activity [65]. More complex regulations in clock protein activities have been proposed in *Arabidopsis*, where not just one but many different clock components apparently participate to various degrees in the oscillation at different temperatures [66,67].

In *Neurospora* and in other organisms mutant phenotypes indicate a role for both transcriptional and posttranscriptional processes in temperature compensation [10]. Genetic evidence indicates that mutations in the known *Neurospora* clock components *frq*, *wc-2*, *chrono (chr)* and *period-3 (prd-3)* alter temperature compensation properties over a range of temperatures [44,68]. Theoretically, transcriptional and posttranscriptional processes that act to increase or decrease period in a temperature-dependent way could feed into temperature compensation. For instance, the phosphorylation state of FRQ and the WHITE COLLAR proteins dictates their activity and stability and mutations or chemicals affecting FRQ stability affect temperature compensation [69,70,71,72,73]. Because FRQ stability is regulated by kinases and phosphatases one would predict that the action of these enzymes will be integral to successful temperature compensation of the clock [74] and this is indeed true [32,75]. The apparent temperature compensation of FRQ degradation rate is brought about by different utilization of FRQ phosphorylation sites at different temperatures. Differential accessibility of FRQ phosphorylation sites is probably regulated by a conformational change in FRQ with changing temperature [32]. In addition, our data imply that temperature-dependent changes in the localization of FRQ are an important aspect of temperature compensation.

To be valid, the proposed mechanism of temperature compensation has to be in agreement with a certain number of experimental observations. Between 21 and 28°C: (1) *frq* RNA levels are unchanged, (2) FRQ protein levels increase by 3–4 fold, (3) the degradation rate of FRQ is unchanged. Thus, the increase in FRQ levels must be due to an increase in *frq* translation. However, if the *frq* translation rate is increased significantly, the model predicts that the *frq* RNA level would decrease and the period shorten. Hence, the increase in *frq* translation has to be compensated by other reactions that: (1) increase the period, (2) increase the *frq* RNA level, and (3) triple the FRQ level. We first tested individual reaction parameters to see whether these conditions could be fulfilled over a range of temperatures. When we considered a fixed activation energy for *frq* translation, no parameter variations could fulfil all three conditions and the oscillation was lost at lower temperatures. We then considered different activation energies below and above 25°C for *frq* translation. The reason why *frq* translation might have different activation energies may lie in the complexity of the mechanisms of translation where multiple enzymes are involved. In addition, the structure of mRNA and the conformation of FRQ may be changed at different temperatures. Similarly, Hong *et al.* [31] employed a curved Arrhenius plot for WCC binding to the *frq* promoter and the degradation of FRQ, and used different activation energies depending on the range of temperature (20–25 °C or 25–30 °C) to explain temperature compensation. Using different activation energies for *frq* translation, we observed that when: (1) the Michaelis constant of nuclear WCC phosphorylation is increased with increasing temperature, or (2) the nuclear localisation of FRQ is decreased with increasing temperature, the three conditions are fulfilled. However, the second modification leads to simulations that are in better agreement with experimental data. Temperature dependent translocation of proteins has been reported in other organisms, for example in rat fibroblasts the temperature-sensitive mutant of p53 ($p53^{val-5}$) is predominantly in the cytoplasm at 37.5 °C but moves to the nucleus at 32.5 °C [76]. Another example of a protein whose localisation is temperature-dependent is the *Antirrhinum* Tam3 transposase, which is restricted to the cytoplasm at 25 °C, but translocates into the nucleus at 15 °C [77]. Interestingly, translocation between cytoplasm and nucleus of the *Drosophila* clock protein PER is restricted in the *ritsu* mutant at higher temperatures, resulting in lengthening the period of the clock [78].

How might subcellular localization of FRQ be regulated? Nuclear translocation may be regulated by FRQ phosphorylation, although more recent evidence suggests that this is not the case and that at least at 25 °C, FRQ's interaction with FRH and overall conformation plays a greater role [79]. This being true one would predict that some other posttranslational modification and/or change in conformation of FRQ regulates nuclear localization with temperature. Our proposed temperature compensation mechanism could be tested by carrying out FRQ subcellular distribution experiments. If our prediction is correct, nuclear localisation of FRQ should be restricted at high temperature. If the ratio of cytoplasmic FRQ to nuclear FRQ is similar at low and high temperature, this would suggest that although FRQ level is essentially increased, the activity of FRQ may be diminished at higher temperature, ensuring that levels of WCC phosphorylation are maintained.

In addition to temperature-regulated FRQ nuclear localization, other posttranscriptional modifications may be required to maintain constant levels and activities of the clock components which seem to be unaffected by the temperature. For example, overall WCC activity appears to stay the same at all temperatures, resulting in similar levels of cycling *frq* RNA. However, this may be due to modification of WC-1 at higher temperatures which renders it less active. Indeed, the WC-1 protein runs at a higher molecular weight at 28°C. What could be the significance of the unchanged levels of *frq* mRNA? We speculate that the purpose of keeping *frq* RNA levels constant could be that transcription is the entry point for resetting of the *Neurospora* clock by light, and possibly also temperature. It seems plausible that in order to retain the ability to respond to light at different temperatures, the transcriptional responsiveness has to be maintained at subsaturated levels at all times. FRQ levels increase with temperature yet we predict much of the FRQ protein is excluded from the nucleus. One reason for this could be that a non circadian function of FRQ in the cytoplasm requires increased FRQ at higher temperatures. Additionally, when temperatures drop high levels of FRQ help to reset the clock to the appropriate circadian time [47,59].

In summary, we provide a comprehensive model for the *Neurospora* circadian clock and its responses to acute and chronic changes in light and temperature. The model predicts a role for FRQ nuclear localisation in temperature compensation and makes predictions that can be experimentally tested in the future to further refine our understanding of circadian oscillators. Both light and temperature can entrain and reset the clock [50,52,59], and in reality organisms are exposed to these conditions simultaneously. An advantage of having a model that incorporates both light response and temperature dependency is that the coupling between both types of environmental signals can be studied to provide a comprehensive understanding of the detailed molecular interactions of the clock.

Materials and Methods

Model construction

The circadian clock model was manually constructed using the CellDesigner™ 4.1 software [80,81,82]. The program was operated in Java Runtime Environment (JRE) Version 6 Update 16 on Windows XP. Model parameters were either derived from experimental data (*frq* ([63] and our data), *wc-1* (our data), *wc-2* (our data) and *vvd* RNA degradation (our data), FRQ degradation [30]) or estimated by comparing simulations to experimental observations. The kinetic equations used in the model are presented in Table S1 and the model is provided in SBML format Level 2 version 4 (Dataset S1). Simulations were carried out in CellDesigner using SOSlib as the numerical solver.

Control analysis

To quantify how model components affect the period and amplitude of the oscillation, we calculated period and amplitude response coefficients. The period response coefficient R_j^T of parameter P_j was defined as the rate of change in period T divided by the rate of change of the parameter value.

$$R_j^T = \frac{\frac{\delta T}{T}}{\frac{\delta P_j}{P_j}}$$

The amplitude response coefficient R_j^A of the parameter P_j was similarly defined as the rate of change in amplitude A divided by the rate of change of the parameter value.

$$R_j^A = \frac{\frac{\delta A}{A}}{\frac{\delta P_j}{P_j}}$$

The effect of a 3% change in the value of each parameter was considered. 200 hours of dark simulation and 200 points per hour were calculated without changing the initial value of the components for period response coefficients. 200 hours of dark simulation and 50 points per hour are calculated without changing the initial value of the components for amplitude response coefficients. The last two peaks of *frq* mRNA level were used to calculate the period and the last peak and trough of the *frq* mRNA oscillation were used to calculate the amplitude.

Light input and photoadaptation

Light activated WCC (laWCC) was introduced in the model and was activated from nuclear hypophosphorylated WCC (hypoWCCn). laWCC can activate the transcription of *vvd* and promote the transcription of *frq* and *wc-1*. The light activation rate (*klact_hypoWCCn*) of WCC is 0 in dark and is increased to 5 to mimic light using SBML events. Photoadaptation occurs because light induced VVD represses the light activity of the WCC through the formation of the laWCC VVD complex (WVC). After interacting with VVD the laWCC disassociates and returns to its dark state.

For phase response curves (PRC) simulated in the model, 0.1 or 0.01 h of duration of light was pulsed every two circadian hours. To simulate a light pulse, the light activation rate (*klact_hypoWCCn*) of WCC was changed from 0 to 5, and returned to 0 to end the pulse. The time of peak *frq* mRNA before and after the light pulse was used to calculate the advance or delay of the clock.

Temperature compensation

The effect of temperature was introduced into the model by use of the Arrhenius equation [27]. For each reaction, temperature influences the value of each kinetic parameter k_i according to equation 1 [30].

$$k_i = A_i e^{-\frac{E_i}{RT}} \quad (1)$$

A_i is the collision factor or pre-exponential factor, which is a constant; E_i is the activation energy; R is the gas constant ($8.314462\ \mathrm{J{\cdot}mol^{-1}{\cdot}K^{-1}}$); T is the temperature in Kelvin. A_i and E_i are independent of the temperature. The activation energy E_a was calculated using equation 2 [30].

$$E_a = \frac{R \cdot \ln \frac{k_{T2}}{k_{T1}}}{\frac{1}{T_1} - \frac{1}{T_2}} \quad (2)$$

R is the gas constant k_{T1} is the parameter value at temperature T_1 and k_{T2} is the parameter value at temperature T_2. Once the activation energy was calculated, the pre-exponential factor A_i was obtained by solving the Arrhenius equation.

While all reactions are temperature-dependent in principle, the reactions that are explicitly made temperature-dependent in the model are sufficient to account for all observations related to temperature change, and as such they represent the most likely mechanism for temperature compensation. All other reactions could indeed be made explicitly temperature-dependent in the model, but their activation energies would remain too small to have any noticeable effect on simulations. This would mean that unnecessary complexity is added to the model that cannot be validated by observations, thereby contravening the principle of parsimony. The activation energy of FRQ nuclear localisation (*kin_hypoFRQc*) is −107 kJ/mol, and the activation energies of *frq* translation (*k_FRQ*) below and above 25°C are 86.7 kJ/mol and 305.7 kJ/mol, respectively.

Model robustness to parameter perturbation

The model robustness analysis was carried out using the parameter scan function in CellDesigner. For the rhythmicity test, each parameter was increased and decreased until the oscillation of *frq* RNA level was lost. 20,000 hours of dark simulation and 10 points per hour were calculated without changing the initial value of the components. A persistent oscillation of *frq* mRNA level was considered as rhythmic. For the period perturbation test, each parameter was increased and decreased until the period lay outside the range of 21.6±0.6 hours. For the amplitude perturbation test, each parameter was increased and decreased until the *frq* RNA oscillation amplitude was increased or decreased by 5% of its original value. For the period and the amplitude perturbation test, 500 hours of dark simulation and 10 points per hour were calculated without changing the initial value of the components. The last two peaks of *frq* mRNA level were used to calculate the period and the last peak and trough of the *frq* mRNA oscillation were used to calculate the amplitude.

Strains and conditions

Minimal medium contained 1× Vogel's salts [83], 2% sucrose, 1.5% agar and 50 ng/ml biotin. Liquid medium consisted of 1× Vogel's salts, 2% glucose, 50 ng/ml biotin and 0.17% arginine. mRNA degradation was assayed in the 54-3 *bd* strain of *Neurospora*. *Neurospora* was grown on slant minimal medium and spores were transferred to plate with liquid medium. After 24 hours culture at 30 °C, tissues were cut into discs and inoculated into flasks with liquid medium. Flasks were shaken at 125 rpm. Discs were grown in shake culture in constant light (LL) for at least 24 hours. At the time point of light to dark (DD) transfer, thiolutin was dissolved in dimethyl sulfoxide (DMSO) and added to a final concentration of 5 µg/ml. To assay mRNA and protein expression in constant conditions but at different ambient temperatures, the 54-3 *bd* or the *wc1-myc* strain of *Neurospora* were grown for 1–2 days at either 21°C, 25°C or 28°C in LL and then transferred to DD at the same constant temperature.

Northern blot analysis

Transcripts were extracted by using the Qiagen RNeasy Mini kit according to the manufacturer's instructions for the isolation of total RNA from filamentous fungus. Total RNA (7–10 µg) was electrophoresed through a 1% agarose–formaldehyde gel, blotted onto Hybond-N+ membrane (Amersham), and probed using radiolabelled antisense riboprobes (Ambion) as described previously [48,49]. Nucleotides 1630–3832 of the *frequency* open reading frame (ORF) were transcribed into an antisense riboprobe using Amersham ^{32}P-dUTP (800 Ci/mmol) to a specific activity of 10^9 counts per minute (cpm) per microgram. For *wc-1* (positions 1756–3067) and *wc-2* (positions 637–1801) gene specific riboprobes were generated by labelling PCR fragments containing T7 polymerase sites to generate antisense riboprobes. Gene-specific riboprobes of *vvd* mRNA were obtained by labelling PCR products (AF338412, positions 239–1173 for *vvd*) containing an appropriate T7 Polymerase site to generate antisense riboprobes. Membranes were hybridized in 10 ml of NorthernMax Prehyb/Hyb (Ambion) containing 2×10^7 cpm/ml of *in vitro* transcribed radiolabelled probe (Ambion). Membranes were exposed to Fuji screens and were scanned using a PhosphorImager (Bio-Rad). RNA data were quantified using ImageJ 1.42q (National Institutes of Health, USA) or Quantity One (Bio-Rad).

Protein analysis

Total protein extracts were obtained as previously described [41]. For western blot analysis, 50 µg of total protein extract was loaded per lane onto an SDS-PAGE gel. After electrophoresis, proteins were blotted onto Immobilon-P membrane (Millipore) by wet transfer. Membranes were hybridised with either anti-FRQ (kindly provided by Prof. Jay Dunlap and Prof. Jennifer Loros, Dartmouth Medical School, Hanover, NH), anti-WC-2 (kindly provided by Prof. Yi Liu, University of Texas Southwestern Medical School, Dallas, TX) or anti-MYC antibody (Santa Cruz Biotechnology) as described previously [22]. Immunodetection was carried out as previously described [49] and the signal quantified using Quantity One (Bio-Rad).

Race tube assay

The period of the clock was assayed in the 54-3 *bd* strain of *Neurospora* at 21°C, 25°C and 28°C. Race tube media contained 1× Vogel's salts, 0.1% glucose, 50 ng/µL biotin, 0.17% arginine, and 1.5% agar. *Neurospora* were grown in constant light (LL) for at least 24 hours and then transferred to DD at the same constant temperature. Growth fronts were first marked at the LD transition and then every 24 h thereafter. All race tubes were analyzed using the CHRONO program [84].

Supporting Information

Dataset S1 *Neurospora* circadian clock model in SBML format Level 2 version 4 for CellDesigner.
(XML)

Figure S1 Period response coefficients. Values of averaged period response coefficients for ±3% variation in each parameter value. 200 points per hour and 200 hours in total were simulated. The last two peaks of *frq* mRNA were used to determine the period.
(DOC)

Figure S2 Amplitude response coefficients. Values of averaged amplitude response coefficients for ±3% variation in each parameter value. 50 points per hour and 200 hours in total were simulated. The last peak and trough of *frq* mRNA were used to determine the amplitude.
(DOC)

Table S1 Kinetic equations used in the model. The rate of reaction *i* is noted *v_i*.
(DOC)

Table S2 List and values of model parameters.
(DOC)

Table S3 Parameter sensitivity test for oscillations. For each parameter, the table gives the lower and upper value that conserves *frq* RNA oscillations, as well as the percentage change with respect to its reference value.
(DOC)

Table S4 Parameter sensitivity test for period. For each parameter, the table gives the lower and upper value for which a period of 21.6±0.6 hours is obtained for *frq* RNA oscillations, as well as the percentage change with respect to its reference value.
(DOC)

Table S5 Parameter sensitivity test for amplitude. For each parameter, the table gives the lower and upper value for which the amplitude of *frq* RNA of oscillations is changed by ±5%, as well as the percentage change with respect to its reference value.
(DOC)

Acknowledgments

We thank Jay Dunlap and Jennifer Loros (both at Dartmouth Medical School, New Hampshire) for the generous gift of FRQ antiserum and Yi Liu (University of Texas Southwestern Medical School, Texas) for the generous gift of WC-2 antiserum. We thank Wen-Ching Tseng and Bi-Yi Fu for their support.

Author Contributions

Conceived and designed the experiments: CH SKC JMS. Performed the experiments: YYT SMH. Analyzed the data: YYT CH. Wrote the paper: YYT SKC JMS.

References

1. Bell-Pedersen D, Cassone VM, Earnest DJ, Golden SS, Hardin PE, et al. (2005) Circadian rhythms from multiple oscillators: lessons from diverse organisms. Nat Rev Genet 6: 544–556.
2. Hunt T, Sassone-Corsi P (2007) Riding tandem: circadian clocks and the cell cycle. Cell 129: 461–464.
3. Harrisingh MC, Nitabach MN (2008) Circadian rhythms. Integrating circadian timekeeping with cellular physiology. Science 320: 879–880.
4. Ko GY, Shi L, Ko ML (2009) Circadian regulation of ion channels and their functions. J Neurochem 110: 1150–1169.
5. Heintzen C, Liu Y (2007) The *Neurospora crassa* circadian clock. Adv Genet 58: 25–66.
6. Dunlap JC, Loros JJ, Colot HV, Mehra A, Belden WJ, et al. (2007) A circadian clock in *Neurospora*: how genes and proteins cooperate to produce a sustained, entrainable, and compensated biological oscillator with a period of about a day. Cold Spring Harb Symp Quant Biol 72: 57–68.
7. Pittendrigh CS (1954) On Temperature Independence in the Clock System Controlling Emergence Time in *Drosophila*. Proc Natl Acad Sci U S A 40: 1018–1029.
8. Dunlap JC (1999) Molecular bases for crcadian clocks. Cell 96: 271–290.
9. Dong G, Golden SS (2008) How a cyanobacterium tells time. Curr Opin Microbiol 11: 541–546.
10. Zheng X, Sehgal A (2008) Probing the relative importance of molecular oscillations in the circadian clock. Genetics 178: 1147–1155.
11. Dardente H, Cermakian N (2007) Molecular circadian rhythms in central and peripheral clocks in mammals. Chronobiol Int 24: 195–213.
12. Loros JJ, Dunlap JC (2001) Genetic and molecular analysis of circadian rhythms in *Neurospora*. Annu Rev Physiol 63: 757–794.
13. Cheng P, Yang Y, Liu Y (2001) Interlocked feedback loops contribute to the robustness of the *Neurospora* circadian clock. Proc Natl Acad Sci U S A 98: 7408–7413.
14. Schafmeier T, Diernfellner A, Schafer A, Dintsis O, Neiss A, et al. (2008) Circadian activity and abundance rhythms of the *Neurospora* clock transcription factor WCC associated with rapid nucleo-cytoplasmic shuttling. Genes Dev 22: 3397–3402.
15. He Q, Cha J, Lee HC, Yang Y, Liu Y (2006) CKI and CKII mediate the FREQUENCY-dependent phosphorylation of the WHITE COLLAR complex to close the *Neurospora* circadian negative feedback loop. Genes Dev 20: 2552–2565.
16. Schafmeier T, Haase A, Káldi K, Scholz J, Fuchs M, et al. (2005) Transcriptional feedback of *Neurospora* circadian clock gene by phosphorylation-dependent inactivation of its transcription factor. Cell 122: 235–246.
17. Neiss A, Schafmeier T, Brunner M (2008) Transcriptional regulation and function of the *Neurospora* clock gene *white collar 2* and its isoforms. EMBO Rep 9: 788–794.
18. Chen CH, Dunlap JC, Loros JJ (2010) *Neurospora* illuminates fungal photoreception. Fungal Genet Biol 47: 922–929.
19. Linden H, Macino G (1997) White collar 2, a partner in blue-light signal transduction, controlling expression of light-regulated genes in *Neurospora crassa*. EMBO J 16: 98–109.
20. Froehlich AC, Liu Y, Loros JJ, Dunlap JC (2002) White Collar-1, a circadian blue light photoreceptor, binding to the *frequency* promoter. Science 297: 815–819.

21. Schwerdtfeger C, Linden H (2003) VIVID is a flavoprotein and serves as a fungal blue light photoreceptor for photoadaptation. EMBO J 22: 4846–4855.
22. Heintzen C, Loros JJ, Dunlap JC (2001) The PAS protein VIVID defines a clock-associated feedback loop that represses light input, modulates gating, and regulates clock resetting. Cell 104: 453–464.
23. Hunt SM, Thompson S, Elvin M, Heintzen C (2010) VIVID interacts with the WHITE COLLAR complex and FREQUENCY-interacting RNA helicase to alter light and clock responses in *Neurospora*. Proc Natl Acad Sci U S A 107: 16709–16714.
24. Chen CH, DeMay BS, Gladfelter AS, Dunlap JC, Loros JJ (2010) Physical interaction between VIVID and white collar complex regulates photoadaptation in *Neurospora*. Proc Natl Acad Sci U S A 107: 16715–16720.
25. Malzahn E, Ciprianidis S, ldi KK, Schafmeier T, Brunner M (2010) Photoadaptation in *Neurospora* by competitive interaction of activating and inhibitory LOV domains. Cell 142: 762–772.
26. Ruoff P, Mohsenzadeh S, Rensing L (1996) Circadian rhythms and protein turnover: the effect of temperature on the period lengths of clock mutants simulated by the Goodwin oscillator. Naturwissenschaften 83: 514–517.
27. Ruoff P, Rensing L (1996) The temperature compensated Goodwin model simulates many circadian clock properties. J Theor Biol 179: 275–285.
28. Leloup J-C, Gonze D, Goldbeter1 A (1999) Limit cycle models for circadian rhythms based on transcriptional regulation in *Drosophila* and *Neurospora*. J Biol Rhythms 14: 433–448.
29. Francois P (2005) A model for the *Neurospora* circadian clock. Biophys J 88: 2369–2383.
30. Ruoff P, Loros JJ, Dunlap JC (2005) The relationship between FRQ-protein stability and temperature compensation in the *Neurospora* circadian clock. Proc Natl Acad Sci U S A 102: 17681–17686.
31. Hong CI, Jolma IW, Loros JJ, Dunlap JC, Ruoff P (2008) Simulating dark expressions and interactions of *frq* and *wc-1* in the *Neurospora* circadian clock. Biophys J 94: 1221–1232.
32. Mehra A, Shi M, Baker CL, Colot HV, Loros JJ, et al. (2009) A role for Casein Kinase 2 in the mechanism underlying circadian temperature compensation. Cell 137: 749–760.
33. Dunlap JC, Loros JJ (2006) How fungi keep time: circadian system in *Neurospora* and other fungi. Curr Opin Microbiol 9: 579–587.
34. Froehlich AC, Loros JJ, Dunlap JC (2003) Rhythmic binding of a WHITE COLLAR-containing complex to the *frequency* promoter is inhibited by FREQUENCY. Proc Natl Acad Sci U S A 100: 5914–5919.
35. Káldi K, González BH, Brunner M (2006) Transcriptional regulation of the *Neurospora* circadian clock gene *wc-1* affects the phase of circadian output. EMBO Rep 7: 199–204.
36. Cheng P, He Q, He Q, Wang L, Liu1 Y (2005) Regulation of the *Neurospora* circadian clock by an RNA helicase. Genes Dev 19: 234–241.
37. Diernfellner ACR, Querfurth C, Salazar C, Höfer T, Brunner M (2009) Phosphorylation modulates rapid nucleocytoplasmic shuttling and cytoplasmic accumulation of *Neurospora* clock protein FRQ on a circadian time scale. Genes Dev 23: 2192–2200.
38. Brunner M, Schafmeier T (2006) Transcriptional and post-transcriptional regulation of the circadian clock of cyanobacteria and *Neurospora*. Genes Dev 20: 1061–1074.
39. Ballario P, Vittorioso P, Magrelli A, Talora C, Cabibbo A, et al. (1996) White collar-1, a central regulator of blue light responses in *Neurospora*, is a zinc finger protein. EMBO J 15: 1650–1657.
40. He Q, Cheng P, Yang Y, Wang L, Gardner KH, et al. (2002) White collar-1, a DNA binding transcription factor and a light sensor. Science 297: 840–843.
41. Garceau NY, Liu Y, Loros JJ, Dunlap JC (1997) Alternative initiation of translation and time-specific phosphorylation yield multiple forms of the essential clock protein FREQUENCY. Cell 89: 469–476.
42. Lee K, Loros JJ, Dunlap JC (2000) Interconnected feedback loops in the *Neurospora* circadian system. Science 289: 107–110.
43. Denault DL, Loros JJ, Dunlap JC (2001) WC-2 mediates WC-1-FRQ interaction within the PAS protein-linked circadian feedback loop of *Neurospora*. EMBO J 20: 109–117.
44. Collett MA, Dunlap JC, Loros JJ (2001) Circadian clock-specific roles for the light response protein WHITE COLLAR-2. Mol Cell Biol 21: 2619–2628.
45. Crosthwaite SK, Loros JJ, Dunlap JC (1995) Light-induced resetting of a circadian clock is mediated by a rapid increase in *frequency* transcript. Cell 81: 1003–1012.
46. Merrow M, Franchi L, Dragovic Z, Gorl M, Johnson J, et al. (2001) Circadian regulation of the light input pathway in *Neurospora crassa*. EMBO J 20: 307–315.
47. Guo J, Cheng P, Yuan H, Liu Y (2009) The exosome regulates circadian gene expression in a posttranscriptional negative feedback loop. Cell 138: 1236–1246.
48. Elvin M, Loros JJ, Dunlap JC, Heintzen C (2005) The PAS/LOV protein VIVID supports a rapidly dampened daytime oscillator that facilitates entrainment of the *Neurospora* circadian clock. Genes Dev 19: 2593–2605.
49. Hunt SM, Elvin M, Crosthwaite SK, Heintzen C (2007) The PAS/LOV protein VIVID controls temperature compensation of circadian clock phase and development in *Neurospora crassa*. Genes Dev 21: 1964–1974.
50. Johnson CH (1999) Forty years of PRCs–what have we learned? Chronobiol Int 16: 711–743.
51. Sargent ML, Briggs WR (1967) The effects of light on a circadian rhythm of conidiation in *Neurospora*. Plant Physiol 42: 1504–1510.
52. Dharmananda S (1980) Studies of the circadian clock of *Neurospora crassa*: light-induced phase shifting. [PhD Thesis]. University of California, Santa Cruz.
53. Hastings JW, Sweeney BM (1957) On the Mechanism of Temperature Independence in a Biological Clock. Proc Natl Acad Sci U S A 43: 804–811.
54. Winfree AT (1980) The geometry of biological time. New York: Springer.
55. Ruoff P (1992) Introducing temperature-compensation in any reaction kinetic oscillator model. J Interdiscipl Cycle Res 23: 92–99.
56. Ruoff P, Zakhartsev M, Westerhoff HV (2007) Temperature compensation through systems biology. FEBS J 274: 940–950.
57. Kageyama H, Nishiwaki T, Nakajima M, Iwasaki H, Oyama T, et al. (2006) Cyanobacterial circadian pacemaker: Kai protein complex dynamics in the KaiC phosphorylation cycle in vitro. Mol Cell 23: 161–171.
58. Terauchi K, Kitayama Y, Nishiwaki T, Miwa K, Murayama Y, et al. (2007) ATPase activity of KaiC determines the basic timing for circadian clock of cyanobacteria. Proc Natl Acad Sci U S A 104: 16377–16381.
59. Liu Y, Merrow M, Loros JJ, Dunlap JC (1998) How temperature changes reset a circadian oscillator. Science 281: 825.
60. Leloup J-C, Goldbeter A (2011) Modelling the dual role of Per phosphorylation and its effect on the period and phase of the mammalian circadian clock. IET Syst Biol 5: 44–49.
61. Pokhilko A, Hodge SK, Stratford K, Knox K, Edwards KD, et al. (2010) Data assimilation constrains new connections and components in a complex, eukaryotic circadian clock model. Mol Syst Biol 6: 416.
62. Nagai T, Terada TP, Sasai M (2010) Synchronization of circadian oscillation of phosphorylation level of KaiC in vitro. Biophys J 98: 2469–2477.
63. Guo J, Cheng P, Liu Y (2010) Functional significance of FRH in regulating the phosphorylation and stability of *Neurospora* circadian clock protein FRQ. J Biol Chem 285: 11508–11515.
64. Isojima Y, Nakajima M, Ukai H, Fujishima H, Yamada RG, et al. (2009) CKIepsilon/delta-dependent phosphorylation is a temperature-insensitive, period-determining process in the mammalian circadian clock. Proc Natl Acad Sci U S A 106: 15744–15749.
65. Kondo T (2007) A cyanobacterial circadian clock based on the Kai oscillator. Cold Spring Harb Symp Quant Biol 72: 47–55.
66. Gould PD, Diaz P, Hogben C, Kusakina J, Salem R, et al. (2009) Delayed fluorescence as a universal tool for the measurement of circadian rhythms in higher plants. Plant J 58: 893–901.
67. Salome PA, Weigel D, McClung CR (2010) The role of the *Arabidopsis* morning loop components CCA1, LHY, PRR7, and PRR9 in temperature compensation. Plant Cell 22: 3650–3661.
68. Gardner GF, Feldman JF (1981) Temperature compensation of circadian periodicity in clock mutants of *Neurospora crassa*. Plant Physiol 68: 1244–1248.
69. Gorl M, Merrow M, Huttner B, Johnson J, Roenneberg T, et al. (2001) A PEST-like element in FREQUENCY determines the length of the circadian period in *Neurospora crassa*. EMBO J 20: 7074–7084.
70. He Q, Liu Y (2005) Degradation of the *Neurospora* circadian clock protein FREQUENCY through the ubiquitin-proteasome pathway. Biochem Soc Trans 33: 953–956.
71. Jolma IW, Falkeid G, Bamerni M, Ruoff P (2006) Lithium leads to an increased FRQ protein stability and to a partial loss of temperature compensation in the *Neurospora* circadian clock. J Biol Rhythms 21: 327–334.
72. Liu Y, Loros J, Dunlap JC (2000) Phosphorylation of the *Neurospora* clock protein FREQUENCY determines its degradation rate and strongly influences the period length of the circadian clock. Proc Natl Acad Sci U S A 97: 234–239.
73. Sancar G, Sancar C, Brunner M, Schafmeier T (2009) Activity of the circadian transcription factor White Collar Complex is modulated by phosphorylation of SP-motifs. FEBS Lett 583: 1833–1840.
74. Sweeney BM, Hastings JW (1960) Effects of temperature upon diurnal rhythms. Cold Spring Harb Symp Quant Biol 25: 87–104.
75. Tang CT, Li S, Long C, Cha J, Huang G, et al. (2009) Setting the pace of the *Neurospora* circadian clock by multiple independent FRQ phosphorylation events. Proc Natl Acad Sci U S A 106: 10722–10727.
76. Ginsberg D, Michael-Michalovitz D, Ginsberg D, Oren M (1991) Induction of growth arrest by a temperature-sensitive p53 mutant is correlated with increased nuclear localization and decreased stability of the protein. Mol Cell Biol 11: 582–585.
77. Fujino K, Hashida S-n, Ogawa T, Natsume T, Uchiyama T, et al. (2011) Temperature controls nuclear import of Tam3 transposase in *Antirrhinum*. Plant J 65: 146–155.
78. Matsumoto A, Tomioka K, Chiba Y, Tanimura T (1999) timrit Lengthens circadian period in a temperature-dependent manner through suppression of PERIOD protein cycling and nuclear localization. Mol Cell Biol 19: 4343–4354.
79. Cha J, Yuan H, Liu Y (2011) Regulation of the activity and cellular localization of the circadian clock protein FRQ. J Biol Chem 286: 11469–11478.
80. Kitano H, Funahashi A, Matsuoka Y, Oda K (2005) Using process diagrams for the graphical representation of biological networks. Nat Biotechnol 12: 961–966.
81. Funahashi A, Matsuoka Y, Jouraku A, Morohashi M, Kikuchi N, et al. (2008) CellDesigner 3.5: A versatile modeling tool for biochemical networks. Proc IEEE Inst Electr Electron Eng 96: 1254–1265.
82. Funahashi A, Morohashi M, Kitano H, Tanimura N (2003) CellDesigner: a process diagram editor for gene-regulatory and biochemical networks. Drug Discov Today Biosilico 1: 159–162.
83. Davis RH, de Serres FJ (1970) Genetic and microbial research techniques for Neurospora crassa. Methods Enzymol 17: 79–143.
84. Roenneberg T, Taylor W (2000) Automated recordings of bioluminescence with special reference to the analysis of circadian rhythms. Methods Enzymol 305: 104–119.